



Thesis titled:

**Different Mass Spectrometers, Widely Differing
Purposes.**

**From Structure Elucidation Tool to Gas Phase
Ion-Molecule Reactions.**

Submitted for the Degree of Doctor of Philosophy (PhD)

by

Micheal (Mike) John Maclean

BSc (Hons) MRACI CChem

GradDipForsSc (DNA Tech) MAIBiol

of the

Department of Chemistry

November 2012

For my special little mate

Maksim Vuk Maclean

28/11/2005 -

“Dad ‘gave-it-a-go’, so should you”

XOXOXO

CONTENTS

ACKNOWLEDGEMENTS	vi
DECLARATION	viii
ABSTRACT	ix
PART I	1
Tetra-Atomic and Hetero-Cumulenic Systems of Potential Primordial Interest. Comparative Experimental & Theoretical Investigations.	1
CHAPTER I	2
Mass Spectrometry & Theoretical Methods	2
1.1 THE VG ZAB 2HF MASS SPECTROMETER	3
1.2 THE GENERATION OF IONS IN THE SOURCE	5
1.2.1 Positive Ions	5
1.2.1.1 Electron Ionisation	5
1.2.2 Negative Ions.....	7
1.2.2.1 Electron or Resonance Capture	7
1.2.2.2 Negative Ion Chemical Ionisation	9
1.2.2.3 Decarboxylation and Desilylation	11
1.2.3 Radical Anions.....	12
1.2.3.1 Radical Loss From Even-Electron Anions	12
1.2.3.2 Reactions of the Oxygen Radical Anion	13
1.3 MASS SPECTROMETRY	15
1.3.1 Mass-Analysed Ion Kinetic Energy Spectrometry	15
1.3.2 Collision Induced Dissociation.....	17
1.3.3 Charge Reversal Mass Spectrometry.....	19
1.3.4 Neutralisation-Reionisation Mass Spectrometry.....	20
1.3.5 The Neutral Ion and Decomposition Difference.....	24

1.4	FRAGMENTATION BEHAVIOUR	26
1.4.1	Positive Ions	26
1.4.1.1	Homolytic Cleavage.....	26
1.4.1.2	Charge Inverted Ions	27
1.4.2	Negative Ions.....	27
1.4.2.1	Homolytic Cleavage.....	27
1.4.2.2	Ion-Neutral Complex Formation	27
1.4.2.3	Rearrangement Reactions.....	28
1.5	THEORETICAL METHODS FOR THE DETERMINATION OF MOLECULAR PROPERTIES.....	29
1.5.1	The Schrödinger Equation.....	29
1.5.2	The Hartree-Fock Approximation	30
1.5.3	The Coupled-Cluster Approximation	32
1.5.4	Density Functional Theory	33
1.5.5	Hybrid Density Functional Theory	34
1.5.6	Basis Sets.....	34
1.5.7	Calculation of Molecular Properties and Energies.....	35
CHAPTER II.....	37
	Formation of CCCN by Charge-Stripping (CCCN)⁻ in the Gas Phase	37
2.1	INTRODUCTION.....	38
2.2	RESULTS & DISCUSSION.....	41
2.2.1	(CCCN) ⁻ Isomers.....	41
2.2.2	Theoretical Studies of (C ₃ N) ⁻ Isomers and Some Decomposition Pathways.....	41
2.2.3	CID Analysis of (CCCN) ⁻ and Labelled Analogues	45
2.2.4	⁻ CR ⁺ and ⁻ NR ⁺ Analysis of (CCCN) ⁻	46
2.2.5	Theoretical Investigation of C ₃ N Cations and Neutrals.....	50
2.2.5.1	C ₃ N Cations.....	51
2.2.5.2	C ₃ N Neutrals.....	52

2.3	SUMMARY & CONCLUSIONS.....	61
2.4	EXPERIMENTAL SECTION	62
2.4.1	Mass Spectrometric Methods	62
2.4.2	Materials	63
2.4.3	Theoretical Methods	63
2.5	APPENDICES	64
2.5.1	Appendix 2(A).....	64
2.5.2	Appendix 2(B).....	65
CHAPTER III.....	66	
	Formation of CH₂CCN by Charge-Stripping CH₂⁻CCN in the Gas Phase	66
3.1	INTRODUCTION.....	67
3.2	RESULTS & DISCUSSION.....	69
3.2.1	CID Analysis of CH ₂ ⁻ CCN and Labelled Analogues.....	69
3.2.2	⁻ CR ⁺ and ⁻ NR ⁺ Analysis of CH ₂ ⁻ CCN.....	72
3.2.3	Theoretical Investigation of CH ₂ CCN	76
3.3	SUMMARY & CONCLUSIONS.....	83
3.4	EXPERIMENTAL SECTION	84
3.4.1	Mass Spectrometric Methods	84
3.4.2	Materials	85
3.4.3	Theoretical Methods	85
3.5	APPENDICES	86
3.5.1	Appendix 3(A).....	86

CHAPTER IV	87
A Theoretical Study on the Behaviour of the Energised Neutrals CCCSi & CCCP	87
4.1 INTRODUCTION.....	88
4.2 RESULTS & DISCUSSION.....	90
4.2.1 Rearrangements of Linear Singlet & Triplet CCCSi	90
4.2.2 Rearrangement of Linear Doublet CCCP	98
4.3 SUMMARY & CONCLUSIONS.....	101
4.4 THEORETICAL METHODS.....	102
4.5 APPENDICES.....	103
4.5.1 Appendix 4(A).....	103
CHAPTER V	104
The Enzymatic Oxidation of (SCN)⁻. What is the Major Product?	104
5.1 INTRODUCTION.....	105
5.2 RESULTS & DISCUSSION.....	108
5.2.1 Theoretical Results.....	108
5.2.2 Syntheses of the Anions (OSCN) ⁻ , (SCNO) ⁻ and (SNCO) ⁻	121
5.2.3 The Mass Spectra of the Isomers 1 ⁻ , 2 ⁻ and 3 ⁻	123
5.3 SUMMARY & CONCLUSIONS.....	128
5.4 EXPERIMENTAL SECTION	129
5.4.1 Mass Spectrometric Methods.....	129
5.4.2 Materials and Synthesis	129
5.4.3 Theoretical Methods.....	130

PART II	131
The Modified Finnigan LCQ Mass Spectrometer. Gas Phase Ion-Molecule Experiments	131
CHAPTER VI	132
Selectively Generated Gas Phase Carbanions + CS₂. Diagnostic Adduct Fragmentations.....	132
6.1 INTRODUCTION.....	133
6.1.1 The Smiles Rearrangement.....	133
6.1.2 The Finnigan LCQ Ion Trap Mass Spectrometer.....	135
6.1.3 Modifications of the Finnigan LCQ Ion Trap Mass Spectrometer.....	137
6.1.4 The Waters/Micromass Q-ToF 2 Mass Spectrometer	139
6.1.5 Electrospray Ionisation	141
6.2 RESULTS & DISCUSSION.....	144
6.2.1 Reaction of the Phenyl Anion with CS ₂	144
6.2.2 The Smiles Rearrangement of (PhCOS) ⁻	149
6.2.3 Reactions of the Benzyl and o-Tolyl Anions with CS ₂	154
6.2.4 Reactions of the β-Phenylethyl Anion and Other C ₈ H ₉ ⁻ Isomers with CS ₂	162
6.3 SUMMARY & CONCLUSIONS.....	173
6.4 EXPERIMENTAL SECTION	174
6.4.1 Mass Spectrometric Methods	174
6.4.2 Materials and Synthesis	174
6.4.3 Theoretical Methods	177
REFERENCES.....	178
PUBLICATIONS	203

ACKNOWLEDGEMENTS

This thesis represents a large amount of work and accordingly a great amount of time. Over the span of this time I have been privileged and in some cases honoured to have met and been associated with some great people both scientific and non scientific alike. Meeting these people, and regular associations, always inspires me, as at sometime they have left an imprint on my thoughts for the things they have either done, accomplished, or have said. I wish not to name any of these people, not for disrespect, but the fact that there are so many that I have shared so many wonderful times with and I wish not to offend anyone if I forget to incorporate them in my thanks.

I believe however the one person I would like to, and should acknowledge is my supervisor Professor John H. Bowie. I would like to thank Prof. Bowie for his time, his patience and for giving me the opportunity to attempt (and hopefully achieve) this milestone. John's commitment to science and his research group is second to none. I recall going into the lab (to pick up work) on a Boxing Day and finding John at work whilst minding his grandchildren. Over the years John and I have had some interesting conversations (and not all heated), not just work or science related but also sharing our common interest in cricket and wine. John and I are very strong willed and like minded individuals, and at times I have not been the easiest student for John to deal with. For this I apologise John and thank you again for your constant support, motivation and opportunities.

In order to get such amount of work done we are constantly reliant on our equipment, machines and chemicals to be in pristine working order and available when needed. When these things break down, when some things are hard to obtain and need to be replicated or constructed, or even alternatives are the best solutions, we are ever so reliant on our technical staff and support. I thank the number of people that I have had help me on the way to get my work done and overcome some of the technical difficulties I have faced. I have met some great people in these areas, mainly at the university, however some from abroad as well. Thank you all very much, your services are invaluable.

PREFACE

Also through the time frame of this work I have been to and seen some wonderful places both home and abroad. Along with these travels I have encountered and challenged my taste buds and culinary interests. Some of the wonderful experiences I have had include: International Conferences, Dinners, Lunches, Weddings, Birthdays, Wine Tastings, House Warmings and Scotch Tastings. Some truly wonderful experiences.

To all that have helped or participated in some way either directly, indirectly or not even associated to the writing of this thesis, I thank you all sincerely.

I would also like to thank Dr Daniel Bilusich and (soon to be Dr) Anton Calabrese for the proof reading of this work.

Finally and most importantly I would like to thank my partner and son, for they are the ones who have supported me the most throughout the time span of my studies and research. They are also the ones who had to bare my grumpiness, late nights and abrasiveness. I have learnt a lot about myself throughout the journey of my studies. More as to what I enjoy and what I find hard to do as a scientist, putting actions into words is most definitely my weakest point. I envisaged before starting, and some way into my PhD, that it would be honourable and an accomplishment to be called 'Doctor', however, now I have a family I think that being called 'Dad' has far superseded that theory.

DECLARATION

This work contains no material which has been accepted for the award of any other degree or diploma in any university or other tertiary institution to Micheal J. Maclean and, to the best of my knowledge and belief, contains no material previously published or written by another person, except where due reference has been made in the text.

I give consent to this copy of my thesis when deposited in the University Library, being made available for loan and photocopying, subject to the provisions of the Copyright Act 1968.

I also give permission for the digital version of my thesis to be made available on the web, *via* the University's digital research repository, the Library catalogue, the Australasian Digital Theses Program (ADTP) and also through web search engines, unless permission has been granted by the University to restrict access for a period of time.

Micheal (Mike) John Maclean

BSc (Hons) MRACI CChem

GradDipForsSc (DNA Tech) MAIBiol

28th November 2012

ABSTRACT

This thesis is comprised of two parts with all the work carried out centred around the use of two mass spectrometers with vastly differing capabilities and with the experimental results obtained supported or refuted with the aid of theoretical quantum chemical calculations.

For the last two decades our research group has been interested in cumulenes and hetero-cumulenes, some detected and some not as yet in their interstellar environs. The work discussed in the first part of this thesis is a continuation of some of that work and a comparison with the new work undertaken within. Our interest is predominantly orientated towards the neutral systems and their rearrangements. Our work on interstellar molecules is of interest because some of the systems investigated here and in the past, along with their precursor molecules are already known interstellar molecules and some have been implicated as possible precursors for the building blocks of life and some as possible antibiotics.

The first part of this thesis uses a combination of mass spectrometric techniques using a VG ZAB 2HF mass spectrometer (mainly charge reversal mass spectrometry) and/or theoretical quantum calculations to investigate the structures and energetics of the neutral tetra-atomic and hetero-cumulenic systems CCCN, CCCSi, CCCP, H₂CCCN, and ONCS (a possible primordial antibiotic).

The second part of this thesis involves the modification of a Finnigan LCQ ion trap mass spectrometer in order to perform gas phase ion-molecule reactions between selectively generated carbanions and carbon disulfide.

The investigation carried out in the second part of this thesis is a revisit on our earlier group research on the gas phase *ipso* (Smiles) rearrangement. It was proposed that the adducts formed between the carbanions and CS₂ undergo Smiles type rearrangements *via ipso* intermediates upon collision induced dissociation CID.

PART I

Tetra-Atomic and Hetero-Cumulenic Systems of Potential Primordial Interest. Comparative Experimental & Theoretical Investigations.

CHAPTER I

Mass Spectrometry & Theoretical Methods

1.1 THE VG ZAB 2HF MASS SPECTROMETER

The ions generated and analysed in this part of the thesis were formed in the VG ZAB 2HF* mass spectrometer (Figure 1.1) at The University of Adelaide. The sector configuration of the instrument has the magnetic sector (B) positioned before the electric sector (E) and therefore is commonly referred to as reverse sector geometry¹ [*cf.* conventional (EB) or Nier-Johnson geometry].² This configuration has the advantage of allowing the user to select an ion of choice by its mass-to-charge ratio (m/z) using the magnetic field strength to select the ion, and then to resolve the fragmentation ion masses by varying the voltage in the electric sector in a process referred to as mass analysed ion kinetic energy (MIKE)³ spectrometry, also known as MS/MS or MS² (see section 1.2.1).

* VG ZAB 2HF is an acronym for Vacuum Generators, Zero aberrations on the first and second order focussing, denoted Alpha and Beta, 2 is double sector, HF is for High Field magnet.

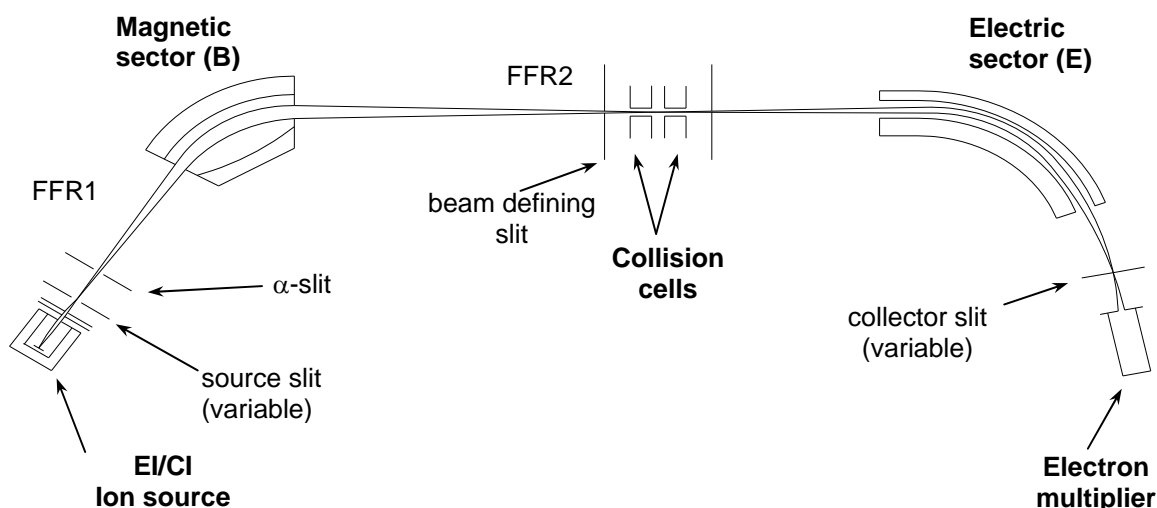


Figure 1.1 A schematic of The University of Adelaide's VG ZAB 2HF mass spectrometer (FFR denotes field free region).*

* An examiner has asked to briefly mention some of the current state-of-the-art mass spectrometric approaches for probing the connectivity of cumulenic structures and why we used the VG ZAB 2HF mass spectrometer in these studies. Firstly, supersonic molecular beam techniques, including Fourier Transform Microwave (FTM) spectroscopy and Cavity Ringdown Spectroscopy (CRDS) have also been utilised to detect carbon molecules including a wide range of bare carbon chains and nitrogen or sulphur-substituted cumulenes (see Reference 100 and references sited therein). These techniques were developed to overcome the problematic formation of unstable cumulenic compounds. Secondly, the use of the VG ZAB 2HF mass spectrometer was in order to make a fair and direct comparison of the results obtained in the first part of this thesis with those previously reported.

1.2 THE GENERATION OF IONS IN THE SOURCE

Within the ion source of the mass spectrometer, both positive and negative ions may be produced.

1.2.1 Positive Ions

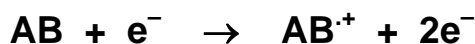
1.2.1.1 Electron Ionisation

Electron ionisation (EI) was the first method used for the formation of positive ions⁴ and is still one of the most widely used forms of generating positive ions in the mass spectrometer. Electrons are generated by heating a filament (by passing a current through it) made of tungsten wire (or rhenium ribbon) *in vacuo* in the source by a process known as thermionic emission (the amount of current controls the number of electrons emitted). The electrons are then accelerated from the hot filament to an anode by applying a small voltage of generally 70 eV*, which, by convention is used for most standard reference mass spectra[#]. This produces an electron beam that is then reduced to a narrow helical path by applying a weak magnetic field in the order of 300 Gauss - the Lorentz force constrains electrons to spiral around magnetic field lines**. When an accelerated electron (70 eV) in the beam collides with a volatilised gas phase neutral molecule (AB) it does not deposit all of its energy into the molecule. Typically, if it causes ionisation, it will then deposit only 0-6 eV of internal energy in the resulting ion.⁵ If the energy absorbed by AB is greater than its ionisation energy, then AB may become ionised by losing an electron and producing a radical cation AB^{•+} (Scheme 1.1).

* 1 eV = 23.061 kcal mol⁻¹ = 96.485 kJ mol⁻¹, a 70 eV electron has sufficient energy not only to ionise an organic molecule (requiring about 7-10 eV) but also to cause extensive fragmentation (the strongest bonds have strengths of about 5 eV).

Standard reference mass spectra are recorded with electrons accelerated to 70 eV.

** $e\mathbf{v} \times \mathbf{B}$.



Scheme 1.1

Since organic molecules, almost without exception, contain electrons in pairs in filled orbitals, ionisation of AB by removing an electron leaves behind an electron that is unpaired, *i.e.* the product is a radical cation.

Due to the chance involved in a collision between the electron and the volatilised compound, this form of ionisation has a relatively low probability of occurrence, with an estimated 1 in 1000 (0.1%) molecules being ionised.⁵

Electron ionisation is referred to as a vertical electronic transition in that when an electron has been removed from the neutral precursor, the nuclear geometry of the resulting product ion is the same as that of the nuclear geometry of the neutral precursor (as governed by the Franck-Condon principle). This principle describes the electrons as being considerably smaller and moving much more rapidly than the nucleus. Therefore, during an electronic transition, it is a satisfactory approximation to assume that the nuclei do not alter their positions or momenta while electronic redistribution occurs.^{6,7}

Due to the charge redistribution time frame, the radical cation formed in Scheme 1.1 may retain this structure or conversely it may be unstable and therefore, form any number of stable dissociation products or 'product' ions. The latter process is referred to as dissociative ionisation and both of these ionisation processes are illustrated by the Morse potential energy curves in Figure 1.2.

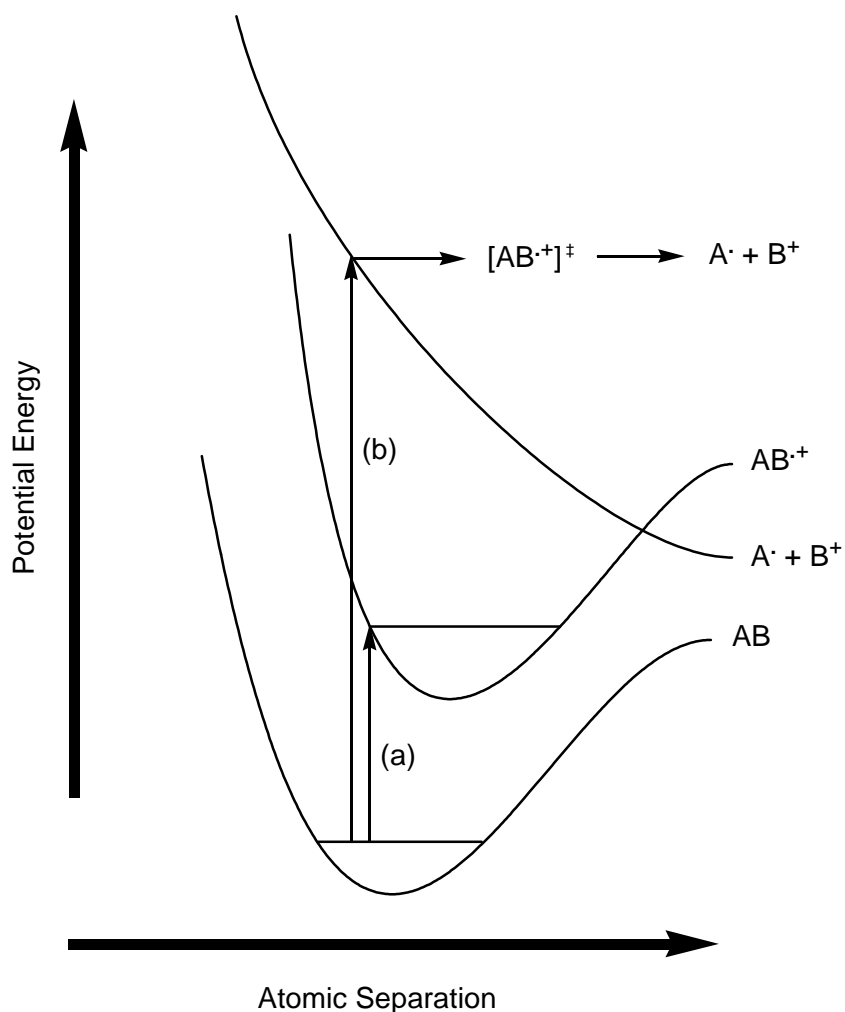


Figure 1.2 Morse potential energy curves for the diatomic neutral molecule AB. Vertical electron ionisation (EI) produces: (a) a stable (bound) radical cation $AB^{\bullet+}$, or (b) an unstable excited ion $[AB^{\bullet+}]^{\ddagger}$ that dissociates to form $A^{\bullet} + B^+$ (dissociative ionisation). The products $AB^{\bullet+}$ and AB may also have dissociation pathways.

1.2.2 Negative Ions

1.2.2.1 Electron or Resonance Capture

Under the conditions of EI, radical anions can also be generated, however the capture of an electron from the electron beam greatly relies on the electron affinity of the

investigating substrate, AB (apart from electron capture, other contributing factors include ion source conditions and the nature of the substrate). Electron capture does not occur to a significant extent (typically about 100 times less probable than electron removal)⁸ since the bombarding electrons have such high translational energies that they cannot be readily captured. This process is also referred to as resonance capture (Scheme 1.2).



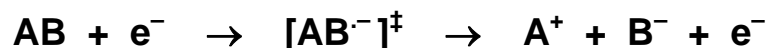
Scheme 1.2

Electron capture, like electron removal is also a vertical transition and excess energy is transferred to the product ion, which may then undergo a number of possible energy lowering processes discussed below.

Analogous to the dissociative ionisation of electron removal, discussed above, electron capture may be followed by fragmentation (Scheme 1.3) and ion-pair formation (Scheme 1.4). This sort of ionisation is referred to as dissociative electron attachment, and both processes occur *via* an excited radical anion (denoted '[‡]').



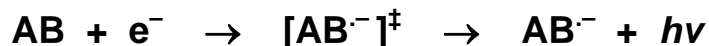
Scheme 1.3



Scheme 1.4

Ion-pair formation generally occurs at above 10-15 eV and is a relatively uncommon process.⁵ If the neutral AB has a high electron affinity and a certain number of internal degrees of freedom to help absorb the excess energy gained from the colliding electron, then electron attachment can produce a radical anion that is more likely to survive on the mass spectrometric timescale (*ca.* 10⁻⁶ seconds).⁹

The excited radical anion formed *via* electron capture may also dissipate its gained excess internal energy by radiative emission ($h\nu$) (Scheme 1.5), or *via* collisions (collisional stabilisation, Scheme 1.6) with other gas phase molecules, X.

**Scheme 1.5****Scheme 1.6**

There are three other alternative pathways for energy dissipation within the excited radical anion system. They are (i) electron ejection (Scheme 1.7), (ii) fragmentation (Scheme 1.3) and, (iii) ion-pair formation (Scheme 1.4).

**Scheme 1.7**

The probability of achieving resonance capture can be enhanced by increasing the source pressure and temperature [molecular ion lifetimes: 10^{-7} - 10^{-12} seconds at low pressures ($<10^{-4}$ Torr), and >10 μ s at *ca.* 0.1 Torr)] resulting in a greater number of interactions between the substrate molecules and the ion beam.⁵ The formation of low energy electrons (Schemes 1.4 and 1.7) promotes further electron capture increasing the abundance of radical ions.¹⁰

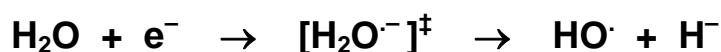
1.2.2.2 Negative Ion Chemical Ionisation

As mentioned previously, increasing the temperature and pressure (to *ca.* 0.1 Torr) within the source of the mass spectrometer promotes the probability of interactions between the substrate molecules and the electron beam. This in turn favours resonance

capture, increasing the yield of low energy electrons (Schemes 1.4 and 1.7) and promoting further electron capture that results in an increased yield of negative ions.

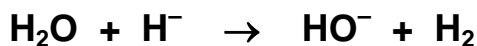
Negative ion chemical ionisation (NICI), commonly referred to as a 'soft' ionisation, is a method that utilises high pressure conditions under which ion-molecule reactions between the reagent anion and the substrate molecules are highly favoured, in turn producing closed-shell anions with low internal energies.¹¹ The partial pressure of the reagent gas is higher than that of the vaporised substrate, so initial ionisation by the electron beam involves the reagent gas with minimal initial ionisation of the sample. This increases the number of ion-molecule reactions between the reagent ion and the substrate molecules.

The methodology behind this technique involves the introduction of a small amount of the substrate molecules into the ion source with a high pressure of reagent gas. The most commonly used reagent gas is water, however, nitrous oxide, methanol and ammonia can also be used. The water undergoes dissociative resonance capture to produce a hydride anion and a hydroxyl radical (Scheme 1.8).¹¹



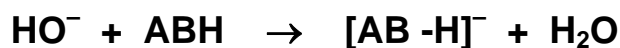
Scheme 1.8

The hydride anion readily deprotonates another water molecule producing dihydrogen and HO^- (Scheme 1.9). This reaction is facilitated by the high pressure conditions of the experiment.



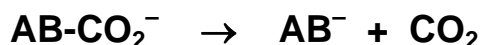
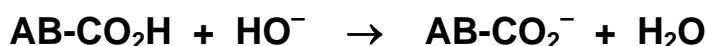
Scheme 1.9

The high concentration of hydroxide anions generated by this process deprotonate the substrate molecule ABH, to produce the closed-shell $[\text{AB}^- \text{H}]^-$ species (Scheme 1.10).

**Scheme 1.10****1.2.2.3 Decarboxylation and Desilylation**

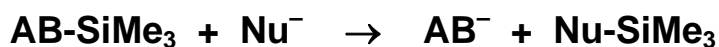
The NICI method discussed above is a good general deprotonation technique, however it is useful only if the molecule has at least one acidic proton. Problems that arise with the use of this technique are (i) if there is more than one acidic proton in the substrate then a number of isomeric anions $[\text{AB -H}]^-$ may be formed, and (ii) for molecules that bear no suitable acidic protons (*i.e.* alkenes and alkanes) deprotonation is difficult using this technique.

An alternative method developed to generate a site specific charge for molecules where deprotonation is unfavourable, involves the decarboxylation of the gas phase carboxylate anion at the location where the negative charge is required.¹² Carboxylate anions are formed subsequent to deprotonation, and decarboxylation will result for anions with sufficient internal energy (Scheme 1.11). If the carboxylate anion does not inherit sufficient internal energy from the deprotonation step, collisional activation may be required to effect decarboxylation.

**Scheme 1.11**

The most practical method for overcoming a majority of the problems encountered so far in generating a site specific AB^- anion involves an $\text{S}_{\text{N}}2$ (Si) reaction between AB-SiMe_3 and an appropriate nucleophile, typically F^- or HO^- (Scheme 1.12). At the site where the negative anion is required, a trimethylsilyl (TMS) group is attached. De Puy *et al.*¹³ first proposed the fluoride anion as the nucleophile of choice because of

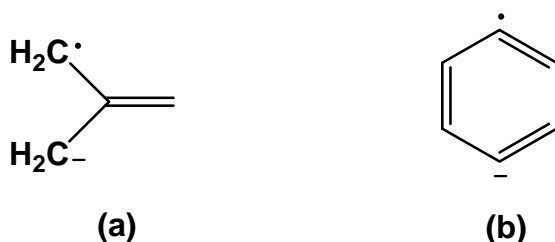
its strong affinity for silicon. It has been shown that as an alternative, hydroxide anions can also be effective gas phase displacement agents of TMS.¹⁴



Where; $\text{Nu}^- = \text{F}^-$ (generated from SF_6 or NF_3) or HO^- (from water)

Scheme 1.12

An extension of the desilylation technique is the double desilylation method, which as the name suggests is the removal of doubly substituted TMS moieties. This method can generate distonic¹⁵ radical anions (radical anions will be discussed in Section C) *i.e.* where the charge and unpaired electron reside on different atoms within the molecule. Two examples of this method are the production of the trimethylene methane [Scheme 1.13(a)]¹⁶ and *para*-benzyne [Scheme 1.13(b)]^{16, 17} anions.



Scheme 1.13

1.2.3 Radical Anions

1.2.3.1 Radical Loss From Even-Electron Anions

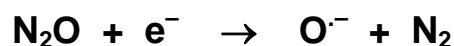
A number of even-electron closed-shell anions can undergo simple homolytic cleavage of their covalent bonds generating a radical anion and the loss of a radical/neutral. An example of this is the generation of the C_5O^- open-shell radical anion in the mass spectrometer source by the fragmentation of the *tert*-butyl radical from the even-electron precursor $^-\text{C}\equiv\text{CC}\equiv\text{CC}(\text{O})\text{C}(\text{CH}_3)_3$ (Scheme 1.14).¹⁸

**Scheme 1.14**

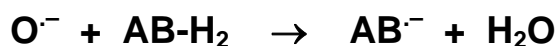
Other examples include the collision induced radical loss of an alkyl group [R]· from deprotonated benzyl ethers [PhCHOR]⁻ to give the benzaldehyde radical anion [PhCHO]⁻,¹⁹ and the generation of the radical anion [R¹CR²]⁻ and N₂ *via* dissociative electron capture of the diazo-substituted systems R¹C(N₂)R².²⁰

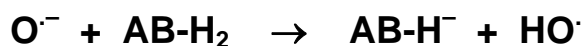
1.2.3.2 Reactions of the Oxygen Radical Anion

The oxygen radical anion is formed by the dissociative electron attachment of nitrous oxide (N₂O) in the source of the mass spectrometer (Scheme 1.15).

**Scheme 1.15**

The oxygen radical anion has been shown to be an effective chemical ionising reagent because it facilitates the formation of radical anions from reactions between organic substrates and O⁻.²¹ Dawson and Jennings²¹ first recognised the potential of the oxygen radical as an ionising reagent by the generation of a number of radical anions from organic substrate precursors. It was shown that for some organic substrates, H atom abstraction by O⁻, followed by proton abstraction by HO⁻ (Scheme 1.16) was as favourable as simple deprotonation (Scheme 1.17).

**Scheme 1.16**

**Scheme 1.17**

An example of this method for generating radical anions is that of the formation of the industrially important radical ion vinylidene from its deuterated precursor ethylene. In the reaction between $\text{O}^{\cdot-}$ and labelled ethylene ($\text{H}_2\text{C}=\text{CD}_2$), only the product radical anions $\text{H}_2\text{C}=\text{C}^{\cdot-}$ and $\text{D}_2\text{C}=\text{C}^{\cdot-}$ (by loss of D_2O and H_2O respectively) are seen and no $\text{HC}=\text{CD}^{\cdot-}$ species is observed.²² From thermodynamic data, one possible mechanism for this reaction is that $\text{O}^{\cdot-}$ removes two hydrogens from the same carbon atom where hydrogen atom abstraction precedes proton abstraction (Scheme 1.18). For example, the initial hydrogen atom abstraction from ethylene is endothermic by $< +0.5 \text{ kcal mol}^{-1}$, whereas proton abstraction is endothermic by almost $+25 \text{ kcal mol}^{-1}$.^{9, 23, 24}

**Scheme 1.18**

1.3 MASS SPECTROMETRY

1.3.1 Mass-Analysed Ion Kinetic Energy Spectrometry

Once ions have been generated in the source of the VG ZAB 2HF mass spectrometer they are accelerated through a potential difference (V) of 7 kV and collimated into a beam by use of adjustable slits. Mass selection within the magnetic sector is achieved by adjusting the magnetic field strength (B) such that only ions with a specific mass to charge ratio, m/z , are permitted to travel the circular radius (r) of the magnetic sector to the collector plate (Equation 1.1, Figure 1.3).

NOTE:
This figure/table/image has been removed
to comply with copyright regulations.
It is included in the print copy of the thesis
held by the University of Adelaide Library.

Figure 1.3 If the poles of the magnet are above and below the plane of the page, then by scanning the magnetic field (B) while r and V are fixed, only the ions with a specific m/z will follow the radial path to the collector plate.⁵

The mass selected ions then pass through the second field free region (FFR2) into the electric sector.

Scanning the electric sector from a maximum voltage (typically 7 kV for the ZAB) through to 0 V separates ions on the basis of their kinetic energies (V). When the ratio of kinetic energy (V) and electric field strength (E) equals the fixed electric sector radius (r) according to Equation 1.2, the ions now have a radial trajectory that corresponds to the fixed electric sector radius, and therefore will be transmitted through to the detector.

$$r = 2V/E$$

Equation 1.2

The spectrum obtained shows a peak that corresponds to the mass selected precursor ion and other 'product' fragmentations that may have formed from the precursor ion in the second field free region. When the precursor ion $(AB)^-$ decomposes in the second FFR2, its kinetic energy $(V_{AB})^-$ is distributed between the charged and neutral fragments (A^- and B) in the ratio of their masses. The fragment ions (A^-) now appear in the spectrum at a voltage (V_A^-) which is related to its mass (M_A^-) according to Equation 1.3.

$$M_A^-/M_{AB}^- = V_A^-/V_{AB}^-$$

Equation 1.3

As the ions generated are detected on the basis of their kinetic energy, this technique is called mass analysed ion kinetic energy (MIKE) spectrometry or MS/MS, MS^n or sometimes also referred to as MS_n , where n denotes the number of mass separations.

1.3.2 Collision Induced Dissociation

When ions are formed in the mass spectrometer they are classified as either, stable, unstable or metastable.

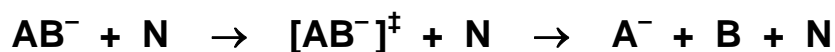
Unstable ions will decompose in the ion source and may be of no practical use unless the desired fragment ion comes from a well selected unstable precursor ion. Metastable ions are ions which decompose in the field free regions of the mass spectrometer.²⁵

Stable ions are able to be accelerated out of the ion source, and detected, after traversing the magnetic and electric sectors intact. In order to obtain any sort of relevant structural data from such ions, they must receive enough energy to effect dissociation of the ion. This transfer of energy comes from colliding the stable ion with a neutral target gas (N) in a collision cell situated in a FFR. Anions generated by the NICI method, discussed earlier, are formed with low internal energies and often do not fragment spontaneously. These ions are allowed to collide with a neutral target gas (*e.g.* argon) in a collision cell located in the FFR2 of the VG ZAB 2HF mass spectrometer allowing the ion to decompose in a process referred to as either collisional activation (CA) or collision induced dissociation (CID)[#].²⁶

Collision induced dissociation is a two-step process where firstly a collision between an energetically activated ion* and a neutral target gas (N) generally results in either vibrational or vertical electronic excitation.²⁵ This is followed by dissociation to redistribute its acquired internal energy (Scheme 1.19).

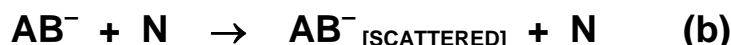
* For CID experiments performed on the VG ZAB 2HF instrument, typically 7 kV of translational energy is imparted upon the ions [(AB)⁻ or (AB)⁺]. Because of these high energies it is generally accepted that vertical electronic excitations are more favoured.²⁷

An examiner has suggested it would be justified and fair to reference Jennings, K. R. Collision-Induced Decomposition of Aromatic Molecular Ions. *Int. J. Mass Spectrom. Ion Phys.* 1968, 1, 227-235.

**Scheme 1.19**

The sensitivity of the CID experiment is dependent upon the choice of the collision gas used and the pressure it is kept at inside the collision cell.²⁸

Apart from the CID process seen above (Scheme 1.19), other competing processes such as electron detachment/neutralisation* [Scheme 1.20(a)], and/or ion scattering [Scheme 1.20(b)] may occur. In order to minimise these two processes, an inert gas such as helium or argon is used.²⁸

**Scheme 1.20**

Ideal pressure conditions for the CID experiment are where a maximum number of single collisions with the neutral target gas are favoured. This is obtained by reducing the intensity of the molecular ion beam by approximately 10 to 20% by increasing the pressure of the neutral target gas inside the collision cell. It has been estimated that with this reduction in intensity of the molecular beam, approximately 1 in every 5 of the precursor ions collide with neutral target gas molecules resulting in 90% of these undergoing single collisions, with the remainder undergoing double or multiple collisions.²⁹

* Electron detachment/neutralisation although undesirable in the CID experiment is the key process in charge reversal mass spectrometry and will be discussed in the next section (Section 1.3.3).

1.3.3 Charge Reversal Mass Spectrometry

Not all negative ions fragment under CID conditions; this can make structure elucidation in such a situation difficult. A technique was developed during the mid 1970's, where under CID type conditions, anions could be stripped of two electrons synchronously forming the corresponding cation - a technique known as charge reversal mass spectrometry *i.e.* ${}^{-}\text{CR}^{+}$ ³⁰⁻³² (*N.B.* the charge states are often included in the nomenclature for charge reversal experiments as there are a number of permutations which are discussed in the next section). The technique involves stripping the precursor negative ion (AB^{-}) of two electrons, in a single step, in a high energy collision with a neutral target gas, N [Scheme 1.21(a) and (b)] (Figure 1.4).

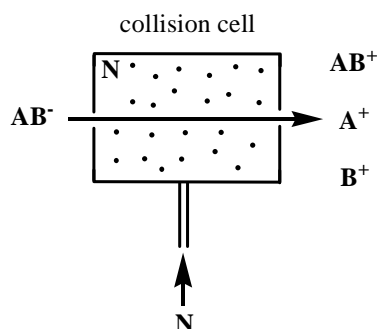
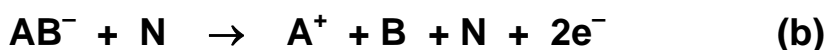


Figure 1.4 A simplified schematic diagram of a charge reversal (${}^{-}\text{CR}^{+}$) experiment. The positive ion spectrum is obtained by scanning the electric sector voltage.



Scheme 1.21

The nature of the neutral target gas, N, used for the collisions in the ${}^{-}\text{CR}^{+}$ experiment plays an important role in the fragmentations obtained. Oxygen is often used as it captures electrons well in collision events and minimises further fragmentation of the

reionised species. For this reason it is often referred to as a ‘soft’ target gas.³³ If a ‘hard’ target gas such as helium were used, extensive fragmentation of the reionised ion would result.

The energy imparted on an anion needed to induce a ${}^{-}\text{CR}^{+}$ experiment is approximately 10 eV for most polyatomic molecules, which is equivalent to the sum of the electron affinity (EA) and ionisation energy (IE) of the corresponding neutral (Equation 1.4).^{30, 34} CID processes such as this, and those mentioned earlier, occur through a vertical Franck-Condon transition, whereby the cation formed initially will have the same structure as its precursor anion.

$$\mathbf{E} = \mathbf{EA}_{(\text{AB})} + \mathbf{IE}_{(\text{AB})}$$

Equation 1.4

The resulting cations generated by the ${}^{-}\text{CR}^{+}$ experiment are also known to undergo fragmentation which can be used diagnostically in the structural characterisation of isomeric anions [Scheme 1.21(b)]. An example of this is the charge reversal spectra of the isomeric anions $\text{CH}_2=\text{C}=\text{CH}^{-}$, $\text{CH}_3\text{C}\equiv\text{C}^{-}$ and *cyc*- $\text{CH}_2\text{CH}=\text{CH}^{-}$ which are all noticeably different.³⁵ The ${}^{-}\text{CR}^{+}$ experiment has also been used to generate various positive ions which cannot be formed *via* conventional ionisation methods (*e.g.* CH_3O^{+}).³⁴

It also must be mentioned that a high energy collision between a cation and the neutral target gas may result in the observation of a negative ion signal (${}^{+}\text{CR}^{-}$).³⁶ However, this method is of limited applicability due to the low probability of the attachment of two electrons from a collisional process.

1.3.4 Neutralisation-Reionisation Mass Spectrometry

Neutrals can also be investigated with the VG ZAB 2HF mass spectrometer employed in an experiment similar to the CID and CR experiments. In the two sector reverse geometry instrument, the precursor ion can be mass selected and then neutralised in the

first of the two collision cells in the FFR2 with an appropriate neutral target gas, N. Due to the fact that a species needs to be charged in order to be detected in the mass spectrometer, the beam of neutrals are then ionised in the second collision cell. The voltage applied to the electric sector is scanned to identify any ionised species.

The methodology behind this technique,³⁷⁻⁴⁰ attributed to McLafferty *et al.*,⁴¹ involves applying a voltage perpendicular to the ion beam path, directly after the first collision cell thus deflecting away any charged ions leaving a beam of pure neutrals to enter the second collision cell (Figure 1.5). Provided that the energy of neutralisation ($E_{neutralisation}$) imparted into the anion during the collision process is greater than the electron affinity (EA) of the resulting neutral, but not more than the sum of the EA and ionisation energy (IE) of the neutral, then some of the anions in the beam will be neutralised (Equation 1.5).

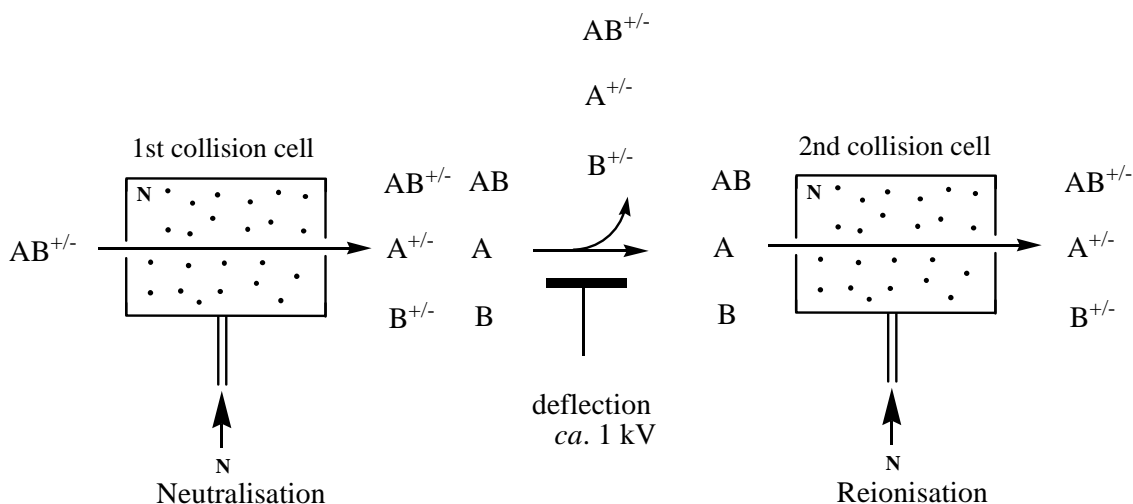


Figure 1.5 A simplified schematic diagram of the neutralisation-reionisation (NR) experiment.

$$EA_{(AB)} < E_{(neutralization)} < [EA_{(AB)} + IE_{(AB)}]$$

Equation 1.5

The reionised species, along with charged fragment particles, are detected by scanning the voltage applied to the electric sector as for an ordinary MS/MS experiment. The fragmentation pattern of a spectrum is often indicative of the bond connectivity of the neutral species. Because of this, NR experiments are a useful tool for the structure determination of elusive neutral species.⁴²

As Figure 1.5 suggests (and analogous to the CR experiment), there are a number of possible charge exchange permutations available and therefore, each experiment is given its specific nomenclature *i.e.* $\bar{\text{NR}}^+$ describes the conversion: anion \rightarrow neutral \rightarrow cation, a process that occurs *via* two sequential one electron oxidations. Other charge permutations include: $\bar{\text{NR}}^-$, $^+\text{NR}^-$, and $^+\text{NR}^+$. The $\bar{\text{NR}}^+$ and the $^+\text{NR}^+$ are the most widely used techniques because the $\bar{\text{NR}}^-$ and $^+\text{NR}^-$ experiments are more difficult due to having to induce electron attachment to a neutral during the collision process⁴³ which often results in little or no ‘recovery signal’[#].

The choice of neutral target gas for NR experiments is important for obtaining maximum intensity and appropriate ion fragmentation and this is why oxygen is used for the NR experiment as well. The use of oxygen* in both collision cells of the NR experiment is because it easily captures electrons and minimises the fragmentation and/or rearrangement of the neutralised and reionised species yielding an optimal ‘recovery signal’. It is able to do this because when it collides with a charged molecule minimal energy is deposited into the nascent neutral, limiting the amount of fragmentation and rearrangement.

Being able to demonstrate the stability or otherwise of the transient neutral is pertinent to the NR experiment. Neutral stability is recognised by obtaining a ‘recovery signal’, which implies that the neutral was stable for the time it took to traverse the distance between the two collision cells.

[#] The signal of the reionised $\text{AB}^{+/-}$. This signal is indicative for a neutral that was stable for the duration of the NR experiment (*ca.* 1 μs).

* Alternatively, vaporised metals such as mercury and sodium have also been used.³³

The distance (d) will vary depending upon the instrument used, however in most instruments the distance between the two collision cells is *ca.* 50 mm. Therefore a neutral (the velocity of the neutral is the same as the incipient ion) accelerated through a potential difference, V, (typically 7 kV) will traverse the distance between the two cells (d) in the order of microseconds ($t = 10^{-6}$ seconds) depending on its mass (m) (Equation 1.6).

$$t = \frac{d}{\sqrt{\frac{2eV}{m}}}$$

Equation 1.6

For k eV collisions, the electron transfer rate is in the order of *ca.* 10^{-15} seconds which at this timeframe can be regarded as instantaneous vertical excitement. Franck-Condon principles may apply* and so there is a geometrical resemblance between the cation initially formed in the second step of the NR experiment and its precursor neutral. Franck-Condon factors govern both steps of the NR experiment and subsequently determine the amount of internal energy of each species and the observed fragmentation patterns. These features are dependent upon the degree of structural difference between the neutral and cation. This is represented in Figure 1.6 where the ${}^+NR^+$ of AB^+ is used as an example, however this representation would be similar for any other type of charge permutation. In the first example [Figure 1.6(A)], there is a situation where AB and AB^+ are bound regards to dissociation and they both have similar geometries so there is a noticeable Franck-Condon overlap. This results in the spectrum displaying a large recovery signal and minor fragmentation peaks due to the neutral forming with minimal excess internal energy and subsequently being able to reionise to reform the cation, also with little excess internal energy.

* The Franck-Condon principle also applies to the first step in the NR experiment, the generation of the neutral from its charged precursor.

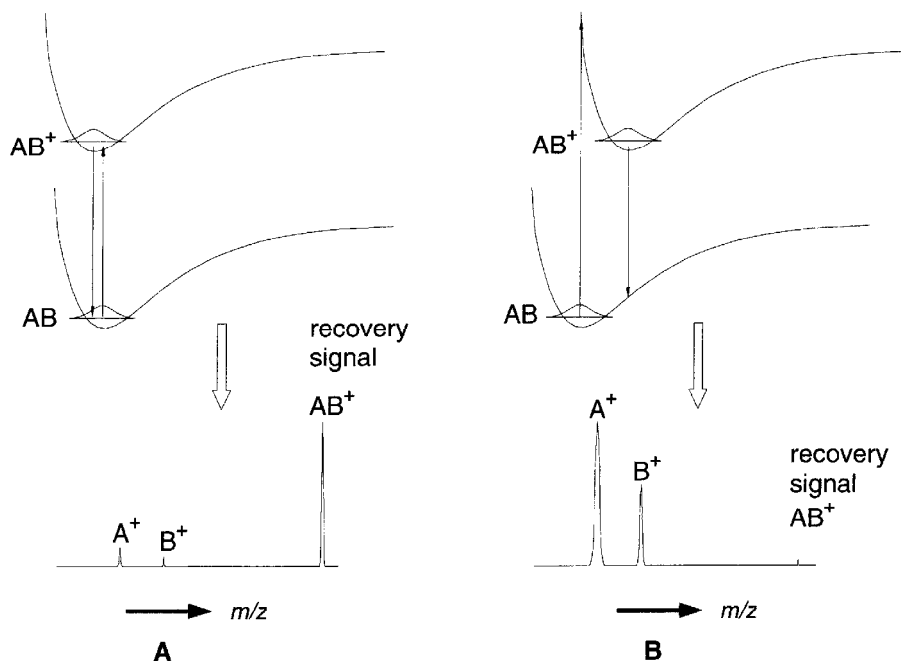


Figure 1.6 Franck-Condon diagrams representing the effects of vertical electron transitions in the ${}^+NR^+$ experiment on AB^+ where (A) the geometries of AB and AB^+ are similar (Franck-Condon principle), and (B) where geometries AB and AB^+ are different.⁴⁴

In the second situation [Figure 1.6(B)], the geometries for AB and AB^+ are different (poor Franck-Condon overlap). This poor overlap produces a cation (or neutral) with significantly more excess internal energy, and as a consequence, it is less stable. Therefore the probability of fragmentation occurring is high, resulting in a small recovery signal and large fragmentation peaks.⁴⁴

1.3.5 The Neutral Ion and Decomposition Difference

When more information is required about the neutral formed from the NR procedure, the neutral ion and decomposition difference (NIDD)⁴⁵ technique is employed. The fragment peaks in a typical ${}^-NR^+$ spectrum are a combination of both neutral and cationic processes that can be differentiated from one another by the use of NIDD analysis. The technique essentially involves the subtraction of the peaks obtained in the

$\bar{\text{CR}}^+$ experiment from the peaks obtained in the $\bar{\text{NR}}^+$ experiment, since the anion is directly converted to the cation, and the $\bar{\text{CR}}^+$ spectrum is due to cationic processes. The experimental conditions for an $\bar{\text{NR}}^+$ and $\bar{\text{CR}}^+$ spectrum should be the same to allow comparison, which is achieved by running an $\bar{\text{NR}}^+$ experiment (deflector on) followed immediately by a $\bar{\text{CR}}^+$ experiment (deflector off).

If both of the $\bar{\text{NR}}^+$ and $\bar{\text{CR}}^+$ spectra are normalised, followed by subtraction of the $\bar{\text{CR}}^+$ from the $\bar{\text{NR}}^+$ peaks (Equation 1.7), this will result in NIDD data where positive peaks represent a neutral process and negative peaks correspond to a cationic process.

$$I_i(\text{NIDD}) = \left[\frac{I_i(\text{NR})}{\sum_i I_i(\text{NR})} \right] - \left[\frac{I_i(\text{CR})}{\sum_i I_i(\text{CR})} \right]$$

Where; I_i = the Intensity of peak i

Equation 1.7

NIDD analysis is most valuable when there is a noticeable difference between the $\bar{\text{NR}}^+$ and $\bar{\text{CR}}^+$ spectra as is the case for the formate anion, HCO_2^- (Scheme 1.22).⁴⁵



Scheme 1.22

In the $\bar{\text{CR}}^+$ spectrum obtained from the formate anion, there is a large recovery signal of the precursor ion compared to the noticeably smaller recovery signal obtained in the $\bar{\text{NR}}^+$ spectrum. After NIDD analysis it can be seen that an observed $\text{CO}_2^{\cdot+}$ peak in the $\bar{\text{NR}}^+$ spectrum, generated from the loss of H, is due predominantly to a neutral process. Theoretical calculations indicate that H radical loss from neutral HCO_2 occurs with minimal activation and that the neutral decomposes upon its formation leaving the CO_2 to be reionised.

1.4 FRAGMENTATION BEHAVIOUR

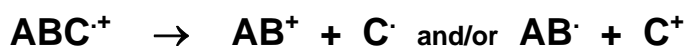
The way in which an ion fragments provides information concerning the structure of the precursor ion. The general patterns for decomposition pathways for both positive and negative ions are now known. Several are summarised below.

1.4.1 Positive Ions

The work performed on the generation of positively charged ions, and in particular their fragmentation, has been widely studied with a number of available books and reviews.^{e.g. 5, 46-48} It is not the purpose here to go into detail of the volume of work in this area, but to provide some insight into several categories of positive ion fragmentation pertinent to the work studied herein.

1.4.1.1 Homolytic Cleavage

A radical cation formed by electron ionisation (EI, discussed earlier) may undergo facile homolytic cleavage of a σ -bond (one electron oxidation) resulting in the generation of a stable cation and a neutral fragment (Scheme 1.23).



Scheme 1.23

The charge has the same probability of being distributed over either atom and theoretical mechanisms have been devised to prove it, however, the fragment that results in the more stable cation generally retains the charge and determines the ratio of the possibly formed cations AB^+ or C^+ .

The relative extent of these processes depends on kinetics and thermodynamics, and also the relative ability of the product ions to fragment further.

1.4.1.2 Charge Inverted Ions

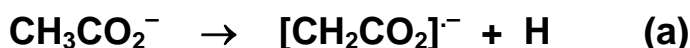
Charge inverted ions are formed *via* the CR or NR procedure. These ions have been shown to exhibit fragmentation behaviour that may be different to that of ions generated from a direct ionisation method (*e.g.* EI). An example of this is the CR spectrum of the nitrobenzene radical anion, which is remarkably different to that of the radical cation generated under EI conditions.³¹ The difference in fragmentation behaviour is attributed to the variation in internal energies of each ion formed by the different techniques.

1.4.2 Negative Ions

There are a number of categories of basic fragmentation behaviour for closed shell anions. There are reviews of negative ion fragmentations^{49, 50} and a brief summary of the major fragmentation types is given below.

1.4.2.1 Homolytic Cleavage

An example of a homolytic cleavage from an organic anion $[M-H]^-$ is the loss of a hydrogen radical. This process often generates a stabilised radical anion *e.g.* Schemes 1.24(a) and (b).

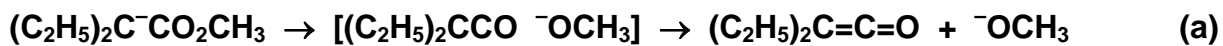


Scheme 1.24

1.4.2.2 Ion-Neutral Complex Formation

If the organic anion $[M-H]^-$ decomposes, it may yield an ion and a neutral fragment *via* charge mediated heterolytic cleavage, with the fragments either completely separating or becoming loosely bound to each other *via* hydrogen bonds or ion-induced dipole interactions [Scheme 1.25(a)].⁵¹ This ion-neutral complex may now become the

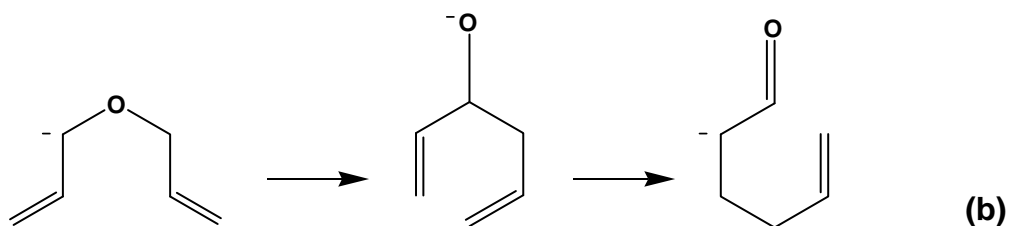
precursor to other reactions including, (i) deprotonation of the neutral by the bound anion [Scheme 1.25(b)], (ii) an S_N2 process [Scheme 1.25(c)], (iii) or hydride transfer from the anion to the neutral [Scheme 1.25(d)].



Scheme 1.25

1.4.2.3 Rearrangement Reactions

It has been demonstrated that in certain circumstances, if simple fragmentation is unfavourable, the initially formed anion $[\text{M} - \text{H}]^-$ may rearrange before undergoing a more favourable fragmentation pathway. This rearrangement reaction may be as simple as a proton transfer [Scheme 1.26(a)], or as complex as a skeletal rearrangement [Scheme 1.26(b)].¹⁹ A rearrangement reaction can be identified by comparing the spectra obtained from the rearranged species with that of the independently derived rearrangement product.



Scheme 1.26

1.5 THEORETICAL METHODS FOR THE DETERMINATION OF MOLECULAR PROPERTIES

Theoretical (or Quantum) chemistry now plays an integral part in our understanding of experimental chemistry, and it is used to fill the gaps where experimental chemistry is not possible. With the advance of computer speed, super-computing power and facilities, and the design of quantum chemistry packages with graphical user interfaces, it is now possible to make highly accurate predictions of molecular structures of interest. Other benefits include being able to investigate molecular stabilities, including any short lived intermediates or transition states, and to predict molecular energies.

Early on in its development, theoretical chemistry was used to rectify and answer pre-existing problems that arose with experimental chemistry. Nowadays it is common for theoretical chemistry to pre-empt an experimental investigation. The sometimes parallel use of theoretical and experimental techniques is used in places throughout this thesis, so a brief synopsis of the methods used is given in this chapter.

1.5.1 The Schrödinger Equation

The time independent Schrödinger equation (Equation 1.8) is a good representation of the nuclear and electronic structure of an atom or molecule and approximate solutions are derived from molecular orbital calculations.⁵²

$$\hat{H}\psi = E\psi$$

Equation 1.8

In this equation \hat{H} , represents the Hamiltonian operator, a differential operator depicting the total energy (both kinetic and potential) of the system, and ‘ ψ ’ represents the wave function, a mathematical function requiring the information of the spatial and spin coordinates of the electrons and the coordinates of the nuclei. The square of the wave function, ψ^2 (or $|\psi|^2$ if ψ is complex), describes the probability of finding an electron at a

given point in space. The electronic energy of the system, E , is the energy relative to a state in which its nuclei and electrons are infinitely separated and at rest.

The Schrödinger equation can be solved exactly for a simple hydrogen molecule, however as the systems become more complex, exact solutions are not possible and are only solvable by adopting the Born-Oppenheimer approximation.⁵³ Within this approximation the electronic and nuclear movements are considered separately, which is a reasonable assumption because the nuclei are many times more massive than the electrons. Thus the nuclei will move much more slowly relative to the electrons and therefore may be considered stationary, eliminating nuclear-nuclear repulsion.

Once the energy of a given molecular geometry is determined, the variation in energy with the variation in geometry can be established and a potential surface can be calculated. Such a surface can exhibit a number of local minima, each of which represents an equilibrium structure of the molecule. Other stationary points on the potential surface occur where there are one or more orthogonal directions where the energy is at a maximum, these points are termed first order saddle points. First order saddle points (transition states) along with local and global minima allow insight into the chemical behaviour of a molecular system.

The Schrödinger equation is still extremely complex for all but the simplest molecular systems and a number of theories have been developed to calculate an approximate solution by applying various mathematical assumptions in order to simplify the calculation and make it applicable for a more diverse range of molecular systems.

1.5.2 The Hartree-Fock Approximation

The most commonly used technique for approximating a wave function for a system is the Hartree-Fock (HF) approximation,^{54, 55} sometimes referred to as the Self Consistent Field (SCF) method. The HF method involves the conversion of the Schrödinger equation into a set of HF equations which describe the approximate electronic wave-function (ψ) as a product of molecular orbitals (ϕ) which in turn can be estimated as a linear combination of one-electron functions (χ) also referred to as basis functions (a

complete set of basis functions for all the electrons of a system is called the basis set) (Equation 1.9). Basis functions are centered on nuclei and hence approximate atomic orbitals.

$$\phi_I = \sum c_{ik} \chi_k$$

Equation 1.9

The molecular orbital expansion coefficients, (c_{ik}) are optimised using the SCF method which involves calculating the electronic energy for each electron separately and thus determining the interactions between particles. Using the smallest possible basis set will incorporate all the electrons of a system, however increasing the size of the basis set will improve the description of the molecular orbitals.

The method involves selecting a single electron, then the spherical potential in which it moves (assumed to be a spherical average of the potential due to all other electrons) is calculated by ‘discarding’ the distribution of all the other electrons, treating them as the source of the potential. A new orbital is then obtained for that electron by solving the Schrödinger equation. Each electron in the system is then individually selected and the process repeated, once again using the electrons in the ‘discarded’ orbitals as the source of the potential. Once a full cycle is completed, a full set of orbitals for all electrons in the system is obtained, which will generally differ from the original set. This overall process is repeated, creating more and more accurate wave functions. Once a repetition of this process leads to (effectively) no change in the orbitals, the system is considered ‘self-consistent’ and the calculation ceases.

A limitation to the HF-SCF method is that inaccuracies arise because the HF method treats electrons as individual particles and does not consider the interaction between electrons, therefore neglects the relative motion of the electron due to this interaction. Realistically electrons move in order to avoid contact, this is the so-called ‘dynamic electron correlation effect’. Omitting this correlation will lead to an error in calculated energy values of approximately one percent and in a majority of cases reasonable geometries can be obtained using this theory. There have been a number of post HF

methods that take into account the electron correlation effects but the level of accuracy in the calculation of the electron correlation problem is determined by available computational resources.

1.5.3 The Coupled-Cluster Approximation

The Coupled-Cluster (CC) approximation^{56, 57} is one of the most accurate approaches for incorporating the electron correlation effects. This is achieved by incorporating an exponential operator, e^T with the HF wave-function (Equation 1.10) resulting in a more accurate representation of the true electronic wave-function.

$$\Psi_{CC} = e^T \Psi_{HF}$$

Equation 1.10

The wave-function Ψ_{CC} is a function of all possible excitations of electrons covering occupied to unoccupied molecular orbitals. The incorporation of these excited states allows the electrons to keep away from one another thereby providing electron correlation. The cluster operator (T) is the sum of one electron (T_1) up to N-electron (T_N) excitation operators, where N represents the number of electrons in the system. It is not practicable to do calculations considering all possible excitations of electrons from occupied orbitals to unoccupied orbitals for all but small systems, so a number of predefined approximations can be used. The CC approximation incorporating only double excitations has been designated CCD (Coupled-Cluster Doubles - derived from the inclusion of T_2), allowing it to be distinguished from more general versions of the theory which include singles and doubles (CCSD - derived from T_1 and T_2), or the very computationally expensive singles, doubles and triples (CCSDT - derived from T_1 , T_2 and T_3). The extreme computational complexity of the CCSDT method has led to the development of several approximate forms of this level of theory, for example CCSD(T), where the contribution of triple excitations has been simplified.⁵⁸

1.5.4 Density Functional Theory

The Density Functional Theory (DFT) is a different approach for calculating molecular properties in which it attempts to calculate the electron probability density (ρ) rather than calculating the wave-function (ψ). The DFT is best utilised when the system under investigation contains five or more atoms and modest accuracy is acceptable.⁵⁹ The theory behind this method was developed by Hohenberg and Kohn⁶⁰ where they determined that the ground state molecular energy, wave-function and any other molecular properties may in principle be described as functionals of the electron probability density, ρ . Further studies into this work by Kohn and Sham⁶¹ which lead to the Kohn-Sham approximation, separates the electronic energy into a number of individual parameters (Equation 1.11).

$$E = E^T + E^V + E^J + E^{XC}$$

Equation 1.11

In this equation the total electronic energy of the system, E , is separated into terms determined by the charge density (E^T represents the kinetic energy that arises from the motion of the electrons, E^V represents the potential energy of the nuclear-electron interactions and E^J represents the electron-electron repulsions) and the exchange-correlation energy E^{XC} , which accounts for additional electron-electron interactions. For molecular systems, the Kohn-Sham approximation leads to a molecular orbital picture analogous to the HF approximation.

The starting point of most DFT methods is the Local Density Approximation (LDA). However, the LDA in itself is usually inadequate in describing most molecular systems so to compensate, Becke⁶² and Perdew⁶³ introduced gradient corrections to the LDA for the exchange and correlation energy, forming the corrected LDA-BP functional. The LDA-BP functional is defined by the pairings of exchange and correlation, similarly, the substitution of the Perdew correlation function with that of Lee, Yang and Parr,⁶⁴ forms the popular BLYP method. DFT calculations incorporate electron correction with no significant additional computational cost compared to an HF calculation.

1.5.5 Hybrid Density Functional Theory

Electron exchange is more accurately described by the HF-SCF method, rather than DFT methods leading to a further modification of the technique. The result, introduced by Becke,⁶⁵ is a hybrid density functional theory (DFT-HF), where both DFT and HF methods are combined. This is a way to obtain consistently reliable computational results using modest computational resources and time. The B3LYP method (the most popular DFT-HF method for delivering accurate results for a large range of molecular systems) involves the combination of LDA, HF, BP, and LYP functionals.

Hybrid density functional theory has become widely used for the study of a wide range of molecular systems, largely due to their computationally inexpensive nature and proven accuracy, which is coupled with an inherent consideration of electron correlation effects.

1.5.6 Basis Sets

A basis set (a set of one-electron basis functions) is a mathematical description of the orbitals within a system. The basis set therefore, when applied to a level of theory (*e.g.* HF), defines that level of theory by restricting the region electrons may occupy in a molecule or atom to confined regions in space close to the nucleus. One way in which a basis set may be modified to increase the accuracy of a calculation is by increasing the number of basis functions per atom *e.g.* the split valence sets of 3-21G and 6-31G (one of the simplest split-valence basis sets) allow for two sizes of basis function per valence orbital, and is named double zeta. An example of the application of a double zeta basis set on both H and C atoms is seen in Scheme 1.27, where orbitals that are primed differ in size to those that are not.

H: 1s, 1s'

C: 1s, 2s, 2s', 2p_x, 2p_y, 2p_z, 2p_x', 2p_y', 2p_z'

Scheme 1.27

Similarly, a triple split valence set (triple zeta), such as 6-311G, will use three different sizes of basis function for each valence orbital.

Where split valence basis sets allow an orbital to change size, polarised basis sets allow orbitals to change shape. This is done *via* the addition of orbitals with angular momentum greater than that required for their ground state (to the description of each atom). A widely used example of this is given by the notation 6-31G* [or 6-31G(d)], where the '*' [or (d)] is indicative of the addition of *d*-type functions to the heavy atoms.

For systems where the electrons are likely to be located relatively far from the nucleus, such as molecules with lone pairs or significant negative charge, the addition of diffuse functions is often required. Diffuse functions are essentially larger *s*- and *p*-type functions, allowing orbitals to once again occupy larger regions in space in an attempt to better represent the electronic wave-function. Diffuse functions are designated with either a '+' symbol or the prefix 'aug' (augmented), for example the correlation consistent (cc) double-zeta Dunning's basis set aug-cc-pVDZ.

1.5.7 Calculation of Molecular Properties and Energies

The approach used within this work to determine the physical and geometrical properties of the investigated compounds was to calculate the molecular geometries at a modest level of theory, then to subsequently calculate a single point energy at a higher level of theory.

Firstly, the geometry optimisation of the compounds investigated needed to be carried out using a modest level of theory, so the hybrid density functional theory of B3LYP was used in conjunction with the 6-31+G(d) basis set (unless otherwise stated). This combination has the advantage of accurately being able to predict molecular geometries at low computational costs, and has allowed the calculation of vibrational frequencies of over 100 molecules with an average experimental variant of $< 50 \text{ cm}^{-1}$.⁶⁶ The geometries presented in this thesis were optimised using the B3LYP level of theory with

the 6-31+G(d) basis set within the Gaussian 03⁶⁷ suite of programs, unless otherwise stated.*

Finally, the more accurate representation of the single point energy is calculated at the higher level of theory, CCSD(T) with the aug-cc-pVDZ basis set. The reasoning for this application is that many of the compounds studied in this work are anionic. The need to incorporate diffuse functions in the basis set for a more sophisticated approach at electron correlation is a requirement for the accurate prediction of energies of anions. The energies presented in this thesis were optimised using the CCSD(T) level of theory with the aug-cc-pVDZ basis set within the Gaussian 03⁶⁷ suite of programs, unless otherwise stated.

Throughout this work theoretical calculation parameters are designated like so:

CCSD(T)/aug-cc-pVDZ//B3LYP/6-31+G(d)

which reads from left to right;

ENERGY level of theory/ENERGY basis set//GEOMETRY level of theory/GEOMETRY basis set

* *An examiner has asked why the B3LYP hybrid density functional was selected (from the many now available) for the structural calculations. Apart from the reasoning given above, and the fact that it is a cost effective method in terms of accuracy, the purpose was in order to make a fair comparison of the results obtained in the first part of this thesis with those previously reported, therefore using the same level of theory. Other hybrid functionals that could have been used, which incorporate more long range interaction or kinetic factors include; X3LYP, O3LYP, MO6, MO6L, and MO62X.*

CHAPTER II

Formation of CCCN by Charge-Stripping (CCCN)⁻ in the Gas Phase

2.1 INTRODUCTION

The neutral cumulene CCCN (cyanoethynyl radical) was first tentatively detected in the molecular envelope of the carbon rich star IRC +10216 in April 1976 whilst obtaining a millimetre wave spectrum of the star.⁶⁸ From the detection of two emission doublets, one centred at 89055 MHz and the other at 98949 MHz, it was concluded, by using theoretical predictions of its microwave spectrum, that the radical was a linear molecule with a $^2\Sigma$ electronic ground state.^{68, 69} The identification of this radical was confirmed by the subsequent discovery of the isoelectronic radical C₄H in the same carbon star (C₄H has a very similar pattern of millimetre wavelength lines but a significantly different rotational constant).⁶⁹

In 1980 the detection of the neutral C₃N radical was seen at the centres of the Taurus molecular (dark) cloudlets TMC-1 and TMC-2.⁷⁰ From this detection it was reported that the interstellar ratio of C₃N/HC₃N at these centres was similar to that observed at IRC +10216.⁷⁰ From the ratio data it was proposed that two mechanisms for the formation of C₃N and HC₃N were possible. For the first mechanism, more applicable to the carbon star IRC +10216, it was proposed that the molecules are formed in the atmosphere of the star, then expelled into the circumstellar envelope with constant relative abundance, the ‘freeze out’ model.⁷¹ The second mechanism involved *in situ* ion-molecule reactions like C₂H₂ + H₂CN⁺ → H_nC₃N⁺, followed by dissociative recombination of H_nC₃N⁺, yielding HC₃N and C₃N.^{70, 72, 73}

Since its initial detection, other molecular environs where C₃N has been detected include the gas condensations of Heiles’ Cloud 2 (HCL2),⁷⁴ the dark nebula that surrounds TMC-1 (this is the strongest observed emission outside of TMC-1), and the gravitational lens* system B0218+357.⁷⁵

* A gravitational lens is formed when light from a distant bright source is ‘bent’ around a massive object, such as a cluster of galaxies, and can both magnify and distort the apparent image of the background source.

The mechanism for the interstellar formation of C₃N (from HCCCN) has undergone a number of theoretical investigations to possibly help support its detection. It was proposed that an ion-molecule reaction between CN and C₂H₂⁺, both interstellar molecules, may produce only the linear species HCCCN⁺ and CCCNH⁺ in cool interstellar regions.⁷⁶ It was also proposed that dissociative recombination of HC₃N⁺ could lead to C₃N with a possibility of the two isomers, CCCN and CCNC forming.⁷⁶ A reaction between neutral CN and neutral C₂H₂ has also been suggested as a possible source of interstellar HCCCN,⁷⁷ as has the reaction between dinitrogen and C₃H₂⁺.⁷⁸

The linear isomer CCNC, derived from the known interstellar precursor isocyanoacetylene (HCCNC), has been studied by quantum mechanical calculations in order to obtain estimates of its rotation constants.⁷⁹ It was suggested that because of the detection of HCCCN and CCCN in the molecular envelope of IRC +10216, it was possible that the isocyanoacetylene molecule (HC≡C-N≡C), and the corresponding isocyanoethynyl radical, (C≡C-N≡C) may also be present.⁷⁹ Although the isocyanoethynyl radical (C≡C-N≡C) has not, to date, been detected in interstellar environs, its precursor HCCNC however is an interstellar molecule detected in the molecular envelope of IRC +10216⁸⁰ and in the Taurus molecular cloud TMC-1.⁸¹

The first experimental production of the linear C₃N radical came from a direct current (DC) discharge through a flowing mixture of low pressure cyanoacetylene and N₂.⁸² The resulting spectral data confirmed the astronomical detection of CCCN at IRC +10216 and in the Taurus molecular cloud TMC-1.⁸²

It has been shown that the neutrals CCCC, CCCO and CCCS can be formed by charge-stripping of (CCCC)⁻, (CCCO)⁻ and (CCCS)⁻ in a collision cell of a mass spectrometer.^{83, 84} These neutrals have all been detected in interstellar dust clouds.⁸⁵ Energised CCCC undergoes scrambling of the atoms *via* a planar rhombic intermediate⁸³ while energised CCCO and CCCS decompose by losses of CO and CS respectively without scrambling of the carbon backbone.⁸⁴

We have now extended this study to investigate the interstellar molecule CCCN with a view to determine whether when energised, it undergoes C scrambling (like CCCC)

and/or rearranges to the less stable isomer CCNC. In this context, it has already been reported that the energised neutral NCCCN undergoes atom scrambling.⁸⁶

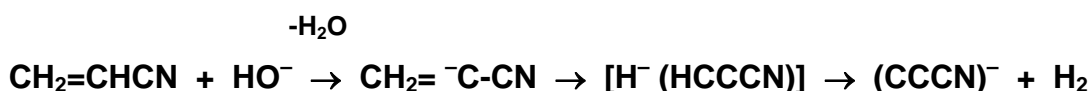
This chapter describes the gas phase formation of neutral CCCN and some of its ¹³C labelled analogues from anionic precursors using the neutralisation-reionisation (NR⁺) procedure,^{*e.g.* see 45, 87} with the aim of investigating the behaviour of energised CCCN. The experimental results are complemented by theoretical calculations. The formation of unlabelled CCCN from a cation precursor has been reported by Schwarz.⁸⁸

2.2 RESULTS & DISCUSSION

2.2.1 (CCCN)⁻ Isomers

The aim of this project was to form the gas phase molecule CCCN and some of its ¹³C labelled analogues from negative ions of known bond connectivity, with the purpose of investigating the behaviour of the energised neutral CCCN. Unlabelled acrylonitrile was selected as the precursor for (CCCN)⁻, mainly because the labelled analogues ¹³CH₂=CHCN and CH₂=CH¹³CN are commercially available.

The ¹³C labelled acrylonitriles will readily form (¹³CCCN)⁻ and (CC¹³CN)⁻ by analogous processes to that forming (CCCN)⁻ shown in Scheme 2.1. The deprotonation site shown in Scheme 2.1 was confirmed by the CID reaction between CH₂=CDCN and HO⁻ which gave exclusively CH₂=⁻CCN [Appendix 2(A)].



Scheme 2.1

Once the three anions (CCCN)⁻, (¹³CCCN)⁻ and (CC¹³CN)⁻ had been generated in the source of the VG ZAB 2HF mass spectrometer, it was necessary to determine that they did not rearrange under the experimental conditions necessary to charge strip them to the neutrals CCCN, ¹³CCCN and CC¹³CN. To do this, it was necessary to determine (i) the structures and relative energies of the (C₃N)⁻ isomers, (ii) the energies for the dissociations of (C₃N)⁻ isomers, and (iii) the collision induced spectra of (CCCN)⁻ and its ¹³C labelled analogues.

2.2.2 Theoretical Studies of (C₃N)⁻ Isomers and Some Decomposition Pathways

There are only three stable singlet anionic (C₃N)⁻ isomers at the CCSD(T)/aug-cc-pVDZ//B3LYP/6-31+G(d) level of theory used for this investigation (Table 2.1). There

are two stable linear isomers, (CCCN)⁻ (¹A) and (CCNC)⁻ (¹C) and a single stable cyclic isomer (¹B) (Table 2.1). The rearrangement of ¹A through ¹B to ¹C is energetically unlikely due to ¹B being +63.3 kcal mol⁻¹ more endothermic than ¹A. The rearrangement through triplet (CCCN)⁻ (³A) was not considered because the ground state triplet (³A) is +83.7 kcal mol⁻¹ more energetic than the ground state singlet (¹A) (Table 2.2).

The energies for the dissociation of C from the isomers (CCCN)⁻ and (CCNC)⁻ are shown in Scheme 2.2 [CCSD(T)/aug-cc-pVDZ//B3LYP/6-31+G(d) level of theory].



Scheme 2.2

From the C dissociation data (Scheme 2.2), if (CC¹³CN)⁻ rearranges to decomposing (CCN¹³C)⁻, loss of ¹³C will be more facile than loss of ¹²C.

TABLE 2.1

The Structures and Energies of the (C₃N)⁻ Isomeric Singlet Anions.

Level of theory used - CCSD(T)/aug-cc-pVDZ//B3LYP/6-31+G(d)

Relative energies in kcal mol⁻¹ relative to ¹A (0 kcal mol⁻¹)

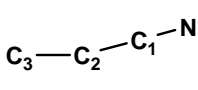
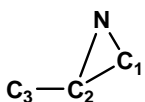
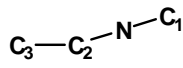
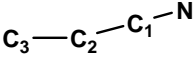
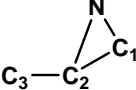
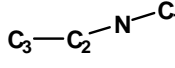
			
	¹ A	¹ B	¹ C
State	¹ A	¹ A'	¹ A'
Symmetry	C ₁	C _s	C _s
Energy (Hartrees)	-168.57243	-168.47161	-168.52221
Energy Relative to ¹A	0	+63.3	+31.5
Dipole Moment (Debye)	2.65	3.49	3.13
Bond Lengths (Å)			
NC ₁	1.180	1.245	1.186
C ₁ C ₂	1.365	1.619	-
C ₂ C ₃	1.256	1.266	1.322
NC ₂	-	1.489	1.255
Bond Angles (°)			
NC ₁ C ₂	180.0	61.0	-
C ₁ C ₂ C ₃	180.0	151.6	-
C ₁ C ₂ N	-	47.0	-
C ₂ NC ₁	-	72.0	180.0
C ₃ C ₂ N	-	161.4	180.0
Dihedral Angle (°)			
NC ₁ C ₂ C ₃	167.3	180.0	-
C ₁ NC ₂ C ₃	-	-	180.0

TABLE 2.2

The Structures and Energies of the (C₃N)⁻ Isomeric Triplet Anions.

Level of theory used - CCSD(T)/aug-cc-pVDZ//B3LYP/6-31+G(d)

Relative energies in kcal mol⁻¹ relative to ³A and ¹A (0 kcal mol⁻¹)

			
	³ A	³ B	³ C
State	³ A	³ A''	³ A'
Symmetry	C ₁	C _s	C _s
Energy (Hartrees)	-168.43901	-168.39722	-168.40585
Energy Relative to ³A	0	+26.2	+20.8
Energy Relative to ¹A	+83.7	+109.9	+104.5
Dipole Moment (Debye)	1.38	2.47	2.47
Bond Lengths (Å)			
NC ₁	1.264	1.357	1.197
C ₁ C ₂	1.358	1.447	-
C ₂ C ₃	1.302	1.395	1.371
NC ₂	-	1.377	1.352
Bond Angles (°)			
NC ₁ C ₂	137.9	58.7	-
C ₁ C ₂ C ₃	166.9	158.3	-
C ₁ C ₂ N	-	57.4	-
C ₂ NC ₁	-	63.9	167.7
C ₃ C ₂ N	-	57.4	130.0
Dihedral Angle (°)			
NC ₁ C ₂ C ₃	-179.7	180.0	-
C ₁ NC ₂ C ₃	-	-	180.0

2.2.3 CID Analysis of (CCCN)⁻ and Labelled Analogues

The CID mass spectrum of (CCCN)⁻ (Figure 2.1) shows the precursor anion (m/z 50) as the base peak (recovery signal). The only fragment anions $\geq 0.5\%$ of the base peak are those formed by losses of C [(0.8%) to m/z 38] and N [(0.5%) to m/z 36] from the precursor anion (CCCN)⁻. There are two other fragments in the CID spectrum that are $\leq 0.5\%$ of the base peak. These are formed by losses of C₂, 24amu (m/z 26) and CN, 26amu (m/z 24) from the precursor anion.

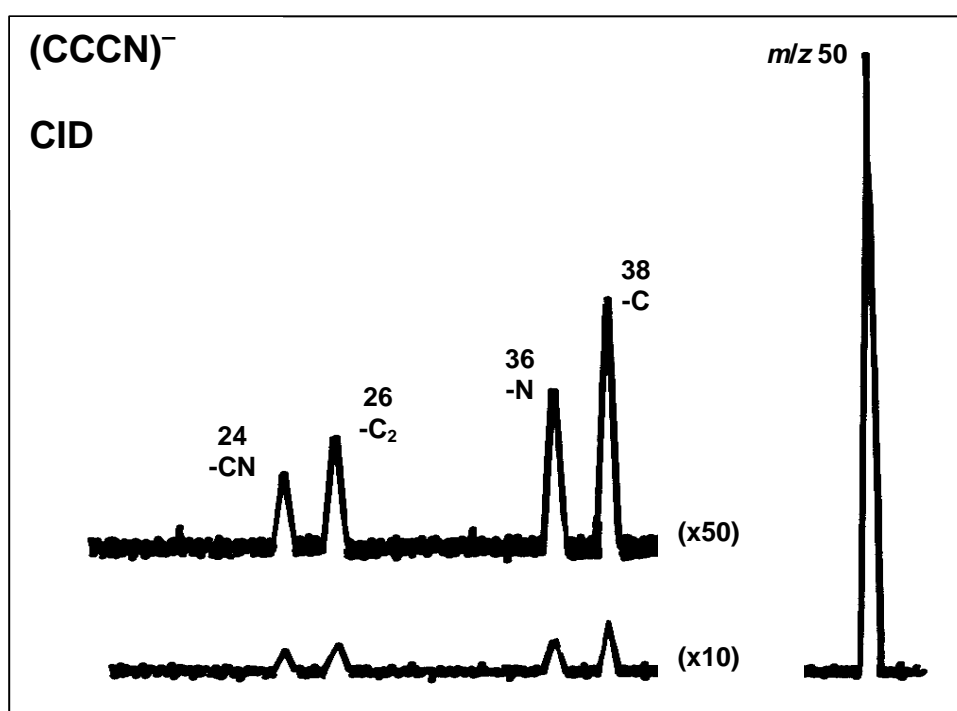


Figure 2.1 CID spectrum of (CCCN)⁻. VG ZAB 2HF mass spectrometer.
For experimental details see Experimental section.

The corresponding fragment ions in the CID spectrum of (CC¹³CN)⁻ (Figure 2.2) are m/z 39[1.0% (-¹²C)], m/z 38[0.05% (-¹³C)] and m/z 37[0.7% (-N)]. Minor fragment ions in the CID spectrum include, m/z 27 (-C₂), 26 (-¹²C¹³C), 25 (-CN) and 24 (-¹³CN). Minor peaks at m/z 38 (loss of ¹³C), 26 (loss of ¹²C¹³C) and 25 (loss of CN) infer that some energised (CC¹³CN)⁻ has rearranged. However, the loss ratio ¹²C:¹³C

(20:1) means that C rearrangement and/or scrambling of (CC¹³CN)⁻ to (CCN¹³C)⁻ and (C¹³CNC)⁻ is at best minimal.

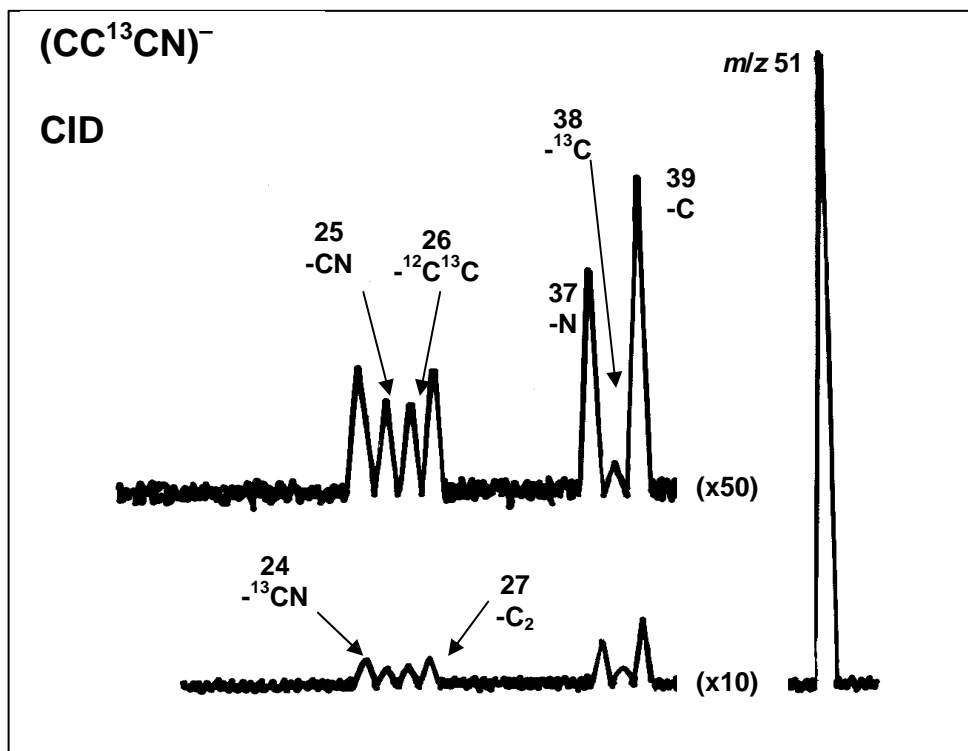


Figure 2.2 CID spectrum of (CC¹³CN)⁻. VG ZAB 2HF mass spectrometer.
For experimental details see Experimental section.

The collision induced dissociation data for the three anions (CCCN)⁻, (¹³CCCN)⁻ and (CC¹³CN)⁻ together with the theoretical data (2.2.2) indicate that (CCCN)⁻ is formed as shown in Scheme 2.1, and has the appropriate bond connectivity for the formation of CCCN since there is only minor rearrangement of (CCCN)⁻ under the conditions necessary to charge strip (CCCN)⁻ to CCCN.

2.2.4 ⁻CR⁺ and ⁻NR⁺ Analysis of (CCCN)⁻

The charge reversal spectrum, ⁻CR⁺ [synchronous two electron stripping of (CCCN)⁻ to (CCCN)⁺]⁸⁹ and neutralisation-reionisation, ⁻NR⁺ [sequential two electron stripping of

(CCCN)⁻ to CCCN to (CCCN)⁺]^{45, 87} spectra of (CCCN)⁻ are shown in Figures 2.3(a) and 2.3(b) respectively. Both spectra show the precursor ion (CCCN)⁺ as the base peak (recovery signal) with fragment cations corresponding to the losses of C (*m/z* 38), N (*m/z* 36), C₂ (*m/z* 26) and CN (*m/z* 24). There is also a peak corresponding to the radical cation C⁺ (*m/z* 12).

The peak in the ⁻NR⁺ spectrum formed by loss of C (*m/z* 38) is more intense than the corresponding peak in the ⁻CR⁺ spectrum. From the difference in the peak intensities we can suggest that whatever the structure(s) of the neutral(s) C₃N formed during the charge stripping of (CCCN)⁻, the neutral(s) are losing more C than the corresponding positive ion(s) (C₃N)⁺. The loss of C from the neutral(s) needs to be investigated theoretically to determine whether the energised neutral C₃N radicals are undergoing any carbon rearrangement prior to or during the loss of C.

The ⁻CR⁺ and ⁻NR⁺ spectra of (¹³CCCN)⁻ are shown in Figure 2.4(a) and (b) respectively. The data for the ⁻CR⁺ and ⁻NR⁺ spectra of (CC¹³CN)⁻ are listed in Table 2.3.

All of the ¹³C labelled spectra (⁻CR⁺ and ⁻NR⁺) confirm that there is significant carbon scrambling within each system. For example, in both spectra of (¹³CCCN)⁻, there is a large peak at *m/z* 39 indicative of the loss of ¹²C, and in both (CC¹³CN)⁻ spectra we see a minor peak at *m/z* 38 representing the loss of ¹³C.

The ⁻NR⁺ spectra of (¹³CCCN)⁻ and (CC¹³CN)⁻ show more loss of ¹²C and ¹³C respectively than their ⁻CR⁺ counterparts, confirming that some of the labelled neutral species ¹³CCCN are decomposing by loss of ¹²C and similarly some CC¹³CN neutrals are decomposing by loss of ¹³C. The ratios for the loss of ¹²C vs ¹³C are as follows: 62:38 (⁻CR⁺) and 66:34 (⁻NR⁺) from ¹³CCCN, and 76:24 (⁻CR⁺) and 73:27 (⁻NR⁺) from the CC¹³CN cation/neutral.

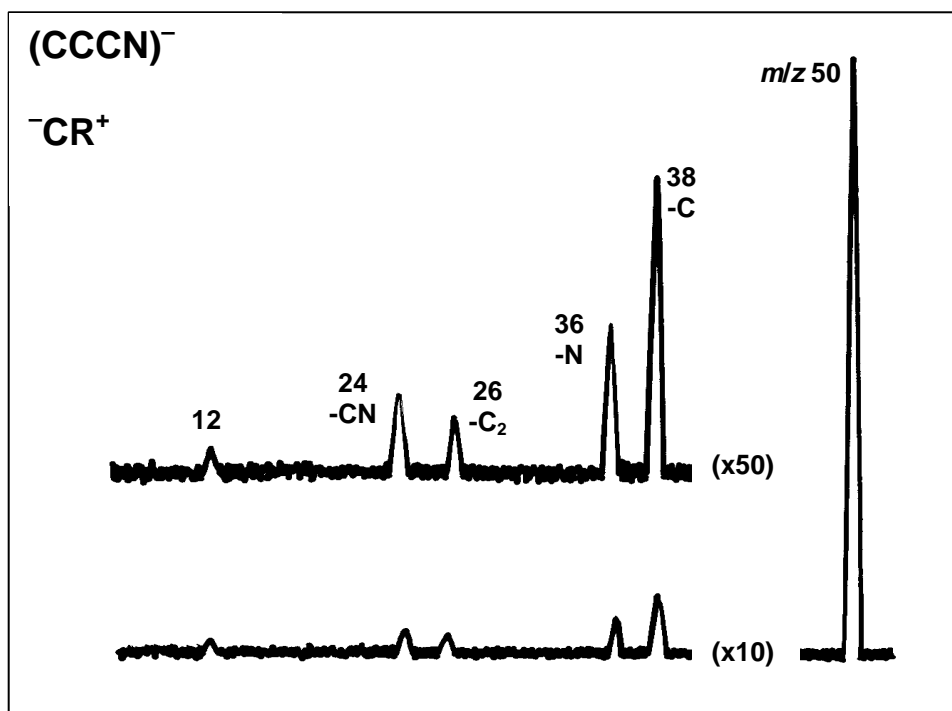


Figure 2.3(a) ⁻CR⁺ spectrum of (CCCN)⁻. VG ZAB 2HF mass spectrometer.
 For experimental details see Experimental section.

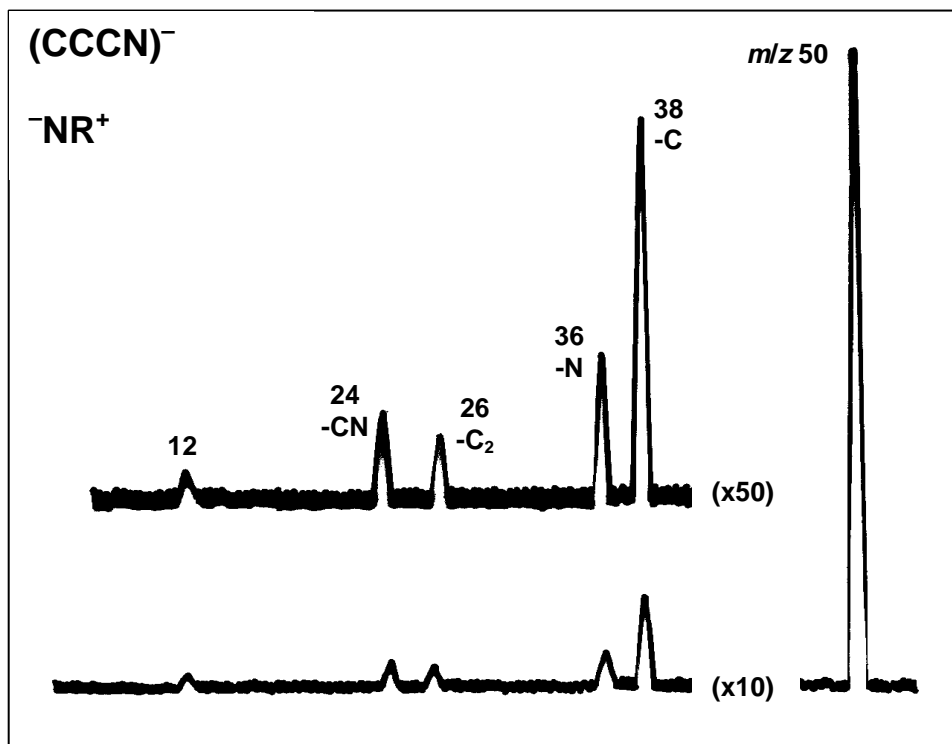


Figure 2.3(b) ⁻NR⁺ spectrum of (CCCN)⁻. VG ZAB 2HF mass spectrometer.
 For experimental details see Experimental section.

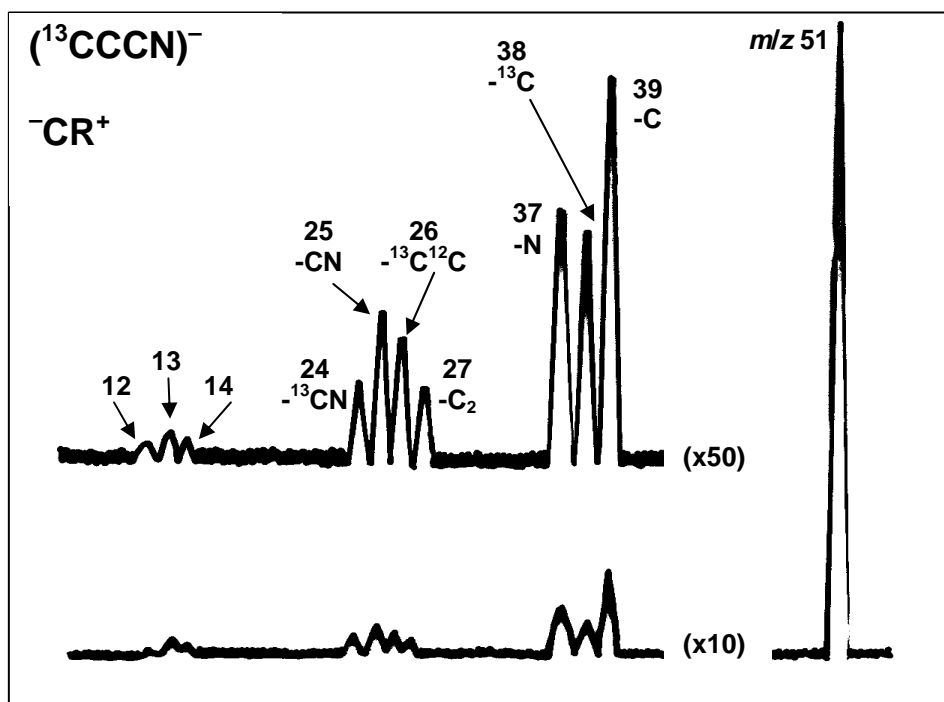


Figure 2.4(a) $^- \text{CR}^+$ spectrum of $(^{13}\text{CCCN})^-$. VG ZAB 2HF mass spectrometer. For experimental details see Experimental section.

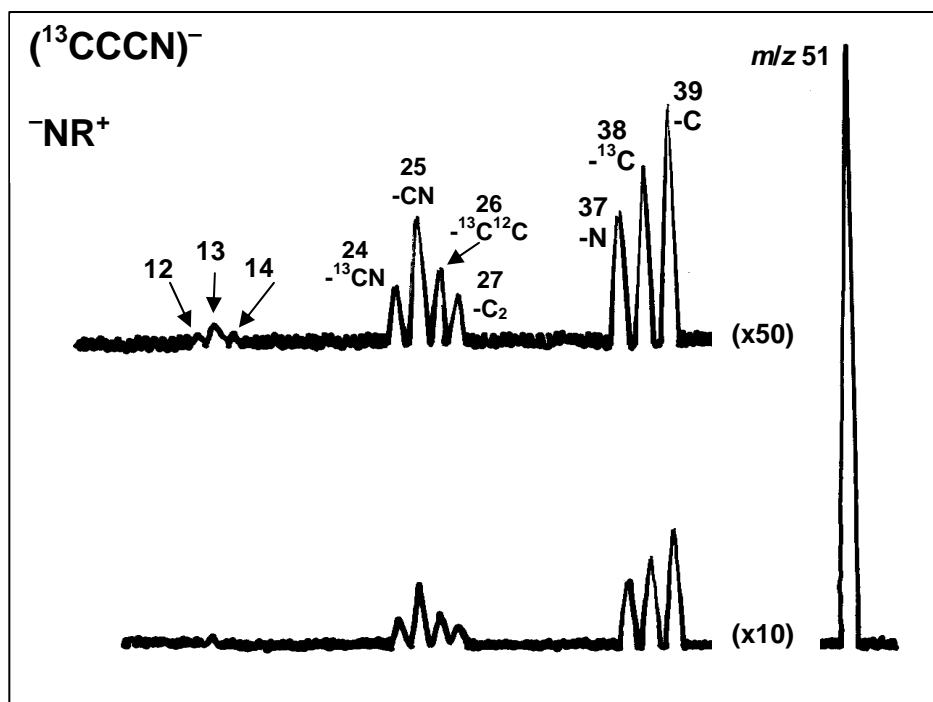


Figure 2.4(b) $^- \text{NR}^+$ spectrum of $(^{13}\text{CCCN})^-$. VG ZAB 2HF mass spectrometer. For experimental details see Experimental section.

TABLE 2.3

⁻CR⁺ and ⁻NR⁺ Spectra of (CC¹³CN)⁻.[*m/z* (relative abundance in %)]

⁻CR⁺	51(100); 39(25.0); 38(7.7); 37(15.5); 27(4.8); 26(2.25); 25(4.9); 24(6.4); 13(0.5); 12(0.8).
⁻NR⁺	51(100); 39(26.5); 38(9.7); 37(10.5); 27(3.6); 26(2.25); 25(5.0); 24(5.0); 13(0.5); 12(0.9).

Other ion fragmentation ratios indicative of carbon scrambling in both labelled systems are the formation of ¹²C¹²C⁺ vs ¹²C¹³C⁺ and ¹²CN⁺ vs ¹³CN⁺.

The ratios for the formation of ¹²C¹²C⁺ vs ¹²C¹³C⁺ are as follows: 21:79 (⁻CR⁺) and 30:70 (⁻NR⁺) for the (¹³CCCN)⁻ analogue and 57:43 (⁻CR⁺) and 50:50 (⁻NR⁺) for CC¹³CN. The ratios for the formation of ¹²CN⁺ vs ¹³CN⁺ are as follows: 80:20 (⁻CR⁺) and 74:26 (⁻NR⁺) for (¹³CCCN)⁻, and 32:68 (⁻CR⁺) and 38:62 (⁻NR⁺) for the (CC¹³CN)⁻ analogue. The small but reproducibly different ratios observed in the ⁻CR⁺ and ⁻NR⁺ spectra indicate that carbon scrambling processes are occurring for both neutral and cationic C₃N, however, there is notably more scrambling observed in each of the ⁻NR⁺ spectras.

In conclusion, the experimental data indicate that carbon scrambling is occurring for both the energised neutral and its positive ion counterpart, but the data do not allow the precise determination of how much scrambling is occurring for the neutral.

2.2.5 Theoretical Investigation of C₃N Cations and Neutrals

The aim of this theoretical investigation was to determine the rearrangement mechanism of energised CCCN and (CCCN)⁺.

2.2.5.1 C₃N Cations

With respect to cationic interconversion of (CCCN)⁺ to (CCNC)⁺ it is important to consider the theoretical results of Ding *et al.*⁹⁰ The reaction coordinate pathway is shown in Figure 2.5 for the ground state triplet interconversion.

The energy difference between (CCCN)⁺ and the less stable isonitrile isomer (CCNC)⁺ is +12 kcal mol⁻¹ at the CCSD(T)/6-311G(d) level of theory, and there are two possible reaction coordinate pathways for the interconversion. The first pathway goes through the rhombic intermediate D, and the second *via* the three membered ring intermediate E. The barriers for these rearrangements are +43 and +45 kcal mol⁻¹ respectively at this level of theory.

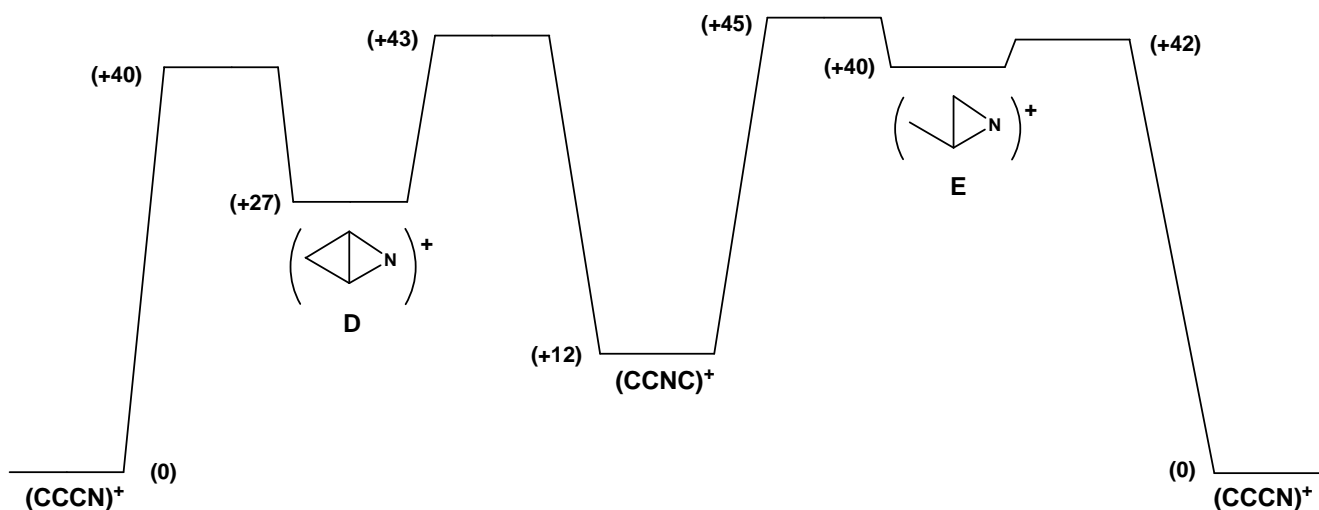
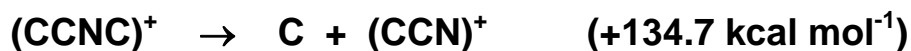
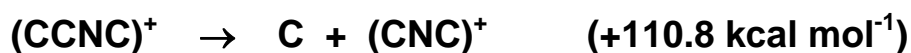
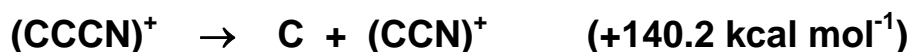


Figure 2.5 Reaction coordinate pathways for the conversion of ground state triplet (CCCN)⁺ to triplet (CCNC)⁺. Taken from Ding *et al.*⁹⁰ Relative energies in kcal mol⁻¹. Level of theory used - CCSD(T)/6-311G(d) with zero-point vibrational energy correction.

In addition, losses of C from the isomers (CCCN)⁺ and (CCNC)⁺ require the energies shown in Scheme 2.3 [CCSD(T)/aug-cc-pVDZ//B3LYP/6-31+G(d) level of theory].



Scheme 2.3

2.2.5.2 C₃N Neutrals

Both the neutrals CCCN and CCNC have bent structures at the level of theory used in this investigation, however previous calculations have reported that CCCN is linear.⁹¹⁻⁹⁹ The calculated structure of CCCN (bent or linear) is dependent upon the level of theory and the basis set used. There has been a report on the rotational spectrum of CCCN indicating that the data best fit 'a nearly pure $^2\Sigma$ (linear) electronic ground state'.¹⁰⁰

Reaction coordinate pathways have been investigated for (i) the bent CCCN system at the CCSD(T)/aug-cc-pVDZ//B3LYP/6-31+G(d) level of theory [for comparison with previous studies on CCCC,⁸³ CCCO⁸⁴ and CCCS⁸⁴ see Appendix 2(B)], and (ii) linear CCCN at the B3LYP/6-311G(d)¹⁰¹ level of theory.

The reaction coordinate pathway for the interconversion of bent CCCN to CCNC is shown in Figure 2.6, with full details of minima and transition states recorded in Tables 2.4 and 2.5 respectively. The reaction coordinate pathway for the interconversion of linear CCCN to CCNC is shown in Figure 2.7, with full details of minima and transition states recorded in Tables 2.6 and 2.7.

The reaction coordinate pathways shown in Figures 2.6 and 2.7 are similar.

After repeating some calculations reported previously, namely (i) CCCN is confirmed as linear at the MP2/6-311G(d,p) level of theory,¹⁰¹ but (ii) at the B3LYP/6-311G(d) level of theory there are two minima, a stable linear structure (as reported⁹⁷), and a bent

structure (C_3C_2 , 1.263 Å; C_2C_1 , 1.353 Å; C_1N , 1.167 Å; $C_1C_2C_3$, 162.1°; C_2C_1N , 178.5°; dihedral angle 180°). The bent structure is the more stable by 6.5 kcal mol⁻¹ [B3LYP/6-311G(d) level of theory] and 6.9 kcal mol⁻¹ [CCSD(T)aug-cc-pVDZ//B3LYP/6-311G(d) level of theory]. CCCN is also bent (there is no stable linear form) at the B3LYP/6-311+G(d) level of theory (C_3C_2 , 1.266 Å; C_2C_1 , 1.352 Å; C_1N , 1.168 Å; $C_1C_2C_3$, 162.9°; C_2C_1N , 178.4°; dihedral angle 180°).

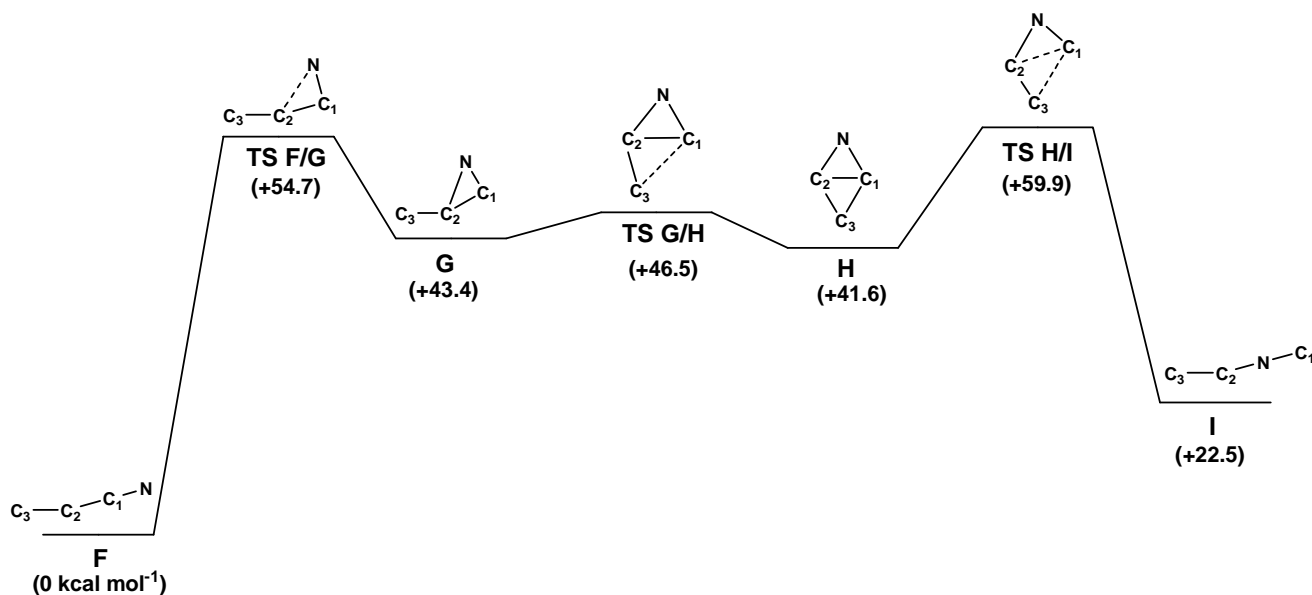


Figure 2.6 Reaction coordinate pathway for the interconversion of bent CCCN (F) to CCNC (I). Relative energies in kcal mol⁻¹. Level of theory used - CCSD(T)/aug-cc-pVDZ//B3LYP/6-31+G(d). Structures shown in the Figure show bond connectivities only. For full structural details see Tables 2.4 and 2.5.

TABLE 2.4

Reaction Coordinate Pathway for the Interconversion of Bent CCCN to CCNC. The Structures and Energies of the Isomeric Doublet Neutral Minima.

Level of theory used - CCSD(T)/aug-cc-pVDZ//B3LYP/6-31+G(d)

Relative energies in kcal mol⁻¹ relative to F (0 kcal mol⁻¹)

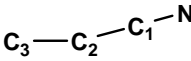
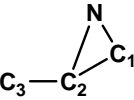
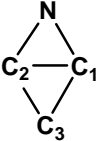
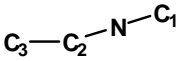
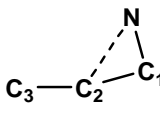
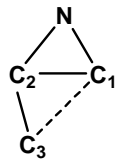
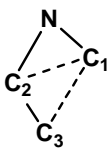
				
	F	G	H	I
State	² A	² A''	² A''	² A'
Symmetry	C ₁	C _s	C _s	C _s
Energy (Hartrees)	-168.41367	-168.34450	-168.34732	-168.37778
Energy Relative to F	0	+43.4	+41.6	+22.5
Dipole Moment (Debye)	0.83	1.02	1.02	0.77
Bond Lengths (Å)				
NC ₁	1.177	1.279	1.379	1.198
C ₁ C ₂	1.355	1.551	1.495	-
C ₂ C ₃	1.278	1.318	1.458	1.285
NC ₂	-	1.390	1.379	1.293
C ₁ C ₃	-	-	1.457	-
Bond Angles (°)				
NC ₁ C ₂	178.5	57.9	57.2	-
C ₁ C ₂ C ₃	163.6	148.6	59.1	-
C ₁ C ₂ N	-	51.2	57.2	-
C ₂ NC ₁	-	70.9	65.6	178.2
C ₃ C ₂ N	-	160.2	116.3	165.2
C ₁ C ₃ C ₂	-	-	61.7	-
C ₂ C ₁ C ₃	-	-	59.2	-
NC ₁ C ₃	-	-	116.3	-
Dihedral Angle (°)				
NC ₁ C ₂ C ₃	-179.8	180.0	180.0	-
C ₁ NC ₂ C ₃	-	-	-	180.0
NC ₂ C ₁ C ₃	-	-	180.0	-

TABLE 2.5

Reaction Coordinate Pathway for the Interconversion of Bent CCCN to CCNC. The Structures and Energies of the Doublet Neutral Transition States.

Level of theory used - CCSD(T)/aug-cc-pVDZ//B3LYP/6-31+G(d)

Relative energies in kcal mol⁻¹ relative to F (0 kcal mol⁻¹)

			
	TS F/G	TS G/H	TS H/I
State	² A	² A''	² A'
Symmetry	C ₁	C _s	C _s
Energy (Hartrees)	-168.32649	-168.33957	-168.31821
Energy Relative to F	+54.7	+46.5	+59.9
Dipole Moment (Debye)	1.62	1.03	0.80
Bond Lengths (Å)			
NC ₁	1.219	1.316	1.240
C ₁ C ₂	1.458	1.576	1.811
C ₂ C ₃	1.296	1.338	1.300
NC ₂	1.725	1.377	1.534
C ₁ C ₃	-	1.942	1.820
Bond Angles (°)			
NC ₁ C ₂	79.7	56.0	56.7
C ₁ C ₂ C ₃	167.5	83.1	69.4
C ₁ C ₂ N	44.0	52.4	42.5
C ₂ NC ₁	56.2	71.6	80.8
C ₃ C ₂ N	130.7	135.5	112.0
C ₁ C ₃ C ₂	-	53.7	68.7
C ₂ C ₁ C ₃	-	43.2	41.8
NC ₁ C ₃	-	99.2	98.6
Dihedral Angle (°)			
NC ₁ C ₂ C ₃	-70.8	180.0	180.0
C ₁ NC ₂ C ₃	164.4	-	-
NC ₂ C ₁ C ₃	-	180.0	180.0

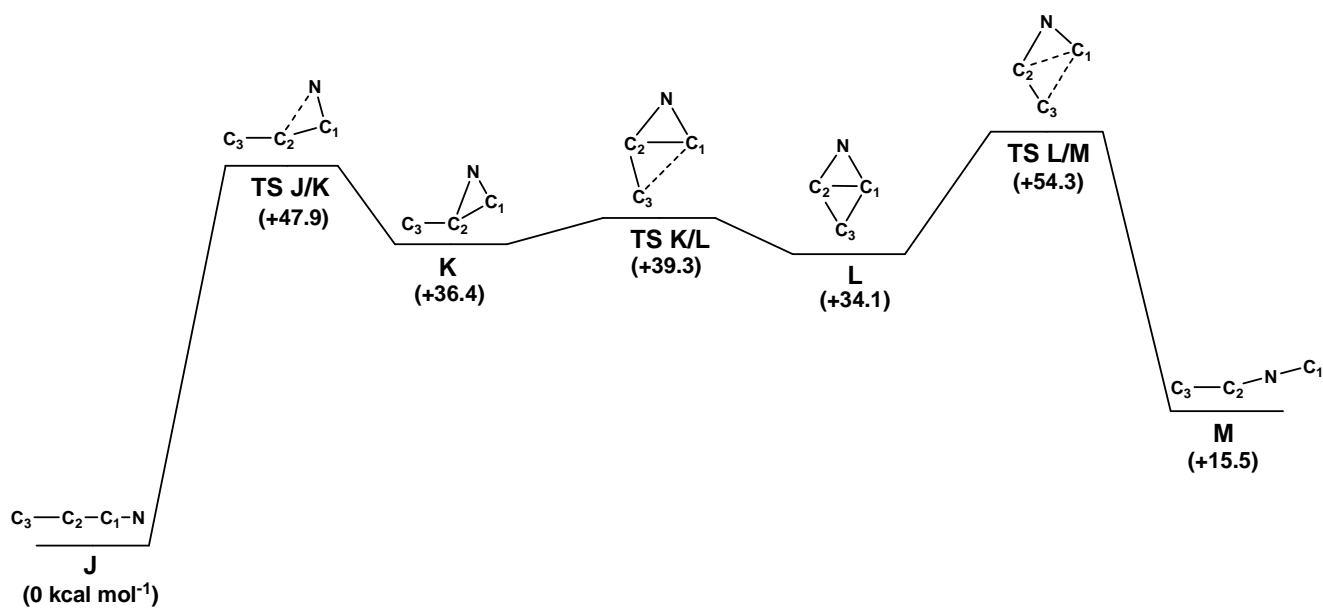


Figure 2.7 Reaction coordinate pathway for the interconversion of linear CCCN (J) to CCNC (M). Level of theory used - CCSD(T)-aug-cc-pVDZ//B3LYP/6-311G(d). Relative energies in kcal mol⁻¹. Structures show bond connectivities only. For full structural details see Tables 2.6 and 2.7.

TABLE 2.6

Reaction Coordinate Pathway for the Interconversion of Linear CCCN to CCNC. The Structures and Energies of the Isomeric Doublet Neutral Minima.

Level of theory used - CCSD(T)/aug-cc-pVDZ//B3LYP/6-311G(d)

Relative energies in kcal mol⁻¹ relative to J (0 kcal mol⁻¹)

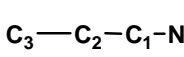
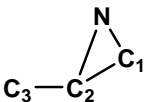
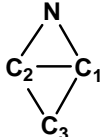
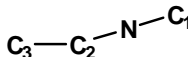
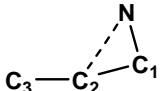
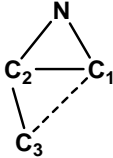
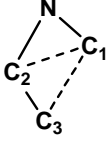
				
	J	K	L	M
State	-	² A''	² A''	² A'
Symmetry	C _{∞v}	C _s	C _s	C _s
Energy (Hartrees)	-168.40188	-168.34382	-168.34685	-168.37717
Energy Relative to J	0	+36.4	+34.1	+15.5
Dipole Moment (Debye)	0.34	1.11	1.03	0.68
Bond Lengths (Å)				
NC ₁	1.173	1.271	1.377	1.192
C ₁ C ₂	1.341	1.564	1.490	-
C ₂ C ₃	1.291	1.311	1.456	1.273
NC ₂	-	1.385	1.377	1.292
C ₁ C ₃	-	-	1.456	-
Bond Angles (°)				
NC ₁ C ₂	180.0	57.4	57.2	-
C ₁ C ₂ C ₃	180.0	145.4	59.2	-
C ₁ C ₂ N	-	50.6	57.3	-
C ₂ NC ₁	-	72.0	65.5	177.4
C ₃ C ₂ N	-	163.9	116.5	163.9
C ₁ C ₃ C ₂	-	-	61.5	-
C ₂ C ₁ C ₃	-	-	59.2	-
NC ₁ C ₃	-	-	116.5	-
Dihedral Angle (°)				
NC ₁ C ₂ C ₃	0.0	180.0	180.0	-
C ₁ NC ₂ C ₃	-	-	-	180.0
NC ₂ C ₁ C ₃	-	-	180.0	-

TABLE 2.7

Reaction Coordinate Pathway for the Interconversion of Linear CCCN to CCNC. The Structures and Energies of the Doublet Neutral Transition States.

Level of theory used - CCSD(T)/aug-cc-pVDZ//B3LYP/6-311G(d)

Relative energies in kcal mol⁻¹ relative to J (0 kcal mol⁻¹)

			
	TS J/K	TS K/L	TS L/M
State	² A	² A''	² A'
Symmetry	C ₁	C _s	C _s
Energy (Hartrees)	-168.32547	-168.33919	-168.31537
Energy Relative to J	+47.9	+39.3	+54.3
Dipole Moment (Debye)	1.51	1.04	0.75
Bond Lengths (Å)			
NC ₁	1.212	1.313	1.231
C ₁ C ₂	1.463	1.570	1.819
C ₂ C ₃	1.288	1.337	1.293
NC ₂	1.718	1.378	1.548
C ₁ C ₃	-	1.908	1.814
Bond Angles (°)			
NC ₁ C ₂	79.3	56.3	57.2
C ₁ C ₂ C ₃	166.4	81.6	68.9
C ₁ C ₂ N	43.9	52.4	41.9
C ₂ NC ₁	56.8	71.3	80.9
C ₃ C ₂ N	129.9	134.0	110.9
C ₁ C ₃ C ₂	-	54.5	69.4
C ₂ C ₁ C ₃	-	43.9	41.7
NC ₁ C ₃	-	100.2	98.9
Dihedral Angle (°)			
NC ₁ C ₂ C ₃	68.7	180.0	180.0
C ₁ NC ₂ C ₃	-163.4	-	-
NC ₂ C ₁ C ₃	-	180.0	180.0

The rearrangement pathway shown in Figure 2.6 is different from that of the cation depicted in Figure 2.5 in that there is only one interconversion pathway found for the neutrals. The rearrangement pathway for CCCN (Figure 2.6) shows some similarity to that of CCCC.⁸³ Both rearrangements proceed *via* ‘rhombic’ intermediates (see H, Figure 2.6). The largest difference between the two systems is predominantly energetic *i.e.* C randomisation *via* the triplet ground state of CCCC has a calculated barrier of only +28.6 kcal mol⁻¹,⁸³ whereas the maximum barrier shown in Figure 2.6 is +59.9 kcal mol⁻¹.

If carbon scrambling in CCCN is a consequence of direct isomerisation to CCNC then for the labelled neutrals there should be mixtures of ¹³CCCN and ¹³CCNC (from ¹³CCCN) and CC¹³CN and CCN¹³C (from CC¹³CN). No combination of either pair of these decomposing isomer pairs can account for the experimental loss ratios ¹²C:¹³C from ¹³CCCN and from CC¹³CN which are approaching the theoretical ratio of 67:33 for complete randomisation of carbon.

The calculated energies for the losses of C from the two isomers CCCN and CCNC are shown in Scheme 2.4 (calculations at the CCSD(T)/aug-cc-pVDZ//B3LYP/6-31+G(d) level of theory). Experimental values are not known for all species shown in Scheme 2.4, so we are unable to compare computational and experimentally derived values. Losses of C from either end of CCNC are more energetically favourable than loss of C from CCCN.



Scheme 2.4

The Franck-Condon energy [the difference in energy between ground state CCCN and that structure (of CCCN) with the same geometry as (CCCN)⁻] is calculated to be only

1 kcal mol⁻¹ at the CCSD(T)/aug-cc-pVDZ//B3LYP/6-31+G(d) level of theory. The energy required to affect any of the various dissociation processes (Scheme 2.4) is significantly more than the Franck-Condon energy of this vertical process, and this excess energy presumably originates, at least in part, from subsequent collisions of the first formed neutral in the collision cell.

2.3 SUMMARY & CONCLUSIONS

In conclusion, although we are not in a position to determine precisely how much carbon scrambling occurs through individual neutral and cationic CCCN in the NR^+ system, the combined scrambling through both is approaching statistical for loss of C. The most likely scenario for the carbon randomisation of neutral CCCN involves equilibration with, and random cleavage of bonds in the planar ‘rhombohedral’ intermediate (H) (Figure 2.6) to yield mixtures of CCCN and CCNC in which the carbons will be (ultimately) statistically randomised. Losses of carbon from these neutrals are most likely to occur by the decomposition pathways shown in Scheme 2.4. Carbon randomisation of the initially formed cation (CCCN)⁺ may also occur through the equilibrating and planar ‘rhombohedral’ intermediate (D) shown in Figure 2.5.

2.4 EXPERIMENTAL SECTION

2.4.1 Mass Spectrometric Methods

Experiments were performed using a two-sector modified VG ZAB 2HF mass spectrometer with BE configuration, where B and E represents the magnetic and electric sectors, respectively (discussed in Chapter 1). The precursor anion (CCCN)⁻ was formed in the chemical ionisation source by reaction of CH₂=CHCN with HO⁻ (from H₂O) to form CH₂=⁻CCN which then decomposes through intermediate [H⁻ (HCCCN)] to yield (CCCN)⁻ and H₂. Similar reactions of HO⁻ with ¹³CH₂=CHCN and CH₂=CH¹³CN yield (¹³CCCN)⁻ and (CC¹³CN)⁻ respectively, while the reaction of DO⁻ (from D₂O) with CH₂=CDCN gave CH₂=⁻CCN exclusively, which decomposes to (CCCN)⁻. Source conditions were as follows: source temperature 100°C, repeller voltage -0.5 V, ion extraction voltage 7 kV, mass resolution m/Δm ≥ 1500. Acrylonitrile (or labelled acrylonitrile as required) is added through the septum inlet (unheated) to give a pressure of 10⁻⁵ Torr measured in the source housing. Water (or D₂O) is then introduced through the septum inlet (unheated) to give a constant pressure of 10⁻⁴ Torr in the source housing. The estimated pressure in the ion source is 10⁻¹ Torr.⁸³ Collision Induced Dissociation (CID) spectra were determined using the magnetic sector to select the precursor anion, and utilising argon as the collision gas in the first collision cell following the magnetic sector. The pressure of argon in the first cell was maintained such that 80% of the precursor ion beam was transmitted through the cell. This corresponds to an average of 1.1-1.2 collisions per ion.²⁹ Product anion peaks resulting from CID processes were recorded by scanning the voltage applied to the electric sector.

Neutralisation-reionisation (⁻NR⁺)^{45, 87} spectra were performed for mass selected anions utilising the dual collision cells located between the magnetic and electric sectors. Neutralisation of anions was effected by collisional electron detachment using O₂ at 80% transmission (of the ion beam) as collision gas in the first collision cell, while reionisation to cations was achieved by collision of neutrals with O₂ (80% transmission) in the second collision cell. To detect a reionisation signal due to the precursor neutral, the neutral species must be stable for the one microsecond time frame of this

experiment. Charge Reversal ($\bar{\text{C}}\text{R}^+$) spectra⁸⁹ were recorded using single collision conditions in collision cell 1 (O₂, 80% transmission of main beam). Comparison of $\bar{\text{C}}\text{R}^+$ and $\bar{\text{N}}\text{R}^+$ data for a given precursor anion provides information concerning the neutral formed from the precursor anion: see¹⁰² for a full description of this procedure.

2.4.2 Materials

The neutral precursors CH₂=CHCN, CH₂=CDCN (d₁ > 99%), ¹³CH₂=CHCN and CH₂=CH¹³CN (¹³C > 99%) were all commercially available, and were used without further purification.

2.4.3 Theoretical Methods

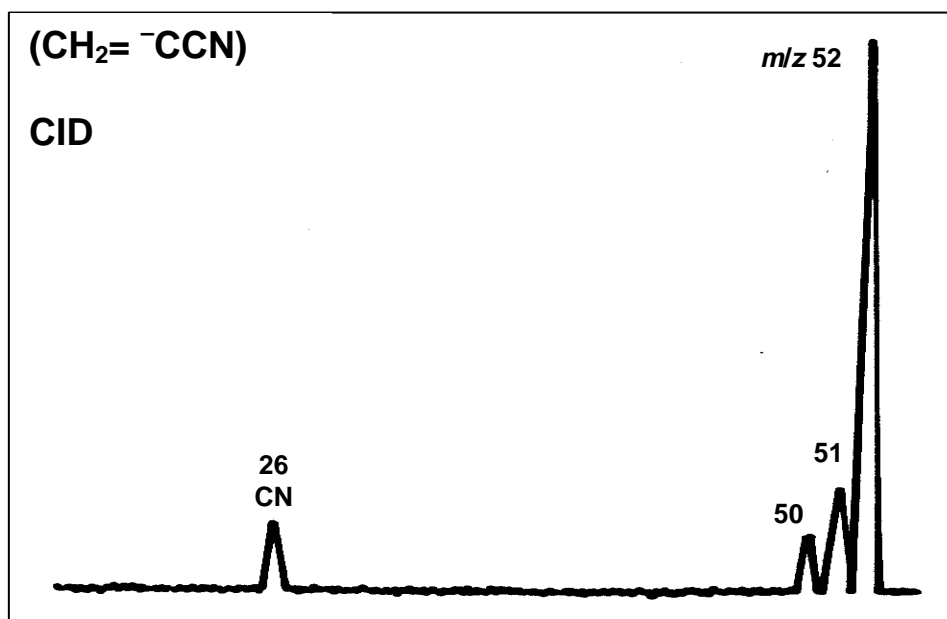
Geometry optimisations were carried out with the Becke 3LYP method^{65, 103} using the 6-31+G(d) basis set¹⁰⁴⁻¹⁰⁶ within the GAUSSIAN 03⁶⁷ suite of programs. Stationary points were characterised as either minima (no imaginary frequencies) or transition states (one imaginary frequency) by calculation of the frequencies using analytical gradient procedures. The minima connected by a given transition structure were confirmed by Intrinsic Reaction Coordinate (IRC) calculations.¹⁰⁷ The calculated frequencies were also used to determine zero-point vibrational energies which were then scaled by 0.9804⁶⁶ and used as a zero-point correction for electronic energies. We have reported the success of this method in predicting geometries of unsaturated chain structures, and that this method produces optimised structures, at low computational cost, that compare favourably with higher level calculations*.¹⁰⁸ More accurate energies for the B3LYP geometries were determined using the CCSD(T) method^{109, 110} including zero-point energy correction (calculated by vibrational frequencies at the B3LYP/6-31+G(d) level of theory). All calculations were carried out using the South Australian Partnership for Advanced Computing (SAPAC) facility.

* To cite a particular example, the value of the adiabatic electron affinity of CCCC was calculated to be 3.65 eV at the same level of theory used in this study,⁸³ while the experimental value is reported to be 3.88 eV.^{111, 112}

2.5 APPENDICES

2.5.1 Appendix 2(A)

CID spectrum of CH₂=⁻CCN (*m/z* 52), from the reaction between CH₂=CD-CN and HO⁻.



CID spectrum of CH₂=⁻CCN. VG ZAB 2HF mass spectrometer. For experimental details see Experimental section.

2.5.2 Appendix 2(B)

A comparison of the results on the CCCC, CCCN, CCCO and CCCS systems.

All systems were investigated experimentally and calculations were carried out at the CCSD(T)/aug-cc-pVDZ//B3LYP/6-31+G(d) level of theory.

In summary, the following is proposed:

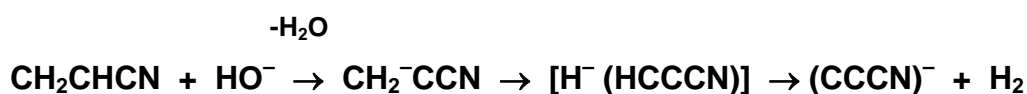
1. CCCC undergoes cyclisation to rhombic C₄ in an exothermic reaction (-10.0 kcal mol⁻¹) over a barrier of +29.5 kcal mol⁻¹. Loss of C comes from largely scrambled C₄ in a reaction endothermic by +122.0 kcal mol⁻¹.⁸³
2. Energised CCCO undergoes fragmentation to yield CC and CO (+79.8 kcal mol⁻¹) without scrambling of the skeleton. Theoretically, rearrangement through a rhomboid C₃O transition state requires an excess energy of +114.5 kcal mol⁻¹.⁸⁴
3. CCCS undergoes minor fragmentation by loss of S (+144.6 kcal mol⁻¹) during the ⁻NR⁺ timeframe of a microsecond. Theoretically, the rearrangement of CCCS to an intermediate rhomboid C₃S is endothermic (+51.6 kcal mol⁻¹) with a barrier of +80.3 kcal mol⁻¹. No appropriate neutral fragmentation occurs which can be used as a probe to test for the rearrangement in the neutral.⁸⁴
4. CCCN rearranges to CCNC *via* a rhombic C₃N (+41.6 kcal mol⁻¹) over a barrier of +54.7 kcal mol⁻¹. The partially scrambled neutral CCCN/CCNC system loses C. This loss of C is most favourable from CCNC [C + CNC (+115.6 kcal mol⁻¹); C + CCN (+117.0 kcal mol⁻¹)].

CHAPTER III

Formation of CH_2CCN by Charge-Stripping CH_2^-CCN in the Gas Phase

3.1 INTRODUCTION

We have recently used 2-d₁-cyanoethylene to produce the anion (CCCN)⁻ in the gas phase (shown in Scheme 3.1 for CH₂CHCN).¹¹³ Frank-Condon vertical electron stripping of this anion yielded the possible interstellar radical CCCN.¹¹³ The first step in this sequence is the deprotonation of CH₂CDCN to form CH₂⁻CCN. This work investigates the possibility of charge-stripping this anion (CH₂⁻CCN) to form the neutral CH₂CCN.



Scheme 3.1

The radical CH₂CCN has not, to date, been detected in interstellar dust clouds, circumstellar envelopes or interstellar ice. However, the precursor acrylonitrile (CH₂CHCN) is an interstellar molecule⁸⁵ and regio-specific hydrogen abstraction from this neutral could yield CH₂CCN. This radical may be a precursor of biologically important molecules like nucleotide bases and amino acids.

There has long been controversy as to whether biomolecules originate in stellar regions,¹¹⁴ and, in particular, whether the prototypical amino acid glycine (NH₂CH₂CO₂H) has been identified in interstellar dust clouds.¹¹⁵⁻¹¹⁷ The likelihood is that the carboxylic acid group of glycine would be unstable under the radiative conditions found in interstellar dust clouds.^{118, 119} The nitrile NH₂CH₂CN has been proposed as a possible precursor to glycine because (i) the nitrile group is more stable to ultraviolet radiation than a carboxyl group,^{120, 121} and (ii) the nitrile analogue should be converted to glycine in interstellar ice.¹²² There are a number of ways that NH₂CH₂CN might be formed in interstellar dust clouds; one might be by the reaction between the interstellar radicals NH₂ and CH₂CN.¹²¹ In a similar way, one of the possible products of the reaction between CH₂CCN and NH₂ is CH₂C(NH₂)CN and perhaps this neutral might be the precursor of amino acids of the general formula RCH₂CH(NH₂)CN.

The aims of this work are to determine (i) whether the radical CH₂CCN can be formed by Franck-Condon charge-stripping of CH₂⁻CCN in the gas phase using the neutralisation-reionisation method,^{45, 87} (ii) whether CH₂CCN is stable during the microsecond time frame of the neutralisation-reionisation experiment, and (iii) identify how CH₂CCN behaves when energised.

3.2 RESULTS & DISCUSSION

The precursor anions CH_2^-CCN , $^{13}\text{CH}_2^-\text{CCN}$ and $\text{CH}_2^-\text{C}^{13}\text{CN}$ were prepared by the reaction of (i) CH_2CDCN with HO^- , and (ii) reactions of HO^- with $^{13}\text{CH}_2\text{CHCN}$ and $\text{CH}_2\text{CH}^{13}\text{CN}$ respectively in the chemical ionisation source of the VG ZAB 2HF mass spectrometer. The first question to be answered is whether these anions are appropriate precursors for the formation of the neutral radicals CH_2CCN , $^{13}\text{CH}_2\text{CCN}$ and $\text{CH}_2\text{C}^{13}\text{CN}$. In other words, are the anions stable on formation and do they retain their structural integrity when treated under collisional conditions analogous to those required to effect Franck-Condon vertical charge stripping to the appropriate neutral radical?

This question is answered in the affirmative following consideration of the collision induced dissociation (CID) mass spectra of the three anions.

3.2.1 CID Analysis of CH_2^-CCN and Labelled Analogues

The CID mass spectrum of CH_2^-CCN (Figure 3.1) shows the precursor anion (m/z 52) as the base peak. The only fragment anion $> 1\%$ of the base peak is that formed by the loss of H_2 [(1.5%) m/z 50] from the precursor anion (CH_2^-CCN). There are three other fragments in the CID spectrum that are $< 1\%$ of the base peak. These are formed by losses of radical H [(0.15%) m/z 51], loss of CH_2 or N [(0.15%) m/z 38] and the formation of CN^- [(0.32%) m/z 26] from the precursor anion.

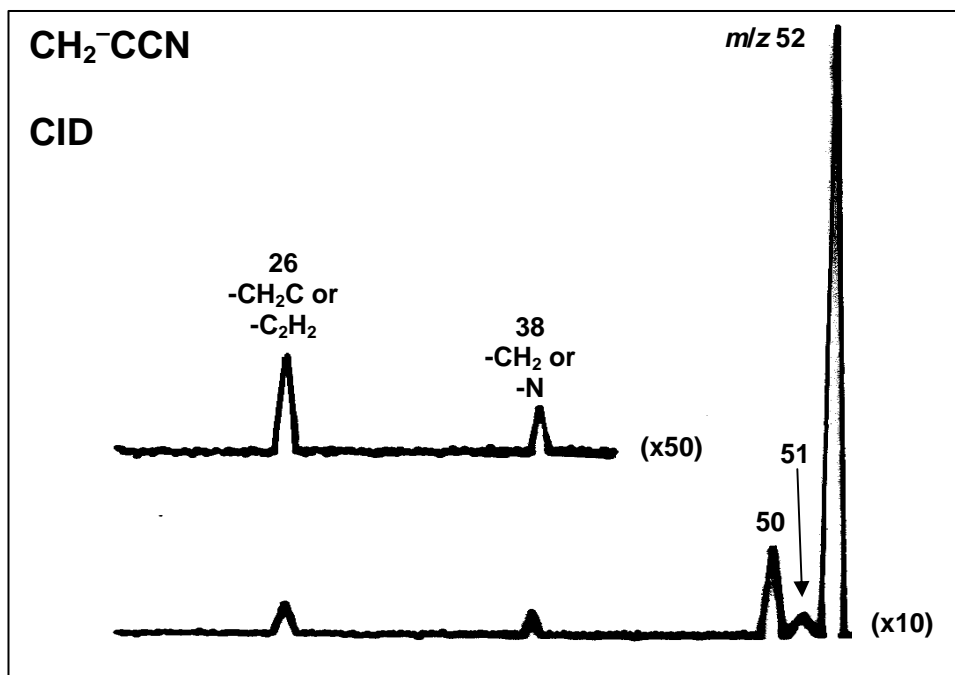


Figure 3.1 CID spectrum of CH_2^-CCN . VG ZAB 2HF mass spectrometer.
For experimental details see Experimental section.

The CID mass spectrum of the labelled analogue $^{13}\text{CH}_2^-\text{CCN}$ (Table 3.1) has the precursor anion (m/z 53) as the base peak. The only fragment ion $> 1\%$ of the base peak is that formed by loss of H_2 [(1.3%) m/z 51] from the precursor anion ($^{13}\text{CH}_2^-\text{CCN}$). There are four other fragments in the CID spectrum that are $< 1\%$ of the base peak. These are formed by losses of radical H [(0.12%) m/z 52], loss of N^* [(0.05%) m/z 39], loss of $^{13}\text{CH}_2$ [(0.12%) m/z 38] and the formation of CN^- [(0.38%) m/z 26] from the precursor anion.

* In theory, this could correspond to the loss of $^{12}\text{CH}_2$, but there is no plausible way that CH_2 could be lost from this species, even if extensive H rearrangement preceded or accompanied the loss.

TABLE 3.1

CID Spectra of $^{13}\text{CH}_2^-\text{CCN}$.[m/z (loss or formation) relative abundance in %] $^{13}\text{CH}_2^-\text{CCN}$

CID 53(precursor ion) 100; 52(H \cdot) 0.12; 51(H_2) 1.3; 39(N) 0.05; 38($^{13}\text{CH}_2$) 0.12; 26(CN^-) 0.38.

The CID mass spectrum of $\text{CH}_2^-\text{C}^{13}\text{CN}$ (Figure 3.2) shows the precursor anion (m/z 53) as the base peak. The only fragment anion $> 1\%$ of the base peak is that formed by the loss of H_2 [(1.8%) m/z 51] from the precursor anion ($\text{CH}_2^-\text{C}^{13}\text{CN}$). There are three other fragments in the CID spectrum that are $< 1\%$ of the base peak. These are formed by losses of radical H [(0.18%) m/z 52], loss of CH_2 or N [(0.14%) m/z 39] and the formation of $^{13}\text{CN}^-$ [(0.36%) m/z 27] from the precursor anion.

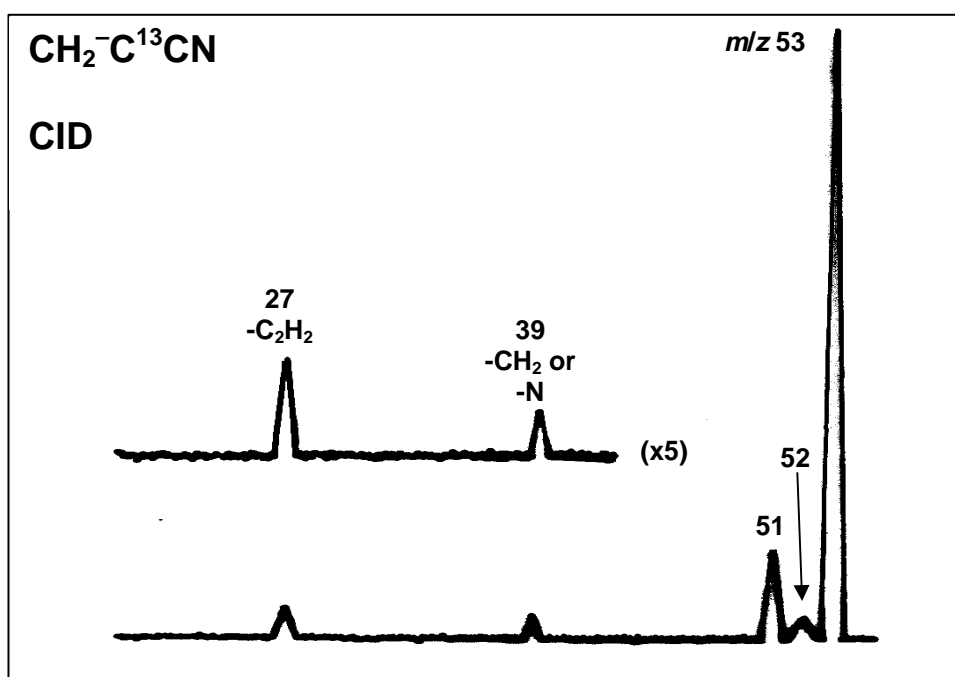


Figure 3.2 CID spectrum of $\text{CH}_2^-\text{C}^{13}\text{CN}$. VG ZAB 2HF mass spectrometer. For experimental details see Experimental section.

With the CID data obtained, there is no indication of rearrangement preceding or accompanying fragmentation of the C skeleton for all of the anions. This is prevalent in the fragmentation involving the formation of the nitrile anion. The CID spectrum of $^{13}\text{CH}_2^-\text{CCN}$ contains CN^- exclusively, while that of $\text{CH}_2^-\text{C}^{13}\text{CN}$ shows only $^{13}\text{CN}^-$. Another example is in the CID spectrum of $\text{CH}_2^-\text{C}^{13}\text{CN}$ which shows no loss of $^{13}\text{CH}_2$. In addition, the spectra do not show losses of C, CH, NH or NH_2 , so no H migration occurs from C or to N in the anion. Therefore it can be concluded that the precursor anions are stable under the conditions required for their charge stripping to the required radicals.

3.2.2 $^-\text{CR}^+$ and $^-\text{NR}^+$ Analysis of CH_2^-CCN

The $^-\text{CR}^+$ (synchronous two electron stripping of CH_2^-CCN to CH_2^+CCN)^{89, 123} and $^-\text{NR}^+$ (sequential two electron stripping, CH_2^-CCN to CH_2CCN then to CH_2^+CCN)^{45, 87} spectra of CH_2^-CCN are shown in Figures 3.3 and 3.4 respectively.

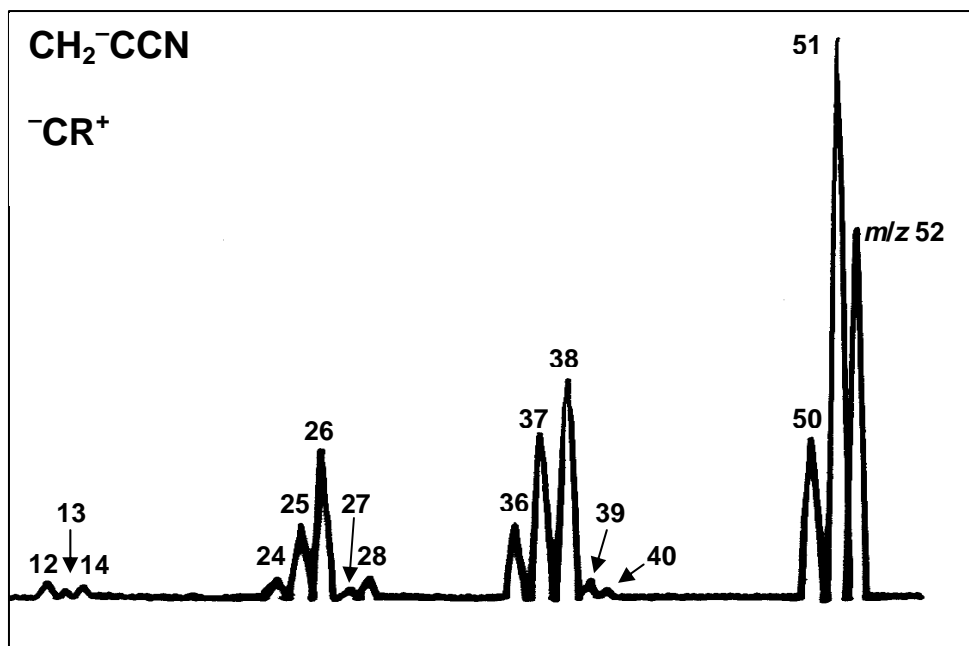


Figure 3.3 $^-\text{CR}^+$ spectrum of CH_2^-CCN . VG ZAB 2HF mass spectrometer.
For experimental details see Experimental section.

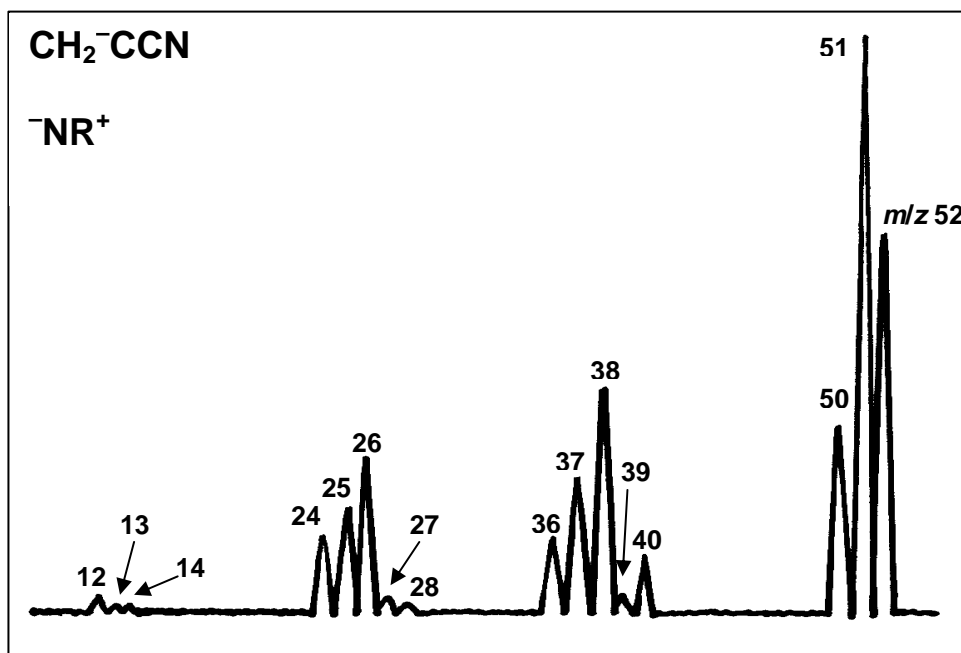


Figure 3.4 NR^+ spectrum of CH_2^-CCN . VG ZAB 2HF mass spectrometer.
For experimental details see Experimental section.

The CR^+ and NR^+ spectra are similar. There are three peaks in the NR^+ spectrum that are visually more intense than those in the corresponding CR^+ spectrum. Namely those corresponding to the loss of C (m/z 40), and to the formation of C_2H^+ (m/z 25) and C_2^+ (m/z 24). This means that the neutral species formed following charge stripping, fragment by loss of C, HCN and H_2CN . The last two processes must be preceded or accompanied by H rearrangement within the initial species CH_2CCN .

Apart from the neutral fragments mentioned above, other peaks in the CR^+ and NR^+ spectra are caused by the dissociation of cations. Many of these peaks are formed following extensive hydrogen rearrangement preceding or accompanying fragmentation: *e.g.* m/z 39 ($-\text{CH}^+$), 37 ($-\text{NH}^+$), 36 ($-\text{NH}_2^+$), 28 ($-\text{C}_2^+$), 27 ($-\text{C}_2\text{H}^+$), 25 ($-\text{HCN}^+$), and 24 ($-\text{H}_2\text{CN}^+$).

The CR^+ and NR^+ spectra of the labelled analogues $^{13}\text{CH}_2^-\text{CCN}$ and $\text{CH}_2^-\text{C}^{13}\text{CN}$ are listed in Table 3.2.

TABLE 3.2

⁻CR⁺ and ⁻NR⁺ Spectra of ¹³CH₂⁻CCN and CH₂⁻C¹³CN.

[*m/z*(loss or formation) relative abundance in %]

¹³CH₂⁻CCN

⁻CR⁺ 53(precursor ion) 73; 52(H⁺) 100; 51(H₂) 26; 41(C) 0.5; 40(¹³C/CH) 1.7; 39(CH₂/¹³CH/N) 7.5; 38(¹³CH₂/NH) 20; 37(NH₂) 5; 29(C₂) 0.5; 28(¹³CC/C₂H) 9; 27(C₂H₂/¹³CCH/CN) 9; 26(¹³CN/HCN) 3; 25(H₂CN/H¹³CN) 1.5; 15(¹³CH₂⁺) 0.2; 14(CH₂⁺/¹³CH/N⁺) 0.3; 13 (CH⁺/¹³C⁺) 0.2; 12 (C⁺) 0.4%.

⁻NR⁺ 53(precursor ion) 76; 52(H⁺) 100; 51(H₂) 26; 41(C) 0.95; 40(¹³C/CH) 1.8; 39(CH₂/¹³CH/N) 8.5; 38(¹³CH₂/NH) 20; 37(NH₂) 6; 29(C₂) 0.5; 28(¹³CC/C₂H) 8; 27(C₂H₂/¹³CCH/CN) 12; 26(¹³CN/HCN) 3.5; 25(H₂CN/H¹³CN) 1.5; 15(¹³CH₂⁺) 0.2; 14(CH₂⁺/¹³CH/N⁺) 0.2; 13 (CH⁺/¹³C⁺) 0.2; 12 (C⁺) 0.4%.

CH₂⁻C¹³CN

⁻CR⁺ 53(precursor ion) 72; 52(H⁺) 100; 51(H₂) 23; 41(C) 0.7; 40(¹³C/CH) 0.6; 39(CH₂/¹³CH/N) 8; 38(¹³CH₂/NH) 7; 37(NH₂) 3.5; 29(C₂) 0.1; 28(¹³CC/C₂H) 0.3; 27(C₂H₂/¹³CCH/CN) 2.5; 26(¹³CN/HCN) 5; 25(H₂CN/H¹³CN) 3.5; 24(H₂¹³CN) 1; 14(CH₂⁺/¹³CH/N⁺) 0.1; 13 (CH⁺/¹³C⁺) 0.2; 12 (C⁺) 0.1%.

⁻NR⁺ 53(precursor ion) 78; 52(H⁺) 100; 51(H₂) 23; 41(C) 4.5; 40(¹³C/CH) 0.9; 39(CH₂/¹³CH/N) 8; 38(¹³CH₂/NH) 7.5; 37(NH₂) 3.5; 29(C₂) 0.5; 28(¹³CC/C₂H) 0.6; 27(C₂H₂/¹³CCH/CN) 2.5; 26(¹³CN/HCN) 5; 25(H₂CN/H¹³CN) 4.5; 24(H₂¹³CN) 1.5; 14(CH₂⁺/¹³CH/N⁺) 0.1; 13 (CH⁺/¹³C⁺) 0.2; 12 (C⁺) 0.1%.

These spectra are very complex. Not only do they confirm extensive H rearrangement in the cationic systems, but they also indicate a complex rearrangement of the carbon skeleton as well. For example, CN⁺ and ¹³CN⁺ are formed in both labelled systems.

A major aim of this investigation is to determine whether neutral CH₂CCN retains its skeletal integrity when energised. The answer is that it does not. The neutral fragmentations yielding C₂H and C₂ indicate H rearrangement preceding or accompanying dissociation. The most interesting fragmentation however, is that which involves loss of C. Loss of carbon from cumulenic systems is normally an indication of an unsubstituted terminal C, however, intact CH₂CCN has no structural feature of this type. If this loss of C comes from terminal C, the process must occur following migration of both hydrogens to other atoms in the neutral radical or skeletal rearrangement followed by dissociation and/or cleavage.

The ⁻NR⁺ spectra of the labelled analogues ¹³CH₂⁻CCN and CH₂⁻C¹³CN respectively show similar and significantly enhanced loss of ¹²C compared with their corresponding ⁻CR⁺ spectra. This means that the C adjacent to N is not lost from CH₂⁻CCN, *i.e.* the process is not involved with a nitrile to isonitrile rearrangement. In contrast, the ⁻NR⁺ and ⁻CR⁺ spectra of ¹³CH₂⁻CCN are not markedly different in the region of the spectra involving losses of ¹³C and ¹²C. These spectra have been measured on many occasions and the results are reproducible. There is a small increase in the intensity of the peak due to loss of ¹²C in the ⁻NR⁺ spectrum [ratio of loss 13 (¹³C/¹²CH):12 (¹²C) is 100:30 (⁻CR⁺) and 100:53 (⁻NR⁺)], without any significant increase in the abundance of the peak produced by loss of 13 Daltons.

3.2.3 Theoretical Investigation of CH₂CCN

Calculations at the CCSD(T)/aug-cc-pVDZ//B3LYP/6-31+G(d) level of theory were used to probe the possibility that the central C is eliminated from CH₂CCN to give CH₂CN. If such a process occurs, it must compete favourably in energy to the H migrations preceding formation of CC and C₂H. The H rearrangements in these systems have not been investigated because of the large number of possible pathways for such reactions, and also since we have previously studied similar rearrangements in other cumulenenic systems. 1,2 and 1,3 H rearrangements in these systems have barriers to transition states in the order of 50-65 kcal mol⁻¹.^{124, 125}

Elimination of C from the centre of CH₂CCN must involve a rearrangement of the C skeleton and this may involve a cyclisation process, most likely a three centre cyclisation. There are two possible cyclisation processes considered. The first involving cyclisation of N to C₂, the second, cyclisation of C₃ to C₁. The first of these is shown in Figure 3.5. This process is of interest because it proceeds through the intermediacy of the rhombic structure C, where similar structures have been proposed to explain the fragmentations of the neutrals CCCC⁸³ and CCCN.¹¹³ However, this process cannot explain the loss of the central C since (i) the barrier to the first transition state (+81.2 kcal mol⁻¹) makes the process non-competitive in comparison with any process involving H rearrangement, and (ii) the rhombic intermediate C is symmetrical and so loss of C should involve both C₁ and C₂ (1:1). Full geometries and energy data for minima and transition states are shown in Figure 3.5 and in Tables 3.3 and 3.4.

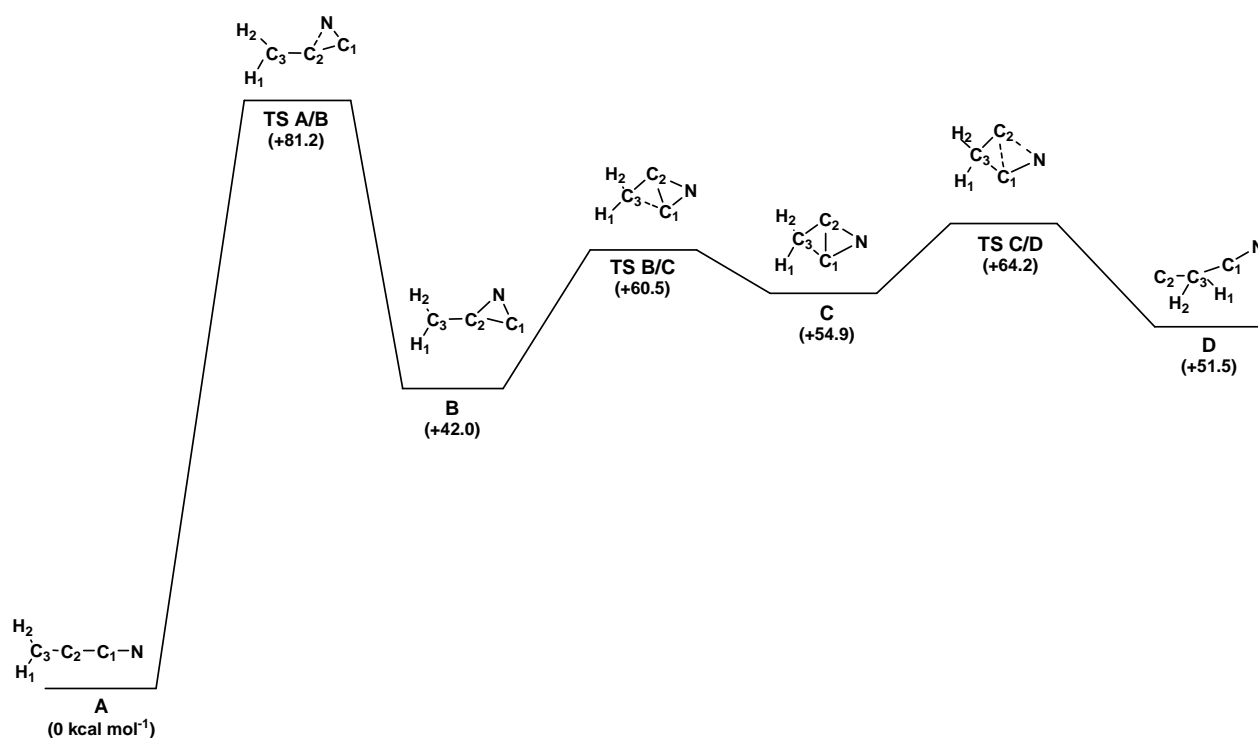


Figure 3.5 Reaction coordinate pathway for the cyclisation of N (A) to C₂ (B). Relative energies in kcal mol⁻¹. Level of theory used - CCSD(T)/aug-cc-pVDZ//B3LYP/6-31+G(d). Structures shown in the Figure show bond connectivities only. For full structural details see Tables 3.3 and 3.4.

TABLE 3.3**Reaction Coordinate Pathway for the Cyclisation of N to C₂.****The Structures and Energies of the Isomeric Doublet Neutral Minima.**

Level of theory used - CCSD(T)/aug-cc-pVDZ//B3LYP/6-31+G(d)

Relative energies in kcal mol⁻¹ with respect to A (0 kcal mol⁻¹)

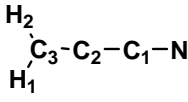
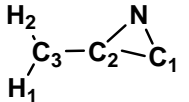
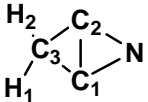
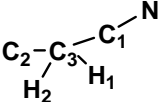
				
	A	B	C	D
State	² A	² A	² A	² A
Symmetry	C ₁	C ₁	C ₁	C ₁
Energy (Hartrees)	-169.68201	-169.61505	-169.59451	-169.59986
Energy relative to A	0	+42.0	+54.9	+51.5
Dipole Moment (Debye)	4.03	1.59	3.10	3.48
Bond Lengths (Å)				
H ₁ C ₃	1.092	1.087	1.090	1.104
H ₂ C ₃	1.092	1.088	1.090	1.114
C ₃ C ₂	1.307	1.311	1.513	1.475
C ₂ C ₁	1.334	1.436	1.726	-
C ₁ N	1.187	1.249	1.349	1.161
C ₁ C ₃	-	-	1.512	1.471
C ₂ N	-	1.519	1.349	-
Bond Angles (°)				
H ₁ C ₃ H ₂	116.2	118.4	113.7	104.6
H ₂ C ₃ C ₂	121.9	121.4	120.4	99.3
C ₃ C ₂ C ₁	180.0	166.5	55.2	-
C ₂ C ₁ N	180.0	68.5	50.2	-
NC ₁ C ₃	-	-	101.9	178.3
H ₁ C ₃ C ₂	121.9	120.2	112.8	112.6
NC ₂ C ₃	-	143.6	101.9	-
Dihedral Angle (°)				
H ₁ C ₃ C ₂ C ₁	-178.5	-0.4	114.1	-
H ₂ C ₃ C ₂ C ₁	1.5	179.6	-107.0	-
C ₃ C ₂ C ₁ N	160.0	-179.7	154.8	-
NC ₁ C ₃ H ₂	-	-	-133.6	-144.8
NC ₁ C ₃ C ₂	-	-	-19.6	-32.1

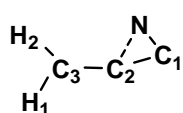
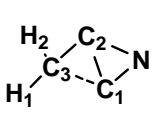
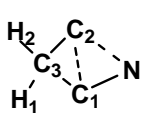
TABLE 3.4

Reaction Coordinate Pathway for the Cyclisation of N to C₂.

The Structures and Energies of the Doublet Neutral Transition States.

Level of theory used - CCSD(T)/aug-cc-pVDZ//B3LYP/6-31+G(d)

Relative energies in kcal mol⁻¹ with respect to A (0 kcal mol⁻¹)

			
	TS A/B	TS B/C	TS C/D
State	² A	² A	² A
Symmetry	C ₁	C ₁	C ₁
Energy (Hartrees)	-169.55253	-169.58553	-169.57970
Energy Relative to A	+81.2	+60.5	+64.2
Dipole Moment (Debye)	2.34	2.84	3.82
Bond Lengths (Å)			
H ₁ C ₃	1.090	1.089	1.095
H ₂ C ₃	1.091	1.090	1.095
C ₃ C ₂	1.311	1.388	1.538
C ₂ C ₁	1.466	1.761	1.815
C ₁ N	1.206	1.291	1.196
C ₁ C ₃	-	1.921	1.460
C ₂ N	1.967	1.388	1.922
Bond Angles (°)			
H ₁ C ₃ H ₂	117.1	116.2	112.7
H ₂ C ₃ C ₂	124.0	120.3	117.7
C ₃ C ₂ C ₁	154.7	74.1	50.8
C ₂ C ₁ N	94.3	51.3	76.3
C ₂ NC ₁	48.0	82.1	66.5
C ₃ C ₂ N	-	115.4	88.0
H ₁ C ₃ C ₂	119.0	121.1	117.7
Dihedral Angle (°)			
H ₁ C ₃ C ₂ C ₁	171.6	119.3	109.9
H ₂ C ₃ C ₂ C ₁	-8.7	-79.2	-
C ₃ C ₂ C ₁ N	20.9	152.2	-
NC ₂ C ₃ H ₂	-	-57.2	-109.9
C ₃ C ₂ NC ₁	-	-29.8	0.0

The C_3 to C_1 cyclisation process is shown in Figure 3.6. Finding the transition state for this process was quite a challenge, geometry and energy data for the transition state (TS A/D) are listed in Table 3.5. Minima data is available in Table 3.3. IRC calculations confirm the transition state connects CH_2CCN and CCH_2CN . It is proposed that this is the mechanism by which the central C of CH_2CCN is lost. The process, with a maximum barrier of $+61.1 \text{ kcal mol}^{-1}$ is certainly competitive with the processes involving possible 1,2 or 1,3 H migrations, and the C eliminated is specifically the central C of CH_2CCN .

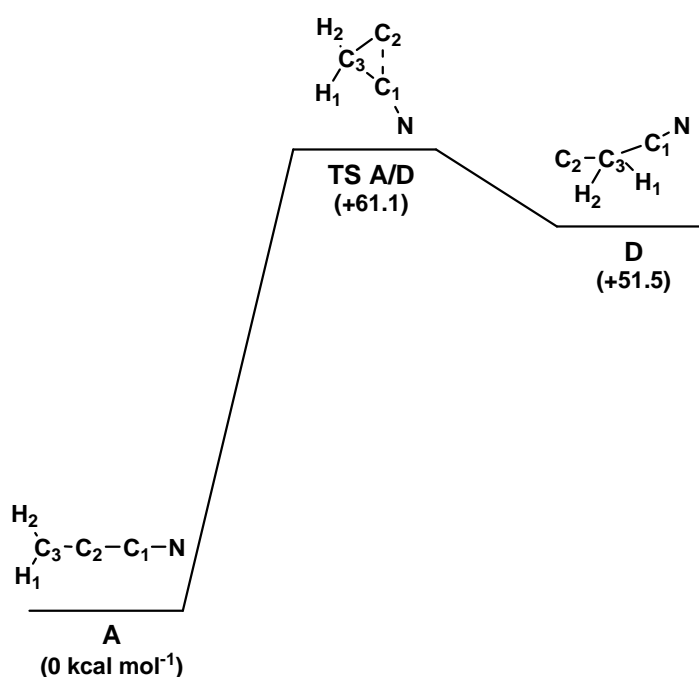


Figure 3.6 Reaction coordinate pathway for the cyclisation of C_3 (A) to C_1 (D). Relative energies in kcal mol^{-1} . Level of theory used - CCSD(T)/aug-cc-pVDZ//B3LYP/6-31+G(d). Structures shown in the Figure show bond connectivities only. For full structural details see Tables 3.3 and 3.5.

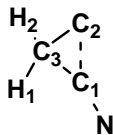
TABLE 3.5

Reaction Coordinate Pathway for the Cyclisation of C₃ to C₁.

The Structure and Energy of the Doublet Neutral Transition State.

Level of theory used - CCSD(T)/aug-cc-pVDZ//B3LYP/6-31+G(d)

Relative energy in kcal mol⁻¹ with respect to A (0 kcal mol⁻¹)



TS A/D

State	-
Symmetry	C ₁
Energy (Hartrees)	-169.58469
Energy Relative to A	+61.1
Dipole Moment (Debye)	3.75
Bond Lengths (Å)	
H ₁ C ₃	1.102
H ₂ C ₃	1.102
C ₃ C ₂	1.439
C ₂ C ₁	1.755
C ₁ N	1.170
C ₁ C ₃	1.855
Bond Angles (°)	
H ₁ C ₃ H ₂	112.7
H ₁ C ₃ C ₂	121.4
C ₃ C ₂ C ₁	56.7
C ₂ C ₁ N	144.9
C ₁ C ₃ C ₂	72.0
NC ₁ C ₃	163.9
H ₂ C ₃ C ₁	110.0
Dihedral Angle (°)	
H ₁ C ₁ C ₂ N	62.3
C ₂ C ₃ C ₁ N	180.0

The energy for the dissociation of C from the doublet neutral isomer CCH₂CN (D) is shown in Scheme 3.1 [CCSD(T)/aug-cc-pVDZ//B3LYP/6-31+G(d) level of theory].



Scheme 3.1

* Energy values were determined from the following theoretically calculated values in Hartrees calculated at the CCSD(T)/aug-cc-pVDZ//B3LYP/6-31+G(d) level of theory: CH₂CN = -131.73106, C = -37.76487.

3.3 SUMMARY & CONCLUSIONS

In conclusion, we (i) were able to generate the neutral CH₂CCN by Franck-Condon charge stripping of the precursor anion CH₂⁻CCN using the neutralisation-reionisation method, and (ii) determined that the neutral CH₂CCN is stable during the microsecond time frame needed for this method, however (iii) energised CH₂CCN undergoes loss of C, and H migration precedes or accompanies decomposition of CH₂CCN to form CC and C₂H. A combination of experimental investigation and theoretical calculations suggests that a cyclisation/cleavage process results in the loss of the central C from CH₂CCN to give CH₂CN.

3.4 EXPERIMENTAL SECTION

3.4.1 Mass Spectrometric Methods

The experiments were performed using a two-sector modified VG ZAB 2HF mass spectrometer with BE configuration, where B and E represents the magnetic and electric sectors, respectively (discussed in Chapter I). The reaction between CH_2CCN and HO^- (from H_2O) form CH_2^-CCN exclusively [see Appendix 3(A)]. Similar reactions of HO^- with $^{13}\text{CH}_2\text{CHCN}$ and $\text{CH}_2\text{CH}^{13}\text{CN}$ yield $^{13}\text{CH}_2^-\text{CCN}$ and $\text{CH}_2^-\text{C}^{13}\text{CN}$ respectively. Source conditions were as follows: source temperature 100°C , repeller voltage -0.5 V , ion extraction voltage 7 kV , mass resolution $m/\Delta m \geq 1500$. Acrylonitrile (or labelled acrylonitrile as required) is added through the septum inlet (unheated) to give a pressure of 10^{-5} Torr measured in the source housing. Water (or D_2O) is then introduced through the septum inlet (unheated) to give a constant pressure of 10^{-4} Torr in the source housing. The estimated pressure in the ion source is 10^{-1} Torr. Collision Induced Dissociation (CID) spectra were determined using the magnetic sector to select the precursor anion, and utilising argon as the collision gas in the first collision cell following the magnetic sector. The pressure of argon in the first cell was maintained such that 80% of the precursor ion beam was transmitted through the cell. This corresponds to an average of 1.1-1.2 collisions per ion.²⁹ Product anion peaks resulting from CID processes were recorded by scanning the voltage applied to the electric sector.

Neutralisation-reionisation ($^-\text{NR}^+$)^{45, 87} spectra were performed for mass selected anions utilising the dual collision cells located between the magnetic and electric sectors. Neutralisation of anions was effected by collisional electron detachment using O_2 at 80% transmission (of the ion beam) as collision gas in the first collision cell, while reionisation to cations was achieved by collision of neutrals with O_2 (80% transmission) in the second collision cell. To detect a reionisation signal due to the precursor neutral, the neutral species must be stable for the one microsecond time frame of this experiment. Charge reversal ($^-\text{CR}^+$) spectra⁸⁹ were recorded using single-collision conditions in collision cell 1 (O_2 , 80% transmission of main beam). Comparison of

⁻CR⁺ and ⁻NR⁺ data for a given precursor anion provides information concerning the neutral formed from the precursor anion: see¹⁰² for a full description of this procedure.

3.4.2 Materials

The neutral precursors CH₂CHCN, CH₂CDCN (d₁ > 99%), ¹³CH₂CHCN and CH₂CH¹³CN (¹³C > 99%) were all commercially available, and were used without further purification.

3.4.3 Theoretical Methods

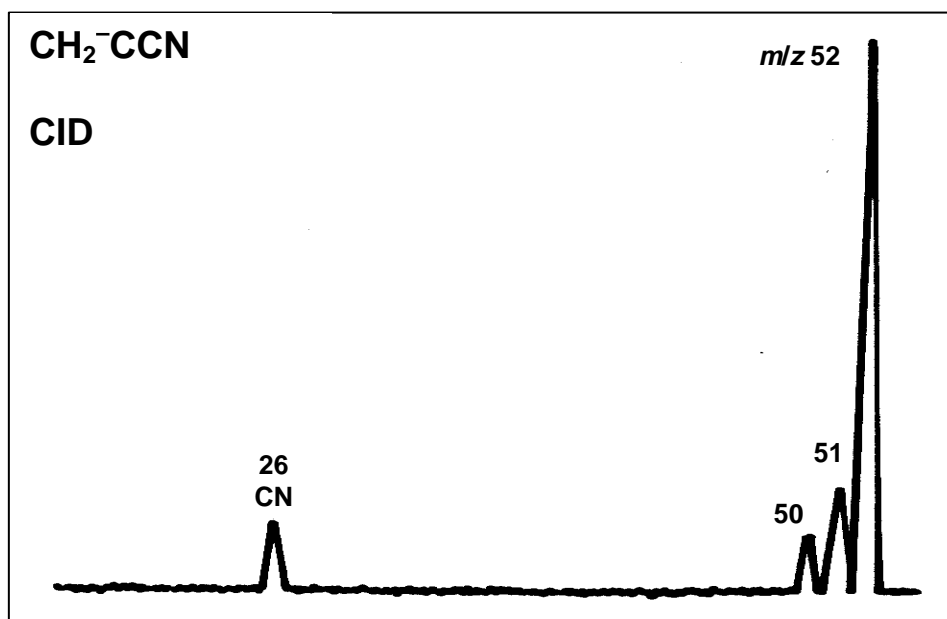
Geometry optimisations were carried out with the Becke 3LYP method^{65, 103} using the 6-31+G(d) basis set¹⁰⁴⁻¹⁰⁶ within the GAUSSIAN 03⁶⁷ suite of programs. Stationary points were characterised as either minima (no imaginary frequencies) or transition states (one imaginary frequency) by calculation of the frequencies using analytical gradient procedures. The minima connected by a given transition structure were confirmed by Intrinsic Reaction Coordinate (IRC) calculations.¹⁰⁷ The calculated frequencies were also used to determine zero-point vibrational energies which were then scaled by 0.9804⁶⁶ and used as a zero-point correction for electronic energies. We have reported the success of this method in predicting geometries of unsaturated chain structures, and that this method produces optimised structures, at low computational cost, that compare favourably with higher level calculations*.¹⁰⁸ More accurate energies for the B3LYP geometries were determined using the CCSD(T) method^{109, 110} including zero-point energy correction (calculated by vibrational frequencies at the B3LYP/6-31+G(d) level of theory). All calculations were carried out using the South Australian Partnership for Advanced Computing (SAPAC) facility.

* To cite a particular example, the value of the adiabatic electron affinity of CCCC was calculated to be 3.65 eV at the same level of theory used in this study,⁸³ while the experimental value is reported to be 3.88 eV.^{111, 112}

3.5 APPENDICES

3.5.1 Appendix 3(A)

CID spectrum of CH_2^-CCN (m/z 52), from the reaction between CH_2CDCN and HO^- .



CID spectrum of (CH_2^-CCN). VG ZAB 2HF mass spectrometer. For experimental details see Experimental section.

CHAPTER IV

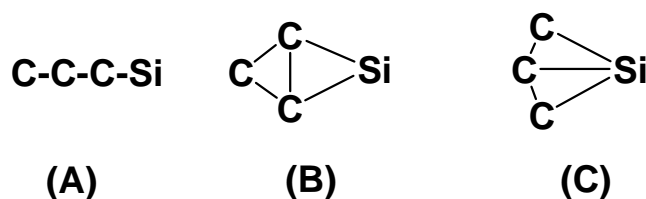
A Theoretical Study on the Behaviour of the Energised Neutrals CCCSi & CCCP

4.1 INTRODUCTION

To date the cumulenes CCCC^{126} and CCCN ,^{68, 69} have been identified in interstellar dust clouds, while CCCO and CCCS are known to be abundant in interstellar regions.^{85, 127-131} All four of these cumulenes have been shown theoretically to be stable species, but, when energised, they may undergo some interesting reactions. For example, energised singlet CCCC undergoes cyclisation to a planar ‘rhombic’ C_4 in an exothermic reaction ($-10.0 \text{ kcal mol}^{-1}$) over a barrier of $+29.5 \text{ kcal mol}^{-1}$ at the $\text{CCSD(T)/aug-cc-pVDZ//B3LYP/6-31G(d)}$ level of theory.⁸³ The corresponding reaction of the ground state triplet CCCC is endothermic by $+17.2 \text{ kcal mol}^{-1}$ with a barrier of $+25.8 \text{ kcal mol}^{-1}$. Loss of carbon (in a reaction endothermic by $+122.0 \text{ kcal mol}^{-1}$ for triplet CCCC) occurs such that the C is scrambled within an equilibrating CCCC/rhombic C_4 system.⁸³ In comparison, energised CCCO decomposes to yield CC and CO (endothermicity $+79.7 \text{ kcal mol}^{-1}$) without any scrambling of the skeleton,⁸⁴ while CCCS fragments to CCC and S [also at the $\text{CCSD(T)/aug-cc-pVDZ//B3LYP/6-31G(d)}$ level of theory]. The calculated barrier for the conversion of CCCS to a ‘rhomboid’ C_3S is $+80.3 \text{ kcal mol}^{-1}$, which makes this process energetically unfavourable.⁸⁴ Finally, the loss of C from doublet CCCN occurs following partial scrambling from an equilibrating CCCN/CCNC system through planar ‘rhombic’ C_3N .¹¹³ The barrier to this process [$+59.9 \text{ kcal mol}^{-1}$ at the $\text{CCSD(T)/aug-cc-pVDZ//B3LYP/6-31+G(d)}$ level of theory] is significantly higher than that required for the CCCC/rhombic C_4 process.^{83, 113}

In order to complete the comparisons for the series of cumulenes (groups 6, 7 and 8 of the second and third periods of the Mendeleev periodic classification), the rearrangements of CCCSi and CCCP need also to be studied. In the experimental studies of the CCCX systems discussed above, the appropriate hetero-cumulenes were prepared by charge stripping (in the collision cell of a mass spectrometer) an anion of known bond connectivity.^{83, 113} Preparation of $(\text{CCCSi})^-$ and $(\text{CCCP})^-$ by unequivocal syntheses of this type is not possible and therefore as a consequence, we have studied possible rearrangements of these two systems theoretically.

The C_3Si radical reaction coordinate pathway has been studied extensively,¹³²⁻¹⁵⁰ and is of particular interest because there is experimental evidence to show that there are three stable isomers, a linear triplet A, and two cyclic rings B and C (Scheme 4.1).^{139, 141} Rhomboid B has been identified in the evolved carbon star system IRC +10216,^{137, 139} but linear CCCSi has not been identified to date, even though its higher homologue, linear CCCCSi has.^{135, 137} C_3Si isomers have been studied by photoelectron spectroscopy,¹³⁹ and by Fourier transform microwave spectroscopy.¹⁴⁰⁻¹⁴² A number of theoretical studies have been reported for the C_3Si system also.¹⁴³⁻¹⁵¹ The relative energies of the linear structure A and the two cyclic structures B and C are dependent on the level of theory and the basis set used, with recent work using the MRPT2 level of theory suggesting that singlet B is more stable than triplet A and singlet C by +2.2 and +4.7 kcal mol⁻¹ respectively.¹⁵⁰ C_3Si anions have also been studied theoretically.^{144, 145, 152}



Scheme 4.1

Much less is known about the chemistry of cumulenes containing phosphorus. Although there are several interstellar molecules containing P,¹⁵³ namely CP¹⁵⁴ and NP,^{155, 156} CCP and CCCP have, to date, not been detected. Theoretical studies of linear CCP¹⁵⁷ and CCCP^{158, 159} have also been reported, where CCCP was determined to have a linear 2π electronic state at the MP2/6-31G* level of theory.¹⁵⁸ C_3P cations¹⁵⁹⁻¹⁶¹ and anions¹⁶²⁻¹⁶⁵ have also been studied.

The aims of this work were to examine theoretically whether the behaviour of energised CCCSi and CCCP follow those of CCCC and CCCN and in particular, to determine whether the carbons of CCCSi and CCCP scramble *via* rearrangement through cyclic intermediates like that of ‘rhomboid’ B.

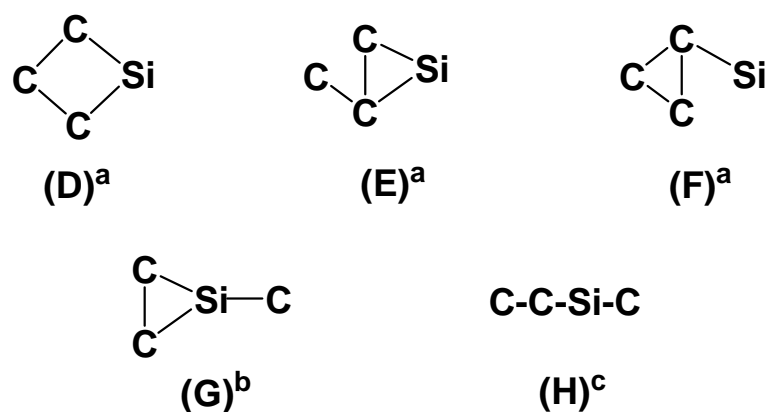
4.2 RESULTS & DISCUSSION

4.2.1 Rearrangements of Linear Singlet & Triplet CCCSi

The three important isomers of C_3Si that were considered in this study are linear CCCSi (A), and the two cyclic structures B and C (Scheme 4.1). Using the CCSD(T)/aug-cc-pVDZ//B3LYP/6-31+G(d) level of theory, triplet A is more stable than the singlet A by $8.1 \text{ kcal mol}^{-1}$, while the singlet forms of B and C are more stable than their triplet states by 22.3 and $8.2 \text{ kcal mol}^{-1}$ respectively. The relative energies of triplet A, singlet B, and singlet C are 0, +5.2 (+2.2), +5.3 (+4.7) kcal mol^{-1} respectively (values in parenthesis are those calculated at the MRPT2 theory¹⁵⁰ and listed for comparison). The question asked here is, can linear CCCSi (A) ring close to B and/or C? If so, and if these processes are equilibria, they will result in atom scrambling of linear CCCSi by processes analogous to those described for linear CCCC.⁸³ The reaction coordinate pathways of such rearrangements have been explored with results summarised in Figures 4.1 to 4.3, with full details of geometries of minima and transition states listed in Tables 4.1 to 4.3. Intersystem crossing between singlet/triplet potential surfaces has not been explored.

The C_3Si potential surface is different from the analogous C_4 surface because a number of the C_3Si analogues of the stable intermediates of C_4 are not stable. Relevant C_3Si isomers are shown in Scheme 4.2. Structure G is the only cyclic isomer shown in Scheme 4.2 where both singlet and triplet are stable, while only the singlet of linear CCSiC is stable.

Because the ground state triplet and singlet CCCSi are separated by only $+8.1 \text{ kcal mol}^{-1}$, we have considered both the singlet and triplet potential surfaces of this system. The rearrangements of triplet A to B and C are summarised in Figure 4.1, while full data concerning geometries and energies of minima and transition states shown in Figure 4.1 are listed in Table 4.1. Stepwise processes of the type proposed for rearrangement of triplet CCCC do not occur, because the required intermediate triplet E is not stable at the level of theory used for this study.



Where; a, both singlet and triplet are unstable; b, both singlet and triplet are stable; c, singlet stable, triplet unstable

Scheme 4.2

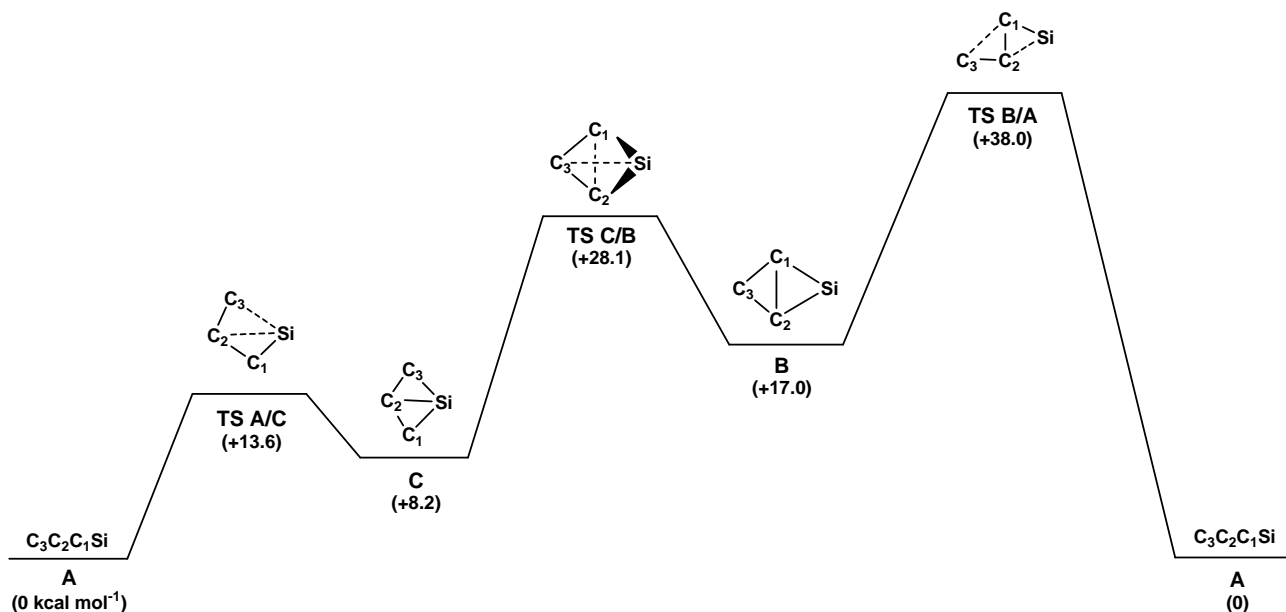


Figure 4.1 Reaction coordinate pathway for the rearrangement of triplet CCCSi (A). Relative energies in kcal mol⁻¹. Level of theory used - CCSD(T)/aug-cc-pVDZ//B3LYP/6-31+G(d). Structures shown in the Figure show bond connectivities only. For full structural details see Table 4.1.

TABLE 4.1

**Reaction Coordinate Pathway for the Rearrangement of Triplet CCCSi.
The Structures and Energies of the Triplet Neutral Minima and Transition States.**

Level of theory used - CCSD(T)/aug-cc-pVDZ//B3LYP/6-31+G(d)

Relative energies in kcal mol⁻¹ relative to ³A (0 kcal mol⁻¹)

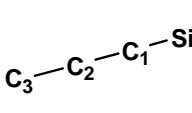
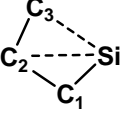
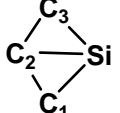
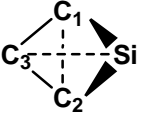
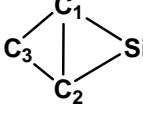
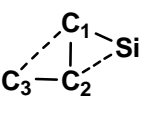
						
	³ A	TS ³ A/ ³ C	³ C	TS ³ C/ ³ B	³ B	TS ³ B/ ³ A
State	³ SG	³ A''	³ B ₁	³ A	³ A''	³ A''
Symmetry	C _{∞v}	C _s	C _{2v}	C ₁	C _s	C _s
Energy (Hartrees)	-402.78612	-402.76438	-402.77305	-402.74133	-402.75895	-402.72555
Energy Relative to ³A	0	+13.6	+8.2	+28.1	+17.0	+38.0
Dipole Moment (Debye)	4.48	3.12	1.75	1.67	0.42	3.27
Bond Lengths (Å)						
SiC ₁	1.736	1.795	1.960	2.093	1.943	1.804
C ₁ C ₂	1.293	1.346	1.345	2.239	1.508	1.430
C ₂ C ₃	1.312	1.323	1.345	1.410	1.362	1.320
SiC ₂	-	2.090	1.974	1.848	1.942	2.01
SiC ₃	-	2.669	1.960	2.268	-	-
C ₁ C ₃	-	-	-	1.319	1.362	1.905
Bond Angles (°)						
SiC ₁ C ₂	180.0	82.1	70.5	50.4	67.2	75.9
C ₁ C ₂ C ₃	180.0	158.8	138.9	33.6	56.4	87.6
C ₁ SiC ₂	-	39.6	40.0	68.9	45.7	43.6
C ₃ C ₂ Si	-	100.5	69.5	87.2	123.5	148.1
C ₁ C ₂ Si	-	58.3	69.5	60.7	67.1	60.5
C ₃ SiC ₁	-	68.7	80.0	34.9	-	-
C ₂ C ₃ C ₁	-	-	-	110.2	67.2	48.6
C ₃ C ₁ Si	-	-	-	79.8	123.6	119.7
C ₃ C ₁ C ₂	-	-	-	36.2	56.4	43.8
Dihedral Angle (°)						
SiC ₁ C ₂ C ₃	0.0	0.0	0.0	138.0	180.0	180.0
C ₃ C ₂ SiC ₁	-	180.0	180.0	-21.7	0.0	0.0

Figure 4.1 shows the conversion of triplet A to B and A to C. The cyclisation of triplet A to B is endothermic ($+17.0 \text{ kcal mol}^{-1}$) with a barrier to the transition state of $+38.0 \text{ kcal mol}^{-1}$. The alternate process, triplet A to triplet C is more facile. It is endothermic ($+8.2 \text{ kcal mol}^{-1}$) with a barrier of only $+13.6 \text{ kcal mol}^{-1}$. The conversion of triplet A to C has a lower barrier ($+13.6 \text{ kcal mol}^{-1}$) than the ring closure of triplet CCCC ($+25.8 \text{ kcal mol}^{-1}$), with the CCCC and CCCSi processes both endothermic ($+17.2$ and $+8.2 \text{ kcal mol}^{-1}$ respectively). Cyclic forms B and C are interconvertible: the barrier is only $+11.1 \text{ kcal mol}^{-1}$ from B to C. Thus energised triplet CCCSi should cyclise readily producing cyclic isomers B and C which on ring opening may reform CCCSi but with the carbon atoms rearranged. The linear species CCSiC cannot be a product in this system since triplet CCSiC is not stable at the level of theory used in this study.

The singlet C_3Si reaction coordinate is shown in Figure 4.2, with details of energies and geometries of minima and transition states (shown in Figure 4.2) recorded in Table 4.2. Singlet CCCSi (A) interconverts in a concerted process to singlet C, but no concerted pathway from singlet A to singlet B (the more stable of the two cyclised singlet isomers) could be found. There is also no stepwise rearrangement forming singlet B, since the required key intermediate, singlet E, is unstable at the level of theory used in this study. However singlet B is convertible synchronously to singlet C over a barrier of $+37.2 \text{ kcal mol}^{-1}$. The cyclisation of singlet A to singlet C is exothermic ($-8.0 \text{ kcal mol}^{-1}$) with the barrier to the transition state being $+16.0 \text{ kcal mol}^{-1}$. This should be compared with the conversion of singlet CCCC to rhombic singlet C_4 : barrier, $+29.5 \text{ kcal mol}^{-1}$; exothermicity ($-10.0 \text{ kcal mol}^{-1}$). So both triplet and singlet A should, (i) form cyclic isomers which when ring opened, may partially scramble the C atoms throughout the backbone of the linear molecule, and (ii) the rearrangement of CCCSi should be more facile than CCCC.

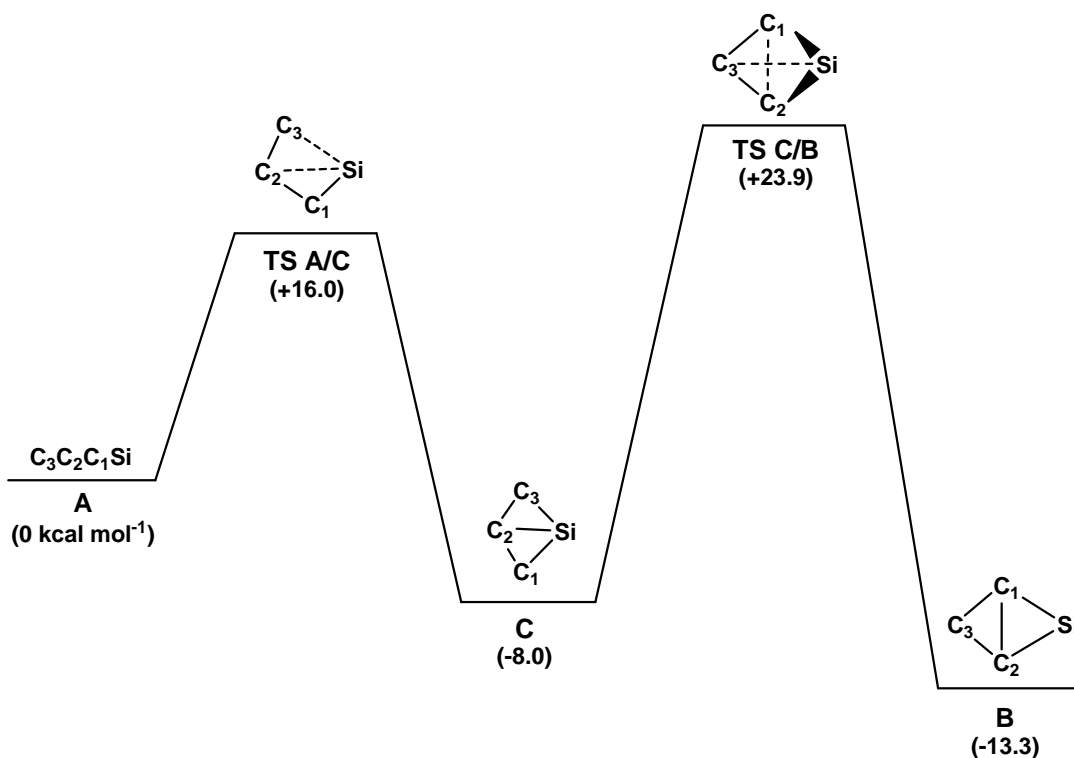


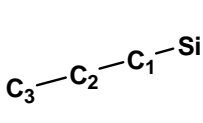
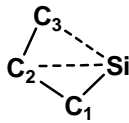
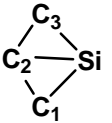
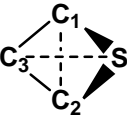
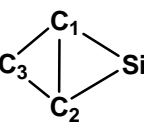
Figure 4.2 Reaction coordinate pathway for the rearrangement of singlet CCCSi (A). Relative energies in kcal mol⁻¹. Level of theory used - CCSD(T)/aug-cc-pVDZ//B3LYP/6-31+G(d). Structures shown in the Figure show bond connectivities only. For full structural details see Table 4.2.

TABLE 4.2

**Reaction Coordinate Pathway for the Rearrangement of Singlet CCCSi.
The Structures and Energies of the Singlet Neutral Minima and Transition States.**

Level of theory used - CCSD(T)/aug-cc-pVDZ//B3LYP/6-31+G(d)

Relative energies in kcal mol⁻¹ relative to ¹A (0 kcal mol⁻¹)

					
	¹ A	TS ¹ A/ ¹ C	¹ C	TS ¹ C/ ¹ B	¹ B
State	-	¹ A'	¹ A'	¹ A	¹ A'
Symmetry	C _s v	C _s	C _s	C ₁	C _s
Energy (Hartrees)	-402.77329	-402.74785	-402.78604	-402.73528	-402.79445
Energy Relative to ¹ A	0	+16.0	-8.0	+23.9	-13.3
Dipole Moment (Debye)	4.31	5.75	2.28	2.02	4.19
Bond Lengths (Å)					
SiC ₁	1.744	1.767	2.056	2.137	1.851
C ₁ C ₂	1.296	1.344	1.343	1.987	1.474
C ₂ C ₃	1.310	1.321	1.343	1.322	1.437
SiC ₂	-	2.415	1.909	1.820	1.852
SiC ₃	-	3.454	2.056	2.046	-
C ₁ C ₃	-	-	-	1.404	1.437
Bond Angles (°)					
SiC ₁ C ₂	180.0	101.0	64.4	52.2	66.5
C ₁ C ₂ C ₃	180.0	178.9	152.4	44.9	59.1
C ₁ SiC ₂	-	33.1	39.4	59.6	46.9
C ₃ C ₂ Si	-	133.0	76.2	98.7	125.6
C ₁ C ₂ Si	-	45.9	76.2	68.2	66.6
C ₃ SiC ₁	-	30.8	78.8	35.4	-
C ₂ C ₃ C ₁	-	-	-	93.5	61.7
C ₃ C ₁ Si	-	-	-	82.8	125.7
C ₃ C ₁ C ₂	-	-	-	41.6	59.2
Dihedral Angle (°)					
SiC ₁ C ₂ C ₃	0.0	0.0	0.0	129.4	180.0
C ₃ C ₂ SiC ₁	-	180.0	180.0	-35.5	0.0

There is however, a significant difference between the triplet and singlet C_3Si potential surfaces in that singlet $CCSiC$ is stable, whereas triplet $CCSiC$ is not. Singlet $CCSiC$ lies $+79.2 \text{ kcal mol}^{-1}$ above $CCCSi$ and so any processes forming this species from A, B or C will require significant excess energy. We have explored one such process which is shown in Figure 4.3 (see also Table 4.3). Ring opening of C to the only stable isomer containing one three membered ring G has a barrier of $+81.1 \text{ kcal mol}^{-1}$, and once formed, this species should ring open to $CCSiC$. This rearrangement is energetically unfavorable compared with other such processes shown in Figures 4.1 and 4.2.

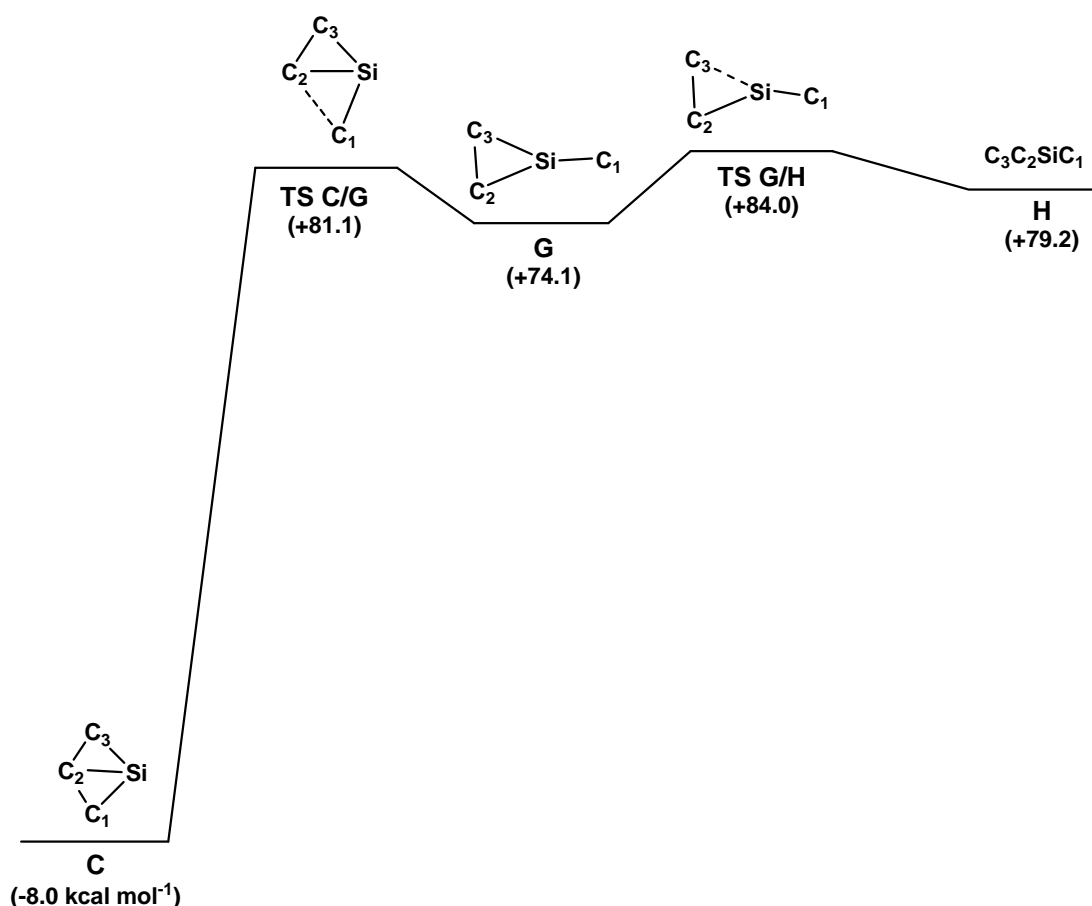


Figure 4.3 Reaction coordinate pathway for the rearrangement of singlet C to $CCSiC$ (H). Relative energies in kcal mol^{-1} . Level of theory used - CCSD(T)/aug-cc-pVDZ//B3LYP/6-31+G(d). Structures shown in the Figure show bond connectivities only. For full structural details see Table 4.3.

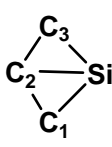
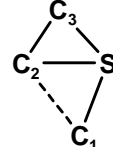
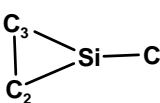
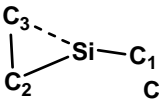
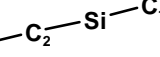
TABLE 4.3

Reaction Coordinate Pathway for the Rearrangement of Singlet (C) to CCSiC.

The Structures and Energies of the Singlet Neutral Minima and Transition States.

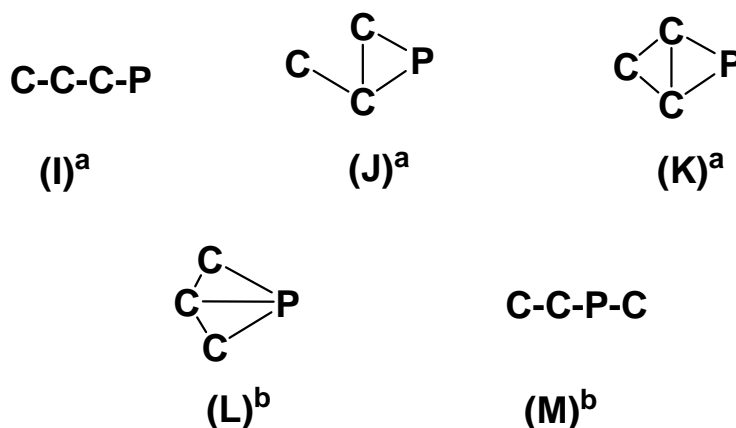
Level of theory used - CCSD(T)/aug-cc-pVDZ//B3LYP/6-31+G(d)

Relative energies in kcal mol⁻¹ relative to ¹A (0 kcal mol⁻¹)

					
	¹ C	TS ¹ C/ ¹ G	¹ G	TS ¹ G/ ¹ H	¹ H
State	¹ A'	¹ A	¹ A'	¹ A	-
Symmetry	C _s	C ₁	C _s	C ₁	C _s
Energy (Hartrees)	-402.78604	-402.64411	-402.65526	-402.63936	-402.64707
Energy Relative to ¹ A	-8.0	+81.1	+74.1	+84.0	+79.2
Dipole Moment (Debye)	2.28	2.71	0.37	1.63	1.71
Bond Lengths (Å)					
SiC ₁	2.056	1.831	1.826	1.820	1.813
C ₁ C ₂	1.343	2.807	-	-	-
C ₂ C ₃	1.343	1.313	1.298	1.294	1.287
SiC ₂	1.909	2.008	1.838	1.706	1.694
SiC ₃	2.056	1.793	1.838	2.533	-
Bond Angles (°)					
C ₁ C ₂ C ₃	152.4	100.2	-	-	-
C ₁ SiC ₂	39.4	93.9	159.3	173.9	180.0
C ₃ C ₂ Si	76.2	61.2	69.3	114.5	180.0
C ₁ C ₂ Si	76.2	40.6	-	-	-
C ₃ SiC ₁	78.8	131.4	159.4	158.4	-
SiC ₃ C ₂	64.4	78.9	69.3	37.8	-
C ₂ SiC ₃	39.4	39.9	41.3	27.7	-
Dihedral Angle (°)					
SiC ₁ C ₂ C ₃	0.0	15.8	-	-	-
C ₃ C ₂ SiC ₁	180.0	-162.1	180.0	-180.0	0.0

4.2.2 Rearrangement of Linear Doublet CCCP

The key isomers of the doublet C_3P potential surface are linear CCCP (I), the half cyclised isomer J and fully cyclised K. In this case, L [*cf.* the Si isomer (C) above] is not a stable entity at the level of theory used in this study. Interestingly, linear CCPC is also not a stable species, so even if I can transform to K, the only linear species to which K can ring open is CCCP (I). Calculations at the CCSD(T)/aug-cc-pVDZ//B3LYP/6-31+G(d) level of theory (Table 4.4), show that doublet CCCP is linear with essentially CC and CP double bonds. The quartet structure of I (see Table 4.4) lies +38.1 kcal mol⁻¹ above doublet I and we have not considered the quartet potential surface further.



Where; doublet structures; a, stable; b, unstable

Scheme 4.3

The rearrangement of I through J to K is shown in Figure 4.4 with full details of energies and geometries of species shown in Figure 4.4 recorded in Table 4.4. The reaction profile shown in Figure 4.4 is similar to that obtained for the ring closure of doublet CCCN at the same level of theory. The CCCP process is the more energetically favourable with a maximum barrier of +50.4 kcal mol⁻¹ at the CCSD(T)/aug-cc-pVDZ//B3LYP/6-31+G(d) level of theory (Figure 4.4) (*cf.* +54.7 kcal mol⁻¹ for CCCN) and an overall endothermicity of +15.4 kcal mol⁻¹ (+41.6 kcal mol⁻¹ for CCCN). Since we have already shown experimentally that there is partial C scrambling of energised

CCCN,¹¹³ it is probable that (at least) partial C scrambling should also be observed for energised CCCP.

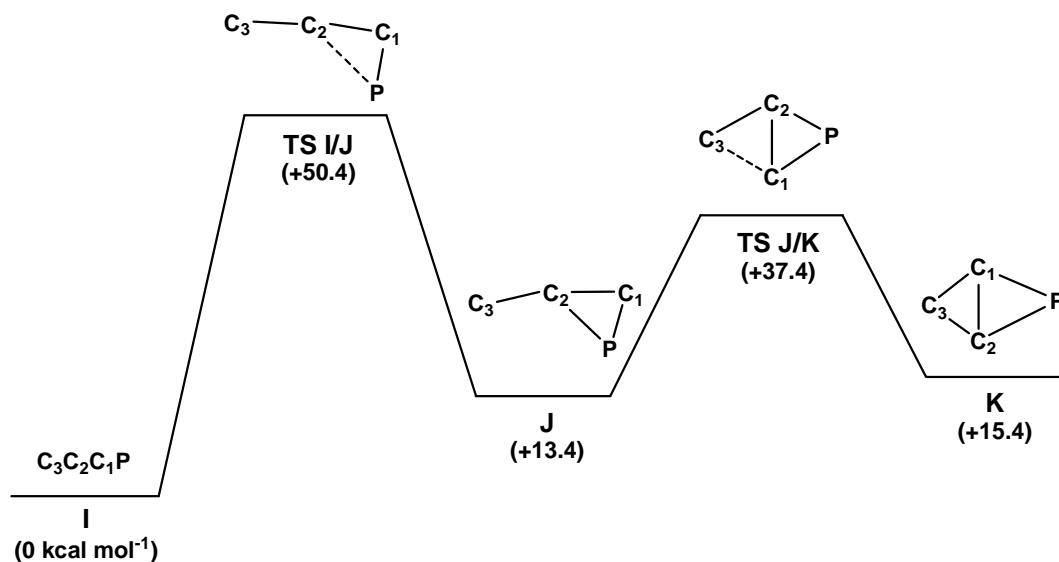


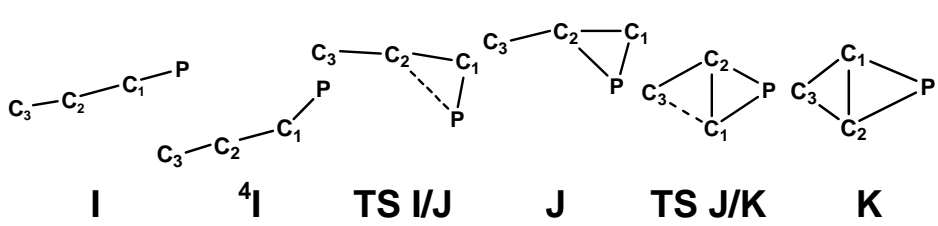
Figure 4.4 Reaction coordinate pathway for the rearrangement of doublet CCCP (I). Relative energies in kcal mol⁻¹. Level of theory used - CCSD(T)/aug-cc-pVDZ//B3LYP/6-31+G(d). Structures shown in the Figure show bond connectivities only. For full structural details see Table 4.4.

TABLE 4.4

Reaction Coordinate Pathway for the Rearrangement of Doublet CCCP.

The Structures and Energies of the Doublet Neutral Minima and Transition States.

Level of theory used - CCSD(T)/aug-cc-pVDZ//B3LYP/6-31+G(d)

Relative energies in kcal mol⁻¹ relative to I (0 kcal mol⁻¹)


	I	⁴ I	TS I/J	J	TS J/K	K
State	-	⁴ A	² A	² A''	² A'	² A''
Symmetry	C _{s,v}	C ₁	C ₁	C _s	C _s	C _s
Energy (Hartrees)	-454.65473	-454.59405	-454.57439	-454.60878	-454.59533	-454.63011
Energy Relative to I	0	+38.1	+50.4	+13.4	+37.3	+15.4
Dipole Moment (Debye)	3.80	3.54	4.37	2.28	3.34	3.66
Bond Lengths (Å)						
PC ₁	1.600	1.742	1.664	1.783	1.788	1.783
C ₁ C ₂	1.314	1.287	1.384	1.403	1.515	1.479
C ₂ C ₃	1.297	1.333	1.309	1.321	1.321	1.434
PC ₂	-	-	2.261	1.839	1.731	1.783
C ₃ C ₁	-	-	-	-	2.306	1.434
Bond Angles (°)						
PC ₁ C ₂	180.0	142.0	95.3	69.3	62.6	65.5
C ₁ C ₂ C ₃	180.0	174.2	179.2	164.0	108.6	59.0
C ₁ PC ₂	-	-	37.5	45.5	51.0	49.0
C ₃ C ₂ P	-	-	133.6	98.9	175.0	124.5
C ₂ C ₃ C ₁	-	-	-	-	38.5	65.1
C ₃ C ₁ C ₂	-	-	-	-	32.9	59.0
C ₃ C ₁ P	-	-	-	-	95.5	124.5
Dihedral Angle (°)						
PC ₁ C ₂ C ₃	0.0	-179.9	178.3	0.0	180.0	180.0
C ₃ C ₂ PC ₁	-	-	-180.0	180.0	0.0	0.0
PC ₁ C ₃ C ₂	-	-	-	-	0.0	0.0

4.3 SUMMARY & CONCLUSIONS

Calculations at the CCSD(T)/aug-cc-pVDZ//B3LYP/6-31+G(d) level of theory have shown that cyclisation of both the ground state triplet and the corresponding singlet state of CCCSi may rearrange to give cyclic isomers which upon ring opening may reform linear C_3Si isomers in which the carbon atoms are scrambled. The cyclisation processes are energetically favorable with barriers to the transition states from +13 to +16 kcal mol⁻¹. This should be compared with the analogous process of triplet CCCC to triplet rhombic C_4 which requires an excess energy of +25.8 kcal mol⁻¹ [see Appendix 4(A)]. A similar cyclisation of doublet CCCP requires +50.4 kcal mol⁻¹ of excess energy which should be compared with the same process for CCCN which requires +54.7 kcal mol⁻¹ in order to effect cyclisation [see Appendix 4(A)].

In conclusion, the linear systems CCCSi and CCCP when energised may undergo cyclisation to planar 'rhomboid' systems, which when ring opened to reform CCCSi and CCCP, may cause scrambling of the carbons. The cyclisation of linear CCCSi to 'rhomboid' C_3Si is more energetically favourable than the cyclisation of CCCC to 'rhombic' C_4 . As a consequence, it is likely that linear CCCSi (A) should be detected together with the known 'rhombic' C_3Si (B) in interstellar molecular clouds and environs. Rearrangement of linear CCCP to a cyclic system is more energetically favourable than the analogous cyclisation of the interstellar analogue CCCN. For a summary of the rearrangements of the CCCX systems see Appendix 4(A).

4.4 THEORETICAL METHODS

Geometry optimisations were carried out with the Becke 3LYP method^{65, 103} using the 6-31+G(d) basis set¹⁰⁴⁻¹⁰⁶ within the GAUSSIAN 03⁶⁷ suite of programs. Stationary points were characterised as either minima (no imaginary frequencies) or transition states (one imaginary frequency) by calculation of the frequencies using analytical gradient procedures. The minima connected by a given transition structure were confirmed by Intrinsic Reaction Coordinate (IRC) calculations.¹⁰⁷ The calculated frequencies were also used to determine zero-point vibrational energies which were then scaled by 0.9804⁶⁶ and used as a zero-point correction for electronic energies. We have reported the success of this method in predicting geometries of unsaturated chain structures, and that this method produces optimised structures, at low computational cost, that compare favourably with higher level calculations*.¹⁰⁸ More accurate energies for the B3LYP geometries were determined using the CCSD(T) method^{109, 110} including zero-point energy correction (calculated by vibrational frequencies at the B3LYP/6-31+G(d) level of theory). All calculations were carried out using the South Australian Partnership for Advanced Computing (SAPAC) facility.

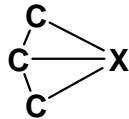
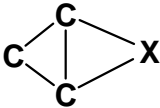
* To cite a particular example, the value of the adiabatic electron affinity of CCCC was calculated to be 3.65 eV at the same level of theory used in this study,⁸³ while the experimental value is reported to be 3.88 eV.^{111, 112}

4.5 APPENDICES

4.5.1 Appendix 4(A)

Rearrangement Summary for the CCCX Systems.

Relative energies in kcal mol⁻¹

	C-C-C-X					
	A	TS A/C	C	TS A/B	TS C/B	B
³ CCCC ^a	0	-	-	+25.8	-	+17.2
¹ CCCC ^a	+7.2	-	-	+36.7	-	-2.8
³ CCCSi ^b	0	+13.6	+8.2	-	+28.1	+17.0
¹ CCCSi ^b	+8.1	+24.1	-8.0	-	+32.0	-5.2
² CCCN ^b	0	-	-	+54.7 ^c	-	+42.6
² CCCP ^b	0	-	-	+50.4 ^d	-	+15.4
¹ CCCO ^a	0	-	-	-	-	not stable
³ CCCO ^a	+65.4	not studied				
¹ CCCS ^a	0	-	-	+80.3 ^e	-	+66.7
³ CCCS ^a	+62.1	not studied				

a CCSD(T)aug-cc-pVDZ//B3LYP/6-31G(d) level of theory

b CCSD(T)aug-cc-pVDZ//B3LYP/6-31+G(d) level of theory

c maximum transition state in this system is **A/CycloC₂N** (+54.7 kcal mol⁻¹)

d maximum transition state in this system is **A/CycloC₂P** (+50.4 kcal mol⁻¹)

e maximum transition state in this system is **A/CycloC₂S** (+80.3 kcal mol⁻¹)

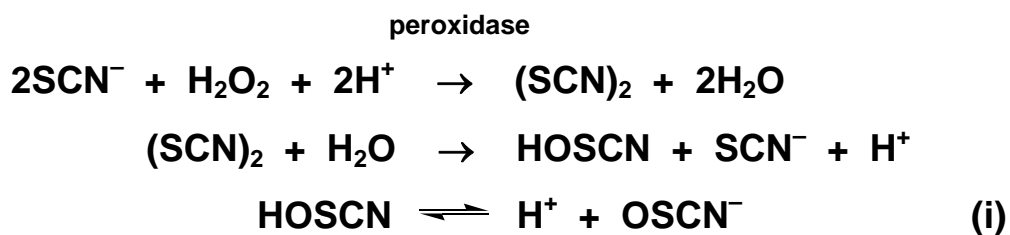
CHAPTER V

The Enzymatic Oxidation of $(\text{SCN})^-$.

What is the Major Product?

5.1 INTRODUCTION

In the early 1960's, the hypothiocyanite anion [(OSCN)⁻ from hypothiocyanous acid (HOSCN)] was initially formed whilst trying to determine the rate of reaction for the oxidation of the thiocyanate anion (SCN)⁻ by hydrogen peroxide using varying catalytic pH-independent and pH dependent conditions.^{166, 167} Also in the sixties, the products of this oxidation reaction, this time enzymatically catalysed with a milk peroxidase (lactoperoxidase), were found to be able to inhibit some strains of *Streptococci*.¹⁶⁸ More than a decade later, it was suggested that the accumulated oxidised form of thiocyanate from the enzyme catalysed reactions was the hypothiocyanite anion (OSCN)⁻¹⁶⁹ formed either by oxidation of (SCN)⁻ to (SCN)₂, followed by hydrolysis, or by direct oxidation of (SCN)⁻ [see Scheme 5.1(i) and (ii)] respectively.¹⁶⁹



Scheme 5.1

There has been a large amount of work undertaken on the thiocyanate anion (SCN)⁻, hydrogen peroxide and peroxidase reaction mixtures, above all because they are natural antimicrobial systems and therefore have the potential to be used as possible preservatives in the food and pharmaceutical industry.¹⁷⁰ The antimicrobial effectiveness relies on the stability of the oxidation products OSCN⁻ and HOSCN, where the decomposition of the hypothiocyanous acid depends on pH and the availability of H₂O₂.¹⁶⁹ These reaction mixtures are active against a number of Gram positive and Gram negative organisms (*e.g.* *Pseudomonas aeruginosa*, *Staphylococcus*

aureus, *Eschericia coli* and *Candida albicans*) however Gram negative bacteria inhibition is more dependent on temperature and pH.¹⁷⁰

Work on the antimicrobial activity and bio-effectiveness of these systems has been extensive especially in the area of dental hygiene. The production of hypothiocyanite is a biologically occurring process that takes place within the oral cavity to reduce the cytotoxicity of hydrogen peroxide. The thiocyanate, which is present in human saliva, is oxidised by hydrogen peroxide and the reaction is catalysed by the salivary peroxidase enzymes which result in the production of hypothiocyanite possessing the required antimicrobial properties which inhibit plaque acid production.¹⁷¹ Reaction mixtures (toothpastes) of $(\text{SCN})^-$ (0.5%) and H_2O_2 (0.1%) without the peroxidase enzymes also have shown to have the required antimicrobial properties to fight the gum disease gingivitis as well as reduce plaque acid formation.¹⁷²

Unfortunately there is also a downside to the enzyme based systems for biological use, as it has been reported that an antimicrobial cocktail of eosinophil peroxidase, H_2O_2 and $(\text{SCN})^-$ has been implicated in promoting cytotoxic tissue damage which occurs in asthma.¹⁷³

The oxidation products of the peroxidase/ H_2O_2 / $(\text{SCN})^-$ systems were poorly characterised until they were probed using nuclear magnetic resonance, electrospray mass spectrometry and quantitative chemical analysis.¹⁷⁴ The results were interpreted in terms of the initial oxidation products being cyanate $(\text{OCN})^-$ and hypothiocyanite $(\text{OSCN})^-$ in abundance and with a cytotoxic potential at roughly a 1:1 ratio.¹⁷⁴ The Collision Induced Dissociation (CID) negative ion mass spectrum of $(\text{OSCN})^-$ (Figure 5.1) is informative in the identification and bond connectivity of the precursor ion [there is a pronounced precursor anion at m/z 74, together with fragment anions at m/z 58 $(\text{SCN})^-$ and 26 $(\text{CN})^-$ consistent with the structure of $(\text{OSCN})^-$]. What is of particular interest in the negative ion mass spectrum of $(\text{OSCN})^-$ is there is a smaller peak at m/z 42 [$(\text{OCN})^-$ or $(\text{CNO})^-$]. This peak either has to be formed (i), from a precursor anion isomeric with $(\text{OSCN})^-$ *i.e.* $(\text{SNCO})^-$ or $(\text{SCNO})^-$, a geometric isomer, or (ii) by rearrangement of $(\text{OSCN})^-$ prior to or during decomposition of the precursor anion. The aim of this project is to determine the origin of m/z 42.

This work is a follow-up on earlier work on the vertical one electron oxidation of $(\text{OCN})^-$ ¹⁷⁵ and $(\text{SCN})^-$ ¹⁷⁶ and because of our particular interest in biological molecules found in interstellar environs. The parent acids HNCO and HNCS are known interstellar molecules,^{85, 177, 178} and $(\text{OCN})^-$ may be a component of interstellar ice (particularly in comets).¹⁷⁹ Therefore the possibility is that if $(\text{SCN})^-$ is present in interstellar ice then the oxidation product $(\text{OSCN})^-$ may have been one of the first antimicrobial agents formed on primeval earth and elsewhere.

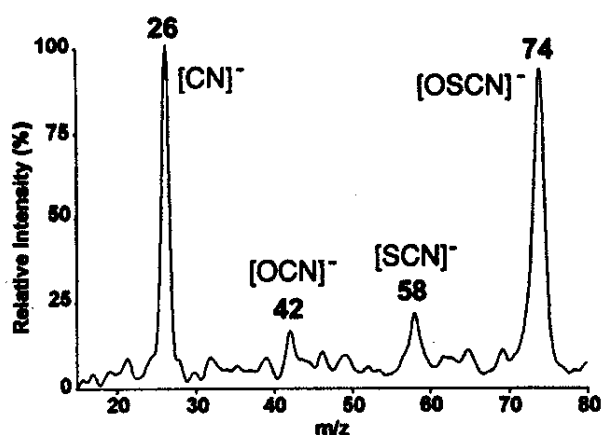
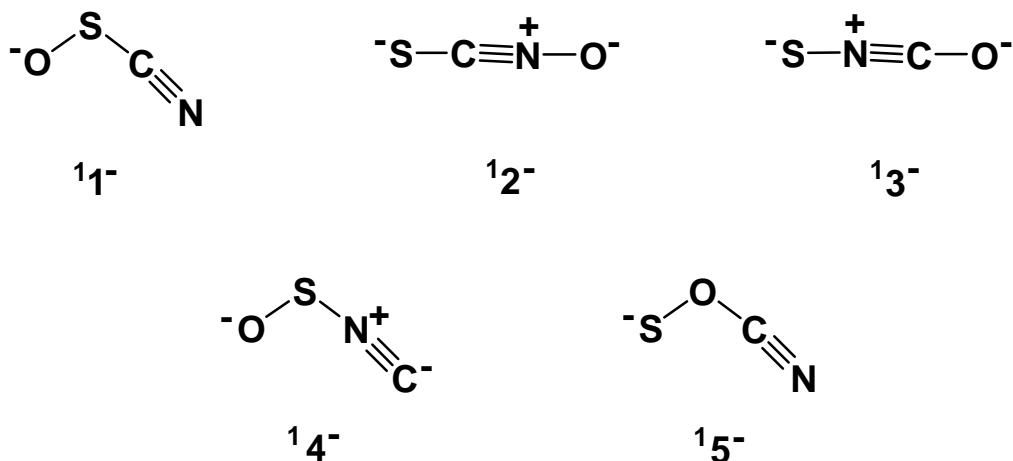


Figure 5.1 MS/MS spectrum of the precursor ion $[\text{OSCN}]^-$ m/z 74. Taken from Arlandson *et al.*¹⁸⁰ Spectrum measured on a Micromass Quatro-2 triple quadrupole mass spectrometer; Ar collision gas in the second quadrupole (1.7×10^{-3} Torr).

5.2 RESULTS & DISCUSSION

5.2.1 Theoretical Results

There may be many possible isomers of an anion containing one atom of each of C, N, O and S. In order to determine the origin of the peak at m/z 42 [$(\text{OCN})^-$ or $(\text{CNO})^-$], isomers of the precursor ion $(\text{OSCN})^-$ *i.e.* $(\text{SNCO})^-$ and $(\text{SCNO})^-$ and the rearrangement of $(\text{OSCN})^-$ need to be investigated theoretically. However, if the oxidation occurs from an intact thiocyanate anion $(\text{SCN})^-$, the only feasible oxidation products are $(\text{OSCN})^-$ and/or $(\text{SCNO})^-$. If the isothiocyanate anion $(\text{SNC})^-$ is present in interstellar ice (either in its own right or as a product of a thiocyanate - isothiocyanate rearrangement), oxidation of this anion could potentially form $(\text{SNCO})^-$ and perhaps $(\text{OSNC})^-$. Before attempting to synthesize the above anions, molecular modeling at the CCSD(T)/aug-cc-pVDZ//B3LYP/6-31+G(d) level of theory was used to determine the structures and relative energies of these isomeric anions together with other possible anions which might be formed by rearrangement of $(\text{OSCN})^-$. Data are listed in Scheme 5.1 and Tables 5.1, 5.2 and 5.3.



Scheme 5.1

TABLE 5.1

Singlet and Triplet Isomer Relative Energies.

STATE **ISOMER (Relative Energy)**

Level of theory used - CCSD(T)/aug-cc-pVDZ//B3LYP/6-31+G(d)

Relative energies in kcal mol⁻¹ relative to ¹1 (0 kcal mol⁻¹)

(OSCN)⁻	(SCNO)⁻	(SNCO)⁻	(OSNC)⁻	(SOCN)⁻
¹ 1 (0 kcal mol ⁻¹)	¹ 2 (+12.9)	¹ 3 (-20.3)	¹ 4 (+21.5)	¹ 5 (-2.5)
³ 1 (+18.1)	³ 2 (+58.2)	³ 3 (+23.8)	³ 4 (+17.2)	³ 5 (unstable) [#]

[#] Decomposes to SO and CN⁻

TABLE 5.2**The Structures and Energies of the Isomeric Singlet Anions.**

Level of theory used - CCSD(T)/aug-cc-pVDZ//B3LYP/6-31+G(d)

Relative energies in kcal mol⁻¹ relative to ¹1 (0 kcal mol⁻¹)

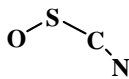
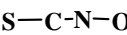
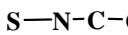
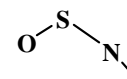
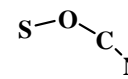
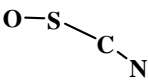
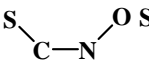
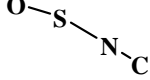
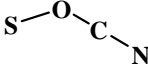
					
	¹1	¹2	¹3	¹4	¹5
State	¹ A ₁	¹ SG	¹ SG	¹ A ₁	¹ A ₁
Symmetry	C _s	C _{∞v}	C _{∞v}	C ₁	C _s
Energy (Hartrees)	-565.38239	-565.36191	-565.41467	-565.3481	-565.38638
Energy Relative to ¹1	0	+12.9	-20.3	+21.5	-2.5
Dipole Moment (Debye)	2.40	0.57	1.25	2.40	1.20
Bond Lengths (Å)					
OS	1.585	-	-	1.561	1.871
SC	1.735	1.673	-	-	-
CN	1.178	1.173	1.181	1.185	1.177
NO	-	1.272	-	-	-
SN	-	-	1.704	1.787	-
CO	-	-	1.221	-	1.267
Bond Angles (°)					
OSC	110.0	-	-	-	-
SCN	177.5	180.0	-	-	-
NCO	-	-	180.0	-	175.0
COS	-	-	-	-	116.8
CNO	-	180.0	-	-	-
OSN	-	-	-	109.2	-
SNC	-	-	180.0	178.8	-
Dihedral Angle (°)					
OSCN	180.0	-	-	-	-
SCNO	-	0.0	-	-	-
SNCO	-	-	0.0	-	-
OSNC	-	-	-	179.8	-
SOCN	-	-	-	-	180.0

TABLE 5.3**The Structures and Energies of the Isomeric Triplet Anions.**

Level of theory used - CCSD(T)/aug-cc-pVDZ//B3LYP/6-31+G(d)

Relative energies in kcal mol⁻¹ relative to ¹1 (0 kcal mol⁻¹)

					
	31	32	33	34	35
State	³ A''	³ A''	-	-	UNSTABLE
Symmetry	C _s	C _s	C ₁	C ₁	
Energy (Hartrees)	-565.35346	-565.28963	-565.34432	-565.35486	
Energy Relative to ¹1	+18.1	+58.2	+23.8	+17.2	
Dipole Moment (Debye)	2.14	1.47	0.65	7.65	
Bond Lengths (Å)					
OS	1.541	-	-	1.537	
SC	2.808	1.654	-	-	
CN	1.181	1.322	1.322	1.184	
NO	-	1.316	-	-	
SN	-	-	1.741	2.676	
CO	-	-	1.222	-	
Bond Angles (°)					
OSC	168.5	-	-	-	
SCN	179.0	140.1	-	-	
NCO	-	-	141.3	-	
CNO	-	118.2	-	-	
OSN	-	-	-	179.4	
SNC	-	-	117.8	178.9	
Dihedral Angle (°)					
OSCN	0.0	-	-	-	
SCNO	-	0.0	-	-	
SNCO	-	-	-0.008	-	
OSNC	-	-	-	0.0	

There are, in principle, singlet and triplet forms of the even-electron anions 1⁻ to 5⁻. An earlier *ab initio* study at the 6-31G(d) level suggested that 1⁻ should be unstable.¹⁸¹ However, the results of this theoretical study indicates that singlet and triplet forms of structures 1⁻ to 5⁻ are stable with the exception of ³5⁻ which is unstable. Singlet structures are the ground states of 1⁻ to 3⁻ and 5⁻ whereas the triplet structure is the ground state of 4⁻ by +4.3 kcal mol⁻¹ at the level of theory used in this investigation. The relative stabilities of the singlet states of the anions are ¹3⁻ > ¹5⁻ > ¹1⁻ > ¹2⁻ > ¹4⁻ whereas the relative stabilities of the triplet states of the anions are ³4⁻ > ³1⁻ > ³3⁻ > ³2⁻ > ³5⁻ (unstable). Details of the structures and relative energies of the anions are recorded in Tables 5.2 and 5.3. While it is difficult to represent each species by a single valence bond structure, the closest representative structures are illustrated in Scheme 5.1. At the level of theory used in this study, the hypothiocyanite anion (¹1⁻) is bent as are ¹4⁻ and ¹5⁻, while ¹2⁻ and ¹3⁻ are linear. For the triplet anions the ground state ³4⁻ is very near linear where ³2⁻ and ³3⁻ are bent and ³1⁻ is slightly bent.

Two questions to be addressed are (i) whether the hypothiocyanite anion (OSCN)⁻ is a stable species under the conditions it may be formed on interstellar ice (as well as in the ion source of a mass spectrometer), or (ii) does it undergo facile rearrangement to an isomeric anion which may decompose to form OCN⁻ [or (CNO)⁻] *i.e.* the origin of the peak seen at *m/z* 42. The singlet state of (OSCN)⁻ (¹1⁻) is +18.1 kcal mol⁻¹ more stable than its corresponding triplet, which is an ion-dipole complex formed between SO and CN⁻ (Table 5.3). As a consequence, rearrangements of this singlet anion are considered first. The possible rearrangements of this anion were investigated at the CCSD(T)/aug-cc-pVDZ//B3LYP/6-31+G(d) level of theory. The rearrangements are summarised in Figures 5.2 to 5.4, with full data provided in Tables 5.2 and 5.4.

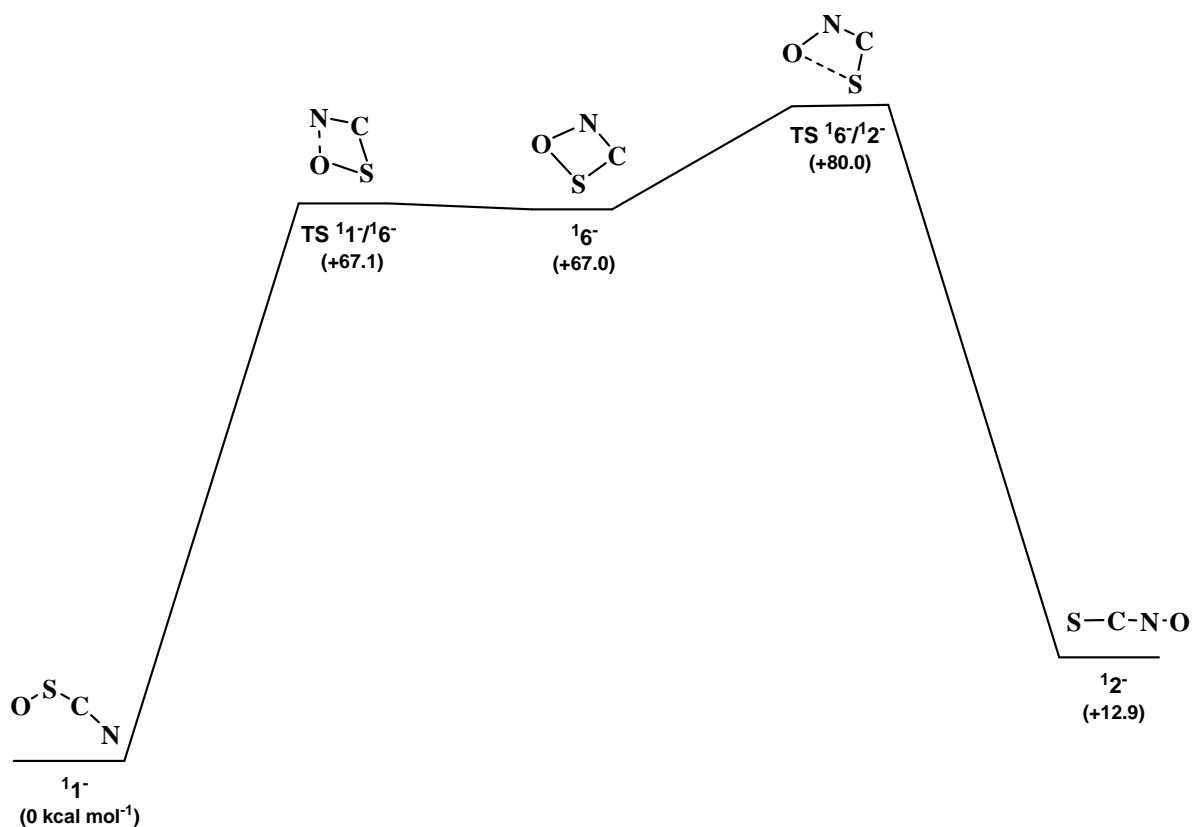


Figure 5.2 Reaction coordinate pathway for the rearrangement of 1^- to 2^- . Level of theory used - CCSD(T)/aug-cc-pVDZ//B3LYP/6-31+G(d). Relative energies in kcal mol^{-1} . Structures shown in the Figure show bond connectivities only. For full structural details see Table 5.2 and 5.4.

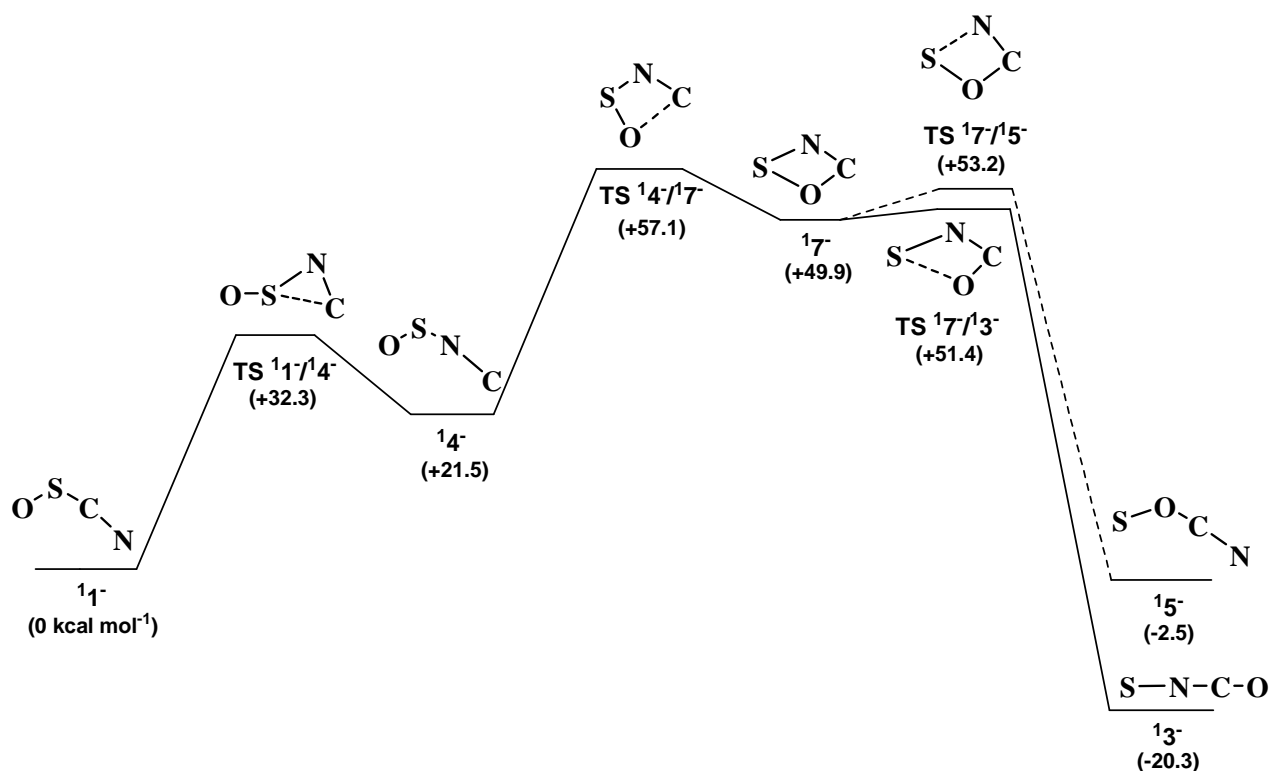


Figure 5.3 Reaction coordinate pathway for the rearrangements 1^- to 13^- , 1^- to 14^- and 1^- to 15^- . Level of theory used - CCSD(T)/aug-cc-pVDZ//B3LYP/6-31+G(d). Relative energies in kcal mol $^{-1}$. Structures shown in the Figure show bond connectivities only. For full structural details see Table 5.2 and 5.4.

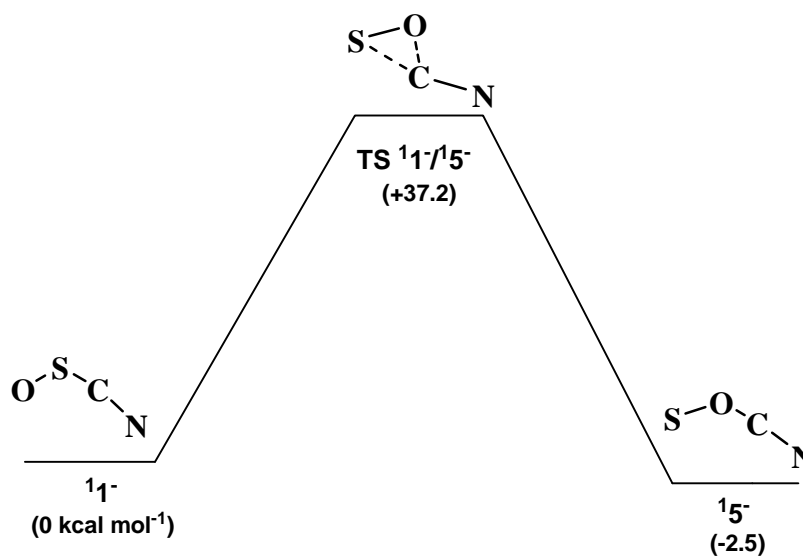


Figure 5.4 Reaction coordinate pathway for the concerted rearrangement of 1^- to 5^- . Level of theory used - CCSD(T)/aug-cc-pVDZ//B3LYP/6-31+G(d). Relative energies in kcal mol^{-1} . Structures shown in the Figure show bond connectivities only. For full structural details see Table 5.2 (minima) and 5.4 (transition state).

TABLE 5.4
The Structures and Energies of the Singlet Anion Transition States and Cyclic Minima.

Level of theory used - CCSD(T)/aug-cc-pVDZ//B3LYP/6-31+G(d)

 Relative energies in kcal mol⁻¹ relative to ¹1⁻ (0 kcal mol⁻¹)

	TS ¹ 1' / ¹ 5'	TS ¹ 1' / ¹ 6'	TS ¹ 6' / ¹ 2'	TS ¹ 1' / ¹ 4'	TS ¹ 4' / ¹ 7'	TS ¹ 7' / ¹ 5'	TS ¹ 7' / ¹ 3'	¹ 6'	¹ 7'
State	1-A'	1-A'	1-A'	-	1-A'	1-A'	1-A'	1-A'	1-A'
Symmetry	Cs	Cs	Cs	C1	Cs	Cs	Cs	Cs	Cs
Energy (Hartrees)	-565.32307	-565.27543	-565.25492	-565.33087	-565.29137	-565.30053	-565.29764	-565.27564	-565.30291
Energy Relative to ¹1'	+37.2	+67.1	+80.0	+32.3	+57.1	+53.2	+51.4	+67.0	+49.9
Dipole Moment (Debye)	-	-	-	-	-	-	-	3.51	4.17
Bond Lengths (Å)									
OS	1.781	1.750	2.195	1.544	1.673	1.808	2.019	1.761	1.600
SC	1.746	1.740	1.711	2.510	-	-	-	1.825	-
CN	1.193	1.277	1.261	1.193	1.271	1.278	1.293	1.304	1.375
NO	-	1.722	1.409	-	-	-	-	1.514	-
SN	-	-	-	2.510	1.691	2.057	1.852	-	1.690
CO	1.711	-	-	-	1.935	1.363	1.315	-	1.664
Bond Angles (°)									
OSC	58.0	81.6	66.5	109.9	-	-	-	76.0	-
SCN	159.6	97.7	105.0	88.1	-	-	-	92.7	-
NCO	138.3	-	-	-	91.0	110.4	112.1	-	121.4
COS	60.0	-	-	-	79.4	95.0	86.1	-	63.6
CNO	-	97.9	109.4	-	-	-	-	103.0	-
NOS	-	82.7	79.1	-	-	-	-	88.4	-
OSN	-	-	-	115.4	87.9	67.9	67.2	-	107.5
SNC	-	-	-	63.5	101.7	86.7	94.1	-	67.5
Dihedral Angle (°)									
OSCN	180.0	0.0	-	-106.7	-	-	-	-	-
SCNO	-	0.0	0.0	-	-	-	-	0.0	-
SNCO	-	-	-	-	-	-	0.0	-	0.0
OSNC	-	-	-	180.0	0.0	0.0	-	-	-
SOCN	180.0	-	-	-	0.0	0.0	-	-	-

The rearrangement of singlet $(\text{OSCN})^- (^1 1^-)$ to singlet $(\text{SCNO})^- (^1 2^-)$ is shown in Figure 5.2. This rearrangement is endothermic (+12.9 kcal mol⁻¹), but the barrier for dissociation of the cyclic intermediate $^1 6^-$ is a prohibitive +80 kcal mol⁻¹. The rearrangement of $^1 1^-$ to $^1 4^-$ is endothermic (+21.5 kcal mol⁻¹) with a barrier of +32.3 kcal mol⁻¹ (Figure 5.3). The process $^1 1^-$ to $^1 4^-$ (Figure 5.3) is possibly energetically unfavourable although it has the lowest barrier of all the rearrangements investigated. Even if there is a possibility the rearrangement occurs, the anion $(\text{OSNC})^-$ cannot be the precursor of the m/z 42 anion seen in Figure 5.1 due to the closeness in energy to that for the decomposition of $\text{CN}^- + \text{SO}^*$.

The stepwise rearrangements $^1 1^-$ to $^1 3^-$ and $^1 1^-$ to $^1 5^-$ (see Figure 5.3) are exothermic (-20.3 and -2.5 kcal mol⁻¹ respectively) and both can proceed through the intermediacy of $^1 4^-$. However, the barrier (+57.1 kcal mol⁻¹) for the two reactions is prohibitively high. The interconversion of $^1 1^-$ to $^1 5^-$ can occur by a concerted exothermic pathway (Figure 5.4), but again, there is a significant barrier (+37.2 kcal mol⁻¹) for this rearrangement.

The dissociation energies of the singlet anions $^1 1^-$ to $^1 5^-$ are shown in Table 5.5. These are all high energy processes and indicate that unless significantly energised, the singlet isomers $^1 1^-$ to $^1 5^-$ should be stable to decomposition.

* The anion $^1 4^-$ is formed requiring +32.3 kcal mol⁻¹ of energy (Figure 5.3) while the decomposition to $\text{CN}^- + \text{SO}$ requires +32.2 kcal mol⁻¹ (Table 5.5).

TABLE 5.5

Dissociation Energies of the Singlet and Triplet Anions.

Level of theory used - CCSD(T)/aug-cc-pVDZ//B3LYP/6-31+G(d). Energies in kcal mol⁻¹. EA [adiabatic electron affinity in kcal mol⁻¹ (energy required to remove an electron from the anion)]

¹ (OSCN) ⁻ (¹ 1 ⁻)	→	NC ⁻ + SO	(+53.7)
(EA, +56.0)	→	O ⁻ + NCS	(+99.7)
	→	OSC ⁻ + N	(+215.4)
¹ (SCNO) ⁻ (¹ 2 ⁻)	→	CS ⁻ + NO	(+92.4)
(EA, +68.7)	→	O ⁻ + NCS	(+86.9)
	→	CNO ⁻ + S	(+103.2)
¹ (SNCO) ⁻ (¹ 3 ⁻)	→	NS ⁻ + CO	(+64.3)
(EA, +60.4)	→	O ⁻ + CNS	(+150.0)
	→	NCO ⁻ + S	(+70.7)
¹ (OSNC) ⁻ (¹ 4 ⁻)	→	CN ⁻ + SO	(+32.2)
(EA, +51.9)	→	O ⁻ + CNS	(+108.2)
	→	NSO ⁻ + C	(+174.7)
¹ (SOCN) ⁻ (¹ 5 ⁻)	→	CN ⁻ + SO	(+56.2)
(EA, +71.5)	→	NCO ⁻ + S	(+52.9)
	→	COS ⁻ + N	(+143.1)
³ (OSCN) ⁻ (³ 1 ⁻)	→	NC ⁻ + SO	(+11.9)
³ (OSNC) ⁻ (³ 4 ⁻)	→	CN ⁻ + SO	(+12.8)

The data listed in Table 5.5 shows that (i) loss of an electron from ¹1⁻ requires +2.3 kcal mol⁻¹ more energy than that required for the lowest energy dissociation, also (ii) loss of an electron from each of ¹2⁻ and ¹3⁻ (+68.7 and +60.4 kcal mol⁻¹ respectively) will compete with the lowest energy dissociation of these anions, and (iii) the electron

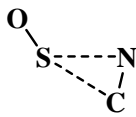
binding energies of ¹4⁻ and ¹5⁻ are higher than the lowest energy dissociation of these anions.

The triplet form of the hypothiocyanite anion (³1⁻) is an ion-dipole complex (OS–CN)⁻ formed between OS and CN⁻ (Table 5.3). The S–C distance is 2.81 angstroms with the angles OSC and SCN being 169° and 179° respectively. The complex ³1⁻ converts to ³4⁻ (OS–NC)⁻ over a barrier of only +0.9 kcal mol⁻¹ (Table 5.6) in a reaction exothermic by 0.9 kcal mol⁻¹. Complex ³4⁻ has an S–N distance of 2.67 angstroms with the angles OSN and SNC each being 179° (near linear). Each of the ion-dipole complexes ³1⁻ and ³4⁻ decompose to SO and NC⁻ in facile reactions which require only +11.9 and +12.8 kcal mol⁻¹ respectively (Table 5.5).

TABLE 5.6**The Structure and Energy of the Triplet Anion Transition State.**

Level of theory used - CCSD(T)/aug-cc-pVDZ//B3LYP/6-31+G(d)

Relative energies in kcal mol⁻¹ relative to ¹1⁻ (0 kcal mol⁻¹)



TS ³1⁻/³4⁻

State	³ A''
Symmetry	C _s
Energy (Hartrees)	-565.35222
Energy relative to ¹1⁻	+18.9
Dipole Moment (Debye)	-
Bond Lengths (Å)	
OS	1.533
SC	3.004
CN	1.183
SN	3.177
Bond Angles (°)	
OSC	163.2
SCN	87.3
OSN	175.0
SNC	70.8
Dihedral Angle (°)	
OSCN	180.0
OSNC	0.0

The conclusions from the theoretical part of this study are, (i) the ground state singlet form of the hypothiocyanite anion (OSCN)⁻ (¹1⁻) is stable *i.e.* no facile rearrangement

process should produce an isomer which can decompose to either (OCN)⁻ or (CNO)⁻, and (ii) the triplet state of (OSCN)⁻ (³1⁻) converts readily to the ground state triplet (OSNC)⁻ (³4⁻), and (iii) both these triplet anions are ion-dipole complexes of SO and NC⁻ which decompose readily to yield NC⁻ and SO.

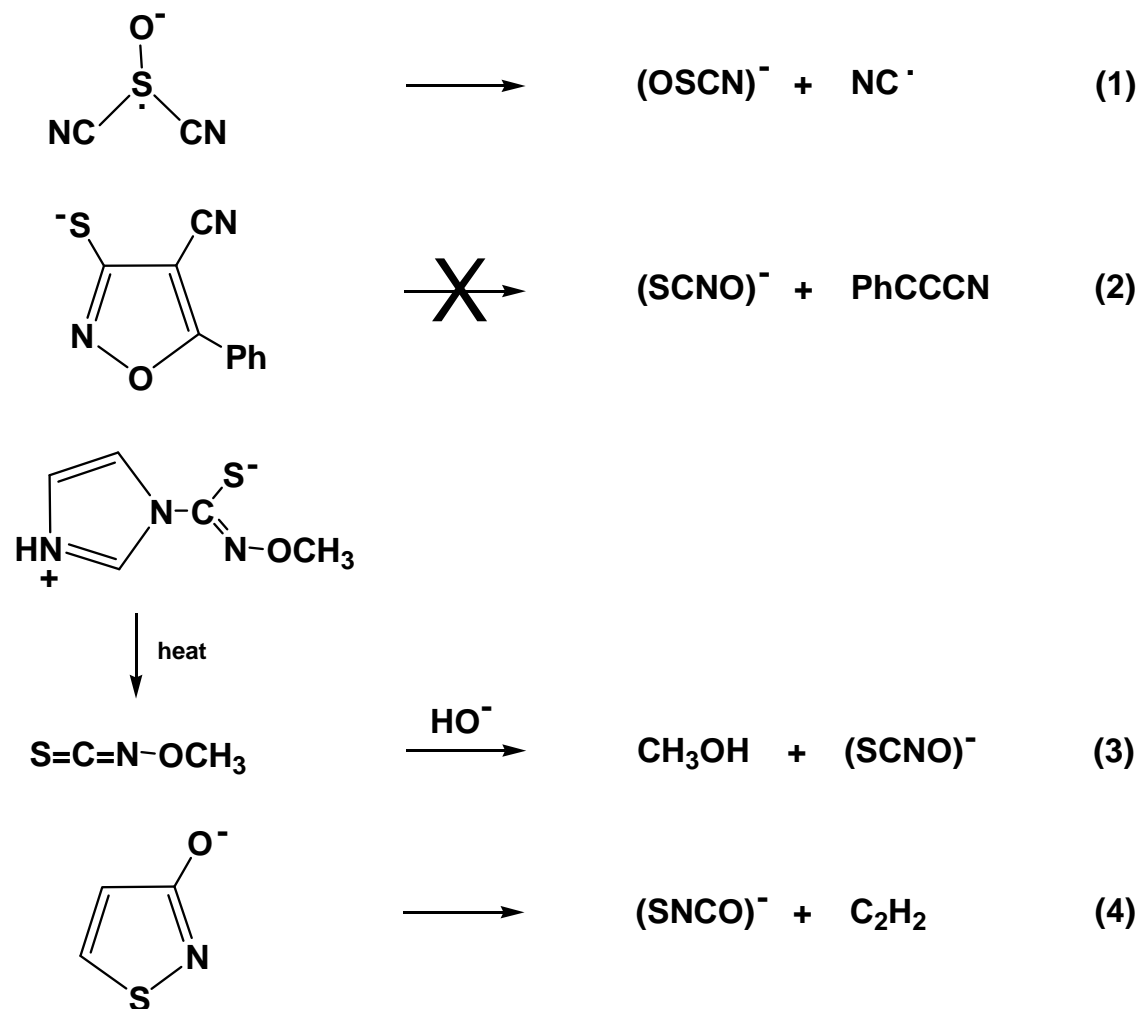
5.2.2 Syntheses of the Anions (OSCN)⁻, (SCNO)⁻ and (SNCO)⁻

Theoretical data suggests that the ground states of the isomers 1⁻ to 5⁻ should be stable. Having determined this, the next task was to synthesise each of these anions, then to examine their spectra in order to rationalise the formation of *m/z* 42 [(OCN)⁻ or (CNO)⁻] seen in the collision induced spectrum of the oxidation product (OSCN)⁻ reported earlier.¹⁷⁴ The anions 1⁻, 2⁻ and 3⁻ were formed by unequivocal routes, however no satisfactory routes to 4⁻ and 5⁻ were found.

The hypthiocyanite anion (OSCN)⁻ (1⁻) was produced (in the source of the VG ZAB 2HF mass spectrometer) by electron capture of NCS(O)CN to form the precursor radical anion which decomposes by loss of a nitrile radical to form the target anion in high yield [Equation (1) Scheme 5.2]. To form (SCNO)⁻ (2⁻) was a little more challenging. An S_N2 reaction between HO⁻ and 1-Thiomethyl-2-cyano-3-phenylisoxazole in the ion source of the mass spectrometer gave the precursor anion shown in Equation (2) (Scheme 5.2). This species was expected to undergo retro cleavage [as shown in Equation (2)] to form (SCNO)⁻. The retro reaction did not occur, instead the precursor anion lost nitric oxide. The required anion (SCNO)⁻ (2⁻) was formed as follows: Thermolysis of the heterocycle shown in Equation (3) (Scheme 5.2) gave neutral SCNOCH₃ as reported by Wentrup *et al.*¹⁸² The S_N2 reaction between HO⁻ and SCNOCH₃ in the ion source of the mass spectrometer gave the required anion (SCNO)⁻ (2⁻) as shown in Equation (3) (Scheme 5.2).

The third isomer, (SNCO)⁻ (3⁻) was made as summarised in Equation (4) (Scheme 5.2). 1-Hydroxyisothiazole was deprotonated in the source of the mass spectrometer using HO⁻ as the base. The CID mass spectrum (MS/MS) of this species is shown in Figure 5.5. There are three fragment anions in this spectrum. The first, the required species (SNCO)⁻ (*m/z* 74), is produced by retro cleavage [Equation (4) (Scheme 5.2)]. The

other two processes proceed through ion complex $[\text{NCO}^- (\text{HCCHS})]$ to form $(\text{NCO})^-$ (m/z 42) and $(\text{HC}_2\text{S})^-$ (m/z 57).



Scheme 5.2

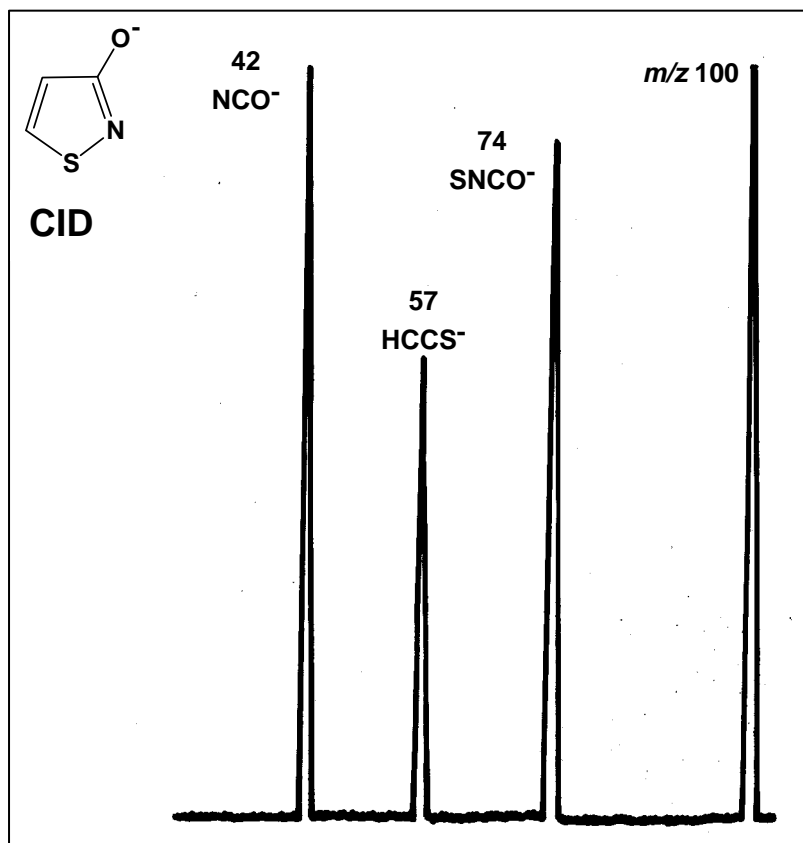


Figure 5.5 CID mass spectrum of the (M-H)⁻ anion of 1-Hydroxyisothiazole. VG ZAB 2HF mass spectrometer. For experimental details see Experimental section.

5.2.3 The Mass Spectra of the Isomers 1⁻, 2⁻ and 3⁻

In order to confirm the structures of the three isomeric anions synthesised as outlined above, we measured both their collision induced (CID) mass spectra (negative ion) and charge-reversal (⁻CR⁺) (positive ion) mass spectra. Charge reversal spectra are obtained by vertical two-electron (Franck-Condon) oxidation of an anion in a collision cell following the magnetic sector of the mass spectrometer. The resulting positive ion decompositions (arising from energised precursor cations) are measured by scanning the electric sector. A combination of the negative ion and positive ion decompositions of the precursor anion can be used to confirm (or refute) the proposed structure/bond connectivity of that anion.

The CID and ⁻CR⁺ mass spectra of the hypothiocyanite anion (OSCN)⁻ (1⁻) are shown in Figure 5.6(a) and (b) respectively. The corresponding spectra of the anions 2⁻ and 3⁻ are listed in Table 5.7. The negative ion CID mass spectrum of (OSCN)⁻ [Figure 5.6(a)] shows fragment anions at *m/z* 58 (SCN)⁻ and 26 (CN)⁻ consistent with the bond connectivity of (OSCN)⁻. There is no fragment anion at *m/z* 42 [(CNO)⁻ or (NCO)⁻] in Figure 5.6(a) analogous to that reported in the CID mass spectrum of *m/z* 74 from the oxidation of (SCN)⁻.¹⁷⁴ The ⁻CR⁺ spectrum of (OSCN)⁻ [Figure 5.6(b)] shows a precursor cation at *m/z* 74, with fragment cations at *m/z* 58 (SCN)⁺, 48 (SO)⁺, and 26 (CN)⁺ consistent with a precursor cation with the bond connectivity OSCN. These data are consistent with the formation of a stable species (OSCN)⁻ by the process shown in Equation (1) (Scheme 5.2). There are two minor peaks in the ⁻CR⁺ spectrum [Figure 5.6(b)] which indicate that some of the energised (OSCN)⁺ species may undergo rearrangement to other isomers [*e.g.* to form *m/z* 42 (CNO)⁻ or (OCN)⁻] and *m/z* 46 (NS)⁺.

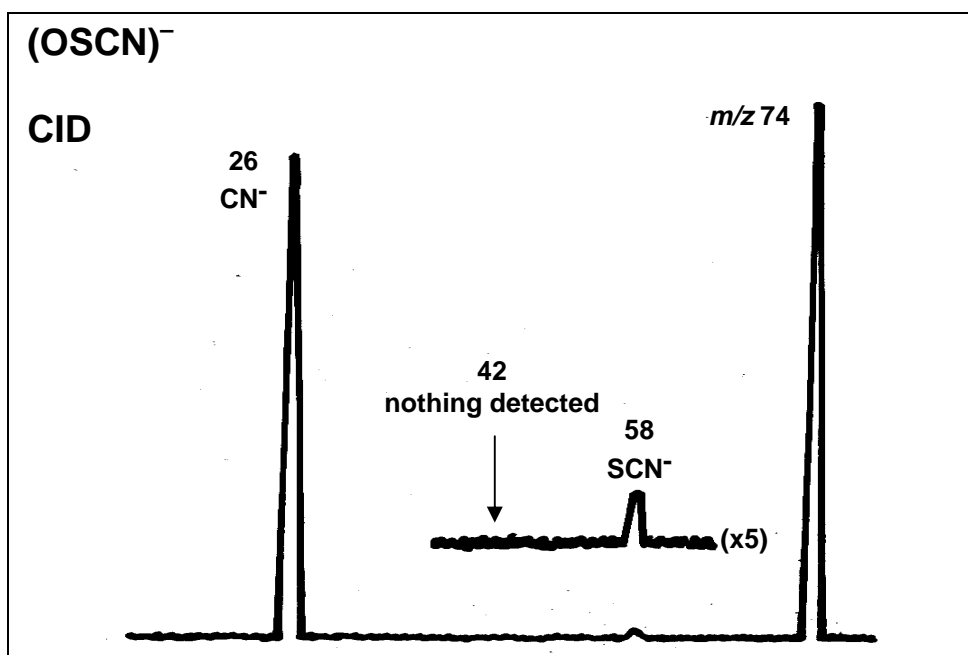


Figure 5.6(a) CID mass spectrum of $(\text{OSCN})^-$. VG ZAB 2HF mass spectrometer. For experimental details see Experimental section.

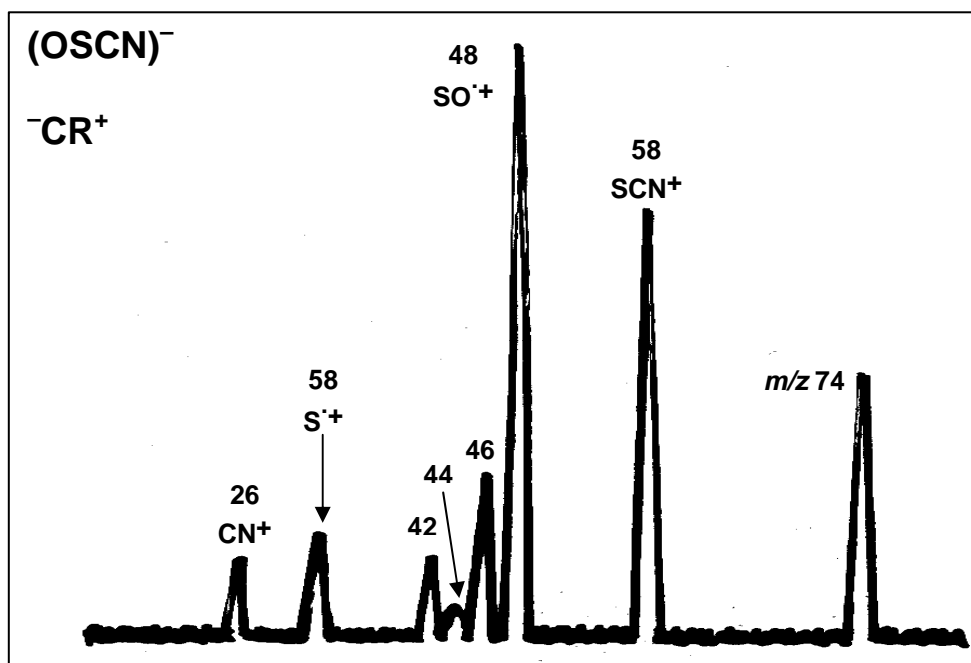


Figure 5.6(b) CR^+ spectrum of $(\text{OSCN})^-$. VG ZAB 2HF mass spectrometer. For experimental details see Experimental section.

TABLE 5.7

CID and ⁻CR⁺ Spectra of (SCNO)⁻ and (SNCO)⁻.

[*m/z* (composition) relative abundance in %]

(SCNO)⁻

CID 74 (SCNO)⁻ 100; 58 (SCN)⁻ 12; 44 (CS)⁻ 2; 42 (CNO)⁻ 9.

⁻CR⁺ 74 (SCNO)⁺ 95; 58 (SCN)⁺ 82^(a); 48 (SO)⁺ 38; 42 (CNO)⁺ 100^(b); 32 (S)⁺ 28; 28 (CO)⁺ 6.

(SNCO)⁻

CID 74 (SNCO)⁻ 68; 46 (NS)⁻ 100.

⁻CR⁺^(c) 74 (SNCO)⁺ no peak; 58 (SNC)⁺ 100; 46 (NS)⁺ 75; 44 (CS)⁺ 25; 42 (NCO)⁺ 18; 32 (S)⁺ 65; 28 (CO)⁺ 8.

- (a) This peak is composite, with a large gaussian peak superimposed on a smaller dish-shaped peak. This means that there are two losses of oxygen from *m/z* 74. This information together with the formation of *m/z* 48 (SO)⁺ and 28 (CO)⁺ indicates some deep seated skeletal reorganisation of a minor proportion of energised precursor cations.
- (b) (CNO)⁺ will rearrange to (NCO)⁺ under the reaction conditions of this experiment.¹⁷⁵
- (c) This spectrum is qualitatively similar to the CID spectrum of (SNCO)⁺ reported by Flammang *et al.*¹⁸³

The CID mass spectrum of $(\text{SCNO})^-$ (2^-) is listed in Table 5.7. The fragment ions observed at m/z 58 $(\text{SCN})^-$, 44 $(\text{CS})^-$ and 42 $(\text{CNO})^-$ are consistent with fragmentation of an anion with a bond connectivity of $(\text{SCNO})^-$. There are no ions in this spectrum that indicate any rearrangement of energised $(\text{SCNO})^-$. The $^- \text{CR}^+$ mass spectrum of the $(\text{SCNO})^+$ cation (Table 5.7) shows major fragment cations at m/z 58 $(\text{SCN})^+$ and 42 $(\text{CNO})^+$ consistent with a precursor cation of bond connectivity $(\text{SCNO})^+$. This spectrum contains smaller peaks at m/z 48 $(\text{SO})^+$ and 28 $(\text{CO})^+$ which must be formed following internal rearrangement of energised and decomposing $(\text{SCNO})^+$.

Finally, the CID mass spectrum of $(\text{SNCO})^-$ (3^-) shows a fragment anion at m/z 46 $(\text{NS})^-$ as the sole anion fragment.¹⁸³ Since there is no peak at m/z 42 $(\text{OCN})^-$ in this spectrum, $(\text{SNCO})^-$ cannot be the precursor of the m/z 42 peak in the CID spectrum of oxidised $(\text{NCS})^-$.¹⁷⁴ The $^- \text{CR}^+$ mass spectrum shown in Table 5.7 is consistent with the structure of the precursor anion being $(\text{SNCO})^-$.

5.3 SUMMARY & CONCLUSIONS

To summarise; (i) the theoretical calculations indicate that the singlet forms of the isomeric anions $(\text{OSCN})^-$ ($^11^-$), $(\text{SCNO})^-$ ($^12^-$), $(\text{SNCO})^-$ ($^13^-$) and $(\text{SOCN})^-$ ($^15^-$) are the ground state stable species, (ii) three of these anions, 1^- , 2^- and 3^- have been produced in the source of the VG ZAB 2HF mass spectrometer by unequivocal synthetic routes, (iii) a combination of CID and $^- \text{CR}^+$ spectra confirm that the three anions do not undergo rearrangement of the skeleton when energised, and (iv) the CID spectra of $(\text{OSCN})^-$ (1^-) and $(\text{SNCO})^-$ (3^-) show no fragment peaks at m/z 42 [$(\text{CNO})^-$ or $(\text{OCN})^-$], while that of $(\text{SCNO})^-$ (2^-) does exhibit a peak at m/z 42 $(\text{CNO})^-$.

From (i) a consideration of the mass spectrometric data given previously,¹⁷⁴ and (ii) the theoretical and experimental evidence provided by the present study, it is concluded that oxidation of $(\text{SCN})^-$ by peroxide gives two isomeric product anions. The major component is the hypothiocyanite anion $(\text{OSCN})^-$. The presented data suggests that the minor component could be $(\text{SCNO})^-$.

5.4 EXPERIMENTAL SECTION

5.4.1 Mass Spectrometric Methods

For a detailed description of the experiment and the instrument used, see Reference¹⁸⁴. In brief, the experiments were performed using a two-sector modified VG ZAB 2HF mass spectrometer with BE configuration, where B and E represents the magnetic and electric sectors, respectively. The anions (OSCN)⁻, (SCNO)⁻ and (SNCO)⁻ were formed in the chemical ionisation ion source by the reactions shown in Scheme 5.2. Typical source conditions were as follows: source temperature 200°C, repeller voltage -0.5 V, ion extraction voltage 7 kV, mass resolution $m/\Delta m \geq 1500$. Each neutral precursor was inserted into the ion source through the direct probe, which was heated to 100°C to give a measured pressure of *ca.* 10⁻⁵ Torr inside the source housing. In the cases of (SCNO)⁻ and (SNCO)⁻, the source also contained HO⁻ (from H₂O) to give a measured source pressure of 10⁻⁴ Torr (estimated total source pressure is 10⁻¹ Torr). Collision Induced Dissociation (CID) spectra were determined using B to select m/z 74 in each case, and utilising argon as the target gas in the first collision cell following B. The pressure of argon in the first cell was maintained such that 80% of the precursor ion beam was transmitted through the cell. This corresponds to an average of 1.1-1.2 collisions per ion.²⁹ Product anion peaks resulting from CID processes were recorded by scanning E.

Charge reversal (⁻CR⁺) spectra^{30, 31, 89} were recorded using single collision conditions in collision cell 1 (O₂, 80% transmission of main beam).

5.4.2 Materials and Synthesis

The precursors used in this study were prepared and supplied by Dr Suresh Dua and Dr Mark Fitzgerald at the University of Adelaide with many thanks. The precursor molecules NCS(O)CN,¹⁸⁵ 1-Thiomethoxy-2-cyano-3-phenylisoxazole,¹⁸⁶ 3-Hydroxyisothiazole,¹⁸⁷ and 1-(*N*-Methoxythiocarbamoyl)imidazole¹⁸² were prepared by literature methods.

5.4.3 Theoretical Methods

Geometry optimisations were carried out with the Becke 3LYP method^{65, 103} using the 6-31+G(d) basis set¹⁰⁴⁻¹⁰⁶ within the GAUSSIAN 98¹⁸⁸ suite of programs. Stationary points were characterised as either minima (no imaginary frequencies) or transition structures (one imaginary frequency) by calculation of the frequencies using analytical gradient procedures. The minima connected by a given transition structure were confirmed by Intrinsic Reaction Coordinate (IRC) calculations.¹⁰⁷ The calculated frequencies were also used to determine zero-point vibrational energies which were used as a zero-point correction for the electronic energies. We have previously reported the success of the B3LYP method in predicting geometries of unsaturated chain structures, and that this method produces optimised structures, at low computational cost, that compare favourably with higher level calculations*.¹⁰⁸ Higher level single point energies were calculated using the CCSD(T) method^{109, 110} together with the Dunning aug-cc-pVDZ basis set.¹⁰⁴⁻¹⁰⁶ All calculations were carried out on the Alpha Server at the Australian Partnership for Advanced Computing (APAC) National Facility (Canberra).

* To cite a particular example, the value of the adiabatic electron affinity of CCCC was calculated to be 3.65 eV at the same level of theory used in this study,⁸³ while the experimental value is reported to be 3.88 eV.^{111, 112}

PART II

The Modified Finnigan LCQ Mass Spectrometer. Gas Phase Ion-Molecule Experiments

CHAPTER VI

Selectively Generated Gas Phase Carbanions

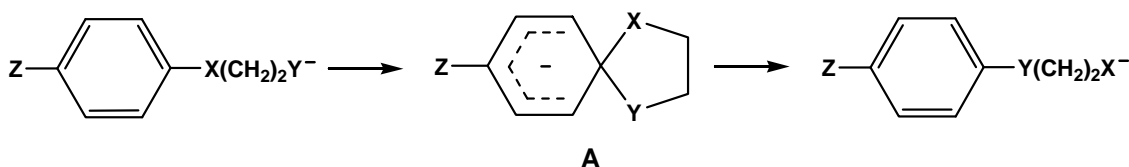
+ CS₂.

Diagnostic Adduct Fragmentations

6.1 INTRODUCTION

6.1.1 The Smiles Rearrangement

The Smiles rearrangement¹⁸⁹⁻¹⁹³ discovered in the early thirties is an intramolecular nucleophilic aromatic substitution reaction and an example is illustrated below in Scheme 6.1.



Scheme 6.1

In the condensed phase Smiles rearrangement above, X is a good leaving group *e.g.* S, SO, SO₂, O or COO, Y is a strong nucleophile, usually a heteroatom *e.g.* O, S or NR, and Z is the substitution activating electron withdrawing group *e.g.* nitro, sulfonyl or halogen. The electron withdrawing group can activate substitution when in the aromatic *ortho* position, preferably, but also in the *para* position as well, with the *ipso** (Smiles) intermediate denoted as A (Scheme 6.1). Recently the condensed phase ionic Smiles rearrangement was investigated to determine whether the electron withdrawing group in the *ortho* position (substituents in the *para* position were found to have little or no effects on the kinetics of reactions)¹⁹⁴ facilitates the substitution due to electronic effects (electron donation) or reaction activation is due to the steric effects at this position. The electronic effects postulation is more favoured over the steric effects.¹⁹⁴⁻¹⁹⁶

The Smiles rearrangement has had a number of synthetic uses including most recently the one pot synthesis of organic compounds.^{197, 198} It has also been utilised in the production of biomolecules¹⁹⁹ and used for the forming of scaffolds for medicinal chemistry.²⁰⁰

* *ipso* describes two substituents sharing the same ring position in an intermediate compound.

There have also been reported examples of radical Smiles type rearrangements in the synthesis of biphenyl derivatives from aryl radicals.²⁰¹⁻²⁰⁴

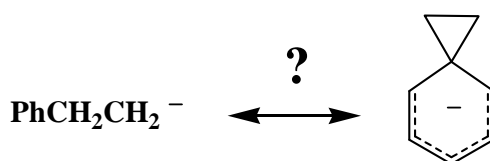
A particular variation on the Smiles rearrangement, the Truce-Smiles rearrangement discovered in the late fifties, has two distinct differences over the Smiles rearrangement. Firstly, it involves attack of a carbanion centre ($Y = RC^-$, Scheme 6.1) rather than a nucleophile at an *ipso* electrophilic centre, and secondly, without the need of the activating electron withdrawing group in the *ortho* or *para* position. The Truce-Smiles variation is more favoured synthetically due to the ability of this reaction selectively forming carbon-carbon (C–C) bonds.²⁰⁵

Gas phase Smiles rearrangement reactions have not been as extensively studied as their condensed phase counterparts. However, it is seen that Smiles rearrangements readily occur in the gas phase without the need for activation of the aromatic ring by electron withdrawing groups in either of the ring substituted positions as seen in the condensed phase. This is possibly due to the solvent effect in the condensed phase reducing the rate of reaction compared to that of the gas phase.²⁰⁶

Earlier gas phase studies using heavy atom labelling (¹³C and ¹⁸O), showed that the product ion PhO^- from $PhO(CH_2)_nO^-$ and products PhO^- and PhS^- from $PhS(CH_2)_nO^-$ (where $n = 2$) are formed exclusively from *ipso* (Smiles) intermediates [(A, Scheme 6.1) where $X=Y=O$ or $X=S, Y=O$].²⁰⁷ However it was also seen that as n increases then the proportion of Smiles rearrangement decreases favouring more competitive S_Ni processes.²⁰⁷

The work carried out here is a return to earlier gas phase *ipso* (Smiles) rearrangement studies.^{208, 209} With the use of a modified Finnigan LCQ ion trap mass spectrometer and aided with theoretical investigations, we wish to determine whether selectively generated gas phase carbanions undergo ion-molecule reactions with CS₂ in the ion trap of the mass spectrometer, producing adducts which undergo collision induced cleavages diagnostic of the structures of the initial carbanions.

The carbanions that have been chosen to react with CS₂ are (i) the phenyl anion (C₆H₅⁻), (ii) the isomers PhCH₂⁻ and (*o*-CH₃C₆H₄⁻) and (iii) the β-phenylethyl anion (PhCH₂CH₂⁻) together with other isomeric anions of C₈H₉⁻. In (iii), we hope also to determine whether the ion-molecule reaction with CS₂ can identify whether the β-phenylethyl anion is a stable species in the gas phase^{210, 211} or does it undergo rearrangement *via* the *ipso* (Smiles) spiro [2,5] octadienyl structure^{211, 212} (Scheme 6.2) or to some other intermediate.



Scheme 6.2

6.1.2 The Finnigan LCQ Ion Trap Mass Spectrometer

A modified Finnigan LCQ ion trap mass spectrometer (San Jose, CA, USA) (discussed later) was used in this work in order to perform ion-molecule reactions within the ion trap. A schematic representation of the mass spectrometer (excluding modifications) is shown in Figure 6.1.

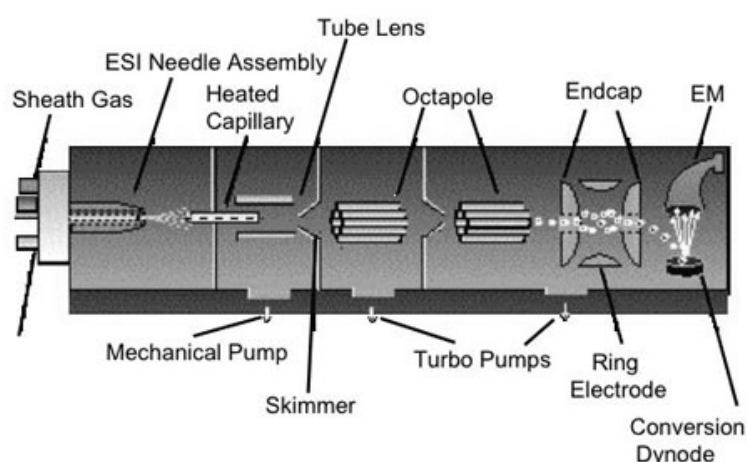


Figure 6.1 A schematic representation of the Finnigan LCQ ion trap mass spectrometer.

Ions are generated in the ion source of the LCQ mass spectrometer by electrospray ionisation (ESI) (discussed later) are then accelerated *via* a potential difference through an octapole focussing region and then into an ion trap.

The ion trap is constructed of three electrodes (two end cap electrodes and a central ring electrode), all of a hyperbolic cross section²¹³ which creates a chamber in which the ions are 'trapped' (Figure 6.2). A RF voltage is applied to the central ring electrode which generates an electric field within the ion trap now imparting a force upon the ion that is proportional to its distance from the centre of the trap. This applied force allows ions of differing mass-to-charge ratios to follow a stable trajectory within the ion trap and remain there for a few seconds. A mass spectrum is generated by increasing the amplitude of the RF voltage which destabilises the trajectories of the ions, ejecting them in m/z sequence from the ion trap through small openings in the end cap to a detector which records the mass spectrum.

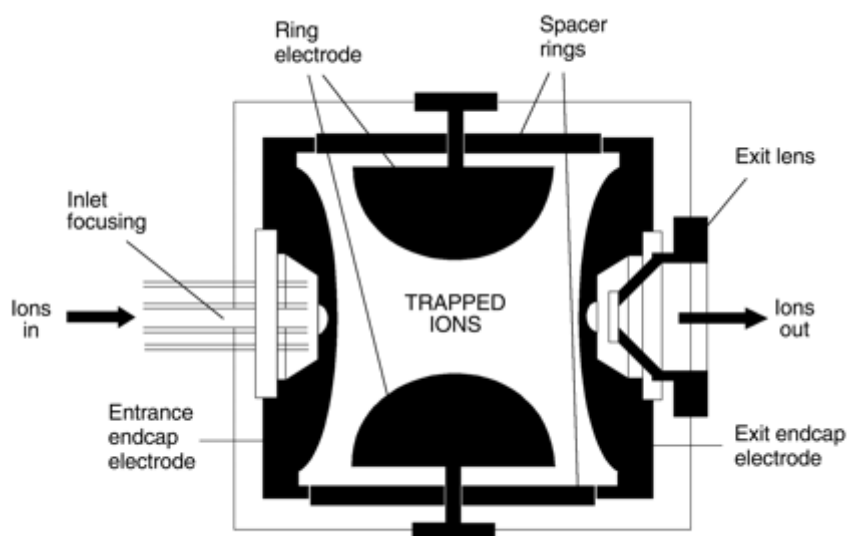


Figure 6.2 A schematic representation of the Finnigan LCQ ion trap.

The LCQ mass spectrometer is able to facilitate MS/MS (MS²) experiments. The ion of interest is isolated within the ion trap and the internal energy of the system is increased so that the ion now undergoes more energetic collisions with the helium gas within the trap generating product fragmentation ions. The product fragmentation ions can now be sequentially ejected from the ion trap and recorded by the detector.²¹⁴

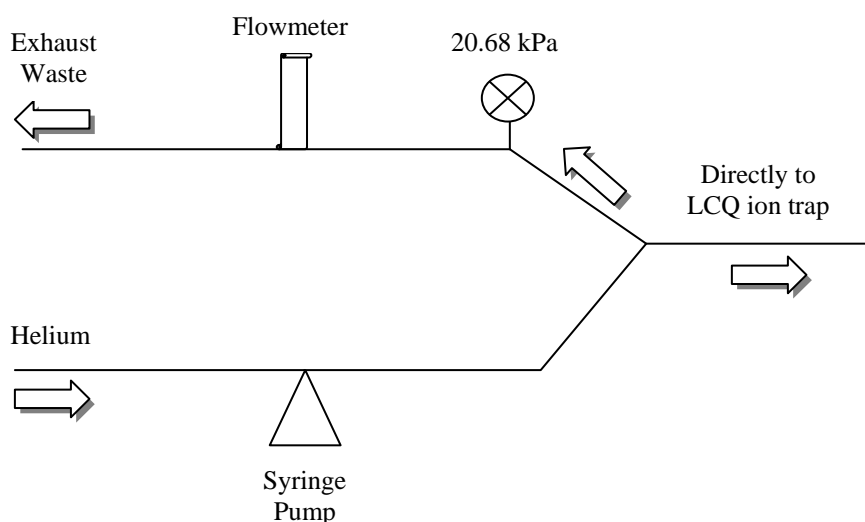


Figure 6.3 A schematic representation of the modifications to the Finnigan LCQ mass spectrometer.

The neutral reagent (CS₂) was introduced continuously into the trap *via* the He background gas flow through a gas tight septum using a Harvard Apparatus Model '11' Plus syringe pump (Holliston, MA, USA) and a 500 μ L gas tight SGE syringe (Ringwood, Victoria, Australia) fitted with a Teflon plunger. Vaporisation of the neutral reagent was done using Thermolyne[®] fibrox-insulated heating tape (2.5 cm x 0.61 m, 208 W) purchased from Sigma-Aldrich (Castle Hill, NSW, Australia) and a Variac Autotransformer (Australia) and an Enviro-Safe[®] thermometer (-10-110°C) as the temperature controller. The heating tape, wound from just before the syringe pump to the external He port, was heated to approximately 60°C (CS₂ b.p. 46°C)²¹⁵ to allow vaporisation and gas phase introduction of the neutral reagent directly into the trap, which operates at atmospheric temperature.^{216, 217}

The Finnigan LCQ uses a constriction capillary (0.4 nm o.d., 0.1 nm i.d.) to control the flow of He into the trap and it is designed to maintain 1.5-1.75 x 10⁻³ Torr of pressure in the trap when 20.68 kPa of helium pressure is applied to the capillary. In the conventional Finnigan LCQ system, the 20.68 kPa is maintained by an internal mechanical pressure regulator that steps down the 275 \pm 70 kPa of He that is delivered

at the external port. To avoid the dead volume in the internal pressure regulator it was bypassed and the He mixture (20.68 kPa) was delivered directly to the capillary.

A majority of the He/reagent mixture exits the system *via* an Aalborg flowmeter (Orangeburg, NY, USA) into the waste exhaust while an external Swagelok 'S' model electronic pressure transducer (Adelaide, South Australia, Australia) maintains the 20.68 kPa required to deliver $\sim 1 \text{ mL min}^{-1,216}$ into the trap in order to maintain optimum operating pressure.

6.1.4 The Waters/Micromass Q-ToF 2 Mass Spectrometer

Another mass spectrometer used in this work is the Waters/Micromass Q-ToF 2 time-of-flight mass spectrometer (Waters/Micromass, Manchester, UK). A schematic representation of this is shown in Figure 6.4.

The Waters/Micromass Q-ToF 2 consists of two sectors, firstly the quadrupole analyser followed by the time-of-flight (ToF) tube.

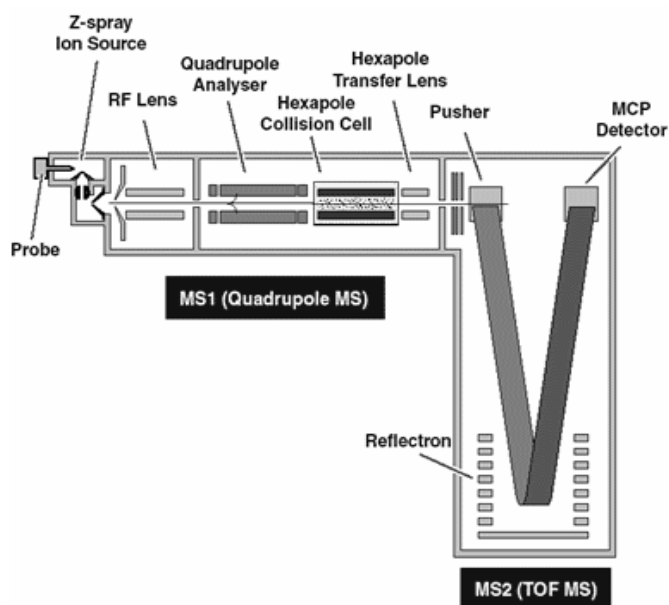


Figure 6.4 A schematic representation of the Waters/Micromass Q-ToF 2 mass spectrometer.

Ionised molecules [*via* electrospray ionisation (ESI) discussed later)] are generated in a Z-spray configured source and accelerated *via* a potential difference towards the quadrupole analyser. Manipulation of the cone voltage allows the selectivity of ions based on their mass-to-charge (m/z) ratios *i.e.* the smaller the voltage the smaller the m/z therefore the smaller the ions.

The quadrupole analyser consists of two pairs of parallel metal rods. Each opposing rod pair is connected together electrically, and a radio frequency (RF) voltage is applied between one pair of rods and the other. A direct current (DC) voltage is then superimposed on the RF voltage. At a given ratio of RF to DC voltages, only ions of a certain mass-to-charge ratio (m/z) (resonated ions) will traverse the quadrupole as an oscillating molecular beam and reach the detector, other ions have unstable trajectories (non-resonated ions) and collide with the rods (Figure 6.5).

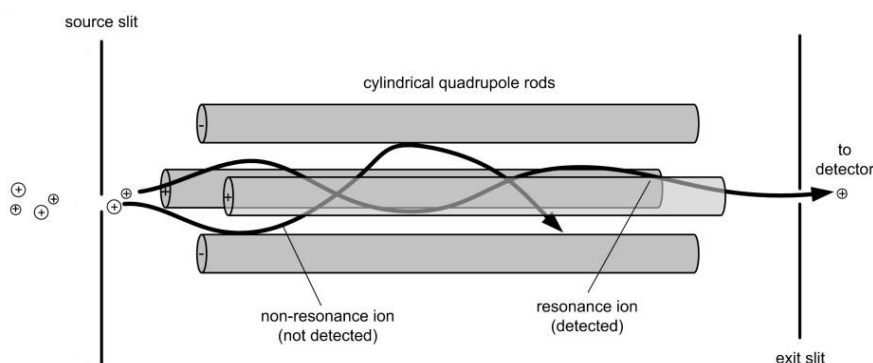


Figure 6.5 A schematic representation of the ion motion through a quadrupole analyser. This process is analogous to that for a octapole arrangement.

The quadrupole analyser allows selection of an ion with a particular mass-to-charge ratio and it also allows the operator to scan for a range of m/z values by continuously varying the applied ratio of RF to DC voltages.

In the MS mode all ions are allowed to pass through the quadrupole analyser where they then accumulate at the pusher so they can leave at the same time. The pusher

accelerates the ions so that they all possess the same translational energy as they pass through the ToF tube. With all the ions having the same translational energy and the translational energy being proportional to both mass and velocity, the heavier the ion the slower it will traverse the ToF tube therefore reaching the detector after lighter ions, which then is interpreted as a mass spectrum.

In MS/MS (MS²) mode, an ion of interest (based on its m/z value) is isolated in the quadrupole analyser and only this ion is allowed to pass into the hexapole collision cell where it is energised by CID (discussed earlier in Chapter 1) using argon or helium as the collision gas.^{218, 219} The resulting product ions are then accelerated into the ToF tube *via* the pusher to produce MS² data of the initially selected ion.

6.1.5 Electrospray Ionisation

Electrospray is the terminology applied to a small flow of liquid (generally 1-10 $\mu\text{L min}^{-1}$) from a heated capillary needle (between 150-200°C) when a potential difference (between 2-5 kV) is applied between the end of the capillary needle and a cylindrical electrode located a small distance away (typically 0.3-2 cm).⁵ If the potential difference applied between the capillary needle and the electrode is positive the droplets/ions will be positive (and the opposite for negative droplets/ions). Due to charge accumulation at the capillary needle, the exiting liquid forms a conical shape referred to as the Taylor cone (Figure 6.6) which becomes unstable at the tip due to an increase in charge density.²²⁰ Under these conditions, which are also near atmospheric, the liquid exits the capillary needle as a fine aerosol plume of very small charged droplets.

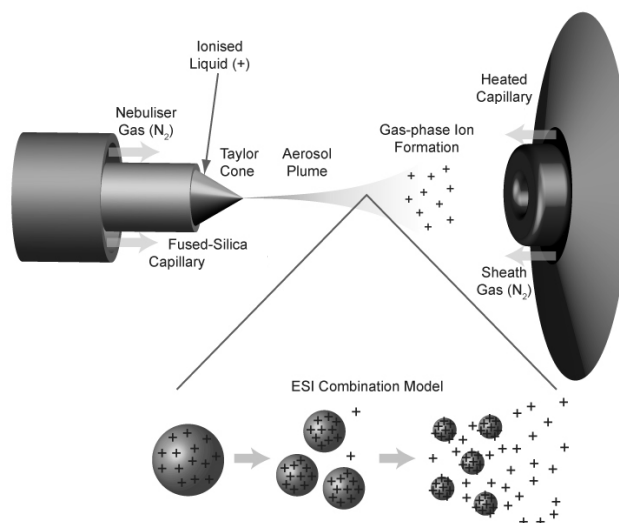


Figure 6.6 Electro spray Ionisation (ESI) overview.

The introduction of nebulising gas (N₂) into to the system, along with warming, aids in desolvating the ions and reducing the radius of the droplet. As the radius (R) (Equation 6.1) of the charged droplet decreases at a constant charge (q), an increase in the concentration of charge leads to an increase in electrostatic (Coulombic) repulsion at the surface of the droplet. At this point, the Rayleigh stability limit, as defined by the Rayleigh equation (Equation 6.1), is reached.^{220, 221}

$$q = 8\pi(\epsilon_0\gamma R^3)^{1/2}$$

Where; ϵ_0 = permittivity of the vacuum, γ = droplet surface tension

Equation 6.1

The Rayleigh stability limit is the point where the electrostatic (Coulombic) repulsion equals the surface tension force and the charged droplet becomes unstable and divides.^{220, 221} Under a continual cycle of these conditions the very small droplets are now reduced to molecular ions (Figure 6.7).

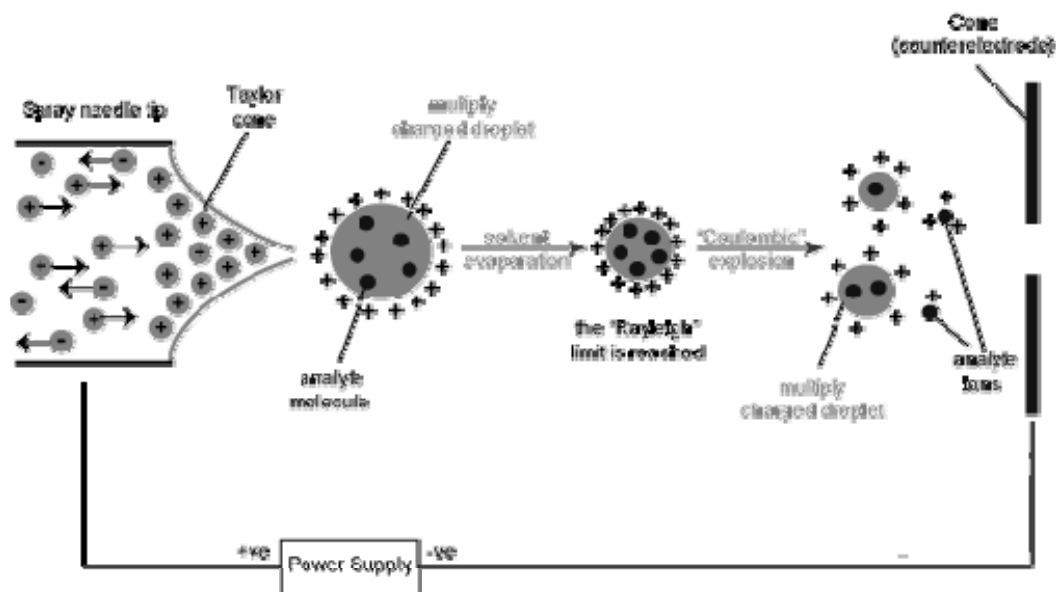


Figure 6.7 A schematic representation of the Electro spray Ionisation (ESI) process and Rayleigh stability limit.

6.2 RESULTS & DISCUSSION

6.2.1 Reaction of the Phenyl Anion with CS₂

The phenyl anion ($C_6H_5^-$) was formed in the Finnigan LCQ ion trap mass spectrometer by decarboxylation of the benzoate anion [$(C_6H_5CO_2^-)$ formed by deprotonating benzoic acid in the ESI source].²²² The reaction of $C_6H_5^-$ with CS₂ forms $C_6H_5CS_2^-$ (m/z 153) and CID MS⁴ of the adduct gives $C_6H_5S^-$ (m/z 109) as the only observable fragment ion. A reduction in the pressure of the added neutral reagent (CS₂) resulted in the detection of a minor peak corresponding to m/z 77 ($C_6H_5^-$) accompanying m/z 109 (Figure 6.8).

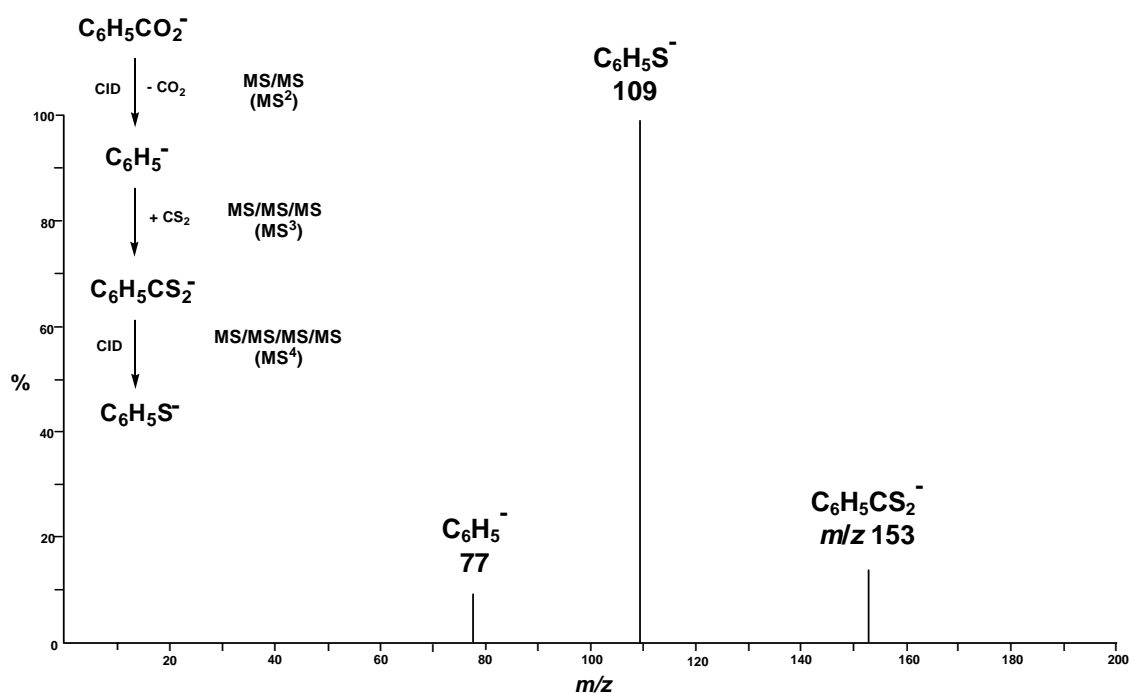


Figure 6.8 CID MS⁴ spectrum of $C_6H_5CS_2^-$ (m/z 153) formed from the reaction of CS₂ with $C_6H_5^-$ ($C_6H_5^-$ formed by decarboxylating $C_6H_5CO_2^-$ in the ESI source). Modified Finnigan LCQ ion trap mass spectrometer.²²³ For experimental details see Experimental section.

Anions can react with CS₂ in the gas phase at either the C or S centre.²²⁴ The ion observed at m/z 153 could therefore have one of two possible bond connectivities [(C₆H₅CS₂⁻) or (C₆H₅S⁻C=S)], so the CID mass spectrum of deprotonated dithiobenzoic acid (C₆H₅CS₂H) was measured using a Waters/Micromass Q-ToF 2 mass spectrometer to deduce the point of reactivity between the anion and the neutral. The Q-ToF 2 was used for this purpose rather than the LCQ because the Q-ToF 2 uses a more efficient gas CID process for accelerated ions than that of the less efficient collisional processes carried out in the mass analyser of the LCQ.

In the CID MS² of C₆H₅CS₂⁻ two fragment ions, m/z 77 [(C₆H₅⁻) 100%] and m/z 109 [(C₆H₅S⁻) 64%] were observed. This is consistent with the adduct (C₆H₅CS₂⁻) seen from the ion-molecule reaction in the LCQ, and confirms that the fragment anion C₆H₅⁻ is produced in the LCQ ion trap but reacts immediately with the C centre of CS₂ on formation before a Smiles type rearrangement.

The reaction coordinate pathway of the possible Smiles rearrangement described above was investigated at the UCCSD(T)/6-31+G(d,p)//B3LYP/6-31+G(d,p) level of theory* and results are shown in Figure 6.9 with full details of geometries and energies listed in Tables 6.1 and 6.1(a). No *ipso* intermediate was able to be isolated. For C₆H₅CS₂⁻ (Figure 6.9), the reaction proceeds through an *ipso* transition state (+314.5 kJ mol⁻¹) to C₆H₅S⁻CS, which is energised and may decompose to C₆H₅S⁻ and CS in an overall reaction endothermic by +235.2 kJ mol⁻¹.

* *An examiner has asked why the UCCSD(T) (unrestricted open-shell) level of theory has been applied to closed-shell singlets in this chapter? In terms of single point calculations, it has been generally accepted that the UCCSD(T) level of theory accounts for spin-polarisation, the process which gives realistic spin densities, and therefore can give a better description for diradicals. However, in terms of this study, the processes do not involve biradicals, the benzene ring stabilises the charge, which makes some transition states have the diradical character. Thus the UCCSD(T) level of theory can provide a qualitatively more correct description of bond breaking.*

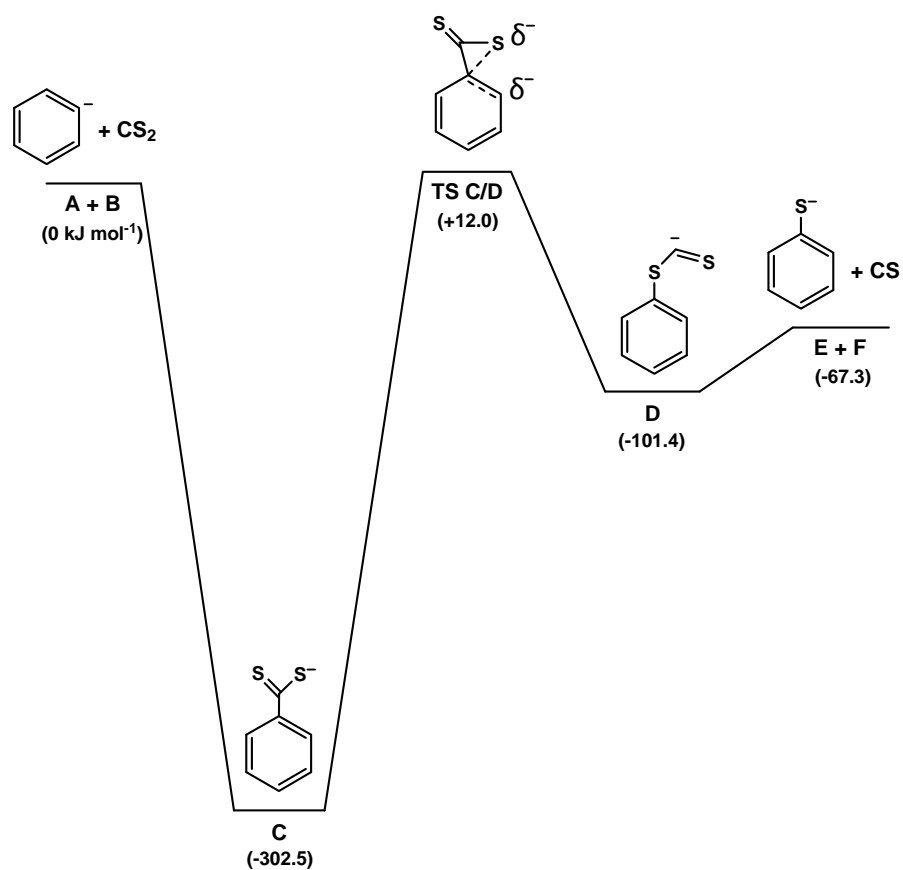


Figure 6.9 Reaction coordinate pathway for the Smiles rearrangement of $C_6H_5CS_2^-$. Relative energies in kJ mol^{-1} . Level of theory used - UCCSD(T)/6-31+G(d,p)//B3LYP/6-31+G(d,p). Structures shown in the Figure show bond connectivities only. For full structural details see Tables 6.1 and 6.1(a).

TABLE 6.1

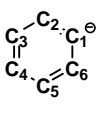
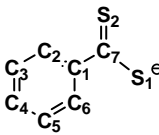
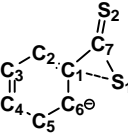
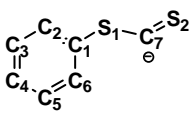
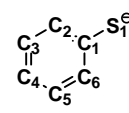
Reaction Coordinate Pathway for the Smiles Rearrangement of C₆H₅CS₂⁻.

Anion Geometries and Energies.

Carbon-Sulfur Skeleton Only.

Level of theory used - UCCSD(T)/6-31+G(d,p)//B3LYP/6-31+G(d,p)

Relative energies in kJ mol⁻¹ relative to A+B (0 kJ mol⁻¹)

					
	A	C	TS C/D	D	E
State	¹ A ₁	¹ A	¹ A	¹ A'	¹ A'
Symmetry	C _{2v}	C ₁	C ₁	C _s	C _s
Energy (Hartrees)	-230.85327 [-1064.1525]	-1064.26773	-1064.14790	-1064.19111	-628.60034 [1064.17814]
Energy Relative to A+B	0 [A+B]	-302.5	+12.0	-101.4	-67.3 [E+F]
Dipole Moment (Debye)	5.63	7.94	3.33	9.53	6.45
Bond Lengths (Å)					
C ₁ S ₁	-	-	3.019	1.791	1.750
C ₁ C ₂	1.421	1.407	1.440	1.405	1.424
C ₁ C ₇	-	1.512	1.491	-	-
C ₂ C ₃	1.407	1.396	1.388	1.396	1.395
C ₃ C ₄	1.402	1.400	1.405	1.401	1.403
C ₄ C ₅	1.401	1.398	1.405	1.399	1.403
C ₅ C ₆	1.407	1.397	1.387	1.397	1.394
C ₆ C ₁	1.422	1.408	1.441	1.407	1.424
C ₇ S ₁	-	1.706	1.937	1.823	-
C ₇ S ₂	-	1.705	1.654	1.682	-
Bond Angles (°)					
S ₁ C ₇ S ₂	-	125.5	104.4	112.4	-
S ₁ C ₁ C ₂	-	-	114.9	123.0	122.4
S ₁ C ₁ C ₆	-	-	118.8	118.4	122.3
S ₁ C ₇ C ₁	-	117.2	75.6	-	-
S ₂ C ₇ C ₁	-	117.2	180.0	-	-
C ₁ C ₂ C ₃	125.0	121.3	120.9	120.3	122.3
C ₂ C ₃ C ₄	119.9	120.4	121.7	121.0	121.0
C ₃ C ₄ C ₅	118.2	119.0	117.5	118.9	118.0
C ₄ C ₅ C ₆	119.9	120.5	121.8	120.5	121.0
C ₅ C ₆ C ₁	124.9	121.2	120.8	120.8	122.3
C ₆ C ₁ C ₂	112.0	117.6	115.1	118.6	115.3
C ₇ C ₁ C ₂	-	121.2	120.0	-	-
C ₇ S ₁ C ₁	-	-	56.7	103.4	-
Dihedral Angle (°)					
C ₁ C ₂ C ₃ C ₄	0.0	1.5	-7.2	0.0	0.0
S ₁ C ₁ C ₂ C ₃	-	-	-118.6	180.0	180.0
C ₂ C ₃ C ₄ C ₅	0.0	-0.8	-2.6	0.0	-0.3
S ₂ C ₇ S ₁ C ₁	-	-	180.0	-	-

S₁=C=S₂ [B]; State ¹A₁, Symmetry C_{2v}, Energy (Hartrees) -833.29923, Dipole 0.003 Debye, S₁-C 1.563Å, C=S₂ 1.563Å, S₁-C=S₂ 179.7°C=S [F]; State ¹SG, Symmetry C_s, Energy (Hartrees) -435.5778, Dipole 1.74 Debye, C=S 1.544Å

TABLE 6.1(a)

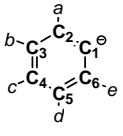
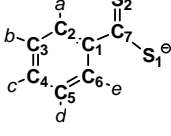
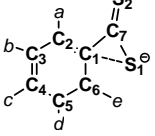
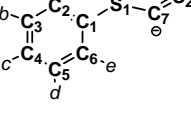
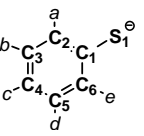
Reaction Coordinate Pathway for the Smiles Rearrangement of C₆H₅CS₂⁻.

Anion Geometries and Energies.

Hydrogens Only.

Level of theory used - UCCSD(T)/6-31+G(d,p)//B3LYP/6-31+G(d,p)

Relative energies in kJ mol⁻¹ relative to A+B (0 kJ mol⁻¹)

					
	A	C	TS C/D	D	E
State	¹ A ₁	¹ A	¹ A	¹ A'	¹ A'
Symmetry	C _{2v}	C ₁	C ₁	C _s	C _s
Energy (Hartrees)	-230.85327 [-1064.1525]	-1064.26773	-1064.14790	-1064.19111	-628.60034 [1064.17814]
Energy Relative to A+B	0 [A+B]	-302.5	+12.0	-101.4	-67.3 [E+F]
Dipole Moment (Debye)	5.63	7.94	3.33	9.53	6.45
Bond Lengths (Å)					
C ₂ a*	1.097	1.085	1.087	1.086	1.087
C ₃ b	1.094	1.088	1.089	1.088	1.090
C ₄ c	1.090	1.087	1.087	1.087	1.088
C ₅ d	1.094	1.089	1.090	1.089	1.090
C ₆ e	1.097	1.084	1.086	1.088	1.087
Bond Angles (°)					
aC ₂ C ₁	118.9	118.1	118.4	117.5	117.8
bC ₃ C ₄	119.6	120.0	119.7	119.7	119.8
cC ₄ C ₅	120.9	120.5	121.2	120.5	121.1
dC ₅ C ₆	120.4	119.5	118.5	119.4	119.8
eC ₆ C ₁	119.0	118.1	118.4	119.2	117.8
Dihedral Angle (°)					
aC ₂ C ₃ C ₄	180.0	-178.1	-179.0	180.0	180.0
cC ₄ C ₃ C ₂	180.0	179.2	-179.6	180.0	180.0
cC ₄ C ₅ C ₆	180.0	179.3	179.6	180.0	180.0
eC ₆ C ₅ C ₄	180.0	-178.1	180.0	-179.0	180.0

* Individual Hydrogens have been designated letters a - e

S₁=C=S₂[B]; State ¹A₁, Symmetry C_{2v}, Energy (Hartrees) -833.29923, Dipole 0.003 Debye, S₁=C 1.563Å, C=S₂ 1.563Å, S₁=C=S₂ 179.7°C=S [F]; State ¹SG, Symmetry C_v, Energy (Hartrees) -435.5778, Dipole 1.74 Debye, C=S 1.544Å

From the reaction coordinate pathway (Figure 6.9) we can see that the reaction between the phenyl anion and CS₂ is more energetically favourable when the phenyl anion attacks at the carbon centre rather than at S (+201.1 kJ mol⁻¹). The theoretical results are consistent with the experimental observations.

The precursor benzoate anion (C₆H₅CO₂⁻) which was used to generate the phenyl anion, is also a possible candidate for a Smiles type rearrangement, so the negative ion CID MS² of C₆H₅CO₂⁻ (C₆H₅CO₂⁻ formed by deprotonating benzoic acid in the ESI source) was measured using the Waters/Micromass Q-ToF 2 mass spectrometer. The only observable fragment was that seen at *m/z* 77 (C₆H₅⁻) confirming that CID of the benzoate anion only generates the decarboxylated phenyl anion and not that of an anion from a Smiles type rearrangement [*m/z* 93 (C₆H₅O⁻)].

6.2.2 The Smiles Rearrangement of (PhCOS)⁻

The possible Smiles rearrangement of the anion (PhCOS)⁻ was investigated to compare with the rearrangements of C₆H₅CS₂⁻ and C₆H₅CO₂⁻ carried out above. The negative ion CID MS² of (PhCOS)⁻ (formed by deprotonating thiobenzoic acid in the ESI source) was measured using the Waters/Micromass Q-ToF 2 mass spectrometer and the spectrum is seen in Figure 6.10.

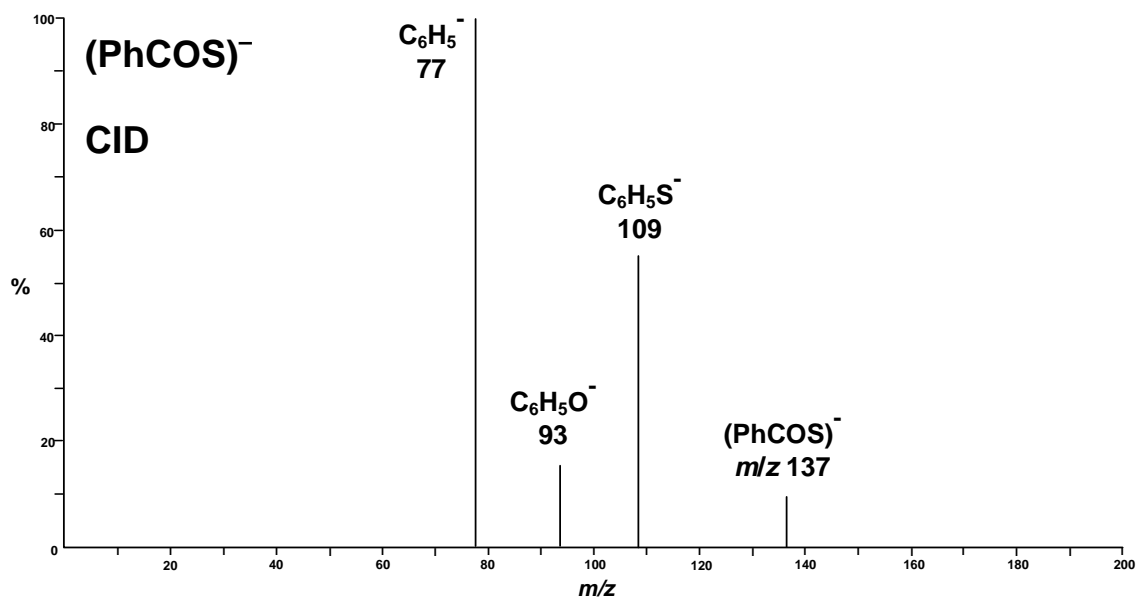


Figure 6.10 CID MS² spectrum of (PhCOS)⁻ (*m/z* 137). Waters/Micromass Q-ToF 2 mass spectrometer. For experimental details see Experimental section.

From the CID MS² spectrum of (PhCOS)⁻ above, the two ions observed at *m/z* 109 (C₆H₅S⁻) and *m/z* 93 (C₆H₅O⁻) indicate that (PhCOS)⁻ undergoes two competitive Smiles type rearrangements.

The reaction coordinate pathways for the two competing Smiles rearrangements described above were investigated at the UCCSD(T)/6-31+G(d,p)//B3LYP/6-31+G(d,p) level of theory and results are shown in Figure 6.11 with full details of geometries and energies listed in Tables 6.2 and 6.2(a). No *ipso* intermediates were able to be isolated.

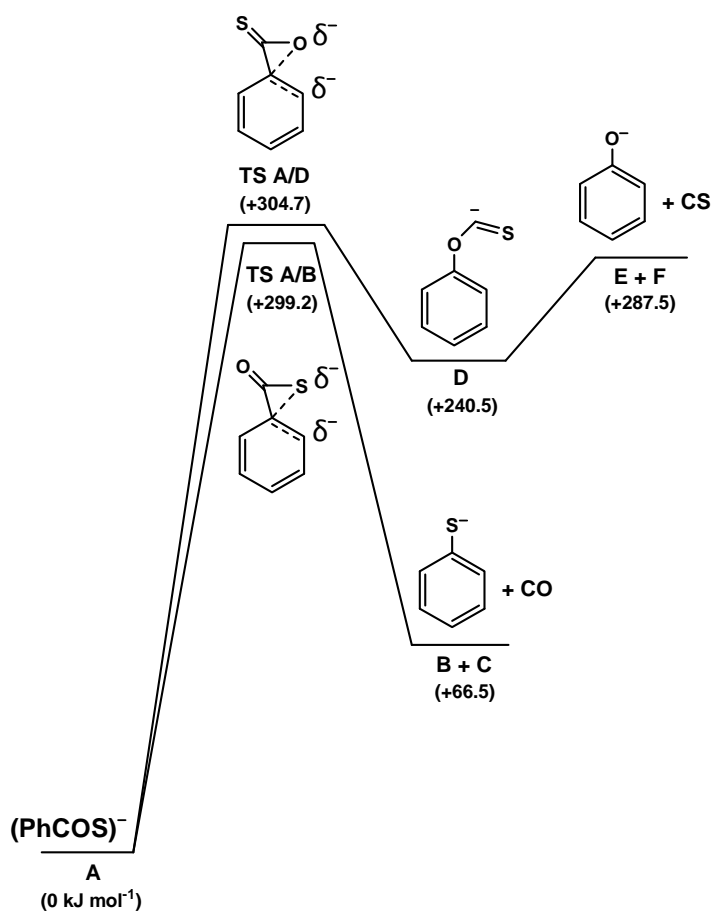


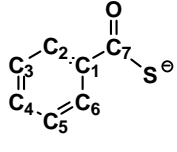
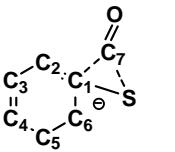
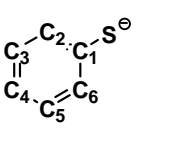
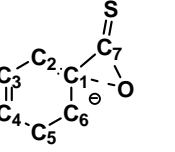
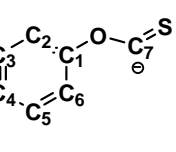
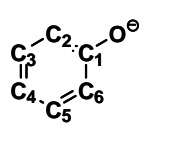
Figure 6.11 Reaction coordinate pathways for the Smiles rearrangements of $(\text{PhCOS})^-$. Relative energies in kJ mol^{-1} . Level of theory used - UCCSD(T)/6-31+G(d,p)//B3LYP/6-31+G(d,p). Structures shown in the Figure show bond connectivities only. For full structural details see Table 6.2 and 6.2(a).

TABLE 6.2

**Reaction Coordinate Pathways for the Smiles Rearrangements of (PhCOS)⁻.
Anion Geometries and Energies. Carbon-Sulfur-Oxygen Skeleton Only.**

Level of theory used - UCCSD(T)/6-31+G(d,p)//B3LYP/6-31+G(d,p)

Relative energies in kJ mol⁻¹ relative to A (0 kJ mol⁻¹)

						
	A	TS A/B	B	TS A/D	D	E
State	¹ A	¹ A	¹ A'	¹ A	¹ A'	¹ A'
Symmetry	C ₁	C ₁	C _s	C ₁	C _s	C _s
Energy (Hartrees)	-741.66644	-741.55247	-628.60034 [-741.64111]	-741.55040	-741.57485	-305.97915 [-741.55695]
Energy Relative to A	0	+299.2	+66.5 [B+C]	+304.7	+240.5	+287.5 [E+F]
Dipole Moment (Debye)	9.1	3.23	6.45	3.68	9.95	4.69
Bond Lengths (Å)						
C ₁ S	-	1.865	1.750	-	-	-
C ₁ C ₂	1.403	1.427	1.424	1.443	1.407	1.448
C ₁ C ₇	1.537	1.686	-	1.537	-	-
C ₂ C ₃	1.398	1.401	1.395	1.389	1.395	1.392
C ₃ C ₄	1.400	1.394	1.403	1.406	1.401	1.407
C ₄ C ₅	1.399	1.415	1.403	1.406	1.400	1.407
C ₅ C ₆	1.399	1.383	1.394	1.389	1.396	1.392
C ₆ C ₁	1.405	1.437	1.424	1.442	1.408	1.449
C ₇ S	1.738	2.033	-	1.686	1.682	-
C ₇ O	1.244	1.187	-	1.342	1.434	-
C ₁ O	-	-	-	1.633	1.362	1.275
Bond Angles (°)						
SC ₇ O	125.7	127.0	-	111.3	109.0	-
SC ₁ C ₂	-	118.5	122.4	-	-	-
SC ₁ C ₆	-	119.8	122.3	-	-	-
SC ₇ C ₁	118.4	69.1	-	180.0	-	-
OC ₇ C ₁	115.9	143.1	-	68.7	-	-
C ₁ C ₂ C ₃	120.9	121.9	122.3	120.6	120.5	122.6
C ₂ C ₃ C ₄	120.4	121.2	121.0	122.2	120.6	121.7
C ₃ C ₄ C ₅	119.3	118.0	118.0	117.4	118.7	117.5
C ₄ C ₅ C ₆	120.2	121.3	121.0	122.2	121.5	121.7
C ₅ C ₆ C ₁	121.1	122.0	122.3	120.6	119.6	122.6
C ₆ C ₁ C ₂	118.2	115.3	115.3	116.0	119.1	113.9
C ₇ C ₁ C ₂	123.4	121.3	-	120.9	-	-
OC ₁ C ₂	-	-	-	115.4	115.9	123.1
C ₇ OC ₁	-	-	-	61.3	118.5	-
Dihedral Angle (°)						
C ₁ C ₂ C ₃ C ₄	0.0	2.8	0.0	5.2	0.0	0.0
C ₂ C ₃ C ₄ C ₅	0.0	0.8	-0.3	1.8	0.0	0.0
OC ₁ C ₂ C ₃	-	-	-	127.8	180.0	-179.0
SC ₇ OC ₁	-	-	-	180.0	-179.0	-

C=O [C]; State ¹SG, Symmetry C_{sv}, Energy (Hartrees) -113.04077, Dipole 0.03 Debye, C=O 1.138Å

C=S [F]; State ¹SG, Symmetry C_{sv}, Energy (Hartrees) -435.5778, Dipole 1.74 Debye, C=S 1.544Å

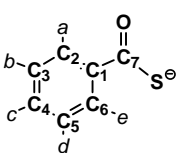
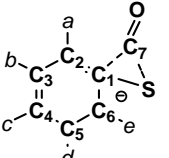
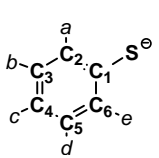
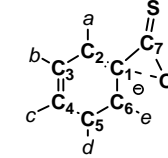
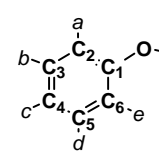
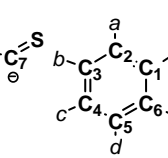
TABLE 6.2(a)

Reaction Coordinate Pathways for the Smiles Rearrangements of (PhCOS)⁻.
Anion Geometries and Energies.

Hydrogens Only.

Level of theory used - UCCSD(T)/6-31+G(d,p)//B3LYP/6-31+G(d,p)

Relative energies in kJ mol⁻¹ relative to A (0 kJ mol⁻¹)

						
	A	TS A/B	B	TS A/D	D	E
State	¹ A	¹ A	¹ A'	¹ A	¹ A'	¹ A'
Symmetry	C ₁	C ₁	C _s	C ₁	C _s	C _s
Energy (Hartrees)	-741.66644	-741.55247	-628.60034 [-741.64111]	-741.55040	-741.57485	-305.97915 [-741.55695]
Energy Relative to A	0	+299.2	+66.5 [B+C]	+304.7	+240.5	+287.5 [E+F]
Dipole Moment (Debye)	9.1	3.23	6.45	3.68	9.95	4.69
Bond Lengths (Å)						
C ₂ a*	1.086	1.087	1.087	1.085	1.085	1.089
C ₃ b	1.088	1.090	1.090	1.091	1.089	1.092
C ₄ c	1.088	1.088	1.088	1.086	1.087	1.087
C ₅ d	1.089	1.090	1.090	1.090	1.089	1.092
C ₆ e	1.085	1.086	1.087	1.086	1.082	1.089
Bond Angles (°)						
aC ₂ C ₁	117.6	118.1	117.8	118.7	118.1	116.9
bC ₃ C ₄	119.9	119.9	119.8	119.5	120.0	119.2
cC ₄ C ₅	120.3	120.8	121.1	121.3	120.7	121.3
dC ₅ C ₆	119.9	119.0	119.8	118.3	118.9	119.0
eC ₆ C ₁	117.5	117.9	117.8	118.7	117.9	116.9
Dihedral Angle (°)						
aC ₂ C ₃ C ₄	-179.0	-178.0	180.0	-178.4	180.0	180.0
cC ₄ C ₃ C ₂	180.0	178.3	180.0	179.1	180.0	-179.0
cC ₄ C ₅ C ₆	180.0	-178.9	180.0	-179.0	180.0	180.0
eC ₆ C ₅ C ₄	180.0	178.5	180.0	178.3	-179.0	180.0

* Individual Hydrogens have been designated letters a - e

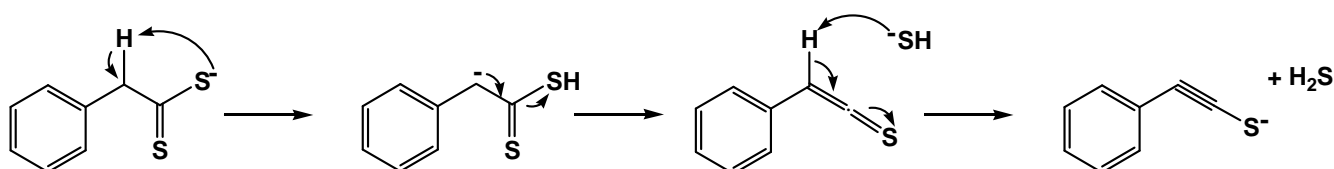
C=O [C]; State ¹SG, Symmetry C_s, Energy (Hartrees) -113.04077, Dipole 0.03 Debye, C=O 1.138ÅC=S [F]; State ¹SG, Symmetry C_s, Energy (Hartrees) -435.5778, Dipole 1.74 Debye, C=S 1.544Å

The formation of C₆H₅S⁻ is kinetically and thermodynamically more favoured than the formation of C₆H₅O⁻. The formation of C₆H₅S⁻ and CO is endothermic (+66.5 kJ mol⁻¹) and proceeds *via* an *ipso* transition state (+299.2 kJ mol⁻¹). In comparison, the competitive formation of C₆H₅O⁻ and CS is more endothermic (+287.5 kJ mol⁻¹) with a transition state slightly higher in energy (+304.7 kJ mol⁻¹).

The theoretical results are consistent with the experimental observations, where the relative abundance of the peak due to C₆H₅S⁻ (*m/z* 109) is greater than that of C₆H₅O⁻ (*m/z* 93) (Figure 6.10).

6.2.3 Reactions of the Benzyl and *o*-Tolyl Anions with CS₂

The benzyl anion (PhCH₂⁻) was formed in the Finnigan LCQ ion trap mass spectrometer by decarboxylation of the phenylacetic anion [(PhCH₂CO₂⁻) formed by deprotonating phenylacetic acid in the ESI source]. Reaction of PhCH₂⁻ with CS₂ forms PhCH₂CS₂⁻ (*m/z* 167) and CID MS⁴ of this adduct gives only one observable fragment ion at *m/z* 133 corresponding to the possible product PhC≡CS⁻. When this procedure was repeated with deuterium labelled PhCD₂⁻, the adduct PhCD₂CS₂⁻ lost only D₂S. A possible mechanism for this process is shown in Scheme 6.4.



Scheme 6.4

A theoretical investigation on the decomposition of PhCH₂CS₂⁻ gives PhC≡CS⁻ and H₂S, a process that is endothermic by +161.4 kJ mol⁻¹ at the UCCSD(T)/6-31+G(d,p)//B3LYP/6-31+G(d,p) level of theory [see Table 6.3 and 6.3(a)].

TABLE 6.3

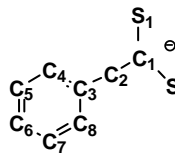
Decomposition Pathway for the CS₂ Addition to the Benzyl Anion.

Anion Minima Geometries and Energies.

Carbon and Sulfur Skeleton Only.

Level of theory used - UCCSD(T)/6-31+G(d,p)//B3LYP/6-31+G(d,p)

Relative energies in kJ mol⁻¹ relative to A (0 kJ mol⁻¹)

	A	B
	A	B
State	¹ A	¹ A'
Symmetry	C ₁	C ₁
Energy (Hartrees)	-1103.43726	-704.55370 [-1103.37578]
Energy Relative to A	0	+161.4 [B+C]
Dipole Moment (Debye)	9.067	9.334
Bond Lengths (Å)		
C ₁ S ₁	1.699	1.656
C ₁ S ₂	1.700	-
C ₁ C ₂	1.549	1.240
C ₂ C ₃	1.516	1.409
C ₃ C ₄	1.404	1.425
C ₄ C ₅	1.397	1.393
C ₅ C ₆	1.399	1.402
C ₆ C ₇	1.399	1.403
C ₇ C ₈	1.398	1.393
C ₈ C ₃	1.404	1.425
Bond Angles (°)		
S ₁ C ₁ S ₂	127.3	-
S ₁ C ₁ C ₂	116.4	180.0
S ₂ C ₁ C ₂	116.3	-
C ₁ C ₂ C ₃	112.9	180.0
C ₂ C ₃ C ₄	121.0	121.9
C ₃ C ₄ C ₅	121.0	121.7
C ₄ C ₅ C ₆	120.3	121.0
C ₅ C ₆ C ₇	119.3	118.4
C ₆ C ₇ C ₈	120.3	121.0
C ₇ C ₈ C ₃	121.0	121.7
C ₈ C ₃ C ₂	120.9	121.9
C ₈ C ₃ C ₄	118.2	116.2
Dihedral Angle (°)		
C ₁ C ₂ C ₃ C ₄	89.7	0.0
S ₁ C ₁ C ₂ C ₃	-89.6	180.0
C ₁ C ₂ C ₃ C ₈	-89.8	0.0
C ₂ C ₃ C ₄ C ₅	-179.7	-179.0

H₁-S-H₂ [C]; State ¹A', Symmetry C_s, Energy (Hartrees) -398.82208, Dipole 1.42 Debye,
H₁-S 1.348 Å, H₂-S 1.348 Å, Angle H₁-S-H₂ 92.7°

TABLE 6.3(a)

Decomposition Pathway for the CS₂ Addition to the Benzyl Anion.

Anion Minima Geometries and Energies.

Hydrogens Only.

Level of theory used - UCCSD(T)/6-31+G(d,p)//B3LYP/6-31+G(d,p)

Relative energies in kJ mol⁻¹ relative to A (0 kJ mol⁻¹)

	A	B
State	¹ A	¹ A'
Symmetry	C ₁	C ₁
Energy (Hartrees)	-1103.43726	-704.55370 [-1103.37578]
Energy Relative to A	0	+161.4 [B+C]
Dipole Moment (Debye)	9.067	9.334
Bond Lengths (Å)		
C ₂ a	1.095	-
C ₂ b	1.094	-
C ₄ a	-	1.087
C ₄ c	1.087	-
C ₈ b	-	1.086
C ₈ d	1.086	-
Bond Angles (°)		
aC ₂ b	108.9	-
aC ₂ C ₁	108.4	-
aC ₂ C ₃	109.0	-
aC ₄ C ₃	-	118.1
bC ₂ C ₁	108.5	-
bC ₂ C ₃	109.0	-
bC ₈ C ₃	-	118.2
cC ₄ C ₃	118.7	-
dC ₈ C ₃	118.7	-
Dihedral Angle (°)		
aC ₄ C ₃ C ₈	-	180.0
bC ₂ C ₃ C ₈	30.9	-
dC ₈ C ₃ C ₄	-178.4	-

H₁-S-H₂ [C]; State ¹A', Symmetry C_s, Energy (Hartrees) -398.82208, Dipole 1.42 Debye, H₁-S 1.348 Å, H₂-S 1.348 Å, Angle H₁-S-H₂ 92.7°

The *o*-tolyl anion was formed in the Finnigan LCQ ion trap mass spectrometer by decarboxylation of the *o*-toluate anion [formed by deprotonating *o*-toluic acid in the ESI

source]. The reaction of *o*-CH₃C₆H₄⁻ with CS₂ forms *o*-CH₃C₆H₄CS₂⁻ (*m/z* 167) and CID MS⁴ of this species gives two observable fragment ions as seen in Figure 6.12.

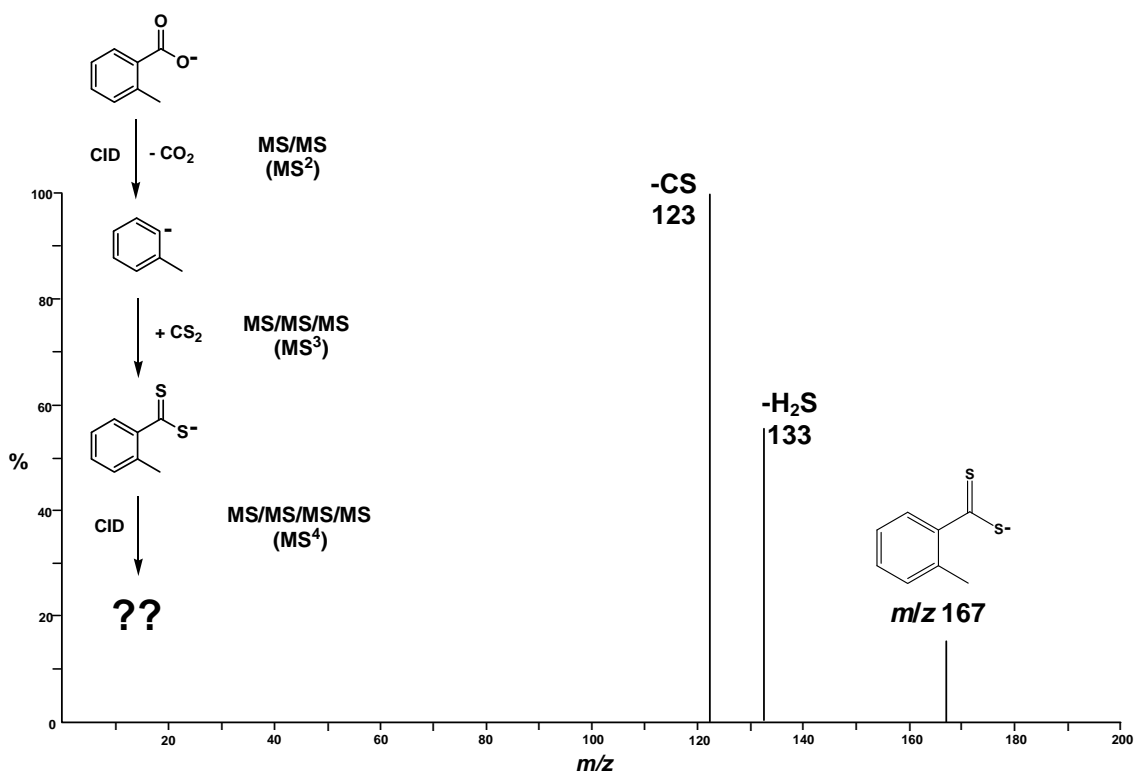
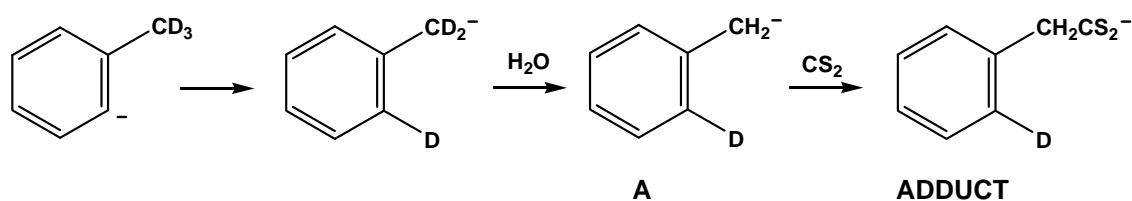


Figure 6.12 CID MS⁴ spectrum of *o*-CH₃C₆H₄CS₂⁻ (*m/z* 167) formed from the reaction of CS₂ with *o*-CH₃C₆H₄⁻ (*o*-CH₃C₆H₄⁻ formed by decarboxylating *o*-CH₃C₆H₄CO₂⁻ in the ESI source). Modified Finnigan LCQ ion trap mass spectrometer.²²³ For experimental details see Experimental section.

The ion observed at *m/z* 123 (-CS) is from the Smiles rearrangement of the expected adduct *o*-CH₃C₆H₄CS₂⁻, however the peak observed at *m/z* 133 (-H₂S) is a little more complicated to explain. Deuterium labelling experiments were used to help rationalise the fragment ion seen at *m/z* 133 (-H₂S).

Deuterium labelled *o*-CD₃C₆H₄CS₂⁻ was formed from the decarboxylation of *o*-CD₃C₆H₄CO₂⁻, with the resulting anion (*o*-CD₃C₆H₄⁻) reacting with CS₂. When the decarboxylated anion (*o*-CD₃C₆H₄⁻) was allowed to react with CS₂ upon its formation, then the expected adduct (*o*-CD₃C₆H₄CS₂⁻) lost only CS *via* a standard Smiles type rearrangement, as observed with the peak at *m/z* 123. However, when the *o*-CD₃C₆H₄⁻

anion was allowed to remain in the ion trap for 10 microseconds, it back exchanged two deuteriums for hydrogens [(A) Scheme 6.5] by a process reported earlier.^{208, 209} The back exchange is a reaction with residual H₂O from the ESI process. The D exchanged ion (A) forms an adduct with CS₂ (Scheme 6.5), which on CID, lost H₂S exclusively in possibly a similar process to that seen for the benzyl adduct (Scheme 6.4), resulting in the ion seen at m/z 133.



Scheme 6.5

The interconversion of the *o*-tolyl and benzyl anions is an exothermic process ($-52.6 \text{ kJ mol}^{-1}$) with a transition barrier of $+180 \text{ kJ mol}^{-1}$ at the UCCSD(T)/6-31+G(d,p)//B3LYP/6-31+G(d,p) level of theory [see Figure 6.13 and Table 6.4 and 6.4(a)]. The theoretical results are consistent with the experimental results obtained where, over a small time frame, the interconversion of the less stable *o*-tolyl anion to the more stable benzyl anion [(A) Scheme 6.5] is seen from the adduct fragmentation[#].

[#] *An examiner has commented that the barrier for the interconversion of the benzyl and o-tolyl anion (Figure 6.13) is prohibitive under the conditions of this experiment and that the experimental and theoretical data point to the process being catalysed with water. Due to the limited availability of computational time and resources, purely due to the complexity of locating a transition state for H₂O facilitating the proton shuttling between these two positions, these calculations were not able to be investigated.*

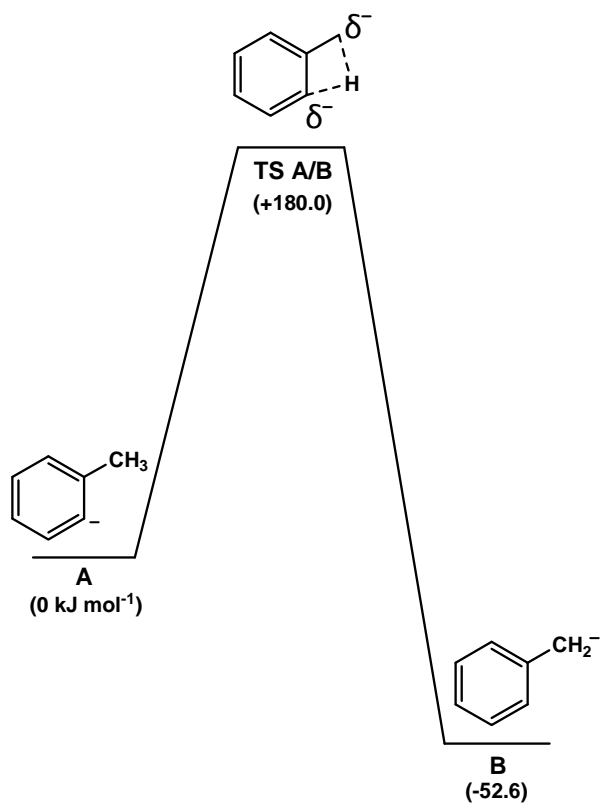


Figure 6.13 Reaction coordinate pathway for the interconversion of the benzyl and *o*-tolyl anion. Relative energies in kJ mol⁻¹. Level of theory used - UCCSD(T)/6-31+G(d,p)//B3LYP/6-31+G(d,p). Structures shown in the Figure show bond connectivities only. For full structural details see Tables 6.4 and 6.4(a).

TABLE 6.4

Reaction Coordinate Pathway for the Interconversion of the Benzyl and *o*-Tolyl Anion.

Anion Minima and Transition State Geometries and Energies.

Carbon Skeleton Only.

Level of theory used - UCCSD(T)/6-31+G(d,p)//B3LYP/6-31+G(d,p)

Relative energies in kJ mol⁻¹ relative to A (0 kJ mol⁻¹)

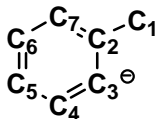
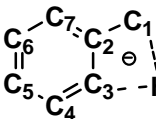
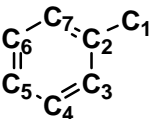
			
	A	TS A/B	B
State	¹ A'	¹ A	¹ A
Symmetry	C _s	C ₁	C ₁
Energy (Hartrees)	-270.03120	-269.96265	-270.05125
Energy Relative to A	0	+180.0	-52.6
Dipole Moment (Debye)	4.74	5.06	2.82
Bond Lengths (Å)			
C ₁ C ₂	1.526	1.509	1.395
C ₂ C ₃	1.422	1.423	1.451
C ₃ C ₄	1.420	1.404	1.386
C ₄ C ₅	1.405	1.412	1.412
C ₅ C ₆	1.401	1.399	1.413
C ₆ C ₇	1.401	1.408	1.386
C ₇ C ₂	1.409	1.403	1.450
Bond Angles (°)			
C ₁ C ₂ C ₃	119.3	105.3	123.2
C ₂ C ₃ C ₄	113.3	118.5	122.8
C ₃ C ₄ C ₅	124.9	120.6	122.1
C ₄ C ₅ C ₆	119.4	120.0	116.7
C ₅ C ₆ C ₇	118.5	120.4	122.1
C ₆ C ₇ C ₂	120.8	119.3	122.8
C ₇ C ₂ C ₁	117.5	133.5	123.2
C ₇ C ₂ C ₃	123.2	121.1	113.6
Dihedral Angle (°)			
C ₁ C ₂ C ₃ C ₄	-179.0	178.7	-179.0
C ₁ C ₂ C ₇ C ₆	180.0	-175.4	180.0
C ₂ C ₃ C ₄ C ₅	0.0	-3.0	0.0
C ₂ C ₇ C ₆ C ₅	0.0	-1.7	0.0

TABLE 6.4(a)

Reaction Coordinate Pathway for the Interconversion of the Benzyl and *o*-Tolyl Anion.

Anion Minima and Transition State Geometries and Energies.

Hydrogens Only.

Level of theory used - UCCSD(T)/6-31+G(d,p)//B3LYP/6-31+G(d,p)

Relative energies in kJ mol⁻¹ relative to A (0 kJ mol⁻¹)

	A	TS A/B	B
State	¹ A'	¹ A	¹ A
Symmetry	C _s	C ₁	C ₁
Energy (Hartrees)	-270.03120	-269.96265	-270.05125
Energy Relative to A	0	+180.0	-52.6
Dipole Moment (Debye)	4.74	5.06	2.82
Bond Lengths (Å)			
C ₁ a	1.102	1.537	-
C ₁ b	1.102	1.105	1.087
C ₁ c	1.093	1.104	1.087
C ₃ a	-	1.421	1.090
C ₄ g	1.097	1.093	1.091
C ₅ f	1.094	1.092	1.087
C ₆ e	1.090	1.091	1.092
C ₇ d	1.095	1.091	1.090
Bond Angles (°)			
aC ₁ C ₂	112.2	72.2	-
aC ₁ b	106.7	132.2	-
aC ₁ c	108.3	110.4	-
bC ₁ C ₂	112.2	115.5	121.3
bC ₁ c	108.3	108.6	117.5
cC ₁ C ₂	108.9	113.0	121.2
dC ₇ C ₆	118.8	119.5	119.2
eC ₆ C ₅	121.0	119.7	119.3
fC ₅ C ₄	120.8	120.4	121.6
gC ₄ C ₃	118.8	120.9	118.6
Dihedral Angle (°)			
aC ₁ C ₂ C ₃	-119.9	-3.2	-
bC ₁ C ₂ C ₃	119.9	-132.2	-179.0

6.2.4 Reactions of the β -Phenylethyl Anion and Other C₈H₉⁻ Isomers with CS₂

The gas phase stability of the β -phenylethyl anion (PhCH₂CH₂⁻) has been in question for the last two decades, as it was uncertain whether the anion is a stable species^{210, 211} in its own right or does it undergo rearrangement *via* the *ipso* intermediate^{211, 212} seen in Scheme 6.2 or maybe some other intermediate.

Our earlier work on the β -phenylethyl anion, carried out using a VG ZAB 2HF mass spectrometer (discussed in Chapter 1), reported the detection of the anion C₈H₉^{-*} and it was suggested that the least stable PhCH₂CH₂⁻ anion was formed before *ipso* rearrangement to the more stable cyclised structure.²¹¹ Other data presented shows that the β -phenylethyl anion rearranges to the cyclised *ipso* form on collisional activation in a conventional mass spectrometer (*cf.* Nibbering *et al.*),²¹² however is stable in a flowing afterglow instrument (*cf.* Squires *et al.*).²¹⁰

The β -phenylethyl anion (PhCH₂CH₂⁻) was formed in the Finnigan LCQ ion trap mass spectrometer by decarboxylation of PhCH₂CH₂CO₂⁻ (formed from deprotonating 3-phenylpropionic acid in the ESI source). The reaction of PhCH₂CH₂⁻ with CS₂ formed an adduct (*m/z* 181) and CID MS⁴ of this adduct gives a single observable fragment ion at *m/z* 147 corresponding to the loss of H₂S. In order to determine the origin of H that makes up the loss of H₂S from the adduct (PhCH₂CH₂CS₂⁻), negative ion CID was carried out on the two deuterium labelled species PhCH₂CD₂CS₂⁻ and PhCD₂CH₂CS₂⁻.

Firstly, the labelled anions (presumably, at least initially) PhCD₂CH₂⁻ and PhCH₂CD₂⁻ were formed in the Finnigan LCQ ion trap mass spectrometer by decarboxylation of their respective carboxylate anions PhCD₂CH₂CO₂⁻ and PhCH₂CD₂CO₂⁻. The adduct formed from PhCD₂CH₂⁻ and CS₂ fragments to lose H₂S, while the adduct formed from PhCH₂CD₂⁻ and CS₂ (Figure 6.14) fragments by loss of D₂S.



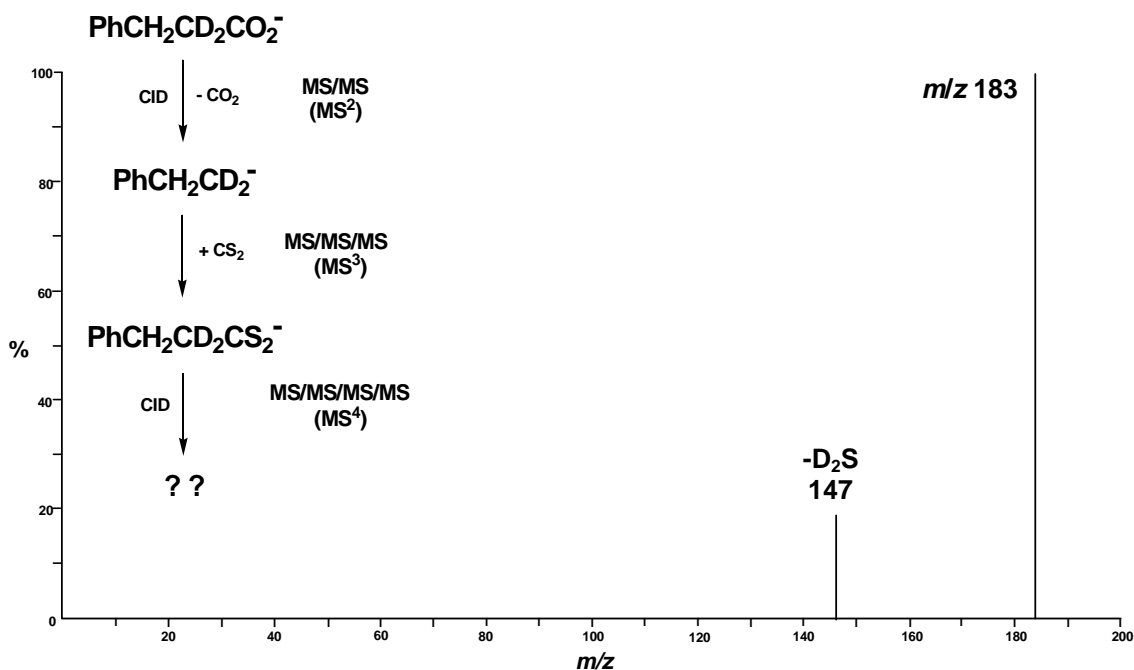


Figure 6.14 The CID MS⁴ spectrum of PhCH₂CD₂CS₂⁻ (*m/z* 183) formed from the reaction of CS₂ with PhCH₂CD₂⁻ (PhCH₂CD₂⁻ formed by decarboxylating PhCH₂CD₂CO₂⁻ in the ESI source). Modified Finnigan LCQ ion trap mass spectrometer.²²³ For experimental details see Experimental section.

Secondly, the species PhCH₂CD₂CS₂⁻ and PhCD₂CH₂CS₂⁻ were formed in a Waters/Micromass Q-ToF 2 mass spectrometer by deprotonation of the acids PhCH₂CD₂CS₂H and PhCD₂CH₂CS₂H respectively. The CID MS² of PhCH₂CD₂CS₂⁻ shows loss of D₂S (Figure 6.15), while the CID MS² of PhCD₂CH₂CS₂⁻ loses H₂S. The CID process of the Q-ToF 2 is able to produce more energised anions than those formed in the LCQ, therefore the peaks observed at *m/z* 92 and 76 in Figure 6.15 are not observed in Figure 6.14.

It is therefore concluded from the experimental data that the hydrogens that make up the loss of H₂S from the adduct (PhCH₂CH₂CS₂⁻) are from the CH₂ next to CS₂⁻.

A possible mechanism for the loss of H₂S from PhCH₂CH₂CS₂⁻ is analogous to that seen in Scheme 6.4.

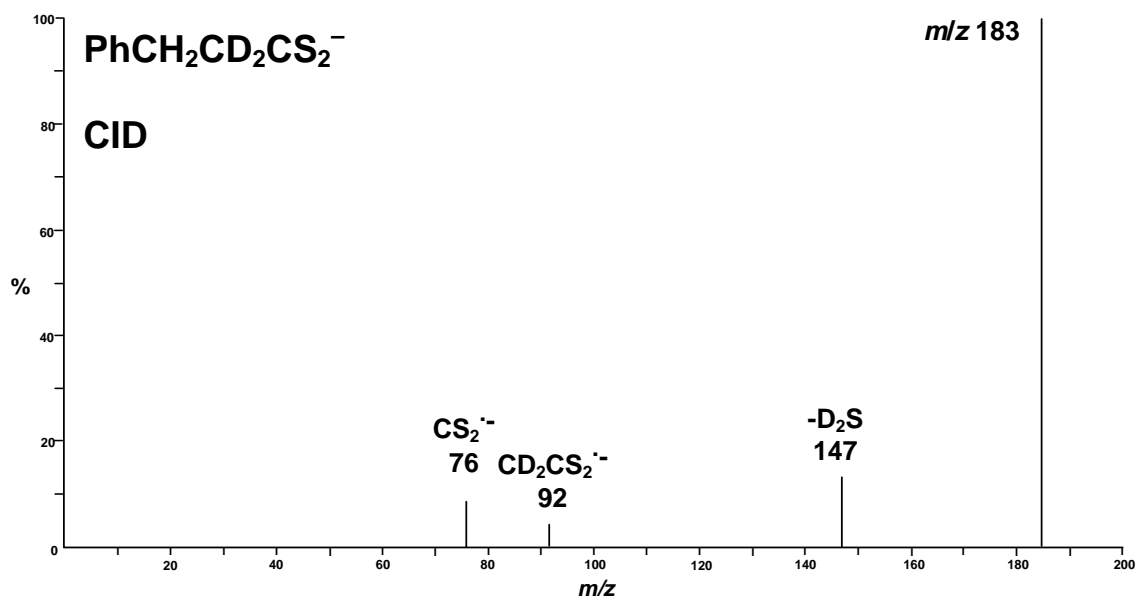
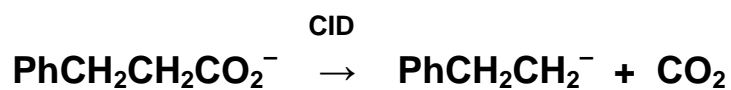


Figure 6.15 CID MS² spectrum of PhCH₂CD₂CS₂⁻ (*m/z* 183). Waters/Micromass Q-ToF 2 mass spectrometer. For experimental details see Experimental section.

The comparative spectra of the isomers Ph(CH₃)CHCS₂⁻ and *o*-C₂H₅-C₆H₄-CS₂⁻ were also investigated. The anion Ph(CH₃)CHCS₂⁻ was formed in the Finnigan LCQ ion trap mass spectrometer from the reaction of Ph(CH₃)CH⁻ (formed from the deprotonation then decarboxylation of 2-phenylpropionic acid) with CS₂. The CID MS⁴ of the adduct [Ph(CH₃)CHCS₂⁻] shows no loss of H₂S analogous to that seen for PhCH₂CH₂CS₂⁻. However, at low CS₂ pressures there is an ion observed at *m/z* 105 [Ph(CH₃)CH⁻] which corresponds to the loss of CS₂. The other isomeric anion *o*-C₂H₅-C₆H₄-CS₂⁻ was formed in the Finnigan LCQ ion trap mass spectrometer from the reaction of *o*-C₂H₅-C₆H₄⁻ (formed from the deprotonation then decarboxylation of *o*-ethylbenzoic acid) with CS₂. The CID MS⁴ of the adduct (*o*-C₂H₅-C₆H₄-CS₂⁻) also shows no loss of H₂S analogous to that seen for PhCH₂CH₂CS₂⁻. However, there is an ion observed at *m/z* 137 (*o*-C₂H₅-C₆H₄-S⁻) which corresponds to the elimination of CS which has occurred *via* a Smiles type rearrangement. It is concluded from the experimental data that the β-phenylethyl anion (PhCH₂CH₂⁻) neither rearranges to Ph(CH₃)CH⁻ nor to *o*-C₂H₅-C₆H₄⁻ prior to or during the reaction with CS₂ in the Finnigan LCQ ion trap mass spectrometer.

A theoretical investigation on the generation and stability of the β -phenylethyl anion (PhCH₂CH₂⁻) along with the stability of other relevant C₈H₉⁻ isomers [at the UCCSD(T)/6-31+G(d,p)//B3LYP/6-31+G(d,p) level of theory] was carried out to help rationalise the observed experimental results.

The energy required for the decarboxylation reaction used to generate the PhCH₂CH₂⁻ anion (Scheme 6.6), is calculated to be +271.5 kJ mol⁻¹ at the UCCSD(T)/6-31+G(d,p)//B3LYP/6-31+G(d,p) level of theory (Table 6.5).



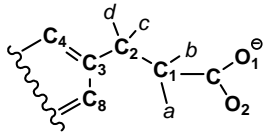
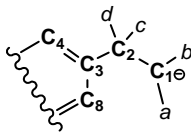
Scheme 6.6

TABLE 6.5

Energies and Geometries of Selected Minima from the Decarboxylation of PhCH₂CH₂CO₂⁻.

Level of theory used - UCCSD(T)/6-31+G(d,p)//B3LYP/6-31+G(d,p)

Relative energies in kJ mol⁻¹ relative to A (0 kJ mol⁻¹)

		
	A	B*
State	¹ A	¹ A
Symmetry	C ₁	C ₁
Energy (Hartrees)	-497.40907	-309.18370 [-497.30566]
Energy Relative to A	0	+271.5 [B+C]
Dipole Moment (Debye)	?	8.82
Bond Length (Å)		
CC ₁	1.571	-
C ₁ C ₂	1.541	1.514
C ₂ C ₃	1.510	1.529
CO ₁	1.261	-
CO ₂	1.259	-
C ₁ a	1.096	1.100
C ₁ b	1.100	1.103
C ₂ c	1.097	1.104
C ₂ d	1.095	1.126
Bond Angle (°)		
CC ₁ C ₂	113.8	-
C ₁ C ₂ C ₃	113.7	116.2
C ₁ CO ₁	116.1	-
C ₁ CO ₂	114.8	-
aC ₁ C ₂	111.1	111.5
bC ₁ C	107.0	-
cC ₂ C ₃	109.5	105.1
dC ₂ C ₃	110.9	103.4
Dihedral Angle (°)		
C ₁ C ₂ C ₃ C ₄	-93.3	177.4
CC ₁ C ₂ C ₃	-171.8	-
O ₁ CC ₁ C ₂	27.9	-
O ₂ CC ₁ C ₂	-153.8	-

O₁-C-O₂ [C]; State ¹A', Symmetry C_s, Energy (Hartrees) -188.12196, O₁-C 1.563 Å, O₂-C 1.563 Å, Angle O₁-C-O₂ 180.0°

* For full geometries of this structure refer to structure A, TABLE 6.6 and 6.6(a).

The reaction coordinate pathways for the interconversion of energised PhCH₂CH₂⁻ and other C₈H₉⁻ isomers is seen in Figure 6.16 with full details of geometries and energies listed Table 6.6 and 6.6(a).

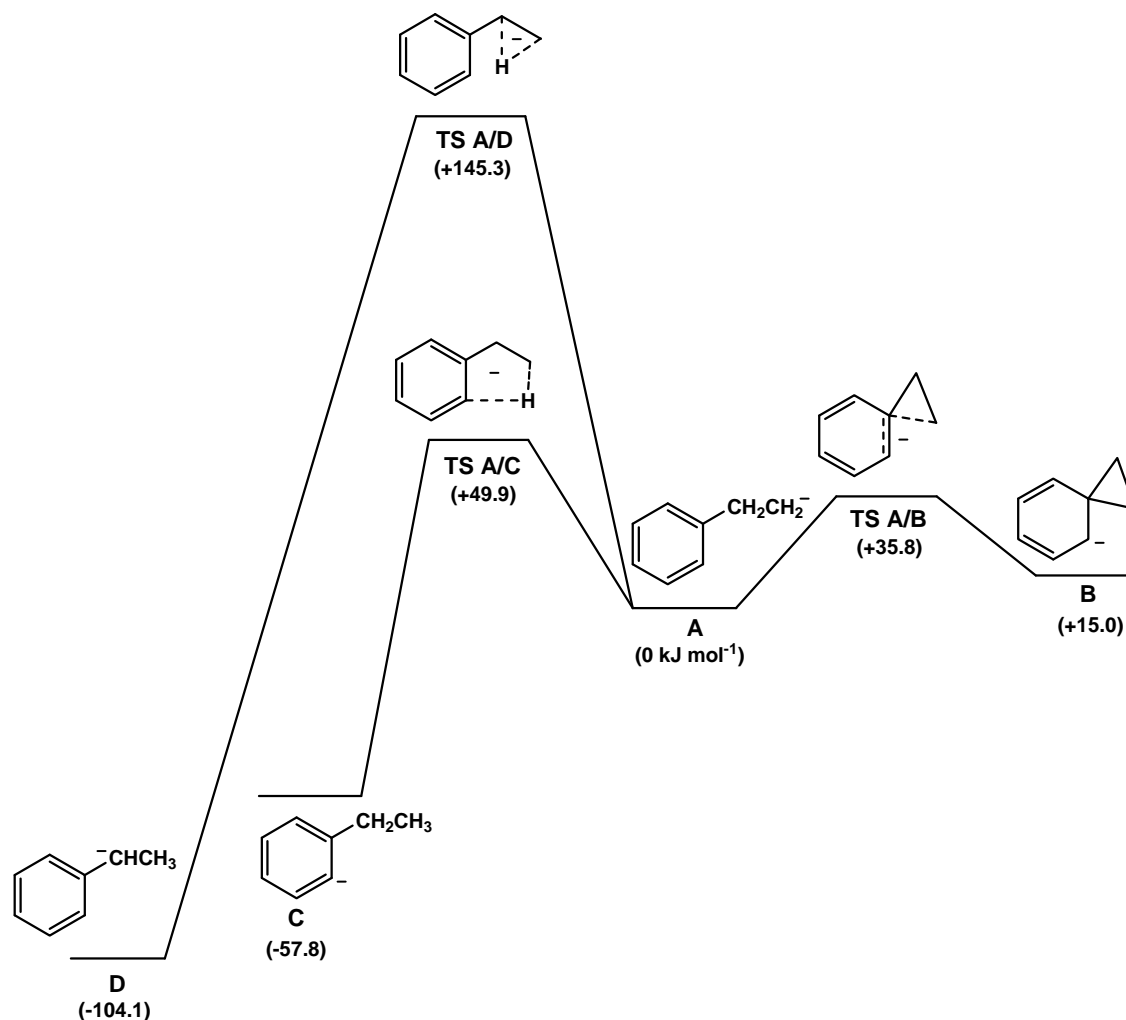


Figure 6.16 Reaction coordinate pathways for the interconversion of the β-phenylethyl anion (PhCH₂CH₂⁻) (A), Ph⁻CHCH₃ (D), o-C₂H₅-C₆H₄⁻ (C) and the cyclised species (B). Relative energies in kJ mol⁻¹. Level of theory used - UCCSD(T)/6-31+G(d,p)//B3LYP/6-31+G(d,p). Structures shown in the Figure show bond connectivities only. For full structural details see Tables 6.6 and 6.6(a).

TABLE 6.6

Reaction Coordinate Pathways for the Interconversion of PhCH₂CH₂⁻ and other C₈H₉⁻ Isomers.

Anion Geometries and Energies.

Carbon Skeleton Only.

Level of theory used - UCCSD(T)/6-31+G(d,p)//B3LYP/6-31+G(d,p)

Relative energies in kJ mol⁻¹ relative to A (0 kJ mol⁻¹)

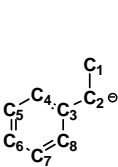
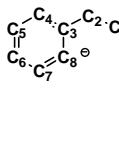
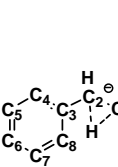
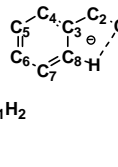
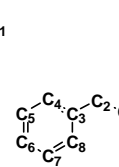
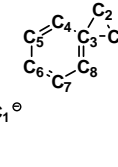
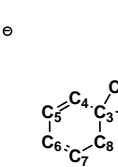
							
	D	C	TS A/D	TS A/C	A	TS A/B	B
State	¹ A	¹ A	¹ A	¹ A	¹ A	¹ A	¹ A
Symmetry	C ₁	C ₁	C ₁	C ₁	C ₁	C ₁	C ₁
Energy (Hartrees)	-309.22336	-309.20572	-309.12837	-309.16471	-309.18370	-309.17008	-309.17799
Energy Relative to A	-104.1	-57.8	+145.3	+49.9	0	+35.8	+15.0
Dipole Moment (Debye)	0.61	4.37	5.17	5.23	8.82	1.26	1.74
Bond Lengths (Å)							
C ₁ C ₂	1.504	1.539	1.564	1.534	1.514	1.503	1.519
C ₂ C ₃	1.392	1.525	1.430	1.555	1.529	1.475	1.517
C ₁ C ₃	-	-	-	-	-	1.902	1.555
C ₃ C ₄	1.453	1.408	1.433	1.399	1.404	1.458	1.499
C ₄ C ₅	1.390	1.403	1.386	1.403	1.399	1.384	1.379
C ₅ C ₆	1.407	1.398	1.414	1.402	1.402	1.415	1.420
C ₆ C ₇	1.417	1.408	1.402	1.406	1.399	1.415	1.420
C ₇ C ₈	1.383	1.416	1.396	1.402	1.402	1.383	1.378
C ₈ C ₃	1.452	1.424	1.435	1.402	1.402	1.458	1.499
Bond Angles (°)							
C ₁ C ₂ C ₃	123.3	112.6	123.7	109.3	116.2	79.4	61.6
C ₂ C ₃ C ₄	123.4	118.2	121.8	124.4	121.0	121.7	119.2
C ₃ C ₄ C ₅	122.3	120.6	122.4	119.8	121.6	121.0	121.3
C ₄ C ₅ C ₆	122.3	118.4	121.1	119.6	119.9	122.0	123.1
C ₅ C ₆ C ₇	116.9	119.6	117.7	119.6	119.1	117.1	116.6
C ₆ C ₇ C ₈	121.9	124.7	121.9	121.6	120.5	122.0	123.1
C ₇ C ₈ C ₃	122.8	113.4	121.4	117.8	121.0	121.0	121.3
C ₈ C ₃ C ₂	122.8	118.5	122.7	114.0	121.2	121.7	119.2
C ₈ C ₃ C ₄	113.8	123.3	115.5	121.6	117.8	114.2	112.3
Dihedral Angle (°)							
C ₁ C ₂ C ₃ C ₄	0.0	-105.2	-173.7	-179.0	177.4	-99.5	-108.0
C ₁ C ₂ C ₃ C ₈	180.0	73.9	7.6	0.0	-3.4	99.5	108.1
C ₂ C ₃ C ₄ C ₅	-179.0	178.8	-177.3	180.0	-179.2	-179.0	-162.2
C ₂ C ₃ C ₈ C ₇	180.0	-178.6	176.6	-179.0	-179.6	179.7	162.2

TABLE 6.6(a)
Reaction Coordinate Pathways for the Interconversion of PhCH₂CH₂⁻ and other C₈H₉⁻ Isomers.
Anion Geometries and Energies. Hydrogens Only.

Level of theory used - UCCSD(T)/6-31+G(d,p)//B3LYP/6-31+G(d,p)

 Relative energies in kJ mol⁻¹ relative to A (0 kJ mol⁻¹)

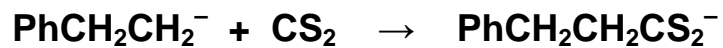
	D	C	TS A/D	TS A/C	A	TS A/B	B
State	¹ A	¹ A	¹ A	¹ A	¹ A	¹ A	¹ A
Symmetry	C ₁	C ₁	C ₁	C ₁	C ₁	C ₁	C ₁
Energy (Hartrees)	-309.22336	-309.20572	-309.12837	-309.16471	-309.18370	-309.17008	-309.17799
Energy Relative to A	-104.1	-57.8	+145.3	+49.9	0	+35.8	+15.0
Dipole Moment (Debye)	0.61	4.37	5.17	5.23	8.82	1.26	1.74
Bond Lengths (Å)							
C ₁ a	1.110	1.098	1.089	1.100	1.100	1.086	1.092
C ₁ b	1.109	1.100	1.095	1.099	1.103	1.085	1.092
C ₁ c	1.098	1.095	1.401	-	-	-	-
C ₁ f	-	-	-	1.528	-	-	-
C ₂ c	-	-	1.220	1.104	1.104	1.098	1.091
C ₂ d	1.089	1.103	1.092	1.104	1.126	1.098	1.091
C ₂ e	-	1.097	-	-	-	-	-
C ₄ e	1.088	-	1.090	1.094	1.091	1.090	1.090
C ₄ f	-	1.095	-	-	-	-	-
C ₈ f	1.090	-	1.085	1.361	1.088	1.090	1.090
Bond Angles (°)							
aC ₁ b	105.0	108.1	115.2	109.1	109.2	118.3	114.8
aC ₁ c	106.4	107.9	112.5	-	-	-	-
aC ₁ C ₂	113.8	110.9	112.1	113.1	111.5	120.1	118.3
bC ₁ c	106.4	108.9	131.5	-	-	-	-
bC ₁ C ₂	113.9	111.9	116.7	113.1	112.9	120.1	118.3
cC ₁ C ₂	110.8	108.9	48.2	-	-	-	-
cC ₂ C ₁	-	-	58.9	113.1	-	120.1	-
cC ₂ C ₃	-	-	112.2	108.0	105.1	113.9	-
cC ₂ d	-	-	115.4	105.1	103.4	109.8	113.5
dC ₂ C ₁	117.8	109.2	116.6	113.2	117.4	116.8	118.4
dC ₂ C ₃	118.8	110.8	116.1	107.9	103.4	115.7	117.8
eC ₂ C ₃	-	108.3	-	-	-	-	-
eC ₄ C ₃	118.8	-	118.3	120.5	118.8	118.7	118.1
fC ₈ C ₃	117.9	-	119.0	95.3	116.6	118.7	118.1
fC ₄ C ₃	-	120.4	-	-	-	-	-
Dihedral Angle (°)							
aC ₁ C ₂ C ₃	60.2	63.0	161.6	-117.7	-166.0	-97.0	106.9
dC ₂ C ₃ C ₈	0.0	-163.5	165.4	123.5	126.7	-145.7	-1.0
eC ₄ C ₃ C ₈	180.0	-	-178.6	180.0	-179.0	166.8	166.9
fC ₈ C ₃ C ₄	-179.0	-	178.6	180.0	-178.0	-166.8	-166.9

Firstly, from the reaction coordinate pathways for the rearrangements of the energised β -phenylethyl anion (Figure 6.16), it is calculated that $\text{PhCH}_2\text{CH}_2^-$ (A) can interconvert *via* a 1,2 proton transfer over a transition state of $+145.3 \text{ kJ mol}^{-1}$ to yield the anion $\text{Ph}(\text{CH}_3)\text{CH}^-$ (D) in an overall exothermic rearrangement ($-104.1 \text{ kJ mol}^{-1}$). However, there is no experimental evidence confirming the rearrangement (A) to (D) because CID of the adduct $[\text{Ph}(\text{CH}_3)\text{CHCS}_2^-]$ shows loss of CS₂ rather than loss of H₂S from $\text{PhCH}_2\text{CH}_2\text{CS}_2^-$.

Secondly, it was calculated that $\text{PhCH}_2\text{CH}_2^-$ [(A) Figure 6.16] can proton transfer from the *ortho* position to give $o\text{-C}_2\text{H}_5\text{C}_6\text{H}_4^-$ (C) over a transition barrier of $+49.9 \text{ kJ mol}^{-1}$ in an overall exothermic reaction ($-57.8 \text{ kJ mol}^{-1}$). As before, there is no experimental evidence supporting this rearrangement [(A) to (C)] because the adduct formed from $\text{PhCH}_2\text{CH}_2^- + \text{CS}_2$ loses H₂S while the adduct formed from $o\text{-C}_2\text{H}_5\text{C}_6\text{H}_4^- + \text{CS}_2$ rearranges *via* a possible *ipso* intermediate to lose CS.

Finally, and more interestingly, the reaction coordinate pathways in Figure 6.16 show that energised $\text{PhCH}_2\text{CH}_2^-$ (A) can convert to the cyclic *ipso* isomer (B) over a barrier of $+35.8 \text{ kJ mol}^{-1}$. The conversion from (A) to (B) is an endothermic process ($+15.0 \text{ kJ mol}^{-1}$) and is energetically more favourable than the rearrangement of (A) to isomers (C) and (D). The experimental results from the reactions of $\text{PhCH}_2\text{CD}_2^-$ and $\text{PhCD}_2\text{CH}_2^-$ with CS₂ provide no evidence of the *ipso* anion (B) reacting with CS₂. If the two D labelled analogues were to rearrange *via* the *ipso* anion (B) (either prior to or during the ion-molecule reaction with CS₂), then the ratio of H₂S and D₂S loss should be the same for both labelled adducts. This is not the case. The CID MS⁴ of $\text{PhCH}_2\text{CD}_2\text{CS}_2^-$ (Figure 6.14) and the CID MS² of $\text{PhCH}_2\text{CD}_2\text{CS}_2^-$ (Figure 6.15) show only a loss of D₂S (*m/z* 147) from both their corresponding adducts. From the observed experimental results and theoretical calculations we can deduce that CS₂ reacts with β -phenylethyl anions that have less than 35.8 kJ mol^{-1} of excess energy. The theoretical results support earlier reported work on the stability of the β -phenylethyl anion in a conventional mass spectrometer²¹² (more energised ions - ion rearrangement) and flowing afterglow instrument (He thermalised ions - ion stability),²¹⁰ indicating both Nibbering and Squires were correct.

The energy required for the addition of CS₂ to PhCH₂CH₂⁻ (Scheme 6.7), is exothermic by 342.7 kJ mol⁻¹ at the UCCSD(T)/6-31+G(d,p)//B3LYP/6-31+G(d,p) level of theory (Table 6.7).



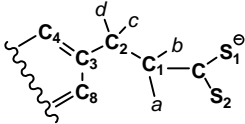
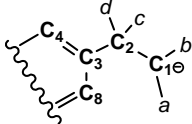
Scheme 6.7

TABLE 6.7

Energies and Geometries of Selected Minima for the CS₂ Addition to PhCH₂CH₂⁻.

Level of theory used - UCCSD(T)/6-31+G(d,p)//B3LYP/6-31+G(d,p)

Relative energies in kJ mol⁻¹ relative to B + C (0 kJ mol⁻¹)

		
	A	B*
State	¹ A	¹ A
Symmetry	C ₁	C ₁
Energy (Hartrees)	-1142.61346	-309.18370 [-1142.48293]
Energy Relative to B + C	+342.7	0 [B+C]
Dipole Moment (Debye)	?	8.82
Bond Length (Å)		
CC ₁	1.535	-
C ₁ C ₂	1.550	1.514
C ₂ C ₃	1.511	1.529
CS ₁	1.702	-
CS ₂	1.703	-
C ₁ a	1.095	1.100
C ₁ b	1.095	1.103
C ₂ c	1.096	1.104
C ₂ d	1.096	1.126
Bond Angle (°)		
CC ₁ C ₂	111.1	-
C ₁ C ₂ C ₃	113.0	116.2
C ₁ CS ₁	116.4	-
C ₁ CS ₂	116.4	-
aC ₁ C	109.6	-
bC ₁ C	109.6	-
cC ₂ C ₃	110.0	105.1
dC ₂ C ₃	110.0	103.4
Dihedral Angle (°)		
C ₁ C ₂ C ₃ C ₄	-89.4	177.4
CC ₁ C ₂ C ₃	180.0	-
S ₁ CC ₁ C ₂	88.9	-
S ₂ CC ₁ C ₂	-88.8	-

S₁-C-S₂ [C]; State ¹A₁, Symmetry C_{2v}, Energy (Hartrees) -833.29923, Dipole 0.003 Debye, S₁=C 1.563Å, C=S₂ 1.563Å, S₁=C=S₂ 179.7°

* For full geometries of this structure refer to structure A, TABLE 6.6 and 6.6(a).

6.3 SUMMARY & CONCLUSIONS

- (i) The ion-molecule reaction between C₆H₅⁻ and CS₂ in the gas phase gives an adduct C₆H₅CS₂⁻ which, when energised, rearranges *via* an *ipso* (Smiles) transition state to yield C₆H₅S⁻ and CS.
- (ii) The respective ion-molecule reactions of C₆H₅CH₂⁻ and *o*-CH₃C₆H₅⁻ with CS₂ give adducts which can be readily distinguished by their CID. The adduct formed from C₆H₅CH₂⁻ + CS₂ loses H₂S, while the adduct formed from *o*-CH₃C₆H₅⁻ + CS₂ loses both H₂S and CS (CS is lost *via* a Smiles type rearrangement), and
- (iii) Decarboxylation of C₆H₅CH₂CH₂CO₂⁻ produces C₆H₅CH₂CH₂⁻ which reacts with CS₂ without rearrangement to yield C₆H₅CH₂CH₂CS₂⁻. During CID the adduct formed loses H₂S.

6.4 EXPERIMENTAL SECTION

6.4.1 Mass Spectrometric Methods

The gas phase ion-molecule reactions carried out in this study were done using a modified Finnigan LCQ mass spectrometer (discussed earlier) configured with an ESI source. Samples were dissolved in HPLC-grade acetonitrile/water (1:1 v/v) and infused into the ESI source at a flow rate of 3-5 $\mu\text{L min}^{-1}$. Carbanions were generated in the ESI source under the following conditions: needle potential of 4.0 to 5.0 kV and a heated capillary temperature of 180-200°C. The neutral reagent (CS₂) was injected into the system at a rate of 0.2 mL hr⁻¹. Extensive tuning of electrospray conditions was often required due to the low signal-to-noise (SN) ratio and/or low abundance of some species.²²³ Mass selection and CID fragmentation were carried out using the ‘advanced scan’ capabilities of the LCQ software (Tune Plus version 1.3).

The ESI CID MS² spectra of the C₆H₅CO₂⁻, C₆H₅COS⁻, C₆H₅CS₂⁻, PhCH₂CD₂CS₂⁻ and PhCD₂CH₂CS₂⁻ anions were measured using a Waters/Micromass Q-ToF 2 mass spectrometer (discussed earlier). Samples were dissolved in HPLC-grade acetonitrile/water (1:1 v/v) and infused into the ESI source at a flow rate of 5 $\mu\text{L min}^{-1}$. Experimental conditions were as follows: capillary voltage 3.1 kV, source temperature 80°C, desolvation temperature 150°C and cone voltage 50 V. Tandem mass spectrometry (MS/MS) data were acquired using argon as the collision gas and the collision energy was set to give maximum fragmentation.

6.4.2 Materials and Synthesis

The following chemicals were purchased from Sigma-Aldrich (Castle Hill, NSW, Australia) and were used without purification: argon gas, carbon disulfide, benzoic acid, thiobenzoic acid, phenylacetic acid, *o*-toluic acid, 3-phenylpropionic acid, 2-phenylpropionic acid, *o*-ethylbenzoic acid and CD₃I (d₃ > 99.5%).

The other compounds (below) used in this study were prepared and supplied by Dr Scott Walker and Dr Peter C.H. Eichinger at The University of Adelaide with many thanks.

Dithiobenzoic acid

This was prepared by a standard Grignard reaction²²⁵ between bromobenzene and carbon disulfide.²²⁶ (m.p. dec. > 200°C; lit.⁶⁵ 208°C).

o-Methyl(d₃)benzoic acid

This was prepared by a standard Grignard reaction²²⁵ using d₃-methyl iodide (d₃ = 99.5%) and commencing with the diethylacetal of *o*-bromobenzaldehyde.²²⁷ [m.p. 103-104°C, lit.²²⁸ 104-105°C (d₃ = 99.5%)].

2,2-Dideuterophenylacetic acid

This was prepared by two cycles of exchange of phenylacetic acid with deuterium oxide (d₂ = 95%) using a standard method.²²⁹ [m.p. 77-78°C, lit.²²⁹ 78°C (d₂ = 95%)].

2-Phenyl-2,2-dideutero-1-bromoethane

2,2-Dideuterophenylacetic acid (d₂ = 95%) (prepared above) was treated with lithium aluminium hydride in tetrahydrofuran (THF) at 0°C by a standard method²³⁰ giving 2-phenyl-2,2-dideuteroethanol after vacuum distillation [yield 90% (d₂ = 95%)]. This was then treated with bromine and triphenyl phosphine in dichloromethane by a standard method²³¹ to give 2-phenyl-2,2-dideutero-1-bromoethane as a colourless oil after vacuum distillation [yield 65% (d₂ = 95%.)].

2-Phenyl-1,1-dideutero-1-bromoethane

Phenylacetic acid was treated with lithium aluminium deuteride (d₂ = 98%) in THF at 0°C by a standard method²³⁰ giving 2-phenyl-1,1-dideuteroethanol as a colourless oil after vacuum distillation [yield 91% (d₂ = 98%)]. This was then treated with bromine and triphenyl phosphine in dichloromethane by a standard method²³¹ to give 2-phenyl-1,1-dideutero-1-bromoethane as a colourless oil after vacuum distillation [yield 83% (d₂ = 98%)].

2,2-Dideutero-3-phenylpropionic acid

2-Phenyl-1,1-dideutero-1-bromoethane ($d_2 = 98\%$) (prepared above) was allowed to react (by a standard Grignard reaction)²²⁵ with Mg in THF under reflux. Addition of solid CO₂ gave 2,2-dideutero-3-phenylpropionic acid [yield 62%, m.p. 46-48°C, lit.²²⁷ 47-48°C ($d_2 = 98\%$)].

3,3-Dideutero-3-phenylpropionic acid

2-Phenyl-2,2-dideutero-1-bromoethane ($d_2 = 95\%$) (prepared above) was allowed to react (by a standard Grignard reaction)²²⁵ with Mg in THF under reflux. Addition of solid CO₂ gave 3,3-dideutero-3-phenylpropionic acid [yield 65%, m.p. 46-48°C, lit.²²⁷ 47-48°C, ($d_2 = 95\%$)].

2,2-Dideutero-3-phenylpropane dithiolic acid

2-Phenyl-1,1-dideutero-1-bromoethane ($d_2 = 98\%$) (prepared above) in THF was allowed to react with Mg in THF, followed by addition of CS₂ and a catalytic amount of CuCl (in THF) at -50°C.²²⁶ Workup isolated 2,2-dideutero-3-phenylpropanedithiolic acid as an unstable red-orange oil [yield 23%, ($d_2 = 98\%$)]. This was used immediately in the Waters/Micromass Q-ToF 2 mass spectrometer to form PhCH₂CD₂CS₂⁻ via ESI CID.

3,3-Dideutero-3-phenylpropane dithiolic acid

2-Phenyl-2,2-dideutero-1-bromoethane ($d_2 = 95\%$) (prepared above) in THF was allowed to react with Mg in THF, followed by addition of CS₂ and a catalytic amount of CuBr (in THF) at -50°C.²²⁶ Work up isolated 3,3-Dideutero-3-phenylpropane dithiolic acid as an unstable red-orange oil [yield 25%, ($d_2 = 95\%$)]. This was used immediately in the Waters/Micromass Q-ToF 2 mass spectrometer to form PhCD₂CH₂CS₂⁻ via ESI CID.

6.4.3 Theoretical Methods

Geometry optimisations were carried out with the Becke 3LYP method^{65, 103} using the 6-31+G(d,p) basis set¹⁰⁴⁻¹⁰⁶ within the GAUSSIAN 03⁶⁷ suite of programs. Stationary points were characterised as either minima (no imaginary frequencies) or transition states (one imaginary frequency) by calculation of the frequencies using analytical gradient procedures. The minima connected by a given transition structure were confirmed by Intrinsic Reaction Coordinate (IRC) calculations.¹⁰⁷ The calculated frequencies were also used to determine zero-point vibrational energies which were then used as a zero-point correction for electronic energies. More accurate energies for the B3LYP geometries were determined using the UCCSD(T) method^{109, 110} including zero-point energy correction (calculated by vibrational frequencies at the B3LYP/6-31+G(d,p) level of theory). All calculations were carried out using the South Australian Partnership for Advanced Computing (SAPAC) facility.

REFERENCES

1. Beynon, J. H., Caprioli, R.M., Ast, T. The Effect of Deuterium Labelling on the Width of a 'Metastable Peak'. *Org. Mass Spectrom.* **1971**, 5, 229-234.
2. Johnson, E. G., Nier, A.O. Angular Aberrations in Sector Shaped Electromagnetic Lenses for Focusing Beams of Charged Particles. *Phys. Rev.* **1953**, 91, 10-17.
3. Beynon, J. H., Cooks, R. G., Amy, J. W., Baitinger, W. E., Ridley, T. Y. Design and Performance of a Mass-Analyzed Ion Kinetic Energy (MIKE) Spectrometer. *Anal. Chem.* **1973**, 45, 1023A-1031A.
4. Dempster, A. J. A New Method of Positive Ray Analysis. *Phys. Rev.* **1918**, 11, 316-325.
5. Williams, D. H., Fleming, I. *Spectroscopic Methods in Organic Chemistry*. 5th ed.; McGraw-Hill: London: **1995**; p 329.
6. Hamill, W. H., Williams, R.R., MacKay, C. *Principles of Physical Chemistry*. 2nd ed.; Prentice-Hall Inc.: New Jersey: **1966**; p 576.
7. Atkins, P. W. *Quanta: A Handbook of Concepts*. 2nd ed.; Oxford University Press: Oxford: **1991**; p 440.
8. Rose, M. E., Johnstone, R.A.W. *Mass Spectrometry for Chemists and Biochemists*. 2nd ed.; Cambridge University Press: Cambridge: **1996**; p 524.
9. Budzikiewicz, H. Mass Spectrometry of Negative Ions. *Angew. Chem., Int. Ed. Engl.* **1981**, 20, 624-637.
10. Dillard, J. G. Negative Ion Mass Spectrometry. *Chem. Rev.* **1973**, 73, 589-643.

REFERENCES

11. Harrison, A. G. *Chemical Ionisation Mass Spectrometry*. 2nd ed.; CRC Press: Boca Raton: **1983**; p 224.
12. Froelicher, S. W., Freiser, B.S., Squires, R.R. The $C_3H_5^-$ Isomers. Experimental and Theoretical Studies of Tautomeric Propenyl Ions and the Cyclopropyl Anion in the Gas Phase. *J. Am. Chem. Soc.* **1986**, 108, 2853-2862.
13. DePuy, C. H., Bierbaum, V.M., Flippin, L.A., Grabowski, J.J., King, G.K., Schmitt, R.J., Sullivan, S.A. Gas-Phase Reactions of Anions with Substituted Silanes. *J. Am. Chem. Soc.* **1980**, 102, 5012-5015.
14. Klass, G., Trenerry, V.C., Sheldon, J.C., Bowie, J.H. An *Ab Initio* and Ion Cyclotron Resonance Study of the Reactions Between Alkoxide Negative Ions and Silane Systems. Stable Adduct Formation, and Nucleophilic Displacement Reactions. *Aust. J. Chem.* **1981**, 34, 519-529.
15. Yates, B. F., Bouma, W.J., Radom, L. Detection of the Prototype Phosphonium (CH_2PH_3), Sulfonium (CH_2SH_2), and Chloronium (CH_2ClH) Ylides by Neutralization-Reionization Mass Spectrometry: A Theoretical Prediction. *J. Am. Chem. Soc.* **1984**, 106, 5805-5808.
16. Wenthold, P. G., Hu, J., Squires, R.R. Regioselective Synthesis of Biradical Negative Ions in the Gas Phase. Generation of Trimethylenemethane, *m*-Benzyne, and *p*-Benzyne Anions. *J. Am. Chem. Soc.* **1994**, 116, 6961-6962.
17. Wenthold, P. G., Hu, J., Squires, R.R. *o*-, *m*-, and *p*-Benzyne Negative Ions in the Gas Phase: Synthesis, Authentication and Thermochemistry. *J. Am. Chem. Soc.* **1996**, 118, 11865-11871.
18. Dua, S., Blanksby, S.J., Bowie, J.H. Conversion of Neutral C_2COC_2 to C_4CO . Potential Interstellar Molecules. *Int. J. Mass Spectrom.* **2000**, 195/196, 45-54.

REFERENCES

19. Eichinger, P. C. H., Bowie, J.H., Blumenthal, T. Gas-Phase Wittig Rearrangement of Carbanions Derived from Benzyl Ethers. *J. Org. Chem.* **1986**, 51, 5078-5082.
20. McDonald, R. N., Chowdhury, A.K., Setser, D.W. Hypovalent Radicals. 4. Gas-Phase Studies of the Ion-Molecule Reactions of Cyclopentadienylidene Anion Radical in a Flowing Afterglow. *J. Am. Chem. Soc.* **1980**, 102, 6491-6498.
21. Dawson, J. H. J., Jennings, K.R. Production of Gas-Phase Radical Anions by Reaction of O⁻ Ions with Organic Substrates. *J. Chem. Soc. Faraday Trans. II* **1976**, 72, 700-706.
22. Goode, G. C., Jennings, K.R. Reactions of O⁻ Ions with Some Unsaturated Hydrocarbons. *Adv. Mass Spectrom.* **1974**, 797-803.
23. Lee, J., Grabowski, J.J. Reactions of the Atomic Oxygen Radical Anion and the Synthesis of Organic Reactive Intermediates. *Chem. Rev.* **1992**, 92, 1611-1647.
24. Nibbering, N. M. M. Bimolecular Gas-Phase Reactions of Anions. *Recl. Trav. Chim. Pays-Bas.* **1981**, 100, 297-306.
25. Cooks, R. G., Beynon, J.H., Caprioli, R.M., Lester, G.R. *Metastable Ions*. Elsevier: Amsterdam: **1973**; p 296.
26. Haddon, W. F., McLafferty, F.W. Metastable Ion Characteristics. VII. Collision-Induced Metastables. *J. Am. Chem. Soc.* **1968**, 90, 4745-4746.
27. Kim, M. S., McLafferty, F.W. Efficiency of Collisional Activation of Gaseous Organic Ions. *J. Am. Chem. Soc.* **1978**, 100, 3279-3282.
28. Laramée, J. A., Cameron, D., Cooks, R.G. Collision-Induced Dissociation Mass Spectrometry: Target Gas Effects upon Scattering and Charge Exchange. *J. Am. Chem. Soc.* **1981**, 103, 12-17.

REFERENCES

29. Holmes, J. L. Assigning Structures to Ions in the Gas Phase. *Org. Mass Spectrom.* **1985**, 20, 169-183.
30. Szulejko, J. E., Bowie, J.H., Howe, I., Beynon, J.H. The Energetics of the Formation of Positive Ions Produced by Charge-Stripping from Negative Ions. *Int. J. Mass Spectrom. Ion Phys.* **1980**, 34, 99-111.
31. Bowie, J. H., Blumenthal, T. +E Collision Induced Mass Spectra from Negative Ions. *J. Am. Chem. Soc.* **1975**, 97, 2959-2962.
32. Bowie, J. H., Blumenthal, T. Electron Impact Studies. CII* +E Spectra from Negative Ions. Flavones and Quinones. *Aust. J. Chem.* **1976**, 29, 115-121.
33. Danis, P. O., Feng, R., McLafferty, F.W. Neutralization Agents for Neutralization-Reionization Mass Spectrometry. *Anal. Chem.* **1986**, 58, 348-354.
34. Bursey, M. M., Hass, J.R., Harvan, D.J., Parker, C.E. Consequences of Charge Reversal in Gaseous Alkoxide Ions. Oxenium Ions. *J. Am. Chem. Soc.* **1979**, 101, 5485-5489.
35. Burgers, P. C., Holmes, J.L., Mommers, A.A., Szulejko, J.E. Generation and Identification of Four Stable Isomeric $[C_3H_3]^+$ Ions by Direct Dissociative Ionization or by Charge Reversal of Anions. *J. Am. Chem. Soc.* **1984**, 106, 521-525.
36. Keough, T., Beynon, J.H., Cooks, R.G. ^-E Mass Spectra. *J. Am. Chem. Soc.* **1973**, 95, 1695-1697.
37. McLafferty, F. W. Studies of Unusual Simple Molecules by Neutralization-Reionization Mass Spectrometry. *Science* **1990**, 247, 925-929.
38. Terlouw, J. K., Schwarz, H. The Generation and Characterization of Molecules by Neutralization-Reionization Mass Spectrometry (NRMS). *Angew. Chem., Int. Ed. Engl.* **1987**, 26, 805-815.

REFERENCES

39. Zagorevskii, D. V., Holmes, J.L. Neutralization-Reionization Mass Spectrometry Applied to Organometallic and Coordination Chemistry. *Mass Spectrom. Rev.* **1994**, 13, 133-154.
40. Goldberg, N., Schwarz, H. Neutralization-Reionization Mass Spectrometry: A Powerful "Laboratory" to Generate and Probe Elusive Neutral Molecules. *Acc. Chem. Res.* **1994**, 27, 347-352.
41. McLafferty, F. W., Todd, P.J., McGilvery, D.C., Baldwin, M.A. High-Resolution Tandem Mass Spectrometer (MS/MS) of Increased Sensitivity and Mass Range. *J. Am. Chem. Soc.* **1980**, 102, 3360-3363.
42. Bowie, J. H. Charge-stripping of Anions in the Gas Phase: The Formation of Interesting Neutrals and Cations. *Int. J. Mass Spectrom.* **2001**, 212, 249-265.
43. McMahan, A. W., Chowdhury, S.K., Harrison, A.G. Negative-Ion-Negative-Ion Neutralization-Reionization ($^{-}NR^{-}$). *Org. Mass Spectrom.* **1989**, 24, 620-624.
44. Schalley, C. A., Hornung, G., Schröder, D., Schwarz, H. Mass Spectrometric Approaches to the Reactivity of Transient Neutrals. *Chem. Soc. Rev.* **1998**, 27, 91-104.
45. Schalley, C. A., Hornung, G., Schröder, D., Schwarz, H. Mass Spectrometry as a Tool to Probe the Gas-Phase Reactivity of Neutral Molecules. *Int. J. Mass Spectrom. Ion Processes* **1998**, 172, 181-208.
46. McLafferty, F. W. *Decompositions and Rearrangements of Organic Ions*. Academic Press: New York, **1963**; p 730.
47. Budzikiewicz, H., Djerassi, C., Williams, D.H. *Mass Spectrometry of Organic Compounds*. Holden-Day: San Francisco, **1967**; p 690.
48. Williams, D. H., Howe, I. *Principles of Organic Mass Spectrometry*. McGraw-Hill: London, **1972**; p 797.

REFERENCES

49. Bowie, J. H. The Fragmentation of Even-Electron Organic Negative Ions. *Mass Spectrom. Rev.* **1990**, 9, 349-379.
50. Bowie, J. H. The Fragmentations of (M-H)⁻ Ions Derived from Organic Compounds: An Aid to Structure Determination. In *Experimental Mass Spectrometry.*, Russell, D. H., Ed. Plenum Press: New York, **1994**; pp 1-38.
51. Longevialle, P. Ion-Neutral Complexes in the Unimolecular Reactivity of Organic Cations in the Gas Phase. *Mass Spectrom. Rev.* **1992**, 11, 157-192.
52. Foresman, J. B., Frisch, Æ. *Exploring Chemistry with Electronic Structure Methods*. 2nd ed.; Gaussian Inc.: Pittsburgh, **1996**; p 302.
53. Born, M., Oppenheimer, J.R. Quantum Theory of Molecules. *Ann. Phys.* **1927**, 84, 457-484.
54. Hartree, D. R. The Wave Mechanics of an Atom with a Non-Coulomb Central Field. III. Term Values and Intensities in Series in Optical Spectra. *Proceedings of the Cambridge Philosophical Society* **1928**, 24, 426-437.
55. Fock, V. "Self-Consistent Field" with Interchange for Sodium. *Physik* **1930**, 62, 795-805.
56. Scuseria, G. E., Lee, T.J. Comparison of Coupled-Cluster Methods Which Include the Effects of Connected Triple Excitations. *J. Chem. Phys.* **1990**, 93, 5851-5855.
57. Lee, T. J., Scuseria, S.G. The Vibrational Frequencies of Ozone. *J. Chem. Phys.* **1990**, 93, 489-494.
58. Raghavachari, K., Trucks, G.W., Pople, J.A., Head-Gordon, M. A Fifth-Order Perturbation Comparison of Electron Correlation Theories. *Chem. Phys. Lett.* **1989**, 157, 479-483.

REFERENCES

59. Dreuw, A., Head-Gordon, M. Single-Reference *Ab Initio* Methods for the Calculation of Excited States of Large Molecules. *Chem. Rev.* **2005**, 105, 4009-4037.
60. Hohenberg, P., Kohn, W. Inhomogeneous Electron Gas. *Phys. Rev.* **1964**, 136, B864-B871.
61. Kohn, W., Sham, L. Self-Consistent Equations Including Exchange and Correlation Effects. *Phys. Rev.* **1965**, 140, A1133-A1138.
62. Becke, A. D. Density-Functional Exchange-Energy Approximation with Correct Asymptotic Behavior. *Phys. Rev. A* **1988**, 38, 3098-3100.
63. Perdew, J. P. Density-Functional Approximation for the Correlation Energy of the Inhomogeneous Electron Gas. *Phys. Rev. B* **1986**, 33, 8822-8824.
64. Lee, C., Yang, W., Parr, R.G. Development of the Colle-Salvetti Correlation-Energy Formula into a Functional of the Electron Density. *Phys. Rev. B* **1988**, 37, 785-789.
65. Becke, A. D. Density-Functional Thermochemistry. III. The Role of Exact Exchange. *J. Chem. Phys.* **1993**, 98, 5648-5652.
66. Wong, M. W. Vibrational Frequency Prediction using Density Functional Theory. *Chem. Phys. Lett.* **1996**, 256, 391-399.
67. Frisch, M. J., Trucks, G. W., Schlegel, H. B., Scuseria, G. E., Robb, M. A., Cheeseman, J. R., Montgomery, Jr., J. A., Vreven, T., Kudin, K. N., Burant, J. C., Millam, J. M., Iyengar, S. S., Tomasi, J., Barone, V., Mennucci, B., Cossi, M., Scalmani, G., Rega, N., Petersson, G. A., Nakatsuji, H., Hada, M., Ehara, M., Toyota, K., Fukuda, R., Hasegawa, J., Ishida, M., Nakajima, T., Honda, Y., Kitao, O., Nakai, H., Klene, M., Li, X., Knox, J. E., Hratchian, H. P., Cross, J. B., Bakken, V., Adamo, C., Jaramillo, J., Gomperts, R., Stratmann, R. E., Yazyev, O., Austin, A. J., Cammi, R., Pomelli, C., Ochterski, J. W., Ayala, P. Y., Morokuma, K., Voth, G. A., Salvador, P., Dannenberg, J. J., Zakrzewski, V. G., Dapprich, S., Daniels, A. D., Strain, M. C.,

REFERENCES

Farkas, O., Malick, D. K., Rabuck, A. D., Raghavachari, K., Foresman, J. B., Ortiz, J. V., Cui, Q., Baboul, A. G., Clifford, S., Cioslowski, J., Stefanov, B. B., Liu, G., Liashenko, A., Piskorz, P., Komaromi, I., Martin, R. L., Fox, D. J., Keith, T., Al-Laham, M. A., Peng, C. Y., Nanayakkara, A., Chalacombe, M., Gill, P. M. W., Johnson, B., Chen, W., Wong, M. W., Gonzalez, C., Pople, J. A. Gaussian 03, Revision C.02, Gaussian, Inc., Wallingford CT. **2004**.

68. Guélin, M., Thaddeus, P. Tentative Detection of the C₃N Radical. *Astrophys. J.* **1977**, 212, L81-L85.

69. Guélin, M., Green, S., Thaddeus, P. Detection of the C₄H Radical Toward IRC +10216. *Astrophys. J.* **1978**, 224, L27-L30.

70. Friberg, P., Hjalmarsen, A., Irvine, W.M., Guélin, M. Interstellar C₃N: Detection in Taurus Dark Clouds. *Astrophys. J.* **1980**, 241, L99-L103.

71. McCabe, E. M., Smith, R.C., Clegg, R.E.S. Molecular Abundances in IRC +10216. *Nature* **1979**, 281, 263-266.

72. Mitchell, G. F., Huntress, W.T., Jr., Prasad, S.S. Interstellar Synthesis of the Cyanopolynes and Related Molecules. *Astrophys. J.* **1979**, 233, 102-108.

73. Winnewisser, G., Walmsley, C.M. Carbon Chain Molecules in Interstellar Clouds. *Astrophys. Space Sci.* **1979**, 65, 83-93.

74. Cernicharo, J., Guélin, M., Askne, J. TMC1-Like Cloudlets in HCL 2. *Astron. Astrophys.* **1984**, 138, 371-379.

75. Henkel, C., Jethava, N., Kraus, A., Menten, K.M., Carilli, C.L., Grasshoff, M., Lubowich, D., Reid, M.J. The Kinetic Temperature of a Molecular Cloud at Redshift 0.7: Ammonia in the Gravitational Lens B0218+357. *Astron. Astrophys.* **2005**, 440, 893-899.

REFERENCES

76. Redondo, P., Ruiz, M.J., Boronat, R., Barrientos, C., Largo, A. Theoretical Study of the Reaction of CN with $C_2H_2^+$. *Theor. Chem. Acc.* **2000**, 104, 199-202.
77. Woon, D. E., Herbst, E. The Rate of the Reaction Between CN and C_2H_2 at Interstellar Temperatures. *Astrophys. J.* **1997**, 477, 204-208.
78. Barrientos, C., Redondo, P., Largo, A. Reaction of $C_3H_2^+$ with Atomic Nitrogen: A Theoretical Study. *J. Phys. Chem. A* **2000**, 104, 11541-11548.
79. Wilson, S. Theoretical Study of Isocyanoacetylene and the Isocyanoethynyl Radical. *Astrophys. J.* **1978**, 220, 363-365.
80. Gensheimer, P. D. Detection of HCCNC from IRC + 10216. *Astrophys. J.* **1997**, 479, L75-L78.
81. Kawaguchi, K., Ohishi, M., Ishikawa, S.-I., Kaifu, N. Detection of Isocyanoacetylene HCCNC in TMC-1. *Astrophys. J.* **1992**, 386, L51-L53.
82. Gottlieb, C. A., Gottlieb, E.W., Thaddeus, P., Kawamura, H. Laboratory Detection of the C_3N and C_4H Free Radicals. *Astrophys. J.* **1983**, 275, 916-921.
83. Blanksby, S. J., Schröder, D., Dua, S., Bowie, J.H., Schwarz, H. Conversion of Linear to Rhombic C_4 in the Gas Phase: A Joint Experimental and Theoretical Study. *J. Am. Chem. Soc.* **2000**, 122, 7105-7113.
84. Tran, K. M., McAnoy, A.M., Bowie, J.H. Do the Interstellar Molecules CCCO and CCCS Rearrange when Energised? *Org. Biomol. Chem.* **2004**, 2, 999-1006.
85. Wootten, A. The 129 Reported Interstellar and Circumstellar Molecules. <http://www.cv.nrao.edu/~awootten/allmols.html>.
86. Blanksby, S. J., Dua, S., Bowie, J.H., Schröder, D., Schwarz, H. Syntheses of NCN and NC_3N from Ionic Precursors in the Gas Phase and an Unusual Rearrangement of Neutral NC_3N : A Joint Experimental and Theoretical Study. *J. Phys. Chem. A* **2000**, 104, 11248-11256.

REFERENCES

87. Zagorevskii, D. V., Holmes, J.L. Neutralization-Reionization Mass Spectrometry Applied to Organometallic and Coordination Chemistry (Update: 1994-1998). *Mass Spectrom. Rev.* **1999**, 18, 87-118.
88. Sülzle, D., Seemayer, K., Schwarz, H., Witulski, B., Hopf, H. On the Generation of Polycarbon Nitride Radicals $C_nN^{\cdot-}$ ($n = 2-5$) by Neutralization-Reionization Mass Spectrometry. *Chem. Ber.* **1991**, 124, 1481-1483.
89. Bursley, M. M. Charge Inversion of Negative Ions in Tandem Instruments. *Mass Spectrom. Rev.* **1990**, 9, 555-574.
90. Ding, Y. H., Huang, X.R., Lu, Z.Y., Feng, J.N. Theoretical Studies on the Structures and Isomerization of C_3N^+ . *Chem. Phys. Lett.* **1998**, 284, 325-330.
91. Wilson, S., Green, S. Theoretical Study of the Butadiynyl and Cyanoethynyl Radicals: Support for the Identification of C_3N in IRC +10216. *Astrophys. J.* **1977**, 212, L87-L90.
92. Sadlej, J., Roos, B.O. A CASSCF-MRCI Study of the Ground and Lower Excited States of the CCCN Radical. *Chem. Phys. Lett.* **1991**, 180, 81-87.
93. Feher, M. Calculated Spectroscopic Properties of CCCN and CCNC. *Chem. Phys. Lett.* **1992**, 188, 609-612.
94. Botschwina, P., Horn, M., Flugge, J., Seeger, S. *Ab Initio* Calculations on Molecules of Interest to Interstellar Cloud Chemistry. *J. Chem. Soc. Faraday Trans.* **1993**, 89, 2219-2230.
95. Mizuno, S., Fujita, M., Nakao, K. Electronic States of Graphitic Heterocompounds of Carbon, Boron, and Nitrogen. *Synthetic Metals* **1995**, 71, 1869-1870.
96. Sandre, E., Pickard, C.J., Colliex, C. What are the Possible Structures for CN_x Compounds? The Example of C_3N . *Chem. Phys. Lett.* **2000**, 325, 53-60.

REFERENCES

97. Belbruno, J. J., Tang, Z-C., Smith, R., Hobday, S. The Structure and Energetics of Carbon-Nitrogen Clusters. *Molec. Phys.* **2001**, 99, 957-967.
98. Ding, Y. H., Li, Z.S., Huang, X.R., Sun, C-C. Theoretical Study on Potential Energy Surface of the Interstellar Molecule SiC₂N. *J. Phys. Chem. A* **2001**, 105, 5896-5901.
99. Chen, G.-H., Ding, Y.H., Huang, X.R., Sun, C-C. Theoretical Study on Structures and Stability of Si₂CP Isomers. *J. Phys. Chem. A* **2005**, 109, 5619-5624.
100. McCarthy, M. C., Fuchs, G.W., Kucera, J., Winnewisser, G., Thaddeus, P. Rotational Spectra of C₄N, C₆N, and the Isotopic Species of C₃N. *J. Chem. Phys.* **2003**, 118, 3549-3557.
101. Francisco, J. S., Richardson, S.L. Determination of the Heats of Formation of CCCN and HCCCN. *J. Chem. Phys.* **1994**, 101, 7707-7711.
102. McAnoy, A. M., Bowie, J.H., Dua, S. The Formation of Cyanoketene (NCCHCO) and the Isomer NCCCHO from Anionic Precursors in the Gas Phase. The Rearrangement of NCCCHO to NCCHCO. *J. Phys. Chem. A* **2004**, 108, 3994-4001.
103. Stephens, P. J., Devlin, F.J., Chabalowski, C.F., Frisch, M.J. *Ab Initio* Calculation of Vibrational Absorption and Circular Dichroism Spectra using Density Functional Force Fields. *J. Phys. Chem.* **1994**, 98, 11623-11627.
104. Dunning, T. H. Gaussian Basis Sets for use in Correlated Molecular Calculations. I. The Atoms Boron through Neon and Hydrogen. *J. Chem. Phys.* **1989**, 90, 1007-1023.
105. Woon, D. E., Dunning, Jr., T.H. Gaussian Basis Sets for use in Correlated Molecular Calculations. III. The Atoms Aluminium through Argon. *J. Chem. Phys.* **1993**, 98, 1358-1371.

REFERENCES

106. Dunning, T.H., Peterson, K.A., Woon, D.E. Basis Sets: Correlation Consistent. In *Encyclopedia of Computational Chemistry*; Schleyer, P.V.R., Ed; Wiley: Chichester, UK, **1998**; p 88.
107. Fukui, K. The Path of Chemical Reactions - The IRC Approach. *Acc. Chem. Res.* **1981**, 14, 363-368.
108. Blanksby, S. J., Dua, S., Bowie, J.H. Generation of Two Isomers of C₅H from the Corresponding Anions. A Theoretically Motivated Mass Spectrometric Study. *J. Phys. Chem.* **1999**, 103, 5161-5170.
109. Cizek, J. On the use of the Cluster Expansion and the Technique of Diagrams in Calculations of Correlation Effects in Atoms and Molecules. *Adv. Chem. Phys.* **1969**, 14, 35-89.
110. Watts, J. D., Gauss, J., Bartlett, R.J. Coupled-Cluster Methods with Noniterative Triple Excitations for Restricted Open-Shell Hartree-Fock and other General Single Determinant Reference Functions. Energies and Analytical Gradients. *J. Chem. Phys.* **1993**, 98, 8718-8733.
111. Arnold, D. W., Bradforth, S.E., Kitsopolous, T.N., Neumark, D.M. Vibrationally Resolved Spectra of C₂-C₁₁ by Anion Photoelectron Spectroscopy. *J. Chem. Phys.* **1991**, 95, 8753-8764.
112. Xu, C., Burton, G.R., Taylor, T.R., Neumark, D.M. Photoelectron Spectroscopy of C₄⁻, C₆⁻, and C₈⁻. *J. Chem. Phys.* **1997**, 107, 3428-3436.
113. Maclean, M. J., Fitzgerald, M., Bowie, J.H. Interstellar Molecule CCCN May Be Formed by Charge-Stripping of [CCCN]⁻ in the Gas Phase, and When Energized, Undergoes Loss of C with Partial Carbon Scrambling. *J. Phys. Chem. A* **2007**, 111, 12932-12937.
114. Burbidge, E. M., Burbidge, G.R., Fowler, W.A., Hoyle, F. Synthesis of the Elements in Stars. *Rev. Mod. Phys.* **1957**, 29, 547-650.

REFERENCES

115. Charnley, S. B., Ehrenfreund, P., Kuan, Y.-J. Spectroscopic Diagnostics of Organic Chemistry in the Protostellar Environment. *Spectrochim. Acta, Part A*. **2001**, 57, 685-704.
116. Kuan, Y.-J., Charnley, S.B., Huang, H-C., Tseng, W-L., Kisiel, Z. Interstellar Glycine. *Astrophys. J.* **2003**, 593, 848-867.
117. Snyder, L. E., Lovas, F.J., Hollis, J.M., Friedel, D.N., Jewell, P.R., Remijan, A., Ilyushin, V.V., Alekseev, E.A., Dyubko, S.F. A Rigorous Attempt to Verify Interstellar Glycine. *Astrophys. J.* **2005**, 619, 914-930.
118. Bernstein, M. P., Ashbourn, S.F.M., Sandford, S.A., Allamandola, L.J. The Lifetimes of Nitriles (CN) and Acids (COOH) During Ultraviolet Photolysis and Their Survival In Space. *Astrophys. J.* **2004**, 601, 365-370.
119. Boechat-Roberty, H. M., Pilling, S., Santos, A.C.F. Destruction of Formic Acid by Soft X-rays in Star-Forming Regions. *Astron. Astrophys.* **2005**, 438, 915-922.
120. Balucani, N., Asvany, O., Chang, A.H.H., Lin, S.H., Lee, Y.T., Kaiser, R.I. Osamura, Y. Crossed Beam Reaction of Cyano Radicals with Hydrocarbon Molecules. III. Chemical Dynamics of Vinylcyanide ($C_2H_3CN; X^1A'$) Formation from Reaction of $CN(X^2E^+)$ with Ethylene, $C_2H_4(X^1A_g)$ *J. Chem. Phys.* **2000**, 113, 8643-8655.
121. Andrezza, H. J., Fitzgerald, M., Bowie, J.H. The Formation of the Stable Radicals $\cdot CH_2CN$, $CH_3\cdot CHCN$ and $\cdot CH_2CH_2CN$ from the Anions $^-CH_2CN$, CH_3^-CHCN and $^-CH_2CH_2CN$ in the Gas Phase. A Joint Experimental and Theoretical Study. *Org. Biomol. Chem.* **2006**, 4, 2466-2472.
122. Walch, S. P., Bakes, E.L.O. On the Reaction $CH_2NH_2^+ + HCN/HNC \rightarrow NH_2CH_2CNH^+$. *Chem. Phys. Lett.* **2001**, 346, 267-273.
123. Petrie, S., Herbst, E. Some Interstellar Reactions Involving Electrons and Neutral Species: Attachment and Isomerization. *Astrophys. J.* **1997**, 491, 210-215.

REFERENCES

124. Fitzgerald, M., Bowie, J.H., Dua, S. Generation of Neutrals from Ionic Precursors in the Gas Phase. The Rearrangement of CCCCCHO to HCCCCCO. *Org. Biomol. Chem.* **2003**, 1, 1769-1778.
125. Fitzgerald, M., Bowie, J.H., Dua, S. Gas Phase Generation of the Neutrals H₂CCCCO, HCCCCDO and CCCHCHO from Anionic Precursors. Rearrangements of HCCCCDO and CCCHCHO. A Joint Experimental and Theoretical Study. *Org. Biomol. Chem.* **2003**, 1, 3111-3119.
126. Cernicharo, J., Goicoechea, J.R., Benilan, Y. A New Infrared Band in Interstellar and Circumstellar Clouds: C₄ or C₄H? . *Astrophys. J.* **2002**, 580, L157-L160.
127. Trimble, V. The Origin and Abundances of the Chemical Elements. *Rev. Mod. Phys.* **1975**, 47, 877-976.
128. Hirahara, Y., Ohshima, Y., Endo, Y. Laboratory Detection of a New Free Radical C₄S (³S⁻). *Astrophys. J.* **1993**, 408, L113-L115.
129. Kasai, Y., Obi, K., Ohshima, Y., Hirahara, Y., Endo, Y., Kawaguchi, K., Muramaki, A. Laboratory Detection of C₅S by Pulsed-Discharge-Nozzle Fourier Transform Microwave Spectroscopy. *Astrophys. J.* **1993**, 410, L45-L47.
130. Brown, R. D., Godfrey, P.D., Cragg, D.M., Rice, E.H.N., Irvine, W.M., Friberg, P., Suzuki, H., Ohishi, M., Kaifu, N., Morimoto, M. Tricarbon Monoxide in TMC-1. *Astrophys. J.* **1985**, 297, 302-308.
131. Ohishi, M., Suzuki, H., Ishikawa, S.-I., Yamada, C., Kanamori, H., Irvine, W.M., Brown, R.D., Godfrey, P.D., Kaifu, N. Detection of a New Carbon-Chain Molecule, CCO. *Astrophys. J.* **1991**, 380, L39-L42.
132. Merrill, P. W. Note on the Spectrum of UV Aurigae. *Publ. Astron. Soc. Pac.* **1926**, 38, 175-176.

REFERENCES

133. Sanford, R. F. Two Bands in Spectra of Class N. *Publ. Astron. Soc. Pac.* **1926**, 38, 177.
134. Cernicharo, J., Gottlieb, C.A., Guellin, M., Thaddeus, P., Vrtilik, J.M. Astronomical and Laboratory Detection of the SiC Radical. *Astrophys. J.* **1989**, 341, L25-L28.
135. Ohishi, M., Kaifu, N., Kawaguchi, K., Murakami, A., Saito, S., Yamamoto, S., Ishikawa, S.-I., Fujita, Y., Shiratori, Y., Irvine, W.M. Detection of a New Circumstellar Carbon Chain Molecule, C₄Si. *Astrophys. J.* **1989**, 345, L83-L86.
136. Howe, D. A., Millar, T.J. The Formation of Carbon Chain Molecules in IRC +10216. *Mon. Not. R. Astron. Soc.* **1990**, 244, 444-449.
137. Apponi, A. J., McCarthy, M.C., Gottlieb, C.A., Thaddeus, P. Astronomical Detection of Rhomboidal SiC₃. *Astrophys. J.* **1999**, 516, L103-L106.
138. Nakajima, A., Taguwa, T., Nakao, K., Gomei, M., Kishi, R., Iwata, S., Kaya, K. Photoelectron Spectroscopy of Silicon-Carbon Cluster Anions (Si_nC_m⁻). *J. Chem. Phys.* **1995**, 103, 2050-2057.
139. McCarthy, M. C., Apponi, A.J., Thaddeus, P. Rhomboidal SiC₃. *J. Chem. Phys.* **1999**, 110, 10645-10648.
140. Apponi, A. J., McCarthy, M.C., Gottlieb, C.A., Thaddeus, P. The Rotational Spectrum of Rhomboidal SiC₃. *J. Chem. Phys.* **1999**, 111, 3911-3918.
141. McCarthy, M. C., Apponi, A.J., Thaddeus, P. A Second Rhomboidal Isomer of SiC₃. *J. Chem. Phys.* **1999**, 111, 7175-7178.
142. McCarthy, M. C., Gottlieb, C.A., Thaddeus, P. Silicon Molecules in Space and in the Laboratory. *Molec. Phys.* **2003**, 101, 697-704.

REFERENCES

143. Alberts, I. L., Grev, R.S., Schaefer III, H.F. Geometrical Structures and Vibrational Frequencies of the Energetically Low-lying Isomers of SiC₃. *J. Chem. Phys.* **1990**, 93, 5046-5052.
144. Hunsicker, S., Jones, R.O. Structure and Bonding in Mixed Silicon-Carbon Clusters and their Anions. *J. Chem. Phys.* **1996**, 105, 5048-5060.
145. Gomei, M., Kishi, R., Nakajima, A., Iwata, S., Kaya, K. *Ab Initio* MO Studies of Neutral and Anionic SiC_n Clusters (*n* = 2-5). *J. Chem. Phys.* **1997**, 107, 10051-10061.
146. Stanton, J. F., Gauss, J., Christiansen, O. Equilibrium Geometries of Cyclic SiC₃ Isomers. *J. Chem. Phys.* **2001**, 114, 2993-2995.
147. Rintelman, J. M., Gordon, M.S. Structure and Energetics of the Silicon Carbide Clusters SiC₃ and Si₂C₂. *J. Chem. Phys.* **2001**, 115, 1795-1803.
148. Sattelmeyer, K. W., Schaefer III, H.F., Stanton, J.F. The Global Minimum Structure of SiC₃: The Controversy Continues. *J. Chem. Phys.* **2002**, 116, 9151-9153.
149. Kurashige, Y., Nakano, H., Hirao, K. The Most Stable Structure of SiC₃ Studied by Multireference Perturbation Theory with General Multiconfiguration Self-Consistent Field Reference Functions. *J. Phys. Chem. A* **2004**, 108, 3064-3067.
150. Rintelman, J. M., Gordon, M.S., Fletcher, G.D., Ivancic, J. A Systematic Multireference Perturbation-Theory Study of the Low-Lying States of SiC₃. *J. Chem. Phys.* **2006**, 124, 034303-1—034303-5.
151. Inostroza, N., Hochlaf, M., Senent, M.L., Letelier, J.R. *Ab Initio* Characterization of Linear C₃Si Isomers. *Astron. Astrophys.* **2008**, 486, 1047-1052.
152. Davico, G. E., Schwartz, R.L., Lineberger, W.C. Photoelectron Spectroscopy of C₃Si and C₄Si₂ Anions. *J. Chem. Phys.* **2001**, 115, 1789-1794.
153. MacKay, D. D. S., Charnely, S.B. Phosphorus in Circumstellar Envelopes. *Mon. Not. R. Astron. Soc.* **2001**, 325, 545-549.

REFERENCES

154. Guélin, M., Cernicharo, J., Paubert, G., Turner, B.E. Free CP in IRC +10216. *Astron. Astrophys.* **1990**, 230, L9-L11.
155. Turner, B. E., Bally, J. Detection of Interstellar PN: The First Identified Phosphorus Compound in the Interstellar Medium. *Astrophys. J.* **1987**, 321, L75-L79.
156. Ziurys, L. M. Detection of Interstellar PN: The First Phosphorus-Bearing Species Observed in Molecular Clouds. *Astrophys. J.* **1987**, 321, L81-L85.
157. Largo, A., Barrientos, C., Lopez, X., Ugalde, J.M. Theoretical Study of the C₂P Radical and (C₂P)⁺ Species. *J. Phys. Chem.* **1994**, 98, 3985-3988.
158. del Rio, E., Barrientos, C., Largo, A. Theoretical Study of the C₃P Radical and its Cation. *J. Phys. Chem.* **1996**, 100, 585-593.
159. Pascoli, G., Lavendy, H. Theoretical Study of C_nP, C_nP⁺, C_nP⁻ (n = 1-7) Clusters. *J. Phys. Chem. A* **1999**, 103, 3518-3524.
160. Pascoli, G., Lavendy, H. Geometrical Structures of the Phosphorus-Doped Carbon Cluster Cations C_nP⁺ (n = 1-20). *Int. J. Mass Spectrom.* **1999**, 189, 125-132.
161. Pascoli, G., Lavendy, H. Comparative *Ab Initio* Studies of Heteroatom-Doped Carbon Clusters C_nX_p⁺ (X = P, S; n + p = 3-6). *Int. J. Mass Spectrom.* **2001**, 206, 153-176.
162. Zhan, C.-G., Iwata, S. *Ab Initio* Studies on Structures, Vertical Electron Detachment Energies, and Stabilities of C_nP⁻ Clusters. *J. Chem. Phys.* **1997**, 107, 7323-7330.
163. Huang, R.-B., Wang, C.-R., Liu, Z.-Y., Zheng, L.-S., Qi, F., Sheng, L.-S., Yu, S.-Q., Zhang, Y.-W. Studies of Cluster Anions C_nX⁻ (X = N, P, As, Sb, Bi) Produced by Laser Ablation. *Z. Phys. D.* **1995**, 33, 49-52.

REFERENCES

164. Fisher, K., Dance, I., Willett, G. Carbon Phosphide Anions. *Eur. Mass Spectrom.* **1997**, 3, 331-338.
165. Li, G., Tang, Z. Parity Alternation Effects in the Stabilities of the Second-Row-Atom-Doped Linear Carbon Clusters $C_nX/C_nX^+/C_nX^-$ ($n = 1-10$; X = Na, Mg, Al, Si, P, S or Cl). A Comparative Study. *J. Phys. Chem. A* **2003**, 107, 5317-5326.
166. Wilson, I. R., Harris, G.M. The Oxidation of Thiocyanate Ion by Hydrogen Peroxide. I. The pH-Independent Reaction. *J. Am. Chem. Soc.* **1960**, 82, 4515-4517.
167. Wilson, I. R., Harris, G.M. The Oxidation of Thiocyanate Ion by Hydrogen Peroxide. II. The Acid-Catalyzed Reaction. *J. Am. Chem. Soc.* **1961**, 83, 286-289.
168. Oram, J. D., Reiter, B. The Inhibition of *Streptococci* by Lactoperoxidase, Thiocyanate and Hydrogen Peroxide. *Biochem. J.* **1966**, 100, 382-388.
169. Aune, T. M., Thomas, E.L. Accumulation of Hypothiocyanite Ion During Peroxidase-Catalyzed Oxidation of Thiocyanate Ion. *Eur. J. Biochem.* **1977**, 80, 209-214.
170. Bosch, E. H., Van Doorne, H., De Vries, S. The Lactoperoxidase System: The Influence of Iodide and the Chemical and Antimicrobial Stability over the Period of about 18 Months. *J. Appl. Microbiol.* **2000**, 89, 215-224.
171. Christy, A. A., Egeberg, P.K. Oxidation of Thiocyanate by Hydrogen Peroxide - A Reaction Kinetic Study by Capillary Electrophoresis. *Talanta* **2000**, 51, 1049-1058.
172. Rosin, M., Kocher, T., Kramer, A. Effects of SCN^-/H_2O_2 Combinations in Dentifrices on Plaque and Gingivitis. *J. Clin. Periodontol.* **2001**, 28, 270-276.
173. van Dalen, C. J., Kettle, A.J. Substrates and Products of Eosinophil Peroxidase. *Biochem. J.* **2001**, 358, 233-239.

REFERENCES

174. Arlandson, M., Decker, T., Roongta, V.A., Bonilla, L., Mayo, K.H., MacPherson, J.C., Hazen, S.L., Slungaard, A. Eosinophil Peroxidase Oxidation of Thiocyanate. *J. Biol. Chem.* **2001**, 276, 215-224.
175. Dua, S., Bowie, J.H. Formation of Cyanate (OCN) and Fulminate (ONC) Radicals from Anionic Precursors in the Gas Phase. A Joint Experimental and Theoretical Study. *J. Phys. Chem. A.* **2003**, 107, 76-82.
176. Fitzgerald, M., Bowie, J.H. The Generation of the Thiocyanate Radical and Cation from the Thiocyanate Anion [SCN]⁻ in the Gas Phase. The Rearrangements of Neutral and Cationic SCN. A Joint Experimental and Theoretical Study. *J. Phys. Chem. A* **2004**, 108, 3668-3674.
177. Blanksby, S. L., Bowie, J.H. Construction of Interstellar Cumulenes and Heterocumulenes: Mass Spectrometric Studies. *Mass Spectrom. Rev.* **1999**, 18, 131-151.
178. Cottin, H., Gazeau, M.C., Raulin, F. Cometary Organic Chemistry: A Review from Observations, Numerical and Experimental Simulations. *Planet. Space Sci.* **1999**, 47, 1141-1162.
179. Hudson, R. L., Moore, M.H., Gerakines, P.A. The Formation of Cyanite Ion (OCN⁻) in Interstellar Ice Analogs. *Astrophys. J.* **2001**, 550, 1140-1150.
180. Arlandson, M., Decker, T., Roongta, V.A., Bonilla, L., Mayo, K.H., MacPherson, J.C., Hazen, S.L., Slungaard, A. Eosinophil Peroxidase Oxidation of Thiocyanate. Characterization of Major Reaction Products and a Potential Sulfhydryl-Targeted Cytotoxicity System. *J. Biol. Chem.* **2001**, 276, 215-224.
181. Pyykko, P., Runeberg, N. Calculated Properties of OCNS⁻ and Related Species. *J. Chem. Soc., Chem. Commun.* **1991**, 547-548.
182. Bech, A. T., Flammang, R., Pedersen, C.Th., Wong, M.W., Wentrup, C. Alkoxy Isothiocyanates, RO-N=C=S. *J. Chem. Soc. Perkin Trans. 2* **1999**, 1869-1873.

REFERENCES

183. Flammang, R., Gerbaux, P., Wong, M.W. Identification of Singlet and Triplet SCNO⁺ Cations in the Gas Phase: Theory and Experiment. *Chem. Phys. Lett.* **1999**, 300, 183-188.
184. Peppe, S., Blanksby, S.J., Dua, S., Bowie, J.H. Formation of Two Isomeric C₃HO Radicals from Charged Precursors in the Gas Phase. Potential Interstellar Molecules. *J. Phys. Chem. A* **2000**, 104, 5817-5824.
185. Kumar, R. C., Shreeve, J.M. On the Reactions of CF₃SF₄Cl, (CF₃)₂SF₂, SF₄, and OSOCl₂ with Trimethyl Cyanide. *Z. Naturforsch* **1981**, 36, 1407-1410.
186. Anthoni, U., Larsen, C., Nielsen, P.H. N-Alkoxythiocarbamoylimidazoles. *Acta. Chem. Scand.* **1968**, 22, 1050-1051.
187. Crow, W. D., Leonard, N.J. 3-Isothiazolone-*cis*-3-Thiocyanoacrylamide Equilibria. *J. Org. Chem.* **1965**, 50, 2660-2665.
188. Frisch, M. J., Trucks, G.W., Schlegel, H.B., Scuseria, G.E., Robb, M.A., Cheeseman, J.R., Zakrzewski, V.G., Montgomery, J.A., Stratmann, R.E., Burant, J.C., Dapprich, S., Millam, J.M., Daniels, A.D., Kudin, K.N., Strain, M.C., Farkas, O., Tomasi, J., Barone, V., Cossi, M., Cammi, R., Mennucci, B., Pomelli, C., Adamo, C., Clifford, S., Ochterski, J., Pedersson, G.A., Ayala, P.Y., Cui, Q., Morokuma, K., Malick, D.K., Rabuck, A.D., Raghavachari, K., Foresman, J.B., Cioslowski, J., Ortiz, J.V., Baboul, A.G., Stefanov, B., Liu, G., Al-Latam, M.A., Peng, C.Y., Nanayakkara, A., Challacombe, M., Gill, P.M.W., Johnson, B., Chen, W., Wong, M.W., Andres, J.L., Gonzales, C., Head-Gordon, M., Replogle, E.S., Pople, J.A. Gaussian 98; Revision A.9 ed. Gaussian Inc. Pittsburgh, PA. **1998**.
189. Warren, L. A., Smiles, S. Dehydro-2-naphtholsulphone. *J. Chem. Soc.* **1930**, 1327-1331.
190. Warren, L. A., Smiles, S. *iso*-β-Naphthol Sulphide. *J. Chem. Soc.* **1930**, 956-963.

REFERENCES

191. Truce, W. E., Kreider, E.M., Brand, W.W. The Smiles and Related Rearrangements of Aromatic Systems. *Org. React.* **1970**, 18, 99-215.
192. McClement, C. S., Smiles, S. The Rearrangement of *Ortho*-hydroxy-sulphones. Part VI. *J. Chem. Soc.* **1937**, 1016-1021.
193. Schmidt, D. M., Bonvicino, G.E. Halogen-Activated Smiles Rearrangement. 2. *J. Org. Chem.* **1984**, 49, 1664-1666.
194. Musaev, D. G., Galloway, A.L., Menger, F.M. The Roles of Steric and Electronic Effects in the 2-Hydroxy-2'-Nitrodiphenyl Sulfones to 2-(*o*-Nitrophenoxy)-Benzene-Sulfinic Acids Rearrangement (Smiles). Computational Study. *J. Mol. Struct.-Theochem.* **2004**, 679, 45-52.
195. Mitchell, L. H., Barvian, N.C. A Homologous Enolate Truce-Smiles Rearrangement. *Tetrahedron Lett.* **2004**, 45, 5669-5671.
196. Li, J., Wang, L. Elucidation of the Mechanism for the S-N-type Smiles Rearrangement on Pyridine Rings. *Aust. J. Chem.* **2009**, 62, 176-180.
197. Mizuno, M., Yamano, M. A New Practical One-Pot Conversion of Phenols to Anilines. *Org. Lett.* **2005**, 7, 3629-3631.
198. Zuo, H., Meng, L., Ghate, M., Hwang, K.-H., Cho, Y. K., Chandrasekhar, S., Reddy, Ch. R., Shin, D.-S. Microwave-Assisted One-Pot Synthesis of Benzo[*b*][1,4]oxazin-3(4*H*)-ones *via* Smiles Rearrangement. *Tetrahedron Lett.* **2008**, 49, 3827-3830.
199. Xiang, J., Zheng, L., Xie, H., Hu, X., Dang, Q., Bai, X. Pyrrolo-Dihydropteridines *via* a Cascade Reaction Consisting of Iminium Cyclization and O-N Smiles Rearrangement. *Tetrahedron* **2008**, 64, 9101-9107.

REFERENCES

200. Xiang, J., Xie, H., Wen, D., Dang, Q., Bai, X. Synthesis of Pyrido[2,3-*e*]pyrrolo[1,2-*a*]pyrazine Derivatives *via* Tandem Iminium Cyclization and Smiles Rearrangement. *J. Org. Chem.* **2008**, 73, 3281-3283.
201. Motherwell, W. B., Pennell, A.M.K. A Novel Route to Biaryls *via* Intramolecular Free Radical *ipso* Substitution Reactions. *J. Chem. Soc. Chem. Commun.* **1991**, 877-879.
202. Caddick, S., Shering, C.L., Wadman, S.N. Radical Catalysed Cyclisations onto Sulfone-Substituted Indoles. *Tetrahedron* **2000**, 56, 465-473.
203. Ryokawa, A., Togo, H. Synthetic use of 1,1,2,2-Tetraphenyldisilane for the Preparation of Biaryls Through the Intramolecular Free Radical *ipso*-substitution of *N*-(2-bromoaryl)arenesulfonamides. *Tetrahedron* **2001**, 57, 5915-5921.
204. Tada, M., Shijima, H., Nakamura, M. Smiles-type Free Radical Rearrangement of Aromatic Sulfonates and Sulfonamides: Syntheses of Arylethanol and Arylethylamines. *Org. Biomol. Chem.* **2003**, 1, 2499-2505.
205. Snape, T. J. A Truce on the Smiles Rearrangement: Revisiting an Old Reaction - the Truce-Smiles Rearrangement. *Chem. Soc. Rev.* **2008**, 17, 2452-2458.
206. Eichinger, P. C. H., Bowie, J.H. The Gas-Phase Smiles Rearrangement the Effect of Ring Substitution. An ¹⁸O labelling Study. *Org. Mass Spectrom.* **1992**, 27, 995-999.
207. Eichinger, P. C. H., Bowie, J.H., Hayes, R.N. The Gas-Phase Smiles Rearrangement: A Heavy Atom Labelling Study. *J. Am. Chem. Soc.* **1989**, 111, 4224-4227.
208. DePuy, C. H., Bierbaum, V.M. Gas-Phase Reactions of Organic Anions as Studied by the Flowing Afterglow Technique. *Acc. Chem. Res.* **1981**, 14, 146-153.

REFERENCES

209. DePuy, C. H., Grabowski, J.J., Bierbaum, V.M. Chemical Reactions of Anions in the Gas Phase. *Science* **1982**, 218, 955-960.
210. Graul, S. T., Squires, R.R. Generation of Alkyl Carbanions in the Gas Phase. *J. Am. Chem. Soc.* **1990**, 112, 2506-2516.
211. Raftery, M. J., Bowie, J.H., Sheldon, J.C. Collision-Induced Dissociations of Aryl-Substituted Alkoxide Ions. Losses of Dihydrogen and Rearrangement Processes. *J. Chem. Soc. Perkin Trans. II* **1988**, 563-569.
212. Maas, W. P. M., Van Veelen, P.A., Nibbering, N.M.M. On the Generation and Characterization of the Spiro[2,5]Octadienyl Anion in the Gas Phase. *Org. Mass Spectrom.* **1989**, 24, 546-558.
213. Cooks, R. G., Kaiser, R.E. Jr. Quadrupole Ion Trap Mass Spectrometer. *Acc. Chem. Res.* **1990**, 23, 213-219.
214. Jonscher, K.R., Yates, J.R. III. The Quadrupole Ion Trap Mass Spectrometry: A Small Solution for a Big Challenge. *Analyt. Biochem.* **1997**, 244, 1-15.
215. Aldrich. Handbook of Fine Chemicals. **2007-2008**.
216. Gronert, S. Estimation of Effective Ion Temperatures in a Quadrupole Ion Trap. *J. Am. Soc. Mass Spectrom.* **1998**, 9, 845-848.
217. Gronert, S., Pratt, L.M., Mogali, S. Substituent Effects in Gas-Phase Substitutions and Eliminations: β -Halo Substituents. Solvation Reverses S_N2 Substituent Effects. *J. Am. Chem. Soc.* **2001**, 123, 3081-3091.
218. Shukla, A. K., Futrell, J.H. Tandem Mass Spectrometry: Dissociation of Ions by Collisional Activation. *J. Mass Spectrom.* **2000**, 35, 1069-1090.
219. de Hoffmann, E. Tandem Mass Spectrometry: A Primer. *J. Mass Spectrom.* **1996**, 31, 129-137.

REFERENCES

220. Kebarle, P. A Brief Overview of the Present Status of the Mechanisms Involved in Electrospray Mass Spectrometry. *J. Mass Spectrom.* **2000**, 35, 804-817.
221. Gomez, A., Tang, K. Charge and Fission of Droplets in Electrostatic Sprays. *Phys. Fluids* **1994**, 6, 404-414.
222. Graul, S. T., Squires, R.R. Advances in Flow Reactor Techniques for the Study of Gas-Phase Ion Chemistry. *Mass Spectrom. Rev.* **1988**, 7, 263-358.
223. Waters, T., O'Hair, R.A.J., Wedd, A.G. Catalytic Gas Phase Oxidation of Methanol to Formaldehyde. *J. Am. Chem. Soc.* **2003**, 125, 3384-3396.
224. Sheldon, J. C., Bowie, J.H., DePuy, C.H., Damrauer, R. Gas-Phase Reaction of Silyl and Trimethylsilyl Anions. The Formation of Silicon-Oxygen and Silicon-Sulfur Bonds. A Flowing Afterglow and *Ab Initio* Study. *J. Am. Chem. Soc.* **1986**, 108, 6794-6800.
225. Vogel, A. I. A Textbook of Practical Organic Chemistry. In 3rd ed.; Longmans, Green and Co.: London, **1956**; pp 247-260.
226. Westmijze, H., Kleijn, H., Meijer, J., Vermeer, P. Synthesis of Dithioesters from Organocopper(I) Compounds. *Synthesis* **1979**, 6, 432-434.
227. Lee, C. C., Tkachuk, R., Slater, G.P. Rearrangement Studies with ¹⁴C-VIII. External and Internal Returns in the Solvolysis of 2-Phenyl-1-¹⁴C-Ethyl *p*-Toluenesulfonate. *Tetrahedron* **1959**, 7, 206-212.
228. Smith, P. A. S. The Schmidt Reaction on *o*-Substituted Aryl Ketones. *J. Am. Chem. Soc.* **1954**, 76, 431-436.
229. Auwers, K., Roth, W.A. Thermochemische Untersuchungen. I. Über Beziehungen zwischen Konstitution und Verbrennungswarme ungesättigter Verbindungen. *Justus Liebigs Ann. Chem.* **1910**, 373, 239-248.

REFERENCES

230. Blum, J., Kraus, S., Pickholtz, Y. Decarbonylation and Dehydrohalogenation of Aliphatic Acyl Halides by Iridium and Rhodium Complexes. *J. Organomet. Chem.* **1971**, 33, 227-240.
231. Orfanopoulos, M., Smonou, I., Foote, C.S. Intermediates in the Ene Reactions of Singlet Oxygen and *N*-Phenyl-1,2,4-triazoline-3,5-dione with Olefins. *J. Am. Chem. Soc.* **1990**, 112, 3607-3614.

PUBLICATIONS

Is the hypothiocyanite anion (OSCN)⁻ the major product in the peroxidase catalyzed oxidation of the thiocyanate anion (SCN)⁻? A joint experimental and theoretical study.

Dua, S., Maclean, M.J., Fitzgerald, M., McAnoy, A.M., Bowie, J.H. *J. Phys. Chem. A* (2006) *110*, (14) 4930-4936.

Interstellar Molecule CCCN May Be Formed by Charge-Stripping of [CCCN]⁻ in the Gas Phase, and When Energized, Undergoes Loss of C with Partial Carbon Scrambling.

Maclean, M.J., Fitzgerald, M., Bowie, J.H. *J. Phys. Chem. A* (2007) *111*, (50) 12932-12937.

A Theoretical Study of the Cyclization Processes of Energized CCCSi and CCCP.

Maclean, M.J., Eichinger, P.C.H., Wang, T., Fitzgerald, M., Bowie, J.H. *J. Phys. Chem. A* (2008) *112*, (49) 12714-12720.

Diagnostic Fragmentations of Adducts Formed Between Carbanions and Carbon Disulfide in the Gas Phase. A Joint Experimental and Theoretical Study.

Maclean, M.J., Walker, S., Wang, T., Eichinger, P.C.H., Sherman, P.J., Bowie, J.H. *Org. Biomol. Chem.* (2010) *8*, 371-377.

Dua, S., Maclean, M.J., Fitzgerald, M., McAnoy, A.M., Bowie, J.H. (2006) Is the hypothiocyanite anion (OSCN)⁻ the major product in the peroxidase catalyzed oxidation of the thiocyanate anion (SCN)⁻? A joint experimental and theoretical study.

Journal of Physical Chemistry A, v. 110 (14), pp. 4930-4936, 2006

NOTE: This publication is included in the print copy of the thesis held in the University of Adelaide Library.

It is also available online to authorised users at:

<http://dx.doi.org/10.1021/jp058144t>

Maclean, M.J., Fitzgerald, M., Bowie, J.H. (2007) Interstellar Molecule CCCN May Be Formed by Charge-Stripping of [CCCN]⁻ in the Gas Phase, and When Energized, Undergoes Loss of C with Partial Carbon Scrambling.
Journal of Physical Chemistry A, v. 111 (50), pp. 12932-12937, 2007

NOTE: This publication is included in the print copy of the thesis held in the University of Adelaide Library.

It is also available online to authorised users at:

<http://dx.doi.org/10.1021/jp076315j>

Maclean, M.J., Eichinger, P.C.H., Wang, T., Fitzgerald, M., Bowie, J.H. (2008) A Theoretical Study of the Cyclization Processes of Energized CCCSi and CCCP. *Journal of Physical Chemistry A*, v. 112 (49), pp. 12714-12720, 2008

NOTE: This publication is included in the print copy of the thesis held in the University of Adelaide Library.

It is also available online to authorised users at:

<http://dx.doi.org/10.1021/jp807403s>

Diagnostic fragmentations of adducts formed between carbanions and carbon disulfide in the gas phase. A joint experimental and theoretical study†

Micheal J. Maclean, Scott Walker, Tianfang Wang, Peter C. H. Eichinger, Patrick J. Sherman and John H. Bowie*

Received 11th August 2009, Accepted 24th September 2009

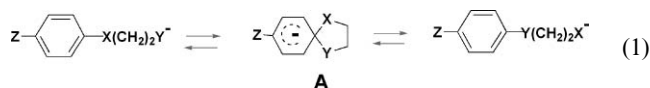
First published as an Advance Article on the web 23rd October 2009

DOI: 10.1039/b916477d

Selected carbanions react with carbon disulfide in a modified LCQ ion trap mass spectrometer to form adducts, which when collisionally activated, decompose by processes which in some cases identify the structures of the original carbanions. For example (i) $C_6H_5^- + CS_2 \rightarrow C_6H_5CS_2^- \rightarrow C_6H_5S^- + CS$, occurs through a 3-membered ring *ipso* transition state, and (ii) the reaction between $C_6H_5CH_2^-$ and CS_2 gives an adduct which loses H_2S , whereas the adduct(s) formed between *o*- $CH_3C_6H_4^-$ and CS_2 loses H_2S and CS . Finally, it is shown that decarboxylation of $C_6H_5CH_2CH_2CO_2^-$ produces the β -phenylethyl anion ($PhCH_2CH_2^-$), and that this thermalized anion reacts with CS_2 to form $C_6H_5CH_2CH_2CS_2^-$ which when energized fragments specifically by the process $C_6H_5CH_2CH_2CS_2^- \rightarrow C_6H_5CH_2^-CHC(S)SH \rightarrow [(C_6H_5CH_2CH=C=S)-SH] \rightarrow C_6H_5CH_2CCS^- + H_2S$. Experimental findings of processes (ii) and (iii) were aided by deuterium labelling studies, and all reaction profiles were studied by theoretical calculations at the UCCSD(T)/6-31+G(d,p)//B3LYP/6-31+G(d,p) level of theory unless indicated to the contrary.

Introduction

A classical (condensed phase) Smiles rearrangement¹ is shown in eqn (1). This nucleophilic *ipso* attack normally requires an electron withdrawing group (*e.g.* nitro, sulfonyl or halogen) either in the *ortho* or *para* position on the aromatic ring; generally X is a good leaving group, Y is a strong nucleophile and Z is shown as a *para* substituent in eqn (1). The anionic Smiles rearrangement has been used extensively synthetically (see *e.g.*^{2–9} for some recent examples), and radical Smiles rearrangements have also been reported.^{10–14} The Truce–Smiles rearrangement (involving attack of a carbanion centre at an *ipso* electrophilic centre) has also been used as a synthetic method.^{15,16}

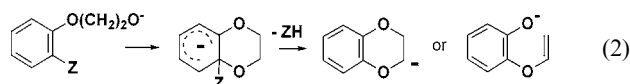


The gas phase Smiles rearrangement has not been studied in such depth as that in the condensed phase. The Smiles rearrangement occurs in the gas phase without the necessity for activation

Department of Chemistry, The University of Adelaide, South Australia, 5005, Australia. E-mail: john.bowie@adelaide.edu.au

† Electronic supplementary information (ESI) available: Tables S1 and S1(a): Anion geometries and energies of reaction pathway for the CS_2 addition to the singlet phenyl anion. Tables S2 and S2(a): Anion geometries and energies of reaction pathway for the collision induced dissociation of the singlet $PhCOS^-$ anion. Tables S3 and S3(a): Anion geometries and energies for the possible reaction pathway for the CS_2 addition to the singlet Benzyl anion. Tables S4 and S4(a): Anion geometries and energies of reaction pathway for the interconversion of the singlet anion *o*- $CH_3(C_6H_4)^-$ to singlet $PhCH_2^-$. Tables S5 and S5(a): Anion geometries and energies of reaction pathway for the interconversion of the singlet $PhCH_2CH_2^-$. Tables S6 and S6(a): Potential energy surface for the dissociation of the singlet $PhCH_2CH_2CS_2^-$ anion. Tables S7 and S7(a): Potential energy surface of dissociation of the singlet $PhCH_2CH_2CO_2^-$ anion. See DOI: 10.1039/b916477d

of the aromatic ring by electron-withdrawing groups. Heavy atom (¹³C and ¹⁸O) labelling shows that the product ion PhO^- from $PhO(CH_2)_2O^-$ and products PhO^- and PhS^- from $PhS(CH_2)_2O^-$ are formed exclusively from Smiles intermediates A ($X = Y = O$ or $X = S, Y = O$).¹⁷ [For the degenerate process where $X = Y = O$, calculations at the CCSD(T)/aug-cc-pVDZ//B3LYP/6-31+G(d) level of theory indicate that *ipso* intermediate A ($\Delta E = +285 \text{ kJ mol}^{-1}$) is reached *via* a transition state 289 kJ mol^{-1} above $PhO(CH_2)_2O^-$].¹⁸ In contrast, the formation of PhO^- from $PhO(CH_2)_3O^-$ occurs by competitive Smiles (85%) and S_N1 reactions (15%), while PhO^- is formed from $PhO(CH_2)_4O^-$ solely by an S_N1 process.¹⁷ ¹⁸O Labelling shows that when there is a substituent in the *ortho* position, the gas phase Smiles rearrangement competes with an *ortho* cyclization process as shown in eqn (2).¹⁹ The classical $[PhNO_2]^-$ to $[PhONO]^-$ gas phase rearrangement is probably an *ipso* process,²⁰ and gas-phase Smiles processes have been proposed for 2-hydroxybenzyl-*N*-pyrimidinylamine,²¹ phenoxy-*N*-phenyl acetamide anions,²² deprotonated 2-(4,6-dimethoxypyrimidine-2-ylsulfanyl)-*N*-phenylbenzamide²³ and other systems.^{24–26}



We wished to revisit our gas-phase *ipso* rearrangement studies in order to determine whether reactions of CS_2 with aryl carbanions give adducts *cf.*^{27,28} which undergo collision-induced cleavages [perhaps *ipso* (Smiles) rearrangements] diagnostic of the structures of the reacting carbanions. The systems we have chosen to react with CS_2 are (a) the phenyl anion, (b) the isomers $PhCH_2^-$ and [*ortho*- $CH_3C_6H_4^-$] and (c) the β -phenylethyl anion ($PhCH_2CH_2^-$) together with some other isomeric anions $C_8H_9^-$. In (c), we wished to determine whether the reaction with CS_2 can settle the old debate^{29–31} as to whether the β -phenylethyl anion is stable or

undergoes side chain rearrangement *via* an *ipso*, or some other intermediate.

Results and discussion

1. Reaction of the phenyl anion with CS₂

The phenyl anion was formed in the LCQ mass spectrometer by decarboxylation of the benzoate anion.³² Reaction of C₆H₅⁻ with CS₂ forms C₆H₅CS₂⁻ and collisional activation of this species gives C₆H₅S⁻ (*m/z* 109) as the only observable fragment ion. Reduction in the pressure of the CS₂ reagent gas in this system results in the detection of a minor peak corresponding to *m/z* 77 (C₆H₅⁻) accompanying *m/z* 109.

Since anions can react with CS₂ in the gas phase either at C or S,³³ the collision induced negative ion mass spectrum of deprotonated dithiobenzoic acid (C₆H₅CS₂H) was measured using a Waters QTOF2 mass spectrometer operating in negative ion electrospray ionization mass spectrometry (ESI MS/MS) mode. We chose the QTOF2 (rather than the LCQ) for this purpose since the QTOF2 uses an efficient gas collision CID MS/MS process for accelerated ions, whereas the LCQ uses a less efficient collisional process in the mass analyser. Two fragment ions, *m/z* 77 [(C₆H₅⁻) 100%] and *m/z* 109 [(C₆H₅S⁻) 64%] were observed. This is consistent with the adduct of the ion molecule reaction being C₆H₅CS₂⁻ and suggests that fragment anion C₆H₅⁻ is produced in the LCQ, but reacts immediately with CS₂ on formation.

In order to compare the reactions of C₆H₅CS₂⁻ with those of oxygen analogues, we have measured the negative ion CID ESI MS/MS of [C₆H₅COS]⁻ and C₆H₅CO₂⁻ using a Waters QTOF2 mass spectrometer. The spectrum of [C₆H₅COS]⁻ shows *m/z* 77 (100%), 93 (C₆H₅O⁻) 15% and 109 (C₆H₅S⁻) 55%, while that of the benzoate anion gives *m/z* 77 (C₆H₅⁻) as the only fragment anion. So C₆H₅CO₂⁻ does not undergo the *ipso* rearrangement, whereas [C₆H₅COS]⁻ undergoes two competitive *ipso* rearrangements.

The reaction coordinate profiles of the possible *ipso* rearrangements described above have been investigated at the UCCSD(T)/6-31+G(d,p)//B3LYP/6-31+G(d,p) level of theory. All relative energies indicated in the text and in the Figures are Δ*G* (free energy) values (as requested by a reviewer rather than Δ*E*). The supplementary tables list both Δ*E* and Δ*G* values. Results for the *ipso* processes of C₆H₅CS₂⁻ and C₆H₅COS⁻ are summarized in Fig. 1 and 2, with full details of geometries and energies listed in supplementary tables 1 and 2.[†] No *ipso* intermediates are identified in any case. In the case of C₆H₅CS₂⁻ (Fig. 1), reaction proceeds through an *ipso* transition state (+316 kJ mol⁻¹) to [C₆H₅SCS]⁻, which is energized and may decompose to C₆H₅S⁻ and CS in an overall endothermic reaction (+193 kJ mol⁻¹).[‡]

The two competitive rearrangements of [C₆H₅COS]⁻ are shown in Fig. 2. Formation of C₆H₅S⁻ and CO is endothermic (+26 kJ mol⁻¹) proceeding *via* an *ipso* transition state (+300 kJ mol⁻¹). In comparison, the competitive formation of C₆H₅O⁻ and CS is more endothermic (+245 kJ mol⁻¹) with a transition state marginally higher in energy (at +306 kJ mol⁻¹).

[‡] A reviewer has asked whether electron detachment of the precursor anion competes with the *ipso* rearrangement to form C₆H₅S⁻. The electron affinity of C₆H₅CS₂⁻ is calculated to be 3.345 eV (332 kJ mol⁻¹) [using the G3B3 level of theory (see Experimental section)] so the process shown in Fig. 1 is more energetically favourable than electron loss.

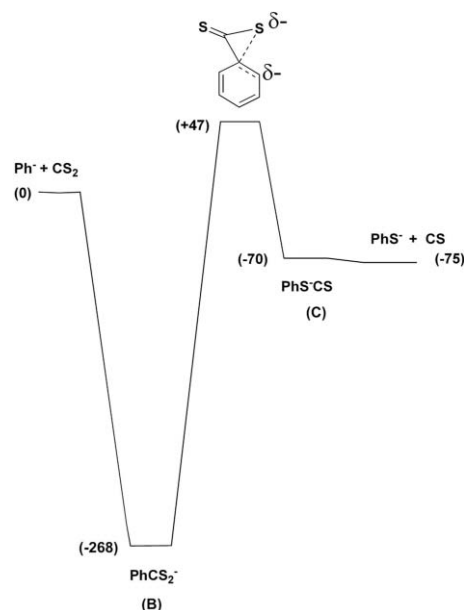


Fig. 1 The *ipso* rearrangement of PhCS₂⁻. Energies at the UCCSD(T)/6-31+G(d,p)//B3LYP/6-31+G(d,p) level of theory. Relative free energies (Δ*G*) in kJ mol⁻¹. Full details of geometries and energies of minima and transition states are recorded in Supplementary table 1.[†]

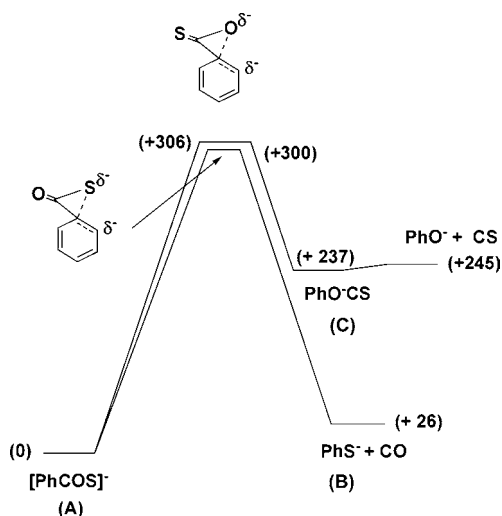


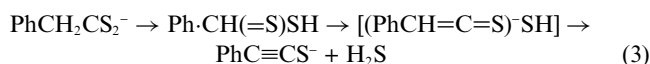
Fig. 2 The *ipso* rearrangements of [PhCOS]⁻. Energies at the UCCSD(T)/6-31+G(d,p)//B3LYP/6-31+G(d,p) level of theory. Relative free energies in kJ mol⁻¹. Full details of geometries and energies of minima and transition states are recorded in Supplementary table 2.[†]

The theoretical results are consistent with experiments, where the relative abundance of the peak due to C₆H₅S⁻ is greater than that of C₆H₅O⁻.

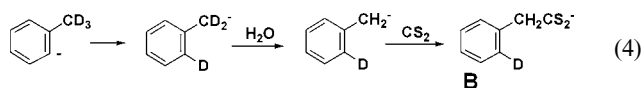
2. Reactions of the benzyl and *ortho*-tolyl anions with CS₂

The reactions of these two anions with CS₂ give adducts whose characteristic fragmentations differentiate between the structures of the original reacting carbanions. The precursors of the two anions were produced following electrospray ionization of phenylacetic acid and *ortho*-toluic acid to yield the two carboxylate anions which were decarboxylated following collisional activation

to yield the benzyl and *ortho*-tolyl anions respectively. The reaction of these two anions with CS₂ gave adducts whose fragmentations were probed using the CID MS4 scanning procedure. Decomposition of PhCH₂CS₂⁻ gave only one fragmentation, yielding a pronounced peak corresponding to the [PhCH₂CS₂⁻ - H₂S]⁻ ion (*m/z* 133). When this procedure was repeated with the D labelled species PhCD₂⁻, the adduct PhCD₂CS₂⁻ lost only D₂S. This process is shown in eqn (3): decomposition of PhCH₂CS₂⁻ gives PhCCS⁻ and H₂S, an endothermic process (+120 kJ mol⁻¹) at the UCCSD(T)/6-31+G(d,p)//B3LYP/6-31+G(d,p) level of theory (see Supplementary Table 3†).



The situation with the *ortho*-tolyl anion is more complex: the adduct formed with CS₂ when collisionally activated shows competitive losses of H₂S and CS. The loss of CS is simply the *ipso* rearrangement (*cf.* Fig. 1) of the expected adduct *ortho*-CH₃C₆H₄CS₂⁻. But how is H₂S lost? This was uncovered when the reaction between the D labelled *ortho*-CD₃C₆H₄⁻ and CS₂ was studied. The decarboxylation process formed *ortho*-CD₃C₆H₄⁻ and if this anion was allowed to react immediately with CS₂, the adduct lost only CS by a standard *ipso* rearrangement. If, in contrast, the *ortho*-CD₃C₆H₄⁻ anion was allowed to remain in the trap for 10 microseconds, it back exchanged two D for H (reaction with residual H₂O from the electrospray ionization process). This ion formed an adduct with CS₂ which, on collisional activation, lost H₂S exclusively. This can only be due to the process shown in eqn (4): namely D transfer to the *ortho* position followed by D/H exchange of the two remaining benzylic deuteriums by water (a process of the type first reported by DePuy *et al.*^{27,28}) to yield the D₁ adduct **B** which then loses H₂S (see eqn (4) and *cf.* eqn (3)). The interconversion of the *ortho*-tolyl and benzyl anions is an exothermic process (-53 kJ mol⁻¹) with a barrier of 179 kJ mol⁻¹ at the UCCSD(T)/6-31+G(d,p)//B3LYP/6-31+G(d,p) level of theory (see Fig. 3 and Supplementary table 4†).



3. The reactions of the β-phenylethyl anion and other isomers with CS₂

The question as to whether the β-phenylethyl anion (PhCH₂CH₂⁻) is stable has been a matter of debate for almost 20 years. Nibbering *et al.*³⁰ presented data which showed that the β-phenylethyl anion rearranges to the cyclised *ipso* form on collisional activation in a conventional mass spectrometer, while Squires and Graul³¹ proposed that the β-phenylethyl anion was stable in a flowing afterglow instrument, because the ion formed by decarboxylation of PhCH₂CH₂CO₂⁻ was thermalised by the helium carrier gas, and had a gas phase basicity (Δ*G*^o_{acid}) of 1699 ± 13 kJ mol⁻¹, a value consistent with that expected for PhCH₂CH₂⁻.

The reaction coordinate calculations [at the UCCSD(T)/6-31+G(d,p)//B3LYP/6-31+G(d,p) level of theory] of relevant C₈H₅⁻ isomers provide some interesting results (see Fig. 4 and Supplementary table 5†). First, PhCH₂CH₂⁻ (**A**) can undergo a 1,2-H transfer over a transition state (+145 kJ mol⁻¹) to yield Ph⁻CHCH₃ (**D**) in an exothermic reaction (-104 kJ mol⁻¹). Second,

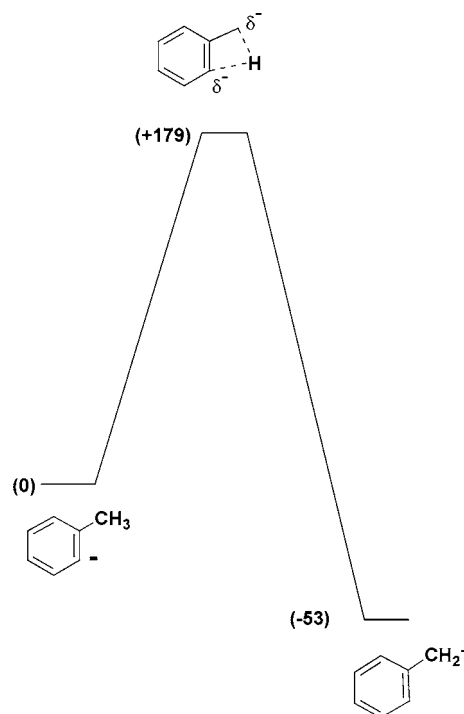


Fig. 3 The interconversion of the benzyl and *ortho*-tolyl anion. Energies at the UCCSD(T)/6-31+G(d,p)//B3LYP/6-31+G(d,p) level of theory. Relative free energies in kJ mol⁻¹. Full details of geometries and energies of minima and transition states are recorded in Supplementary table 4.†

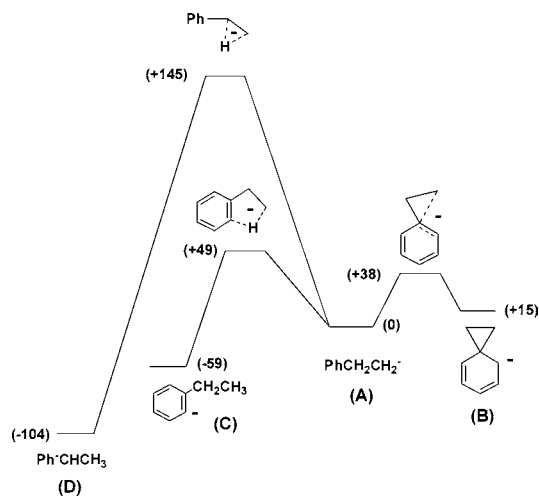


Fig. 4 The interconversions of PhCH₂CH₂⁻ (**A**), Ph⁻CHCH₃ (**D**), *ortho*-C₂H₅-C₆H₄⁻ (**C**) and the cyclised species (**B**). Energies at the UCCSD(T)/6-31+G(d,p)//B3LYP/6-31+G(d,p) level of theory. Relative free energies in kJ mol⁻¹. Full details of geometries and energies of minima and transition states are recorded in Supplementary table 5.†

PhCH₂CH₂⁻ can H⁺ transfer from the *ortho* position to give *ortho*-C₂H₅-C₆H₄⁻ (**C**) [barrier (+49 kJ mol⁻¹), reaction exothermic (-59 kJ mol⁻¹)]. However, the electron affinity of PhCH₂CH₂⁻ at the G3B3 level of theory is calculated to be 0.215 eV (21 kJ mol⁻¹), so these two H transfer processes are unfavourable compared with electron loss from PhCH₂CH₂⁻. Finally, the data shown in Fig. 4 indicates that the conversion of PhCH₂CH₂⁻ (**A**) to the cyclic isomer (**B**) is endothermic (+15 kJ mol⁻¹) and has a modest barrier

to the transition state of 38 kJ mol⁻¹. This interconversion and electron loss from PhCH₂CH₂⁻ should therefore be competitive. These theoretical data are consistent with previous studies, namely (i) Nibbering *et al.* finding rearrangement of PhCH₂CH₂⁻ on collisional excitation,³⁰ and (ii) Squires and Graul suggesting that PhCH₂CH₂⁻ is stable when the ion is efficiently thermalized by the helium carrier gas in the flowing afterglow drift tube.³¹

The collision induced mass spectrum of the adduct formed between “PhCH₂CH₂⁻” (by decarboxylation of PhCH₂CH₂CO₂⁻) and CS₂ shows pronounced loss of H₂S. The analogous spectra of Ph(CH₃)CHCS₂⁻ and *ortho*-C₂H₅-C₆H₄-CS₂⁻ do not exhibit loss of H₂S. *Ortho*-C₂H₅-C₆H₄-CS₂⁻ eliminates CS by the standard *ipso* rearrangement (data not shown but *cf.* Fig. 1)], while Ph(CH₃)CHCS₂⁻ yields Ph(CH₃)CH⁻ at low CS₂ pressures. It can therefore be concluded that PhCH₂CH₂⁻ neither isomerizes to Ph⁻CHCH₃ nor to *ortho*-C₂H₅-C₆H₄⁻ prior to or during reaction with CS₂ in the LCQ mass spectrometer.

The two D labelled species PhCH₂CD₂CS₂⁻ and PhCD₂CH₂CS₂⁻ were formed in the Waters QTOF2 mass spectrometer [by deprotonation under electrospray ionization of PhCH₂CD₂CS₂H and PhCD₂CH₂CS₂H in methanol]. These two dithiocarboxylate anions are those which would be formed by the ion molecule reactions between the appropriately D-labelled β-phenylethyl anion and CS₂ in the LCQ spectrometer. CID MS/MS of PhCH₂CD₂CS₂⁻ shows loss of D₂S (see Fig. 5), while PhCD₂CH₂CS₂⁻ loses H₂S. Loss of H₂S from PhCH₂CH₂CS₂⁻ has been shown by *ab initio* calculations to occur as shown in Fig. 6 (also Supplementary table 6†).

The two D labelled species “PhCD₂CH₂⁻” and “PhCH₂CD₂⁻” were prepared by decarboxylation of their respective carboxylate anions in the LCQ mass spectrometer. If these anions interconvert

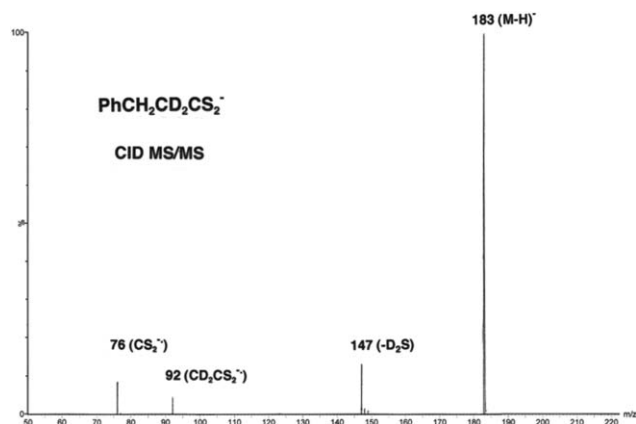


Fig. 5 The CID MS/MS of PhCH₂CD₂CS₂⁻ using electrospray ionization with a Waters QTOF2 mass spectrometer. The collisional activation process in the QTOF2 produces more energized anions than those formed in the LCQ. Thus the peaks observed at *m/z* 92 and 76 in Fig. 5 are not observed in Fig. 7. Since H₂S is lost exclusively from PhCD₂CH₂CS₂⁻, the small peaks at *m/z* 148 and 149 (losses of HDS and H₂S respectively) shown in this Figure are produced by undefined reactions favoured by the operation of a primary deuterium isotope effect occurring for the loss of D₂S from PhCH₂CD₂CS₂⁻.

through the D₂ analogue of cyclic (B) (Fig. 4) prior to or during reaction with CS₂, the subsequent losses of H₂S : D₂S should be the same from both labelled adducts (assuming no deuterium isotope effect is operating). If there is no cyclization then specific losses of H₂S and D₂S should be observed, as seen in the QTOF2 spectra described above. The LCQ data are as follows. The adduct formed from “PhCD₂CH₂⁻” and CS₂ loses H₂S, while that from

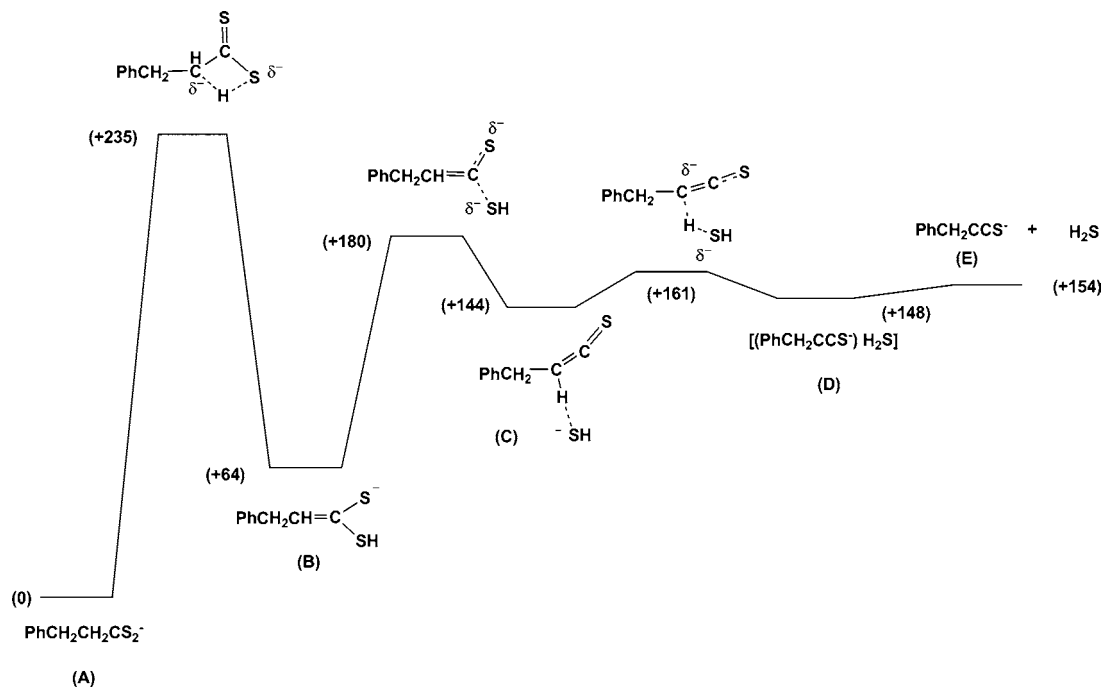


Fig. 6 Reaction coordinate profile for the dissociation of PhCH₂CH₂CS₂⁻ to PhCH₂CCS⁻ + H₂S. Energies at the UCCSD(T)/6-31+G(d,p)//B3LYP/6-31+G(d,p) level of theory. Relative free energies in kJ mol⁻¹. Full details of geometries and energies of minima and transition states are recorded in Supplementary table 6.† The reaction PhCH₂CH₂⁻ + CS₂ → PhCH₂CH₂CS₂⁻ is exothermic by 330 kJ mol⁻¹.

“PhCH₂CD₂⁻” and CS₂ loses D₂S (see Fig. 7). The spectrum shown in Fig. 7 does not change when the trapping time of the reactant ion is increased to 10 μsec.

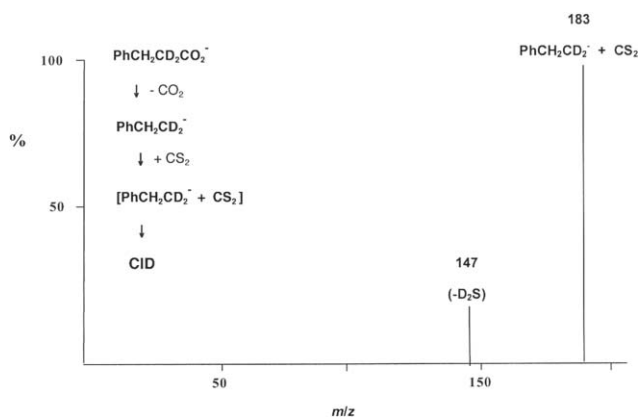


Fig. 7 The CID MS/MS/MS/MS scan of “PhCH₂CD₂CS₂⁻” formed by the reaction of CS₂ with “PhCH₂CD₂⁻” (formed from PhCH₂CD₂CO₂⁻). Electrospray ionization of PhCH₂CD₂CO₂H using a modified³⁶ Finnigan LCQ mass spectrometer.

The decarboxylation reaction shown in eqn (5) is calculated to be endothermic (+231 kJ mol⁻¹) at the UCCSD(T)/6-31+G(d,p)//B3LYP/6-31+G(d,p) level of theory (see Supplementary table 7†). Thus PhCH₂CH₂CO₂⁻ on collisional activation must produce a precursor with sufficient energy (231 kJ mol⁻¹) in order to effect decarboxylation. Collisional processes will produce energized precursor ions with a range of excess energies. The consequence of this is that some product ions PhCH₂CH₂⁻ may have excess energy. The theoretical results shown in Fig. 4 indicate that PhCH₂CH₂⁻ (**A**) needs only 38 kJ mol⁻¹ of excess energy in order to effect conversion to *ipso* species **B**. The experiments already carried out for the reactions of PhCH₂CD₂⁻ and PhCD₂CH₂⁻ with CS₂ show that there is no evidence of the *ipso* anion (**B**) (see Fig. 4) reacting with CS₂ during the ion molecule reaction, or of **B** being involved in an equilibrium process with **A** preceding or accompanying the ion molecule reaction with CS₂. This indicates that only thermalised ions **A** (or more correctly, anions with less than 38 kJ mol⁻¹ of excess energy) are reacting with CS₂ in the LCQ ion trap (*cf.* Gronert^{34,35}).

Conclusions

1. The reaction between C₆H₅⁻ and CS₂ in the gas phase gives an adduct C₆H₅CS₂⁻ which, when energized, rearranges *via* an *ipso* transition state to yield C₆H₅S⁻ and CS.
2. The respective reactions between C₆H₅CH₂⁻ and *ortho*-CH₃C₆H₅⁻ with CS₂ give adducts which can be readily distinguished by their collision induced dissociations; *i.e.* the adduct with C₆H₅CH₂⁻ loses H₂S, while that with *ortho*-CH₃C₆H₅⁻ loses both H₂S and CS₂, and
3. Decarboxylation of C₆H₅CH₂CH₂CO₂⁻ gives C₆H₅CH₂CH₂⁻ which reacts with CS₂ without rearrangement, to yield C₆H₅CH₂CH₂CS₂⁻.

Experimental

Mass spectrometry

All ion molecule reactions were carried out using electrospray ionization with a Finnigan LCQ ion trap mass spectrometer, modified³⁶ to allow ion-molecule reactions to be carried out by the incorporation of additional inlets for introduction of an extra reagent gas or liquid (in this case CS₂). The reagent CS₂ was injected into the system by syringe at a rate of 5 mL min⁻¹. Typical electrospray conditions involved a needle potential of 4.0 to 5.0 kV and a heated capillary temperature of 180 °C. Ions undergoing ion-molecule reactions in the LCQ have been essentially shown to be at room temperature.^{34,35} These experiments were investigated using the MS_n capability of the LCQ instrument. As an example, CID of C₆H₅CO₂⁻ to C₆H₅⁻ and CO₂ utilises an MS/MS scan, reaction of C₆H₅⁻ with CS₂ (MS/MS/MS) and finally, decomposition of the C₆H₅⁻ plus CS₂ adduct utilises an MS/MS/MS/MS scan.

Electrospray CID MS/MS spectra of ArCO₂⁻, ArCOS⁻ and ArCS₂⁻ anions were measured using a Waters QTOF2 hybrid orthogonal acceleration time-of-flight mass spectrometer (Waters/Micromass, Manchester, UK) with a mass range to *m/z* 10,000. The QTOF2 is fitted with an electrospray (ES) source in an orthogonal configuration with a Z-spray interface. Samples were dissolved in acetonitrile–water (1 : 1 v/v) and infused into the ES source at a flow rate of 5 mL min⁻¹. Experimental conditions were as follows: capillary voltage 3.1 kV, source temperature 80 °C, desolvation temperature 150 °C, and cone voltage 50 V. Tandem mass spectrometry (MS/MS) data were acquired using argon as the collision gas and the collision energy was set to give maximum fragmentation.

Theoretical methods

Geometry optimizations were carried out with the B3LYP/6-31+G(d,p) basis set [energies at UCCSD(T)/6-31+G(d,p) within the GAUSSIAN 03 suite of programs.³⁷ Stationary points were characterized as either minima (no imaginary frequencies) or transition states (one imaginary frequency) by calculation of the frequencies using analytical gradient procedures. The minima connected by a given transition structure were confirmed by intrinsic reaction coordinate (IRC) calculations.³⁸ The calculated frequencies were also used to determine zero-point vibrational energies.

The G3B3 level of theory³⁹ was used to calculate electron affinities (the difference in energy between the appropriate anion and the corresponding radical). Three levels of theory were used for chosen standards CH₃CO₂⁻ and HCO₂⁻. The computed values obtained were compared with experimental values as shown below:-

Level of theory	CH ₃ CO ₂ ⁻	HCO ₂ ⁻
Experimental	3.470 eV ⁴⁰	3.541 eV ⁴¹
G2 ⁴²	3.499 eV	3.715 eV
G3B3	3.319 eV	3.555 eV
UCCSD//B3LYP	3.082 eV	3.474 eV

The G3B3 level of theory was used for calculating the following electron affinities because of reasonable accuracy (see above) and efficiency of computer time usage:- PhCS₂⁻ 3.345 eV and PhCH₂CH₂⁻ 0.215 eV.

All calculations were carried out using the South Australian Partnership for Advanced Computing (SAPAC) Facility.

Materials/synthesis

The following were purchased from Sigma-Aldrich and were used without purification: (i) argon gas, carbon disulfide, benzoic acid, thiobenzoic acid, phenylacetic acid, *ortho*-toluic acid, 1-phenylpropionic acid, 2-phenylpropionic acid, *ortho*-ethylbenzoic acid, and 1,2-dibromobenzene; (ii) CD₃I (d₃ > 99.5%).

Dithiobenzoic acid was made by a standard Grignard reaction between bromobenzene and carbon disulfide⁴³ [(M – H)[–] *m/z* 153; m.p. dec. > 200 °C; lit⁴⁴ 208 °C].

Dithiophenyl acetic acid (benzene ethane dithiolic acid) was prepared by a standard Grignard reaction using benzyl chloride and carbon disulfide.⁴³ (yield 57%; m.p. 17–19 °C, lit.⁴⁵ 20 °C

***o*-Methyl(d₃)benzoic acid** [m.p. 103–104 °C (lit.⁴⁶ 104–105 °C; d₃ = 99.5%) was made by a Grignard sequence using d₃-methyl iodide (d₃ = 99.5%) and commencing with the diethylacetal of *o*-bromobenzaldehyde.⁴⁷

2,2-Dideuterophenylacetic acid [m.p. 77–78 °C (lit.⁴⁸ 78 °C; d₂ = 95%) was prepared by two cycles of exchange of phenylacetic acid with deuterium oxide using a standard method.⁴⁸

2-Phenyl-2,2-dideutero-1-bromoethane. 2,2-dideuterophenylacetic acid was treated with lithium aluminium hydride in tetrahydrofuran (THF) at 0° by a standard method⁴⁹ giving 2-phenyl-2,2-dideuteroethanol (90% yield after vacuum distillation; d₂=95%), which was treated with bromine and triphenyl phosphine in dichloromethane by a standard method,⁵⁰ to give 2-phenyl-2,2-dideutero-1-bromoethane as a colourless oil after vacuum distillation (yield 65%; d₂ = 95%).

2-Phenyl-1,1-dideutero-1-bromoethane. Phenylacetic acid was treated with lithium aluminium deuteride in THF at 0° by a standard method⁴⁹ giving 2-phenyl-1,1-dideuteroethanol as a colourless oil (after vacuum distillation) (yield 91%; d₂ = 98%), which was treated with bromine and triphenyl phosphine in dichloromethane by a standard method⁵⁰ to give 2-phenyl-1,1-dideutero-1-bromoethane as a colourless oil (after vacuum distillation) (yield 83%; d₂ = 98%).

2,2-Dideutero-3-phenylpropionic acid. 2-Phenyl-1,1-dideutero-1-bromoethane in THF was allowed to react (by a standard Grignard reaction⁵¹) with magnesium in THF under reflux, followed by addition of solid carbon dioxide to give 2,2-dideutero-3-phenylpropionic acid [m.p. 46–48 °C (lit.⁴⁷ 47–48 °C); yield 62%; d₂ = 98%].

3,3-Dideutero-3-phenylpropionic acid. 2-Phenyl-2,2-dideutero-1-bromoethane in THF was allowed to react with magnesium in THF under reflux.⁵¹ Addition of solid CO₂ gave 3,3-dideutero-3-phenylpropionic acid [m.p. 46–48 °C (lit.⁴⁷ 47–48 °C); yield 65%; d₂ = 95%].

2,2-Dideutero-3-phenylpropane dithiolic acid. 2-Phenyl-1,1-dideutero-1-bromoethane in THF was allowed to react with Mg in THF, followed by addition of CS₂ and a catalytic amount of CuCl (in THF) at –50 °C.⁴³ Workup gave 2,2-dideutero-3-phenylpropanedithiolic acid as an unstable red–orange oil [(M – H)[–] *m/z* 183; 23% yield; d₂ = 98%] which was used immediately in

the gas phase ion chemistry experiments to form PhCH₂CD₂CS₂[–] in the QTOF2 mass spectrometer.

3,3-Dideutero-3-phenylpropane dithiolic acid. 2-Phenyl-2,2-dideutero-1-bromoethane in THF was allowed to react with Mg in THF, followed by addition of CS₂ and a catalytic amount of CuBr in THF at –50 °C.⁴³ 3,3-Dideutero-3-phenylpropanedithiolic acid was isolated as an unstable red–orange oil [(M – H)[–] *m/z* 183; 25% yield, d₂ = 95%]. This was used immediately in the gas phase experiment in the QTOF2 to form PhCD₂CH₂CS₂[–].

Acknowledgements

We thank (i) the Australian Research Council for funding our negative ion mass spectrometry projects, and for Ph.D. (MJM) and research associate (SW, PCHE) stipends, (ii) the South Australian Partners for Advanced Computing (eResearch, The University of Adelaide) for generous provision of time on the Aquila supercomputer, and (iii) Professor R.A.J. O’Hair (University of Melbourne) for providing details of the modification of the Finnigan LCQ mass spectrometer to allow the study of ion–molecule reactions.

References

- 1 L. A. Warren and S. Smiles, *J. Chem. Soc.*, 1930, 1327; C. S. McClement and S. Smiles, *J. Chem. Soc.*, 1937, 1016; W. E. Truce, E. M. Kreider and W. W. Brand, *Org. React.*, 1970, **18**, 99; D. M. Schmidt and G. E. Bonvicino, *J. Org. Chem.*, 1984, **49**, 1664 and references cited therein.
- 2 D. G. Musaev, A. L. Galloway and F. M. Menger, *THEOCHEM*, 2004, **679**, 45.
- 3 L. H. Mitchell and N. C. Barvian, *Tetrahedron Lett.*, 2004, **45**, 5669.
- 4 M. Mizuno and M. Yamano, *Org. Lett.*, 2005, **7**, 3629.
- 5 L. El Kaim, M. Gizolme and L. Grimaud, *Org. Lett.*, 2006, **8**, 5021.
- 6 J. B. Xiang, L. Y. Zheng and H. X. Lie, *Tetrahedron*, 2008, **64**, 9101.
- 7 H. Zuo, L. Meng, M. Ghate, K.-H. Hwang, Y. K. Cho, S. Chandrasekhar, C. R. Reddy and D.-S. Shin, *Tetrahedron Lett.*, 2008, **49**, 3827.
- 8 J. B. Xiang, H. X. Xie and D. S. Wen, *J. Org. Chem.*, 2008, **73**, 3281.
- 9 J. H. Li and J. S. Wang, *Aust. J. Chem.*, 2009, **62**, 176.
- 10 W. B. Motherwell and A. M. K. Pannell, *J. Chem. Soc., Chem. Commun.*, 1991, 877.
- 11 R. Caddick, C. L. Shering and S. N. Wadman, *Tetrahedron*, 2000, **56**, 465.
- 12 Ryokawa and H. Togo, *Tetrahedron*, 2001, **57**, 5915.
- 13 M. Tada, H. Shijuna and M. Nakamura, *Org. Biomol. Chem.*, 2003, **1**, 2499.
- 14 E. Bacqué, M. El Qacemi and S. Z. Zard, *Org. Lett.*, 2005, **7**, 3817.
- 15 T. J. Snape, *Chem. Soc. Rev.*, 2008, **37**, 2452.
- 16 T. J. Snape, *Synlett*, 2008, 2689.
- 17 P. C. H. Eichinger, J. H. Bowie and R. N. Hayes, *J. Am. Chem. Soc.*, 1989, **111**, 4224.
- 18 D. C. Graham and J. H. Bowie, unpublished observations.
- 19 P. C. H. Eichinger and J. H. Bowie, *Org. Mass Spectrom.*, 1992, **27**, 995.
- 20 J. H. Bowie, *Aust. J. Chem.*, 1971, **24**, 989.
- 21 H. Y. Wang, X. Zhang, Y.-L. Guo and L. Lu, *J. Am. Soc. Mass Spectrom.*, 2005, **16**, 1561.
- 22 F. Wang, *Rapid Commun. Mass Spectrom.*, 2006, **20**, 1820.
- 23 Y. P. Zhou, Y. J. Pan and X. T. Cao, *J. Am. Soc. Mass Spectrom.*, 2007, **18**, 1813.
- 24 M. Shafi, M. Hussain and S. G. Peeran, *Phosphorus, Sulfur Silicon Relat. Elem.*, 2007, **182**, 2087.
- 25 M. J. Sun, W. Daim and D. Q. Liu, *J. Mass Spectrom.*, 2008, **43**, 383.
- 26 P. H. Lambert, S. Berlin, J. M. Lacoste, J. P. Volland, A. Krick, E. Furet, A. Botrel and P. Guenot, *J. Mass Spectrom.*, 1998, **33**, 242.
- 27 C. H. DePuy and V. M. Bierbaum, *Acc. Chem. Res.*, 1981, **14**, 146; and references cited therein.
- 28 C. H. DePuy, V. M. Bierbaum and J. J. Grabowski, *Science*, 1982, **218**, 955.

- 29 M. J. Raftery and J. H. Bowie, *J. Chem. Soc., Perkin Trans. 2*, 1988, 563.
- 30 W. P. M. Maas, P. A. van Veelen and N. M. M. Nibbering, *Org. Mass Spectrom.*, 1989, **24**, 546.
- 31 S. T. Graul and R. R. Squires, *J. Am. Chem. Soc.*, 1990, **112**, 2506, and references cited therein.
- 32 S. T. Graul and R. R. Squires, *Mass Spectrom. Rev.*, 1988, **7**, 263 and references cited therein.
- 33 J. C. Sheldon, J. H. Bowie, C. H. DePuy and R. Damrauer, *J. Am. Chem. Soc.*, 1986, **108**, 6794.
- 34 S. Gronert, *J. Am. Soc. Mass Spectrom.*, 1998, **9**, 845.
- 35 S. Gronert, L.M. Pratt and S. Mogall, *J. Am. Chem. Soc.*, 2001, **123**, 3081.
- 36 T. Waters, R. A. J. O'Hair and A. G. Wedd, *J. Am. Chem. Soc.*, 2003, **125**, 3384.
- 37 M. J. Frisch, G. W. Trucks, H. B. Schlegel, G. E. Scuseria, M. A. Robb, J. R. Cheeseman, J. A. Montgomery, T. Vreven, K. N. Kudin, J. C. Burant, J. M. Millam, S. S. Iyengar, J. Tomasi, V. Barone, B. Mennucci, M. Cossi, G. Scalmani, N. Rega, G. A. Petersson, H. Nakatsuji, M. Hada, M. Ehara, K. Topyota, R. Fukuda, J. Hasegawa, M. Ishida, T. Makajima, Y. Honda, O. Kitao, H. Nakai, M. Klene, X. Li, J. E. Know, H. P. Hratchian, J. B. Cross, V. Bakken, C. Adamo, J. Jaramillo, R. Gomperts, R. E. Stratmann, O. Yazyev, A. J. Austin, R. Cammi, C. Pomelli, J. W. Ochterski, P. Y. Ayala, K. Morokuma, G. A. Voth, P. Salvador, J. J. Dannenberg, V. G. Zakrzewski, S. Dapprich, A. D. Daniels, M. C. Strain, O. Farkas, D. K. Malick, A. D. Rabuck, K. Raghavachari, J. B. Foresman, J. V. Ortiz, Q. Cui, A. G. Baboul, S. Cliffor, J. Cioslowski, B. B. Stefanov, G. Liu, A. Liashenko, P. Piskorz, I. Komaromi, R. L. Martin, D. J. Fox, T. Keith, M. A. Al-Latham, C. Y. Peng, A. Nanayakkara, M. Challacombe, P. M. W. Gill, B. Johnson, W. Chen, M. W. Wong, C. Gonzalez and J. A. Pople, *Gaussian 03*, Revision E; Gaussian, Inc., Wallingford, CT, 2004.
- 38 K. Fukui, *Acc. Chem. Res.*, 1981, **14**, 363.
- 39 A. G. Baboul, L. A. Curtiss, P. C. Redfern and K. Raghavachari, *J. Chem. Phys.*, 1999, **110**, 7650; L. A. Curtiss, K. Raghavachari, P. C. Redfern and J. A. Pople, *J. Chem. Phys.*, 2000, **112**, 7373.
- 40 Z. Lu and R. E. Continetti, *J. Phys. Chem. A*, 2004, **108**, 9962.
- 41 G. Caldwell, R. Renneboog and P. Kebarle, *Can. J. Chem.*, 1989, **67**, 611.
- 42 L. A. Curtiss, K. Raghavachari, G. W. Trucks and J. A. Pople, *J. Chem. Phys.*, 1991, **94**, 7221.
- 43 P. Vermeer, *Synthesis*, 1979, 432.
- 44 *NL patent* 1967, 6510637.
- 45 D. F. Aycocock, *J. Org. Chem.*, 1979, **44**, 569.
- 46 P. A. S. Smith, *J. Am. Chem. Soc.*, 1954, **76**, 431.
- 47 C. C. Lee, *Tetrahedron*, 1959, **7**, 206.
- 48 K. Auwers, *Justus Liebigs Ann. Chem.*, 1910, **373**, 239.
- 49 J. Blum, S. Kraus and Y. Pickholtz, *J. Organomet. Chem.*, 1971, **33**, 227.
- 50 M. Orfanopoulos, I. Smonou and C. S. Foote, *J. Am. Chem. Soc.*, 1990, **112**, 3607.
- 51 A. I. Vogel, *A textbook of practical organic chemistry*, Third Edition pp 247-260, Longmans, Green and Co, London, 1956.